The Study of Ruthenium(II) Half-sandwich Phosphido Complexes containing Pentamethylcyclopentadienyl (Cp*) ligand

by

Jin Yang
B.Sc. (Honours), St. Francis Xavier University, 2014

A Thesis Submitted in Partial Fulfillment
of the Requirements for the Degree of

MASTER OF SCIENCE

in the Department of Chemistry

© Jin Yang, 2016
University of Victoria

All rights reserved. This thesis may not be reproduced in whole or in part, by photocopy or other means, without the permission of the author.

Supervisory Committee

The Study of Ruthenium(II) Half-sandwich Phosphido Complexes containing Pentamethylcyclopentadienyl (Cp*) ligand

by

Jin Yang
B.Sc. (Honours), St. Francis Xavier University, 2014

Supervisory Committee

Dr. Lisa Rosenberg, Department of Chemistry
Supervisor

Dr. David Berg, Department of Chemistry
Departmental Member

Abstract

Supervisory Committee
Dr. Lisa Rosenberg, Department of Chemistry
Supervisor
Dr. David Berg, Department of Chemistry
Departmental Member

Previous work in the Rosenberg group showed that the half-sandwich complexes Ru(η^5-indenyl)Cl(PR_2H)(PPh_3) (**2**^{i}), where R = cyclohexyl (Cy), isopropyl (Pr^i), phenyl (Ph), *para*-tolyl (Tol^p), react with the strong, bulky base $KOBu^t$ to give highly reactive complexes Ru(η^5-indenyl)(PR_2)(PPh_3) (**6**^{i}) containing a ruthenium-phosphorus double bond, Ru=PR_2. The reactions of these phosphido complexes **6**^{i} with some reagents, such as alkenes, carbon monoxide and dihydrogen, illustrate their rich and varied reactivity. To better understand the mechanisms of these reactions (whether the indenyl effect is necessary), synthesis of analogous secondary phosphine complexes containing the pentamethylcyclopentadienyl (Cp*) ligand, Ru(η^5-Cp*)Cl(PPh_3)(PR_2H) (**2**) were prepared via ligand substitution at Ru(η^5-Cp*)Cl(PPh_3)$_2$ (**1**). Cp* phosphido complexes Ru(η^5-Cp*)(PR_2)(PPh_3) (**6**) were generated *in situ* and their reactivity was investigated to see if they behaved similarly to the indenyl complexes. Experimental evidence in this thesis suggests that variable hapticity is not necessary in our indenyl system. In addition, these experimental evidence highlights enhanced lability of ligand at the bulky Cp*Ru fragment and higher Bronsted basicity of the phosphido ligand (PR_2^-) in Cp* phosphido **6** relative to the indenyl analogues **6**^{i}.

Table of Contents

List of Tables

List of Figures

List of Schemes

List of Abbreviations

Å	Angstrom (1 x 10^{-10} m)
Anal.	analysis
atm	atmosphere
Ar	aryl
br	broad
Bu	butyl
Bu^t	tert-butyl, -$C(CH_3)_3$
°C	degrees Celsius
C_{ipso}	*ipso*-carbon
C_{meta}	*meta*-carbon
C_{ortho}	*ortho*-carbon
C_{para}	*para*-carbon
Calcd	caculated
$^{13}C\{^1H\}$	observed carbon while decoupling proton
cm^{-1}	wavenumber
COSY	correlation spectroscopy
Cp	cyclopentadienyl group, $C_5H_5^-$
Cp*	1,2,3,4,5-Pentamethylcyclopentadienyl, $C_5(CH_3)_5^-$
Cy	cyclohexyl group, -C_6H_{11}
D	dimension
d	doublet *or* days
DBU	1,8-diazabicyclo[5.4.0]undec-7-ene
dd	doublet of doublets
ddd	doublet of doublet of doublets
dec	decomposes
deg(or °)	degrees
DEPT	distortionless enhanced polarization transfer
DFT	density functional theory
dm	doublet of multiplets
dt	doublet of triplet
δ	NMR chemical shift in parts per million
e^-	electron
equiv	equivalent(s)
eq	equation
ESI	electrospray ionization
Et	ethyl group, -C_2H_5
η^n	hapticity
g	gram
h	hour(s)
^1H	observed proton
H_m	*meta*-proton
H_o	*ortho*-proton
H_p	*para*-proton
HMBC	heteronuclear multiple-bond connectivity
HSQC	heteronuclear single quantum coherence
Hz	hertz
i	iso

IR	infrared
J	scalar nuclear spin-spin coupling constant (NMR)
κ^n	denticity
K	Kelvin
L	liter or neutral donor ligand
LR	low-resolution
M	molarity *or* metal
M^+	parent ion
m	mutiplet (NMR)
Me	methyl,-CH_3
mg	milligram(s)
MHz	megahertz
min	minutes(s)
mL	milliliter
mm	millimeter
mmol	millimole(s)
mol	mole(s)
mp	melting point (°C)
MS	mass spectromertry
m/z	mass to charge ratio
μL	microliter
n	normal
NMR	nuclear magnetic resonance
nOe	nuclear Overhauser effect
NOESY	nuclear Overhauser effect spectroscopy
o	ortho
^{31}P	observed phosphorus
$^{31}P\{^1H\}$	observed phosphorus wihle decoupling proton
p	para
Ph	phenyl group, -C_6H_5
Pr	propyl group, -C_3H_7
R	alkyl *or* aryl group
RT	room temperature
s	singlet (NMR)
T	temperature
t	triplet (NMR)
t	tertiary
td	triplet of doublets
θ	Tolman cone angle
THF	tetrahydrofuran
TOCSY	total correlation spectroscopy
Tol	tolyl group, -$C_6H_4CH_3$
Tol^p	*para*-tolyl group
VT	variable temperature
$\omega_{1/2}$	line width at half height
X	anionic donor ligand
X_i	Tolman electronic factor

List of Numbered Compounds

R= Cy (**a**), Et (**b**), Ph (**c**), Tol^{p} (**d**)

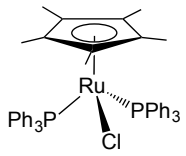

1

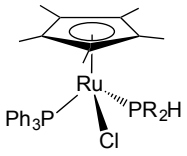

2

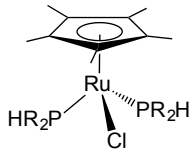

3

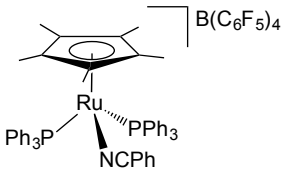

4

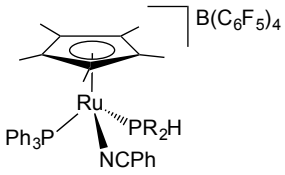

5

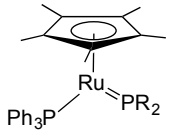

6

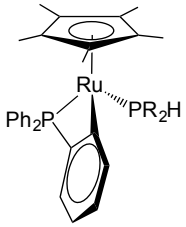

7

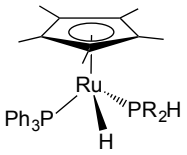

8

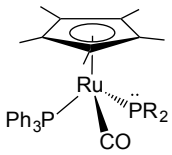

9

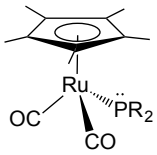

10

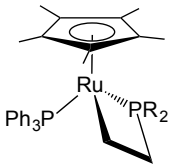

11

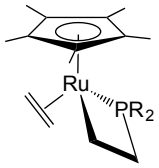

12

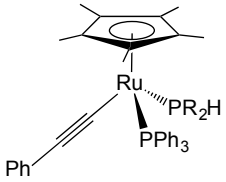

13

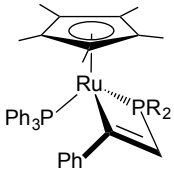

14

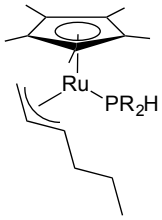

15

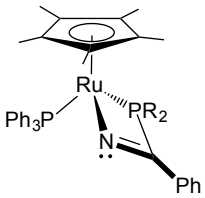

16X

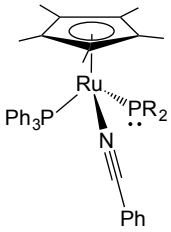

16Y

Indenyl complexes in this thesis are numbered as **number**^{i} for which Cp* analogues are prepared.

Example:

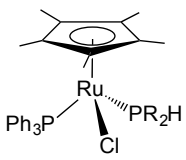

2

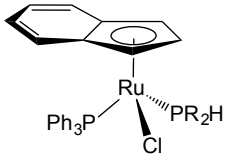

2^{i}

Acknowledgments

Firstly, I would like to express my deep gratitude to my supervisor Dr. Lisa Rosenberg for her patience, invaluable insight and all support throughout my graduate school career. I could not have gotten where I am without her help. During these two years, I am very happy to work with a group of wonderful and hard working people. I am especially grateful to Roman Belli and Dr. Peter Lee for their help and suggestion. I would like to thank Sophie Langis-Barsetti for her contribution for this project.

Various amazing NMR spectroscopy shown in these thesis is impossible without the teaching and assistance of Christopher Barr and I want to thank him. I appreciate Dr. Bob McDonald at the University of Alberta for solving all crystal structures of my complexes in this thesis. I also would like to thank Dr. Jingwei Luo and Haoxuan Zhu for helping me on all MS spectroscopy. In addition, I would like to thank my TA instructor, Jane Browning and Monica Reimer, for their guidance and advice on my teaching. I would like to appreciate all staff in the chemistry department office, science stores and lab at the University of Victoria.

In the end, I am so grateful to my friends and family for their encouragement and support. I specially thank my parent for their infinite love.

Chapter 1 Introduction

1.1 Half-sandwich ruthenium (Ru) complexes of secondary phosphines

The concept of half-sandwich complex was raised by analogy to the well-known "sandwich" complex ferrocene (Cp_2Fe). Organometallic Ru(II) complexes generally exist as an octahedral structure. However, for half-sandwich complexes, the Cp, arene or their derivatives' ring of these complexes occupies one face of the octahedron, which can be treated as one ligand to give pseudo-tetrahedral (three-leg piano stool) structure. Three ligands are present in the rest of the coordination sites as three legs of the "piano stool".[1] The coordination of these Cp, arene or their derivative ligands to metal center is usually strong, regardless of the oxidation states of the metal and effect of the other surrounding ligands.[1] All these considerations are particularly relevant to a lot of ruthenium organometallic chemistry.[1,2,3]

There is a lot of literature describing tertiary phosphine (PR_3) coordination to half-sandwich (e.g. Cp,[4] Cp*[5] and indenyl[6]) Ru species. These tertiary phosphine complexes are known active catalysts in some reactions such as C-C bond formation [7,8,9] Relative to PR_3 ligands, the coordination chemistry of PR_2H is still emerging. Monosubstituted secondary phosphine complexes Ru(η^5-Cp)X(PPh_2H)(PPh_3) (X = H, Cl) were reported by Wilczewski in 1982.[10] Singleton and his coworkers described the synthesis of the disubstituted complex Ru(η^5-Cp)Cl(PPh_2H)$_2$ in 1986.[11] , and more recently Paz-Sandoval and his coworkers reported the synthesis and characterization of Ru(η^5-Cp)Cl(PPh_2H)(PPh_3) and Ru(η^5-Cp*)Cl(PPh_2H)$_2$ complexes. [12 , 13] The Rosenberg group has synthesized a series of indenyl secondary phosphine complexes, such as Ru(η^5-indenyl)X(PR_2H)(PPh_3) (X= H, Cl; R = Cy, Ph, Tol^p, Pr^i).[14,15,16] More recently, the Rosenberg group prepared the cationic secondary phosphine complex

Ru(η^5-indenyl)(NCPh)(PPh_2H)(PPh_3) from its halide precursor in which non-innocent halide ligands have been replaced with labile nitrile ligands.[17] The idea of incorporating labile nitrile ligands is to open a coordination site in the Ru complex for incoming substrate during catalytic reactions (e.g. hydrophosphination).[17] In addition to Ru complexes containing Cp derivatives, η^6-arene secondary phosphine complexes are also an important part of the family of half-sandwich Ru secondary phosphine complexes. Oro and coworkers reported the synthesis of Ru(η^6-*p*-cymene)$Cl_2(PR_2H)$ (R= Cy, Ph) in 1991.[18] Detailed spectroscopic characterization and X-ray crystallography of some η^6-arene Ru complexes containing secondary phosphine were reported in the literature.[19,20]

The P-H bond of PR_2H usually remains intact after coordination to metals in secondary phosphine complexes, but its acidity is enhanced by σ donation to abstract electron density from H to P and π back donation from the metal to σ* orbital of P-H bond.[21,22] As a result, much of the interest in these complexes lies in their use as precursors for phosphido (PR_2^-) complex, which is described below (Section 1.2.1).

1.1.1 Properties of phosphine ligands

Phosphine ligands are important ancillary ligands in homogeneous catalysis and organometallic chemistry.[22] Phosphine ligands in general are considered as strong σ donors.[23] This σ donation arises from their ability to donate lone pair electrons to the metal center (Figure 1.1 left). Meanwhile, π backbonding allows an orbital of π-symmetry with σ* character of a phosphine ligand to accept electron density from a filled d-orbital of the metal (Figure 1.1 right).[24]

Figure 1.1 Representation of σ donation (left) and π acceptance (right) of coordinated phosphine ligand.

Tolman reported the measure of electronic and steric effects of PR_3 ligands depending on their substituents (R).[25] Both of these parameters are known to play an important role in determining the effects of phosphine ligands in transition metal complexes.

Table 1.1 Tolman cone angle (°) and electronic factors (X_i) for selected PR_3 and PR_2H relevant to this project.[a,b]

Phosphine	Electronic factor (X_i)[a]	Cone angle (θ)[b]
PPh_3	12.9	145
PCy_2H	8.5	142
PEt_2H	11.9	117
PPh_2H	16.9	126
$PTol^p{}_2H$	15.3	126

[a] Tolman electronic factor of PR_2H were calculated by equation 1.1.
[b] Tolman cone angles of PR_2H were calculated by equation 1.2.

For electronic properties, the Tolman electronic factor (X_i) can be used to approximate the electron donating ability of a phosphine ligand, which is determined using the ν_{CO} stretching frequency of various $Ni(CO)_3PR_3$ complexes relative to $Ni(CO)_3PBu^t{}_3$.[25] The ability of a phosphine to donate or accept electron density varies by the different substituents (R) on the phosphorus (P) center. In general, the phosphine ligand becomes more electron-donating with electron donating groups (e.g. R = Cy, Et), while these substituents weaken its electon-accepting ability. Electron-withdrawing substituents (e.g. R = F, Cl) increase the π-acidity of a phosphine ligand by attracting electron density from P. The electron-donating ability of PR_3 ligands falls in the order $PCy_3 > PMe_3 > PPh_3 > P(OMe)_3 > P(OPPh)_3 > PF_3$. Moreover, the effect of the substituents on the electronic properties of the phosphine ligand were found to be additive (eq. 1.1).[25] This makes it possible to predict the electronic properties of a PR_2H ligand. Electronic factors for PR_2H ligands relevant to this

project are listed in Table 1.1. The electron-donating ability of PR_2H ligands falls in the order $PCy_2H > PEt_2H > PTol^p{}_2H > PPh_2H$.

$$\nu = 2056.1 + \sum_{i=1}^{3} X_i \quad (1.1)$$

For steric property, the Tolman cone angle (θ) is used quantitatively to represent the phosphine size.[25] The phosphine ligands were fixed at an idealized Ni complex with Ni-P bond distance of 2.28 Å and a cone centered on the metal was set to just touched the outermost van der Waals radii of the substituents (Figure 1.2a, left). This model assumed free rotation of the phosphine ligand. Similar to the electronic factor, Tolman cone angles are not just limited in symmetrical phosphine (PR_3). For PR_2H ligands (Figure 1.2a, right), the Tolman cone angles are calculated by the summing half cone angles ($\theta_i/2$) of the each substituent on PR_2H (eq. 1.2). Tolman cone angles for PR_2H ligand relevant to this project are listed in Table 1.1. The size of PR_2H ligands increases in the order $PEt_2H < PPh_2H \approx PTol^p{}_2H < PCy_2H$. In addition, there is more modern "solid angle" used to describe the sizes of phosphines. The solid angle of a ligand is defined as " the normalized area of the shadow cast by the ligand on a sphere encompassing the entire complex with the metal as the point source of light ".[22,26] The formula of solid angle and related shadow are shown in Figure 1.2b. However, solid angles of PR_2H are not found in the literature. Calculated cone angles for PR_2H ligand are used in this thesis for the phosphine sizes.

$$\theta = \frac{2}{3}\sum_{i=1}^{3}\frac{\theta_i}{2} \quad (1.2)$$

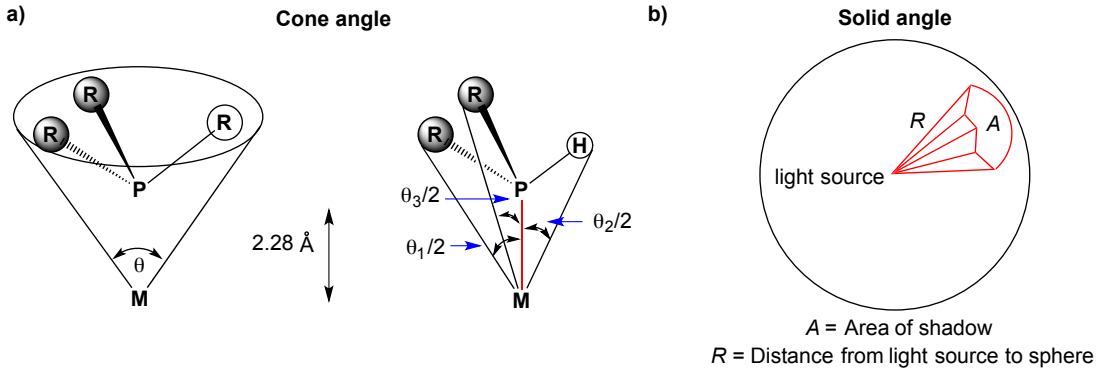

Figure 1.2 a) Definitions of the Tolman cone angle for PR_3 (left) and PR_2H (right). **b)** Definition of the solid angles of phosphines.

Another property of PR_2H relevant to this project is its Bronsted acidity, which allows the deprotonation of the P-H bond. Li et al. calculated pK_a^{DMSO} values for HPR_2 (Table 1.2).[27] More recently, pK_a^{THF} (HA) values for some secondary phosphine base $[PR_2]^-$ (A^-) were also estimated (Table 1.3).[28] The pK_a values of PPh_2H reported in the literature vary a lot.[27,28,29] However, based on these data, the difference in acidity of PR_2H relevant to this project can be approximated, and the acidity increases in the order $PCy_2H \approx PEt_2H < PTol^p_2H < PPh_2H$.

Table 1.2 Selected pK_a^{DMSO} values calculated for HPR_2.

Acid	Base	pK_a
PCy_2H	PCy_2^-	34.6
PEt_2H	PEt_2^-	34.9
PPh_2H	PPh_2^-	22.9

Table 1.3 Selected pK_a^{THF} (HA) values for PR_2H.

Acid	Base	pK_a
PPh_2H	[K(crypt)][PPh_2]	38 ± 4
$PTol^p_2H$	[K(crypt)][$PTol^p_2$]	43 ± 4

[a] crypt = 2.2.2-cryptand.

1.1.2 Properties of nitrile ligands

As mentioned above, adding labile nitrile ligands to half-sandwich secondary phosphine complexes is interesting in some metal-catalyzed reactions. In

organometallic chemistry, nitrile ligands have two types of binding modes to metal centers (Figure 1.3). The more common way that nitrile ligands to coordinate to metals is through its lone pair on the nitrogen (*end-on*). The other coordination mode is to bind through the C-N triple bond (*side-on*).[30] The different coordination modes can be identified by their different ν_{CN} stretches. Relative to end-on nitrile bonding, the side-on mode, which is an analogue of an alkyne, has a smaller ν_{CN} stretching frequency because of π back donation. End-on nitrile bonding is usually less sterically crowding and more labile compared to a phosphine ligand. A recent study of the Rosenberg group shows facile dissociation of a benzonitrile (PhCN) ligand in half-sandwich Ru complexes.[31]

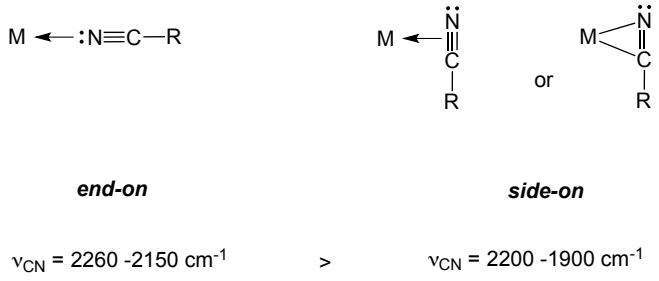

Figure 1.3 Two bonding modes of nitrile ligands to metal centers highlighting their different ν_{CN} stretching frequencies.

1.2 Metal complexes of phosphido ligands (PR_2^-)

Phosphido (PR_2^-) ligands, different from phosphine ligands, are anionic donors with only two substituents on the P center. Various literature are associated with a terminal ligand that is pyramidal at P and has a non-bonding lone pair.[32,33,34,35] Terminal phosphido ligands in metal complexes are somewhat unique due to a "transition metal gauche effect", which is supported by computational and structural studies.[33,36] In this effect, the lone pair on the terminal phosphido ligand occupy space around the P and is repelled by a filled d-orbital on the metal center. As a result, the conformation adopted by terminal phosphido ligands minimizes this steric interaction

as well as the electronic repulsion (Figure 1.4).[37] Structural studies (Table 1.4) found this effect results in elongated M-P bonds (P in terminal phosphido), which are significantly longer than normal M-P bonds (P in PR_3 or PR_2H). Computational studies also found maximizing the distance between metal and terminal phosphido ligands gives an energy minimal conformation around the M-P bond.

Table 1.4 Selected metal-phosphido (pyramidal) and metal-phosphine bond lengths.[12,14,15,17,31]

Complex	M-P Bond Distance (Å)
Ru(η^5-indenyl)(**P**Ph_2)(NCPh)(PPh_3)	2.3824(6)
Ru(η^5-indenyl)(**P**Cy_2)(CO)(PPh_3)	2.4390(7)
[**Ru**(η^5-indenyl)(NCPh)(**P**Ph_2H)(PPh_3)][$B(C_6F_5)_4$]	2.3148(5)
Ru(η^5-indenyl)Cl(**P**Ph_2H)(PPh_3)	2.2307(9)
Ru(η^5-indenyl)Cl(PCy_2H)(**P**Ph_3)	2.3099(9)
Ru(η^5-Cp*)Cl(**P**Ph_2H)(PPh_3)	2.283(3)
Ru(η^5-Cp)Cl(**P**Ph_2H)(PPh_3)	2.282(2)

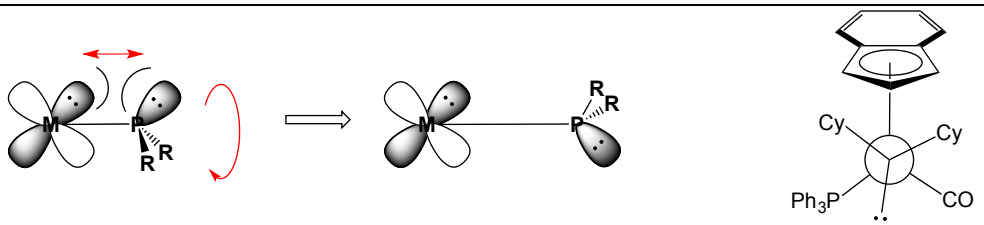

Figure 1.4 The orbitals giving rise to the transition metal gauche effect in coordinatively saturated terminal PR_2 complexes (left) and a Newman projection of the terminal phosphido ligand in Ru(η^5-indenyl)(PCy_2)(CO)(PPh_3) (right).

The lone pair on the terminal phosphido ligands is considered to have high p-character, which confers high *P*-nucleophilicity/basicity. These terminal phosphido ligands have an excellent ability to bridge two or more metal centers to form bridging phosphido complexes (Figure 1.5).[38,39] In addition, the lone pair on the terminal phosphido ligand can participate in π-donation to empty metal-based orbital (see Figure 1.5), which changes its geometry from pyramidal (sp^3) to planar (sp^2). Relative to pyramidal phosphido and normal phosphine ligands (PR_3 or PR_2H), planar phosphido ligand has significantly shorter M-P bonds that more behaves as sp^2

hybridization (Table 1.5). Such rehybridization allows π-stabilized coordinatively unsaturated complexes.[40] Most recently, Rosenberg published a review examining the structural features and reactivities of planar phosphido complexes.[41]

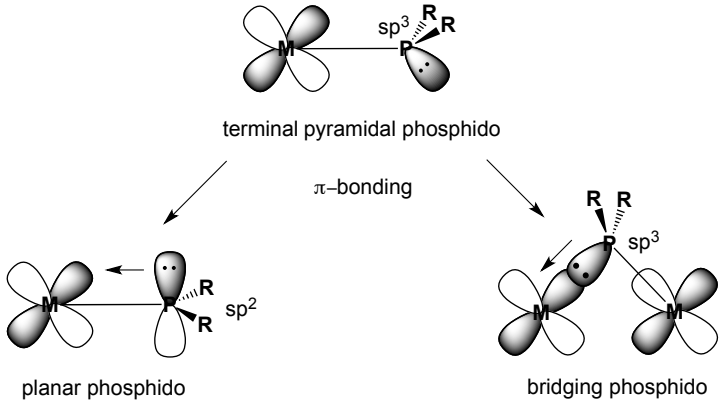

Figure 1.5 The orbitals show the change of bonding mode by π-stabilization in coordinatively unsaturated terminal phosphido complexes.

Table 1.5 Selected metal-phosphido bond lengths with different geometries at the P center.[15]

Complex	M-P Bond Distance (Å)	Geometry
Ru(η^5-indenyl)(**P**Cy_2)(PPh_3)	2.1589(14)	Planar
Ru(η^5-indenyl)(**P**Cy_2)(CO)(PPh_3)	2.4390(7)	Pyramidal

1.2.1 General methods to form phosphido complexes

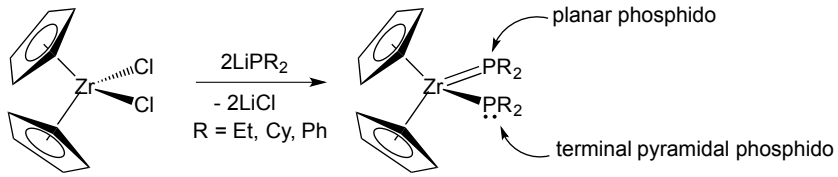

Figure 1.6 An example for generating phosphido ligands by a metal phosphido reagent.[42]

The most common route to phosphido complexes is *via* secondary phosphine precursors. For the other route, phosphido complex can be prepared (see example in Figure 1.6) *via* salt metathesis of metal halide complexes with phosphido reagents (e.g. $LiPR_2$). The early transition metals usually undergo this salt metathesis to give phosphido complexes.[42,43,44,45]

For the main route *via* secondary phosphine precursors, oxidative addition of the P-H bond in PR_2H reagents forms a new complex containing a metal-hydride (M-H) and a PR_2 ligand (Figure 1.7a). By this process, the oxidation state of metal is increased by two. This suggests that the complex precursor for oxidative addition of a P-H bond needs a low oxidation state metal and is coordinatively unsaturated. Oxidative addition of a P-H bond is a key step involved in Pt(0)-catalyzed hydrophosphination and has been thoroughly investigated by Glueck et al. (Figure 1.7b).[46,47] Beletskaya and coworkers also reported oxidative addition of P-H bond to give Ni^{2+} phosphido hydride complexes (Figure 1.7c).[48] Both reactions require ligand dissociation to generate a coordinatively unsaturated intermediate prior to oxidative addition and a metal having a relatively low oxidation state.

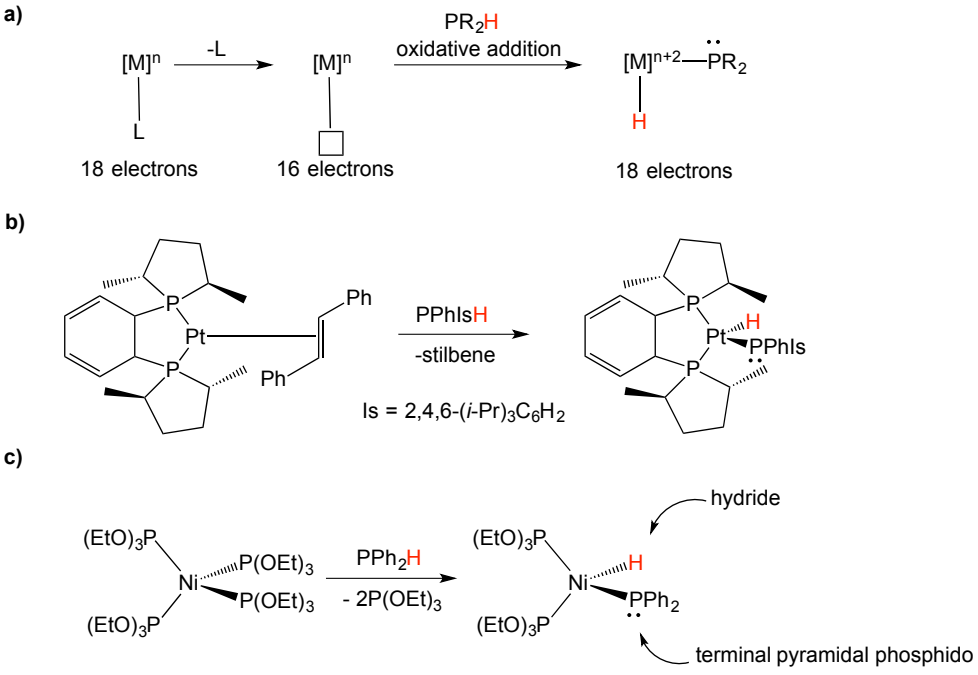

Figure 1.7 General mechanism (a) and examples (b) and (c) for oxidative addition of PR_2H reagents to generate phosphido ligand.

Base-induced P-H bond activation (deprotonation of a P-H bond) is also explored for giving a phosphido (PR_2^-) complex from a secondary phosphine precursor. Different from forming the phosphido complexes *via* oxidative addition of

P-H bond, this deprotonation allows formation of the terminal phosphido ligand in a coordinatively saturated precursor with no change in oxidation state of the metal. To form terminal phosphido complexes *via* deprotonation, the precursor secondary phosphine complex usually needs to be cationic. Since the resulting terminal phosphido is formally negative charged, the cationic precursor and anionic terminal phosphido will make a stable neutral compound (Figure 1.8a). Gladysz et al. reported deprotonating a Ru cationic secondary phosphine complex by $NaN(SiMe_3)_2$ and $KOBu^t$ (Figure 1.8b).[49] Leung and Pullarkat also reported NEt_3 can deprotonate the Pd coordinated PPh_2H to generate a reactive diphenylphosphido (PPh_2^-) ligand for hydrophosphination (Figure 1.8c).[50]

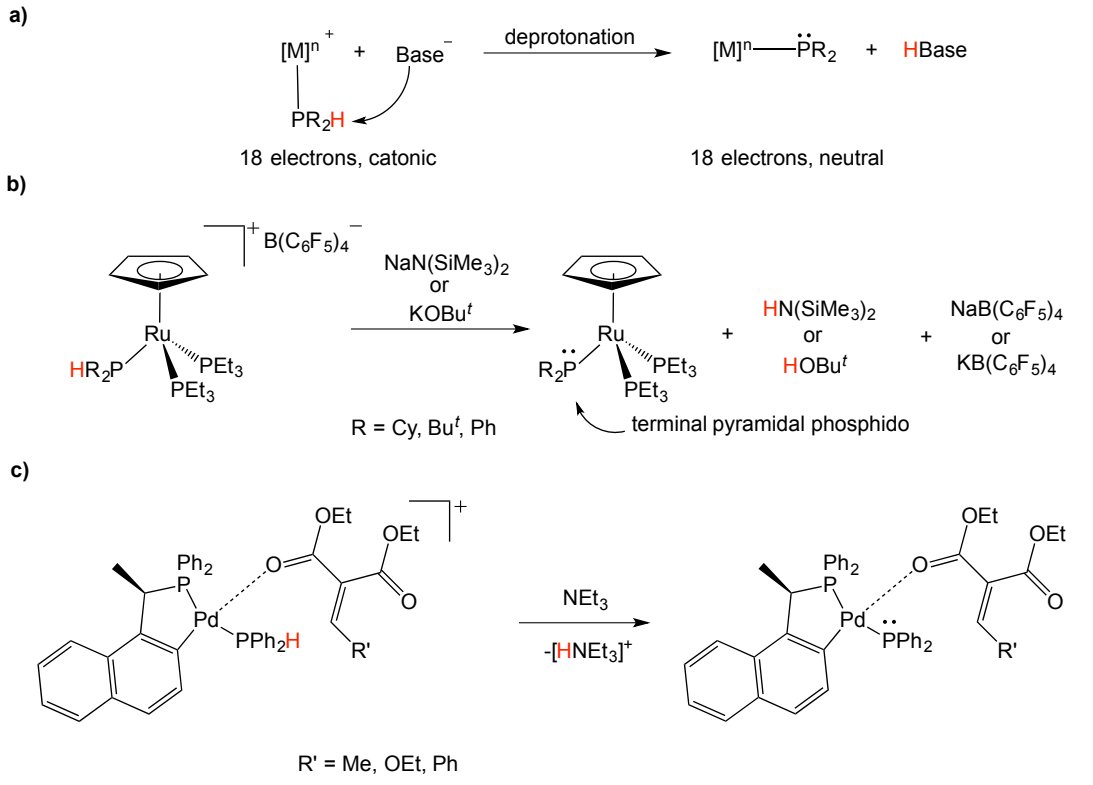

Figure 1.8 General mechanism (a) and examples (b) and (c) for deprotonating PR_2H in cationic complexes to generate terminal phosphido ligands.

The dehydrohalogenation with a neutral precursor containing X-type ligand (i.e. halide) gives a coordinatively unsaturated phosphido complex that will prompt π-bonding of the phosphido lone pair to the metal (Figure 1.9a). This achieves a

coordinatively unsaturated planar phosphido complex. The Rosenberg group prepared planar phosphido complexes *via* dehydrohalogenation of neutral Ru secondary phosphine chloride precursors (Figure 1.9b).[15]

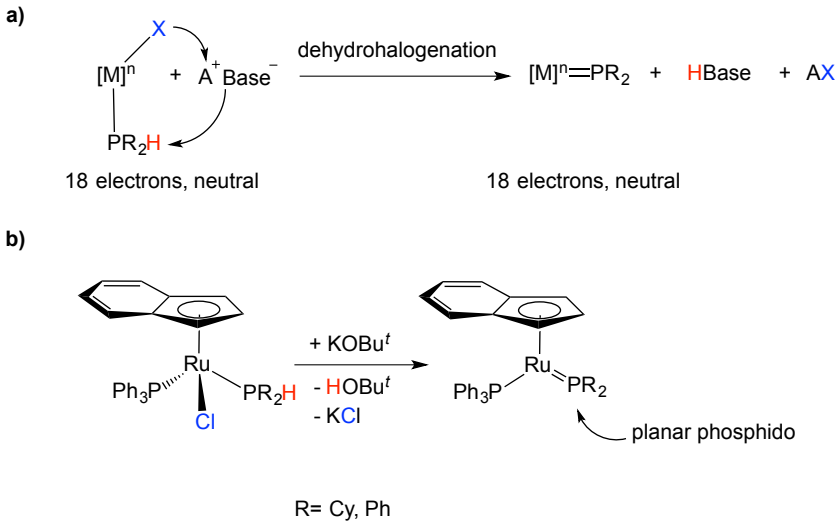

Figure 1.9 General mechanism (a) and an example (b) for dehydrohalogenation of neutral secondary phosphine complexes contain X-type ligands to form planar phosphido ligands.

1.2.2 Reactivity of phosphido complexes

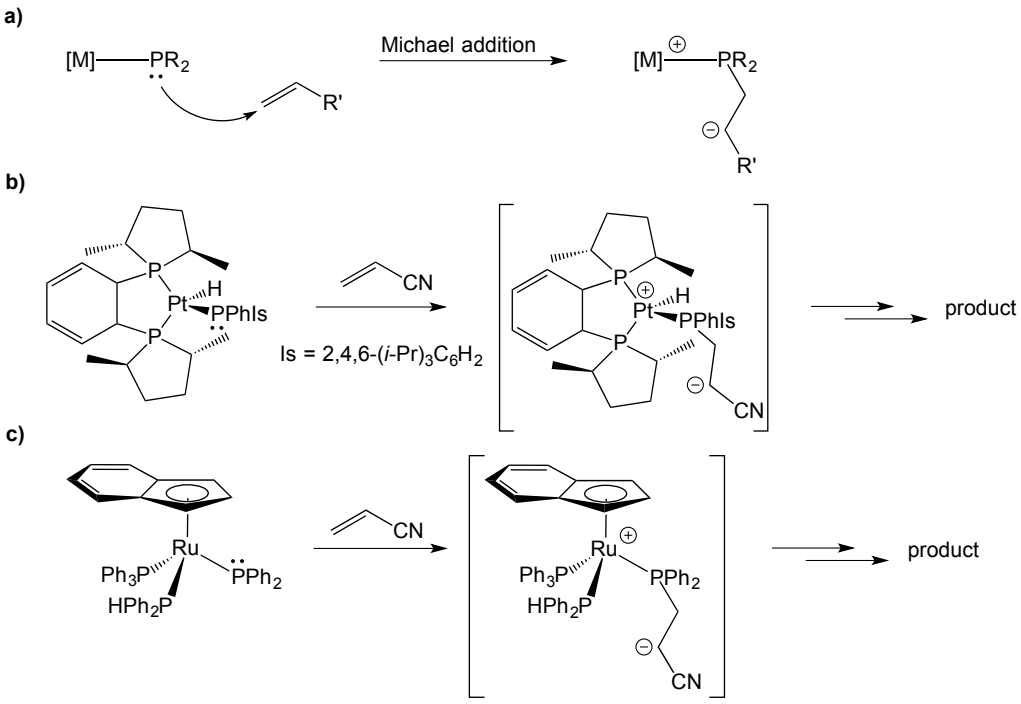

Figure 1.10 General mechanism (a) and examples (b) [47], (c) [17] for Michael addition of terminal PR_2 to activated alkenes.

As described above, phosphido complexes exhibit high *P*-nucleophilicity/basicity at the PR_2 ligand. Terminal phosphido complexes are proposed as key intermediates for P-C bond formation in various metal-catalyzed hydrophosphination[17,28,41,47,51,52,53,54] and phosphination reactions.[55,56] The terminal PR_2 can participate in nucleophilic attack or Michael-type addition at unsaturated molecules, such as activated alkenes (Figure 1.10). For bridging phosphido complex, it is inactive as a nucleophile or base because the lone pair is used to bind to another metal and this binding is usually stable.[57]

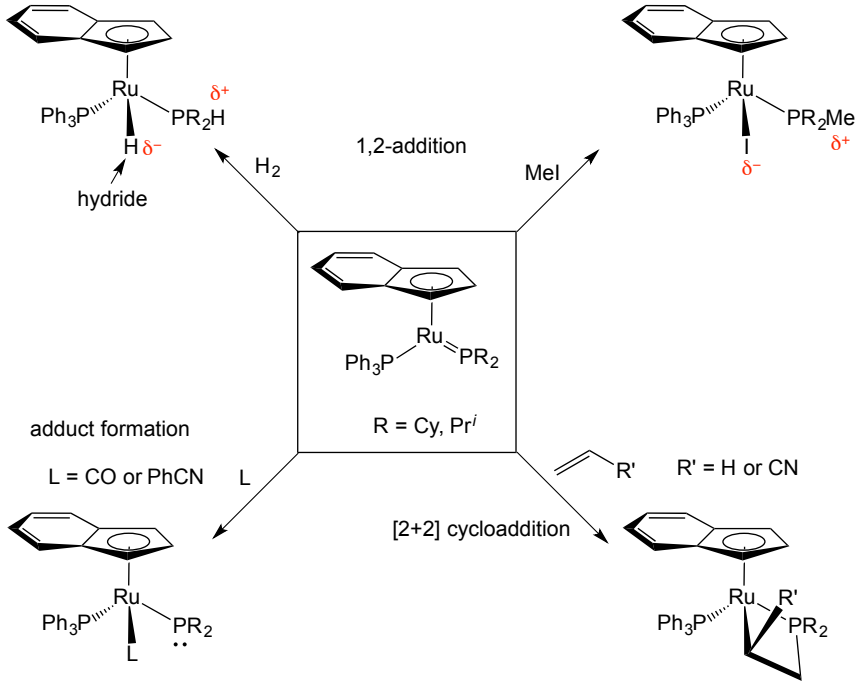

Figure 1.11 Reactivities of indenyl Ru planar phosphido complexes.

For planar phosphido complex, its reactivities are unique due to its high *P*-nucleophilicity and coordinative unsaturation (18 e^-, but 5-coordinate). This type of planar phosphido is unusual and their reactivity is little studied. The Rosenberg group studied a range of reactions of planar phosphido Ru complexes (Figure 1.11).[15,16,31,58] Some polar (e.g. MeI) and non-polar addenda (e.g. H_2) can undergo 1,2-addition across M-P double bond in these planar phosphido complexes. The planar PR_2 also

can transform to a terminal PR_2 with the addition of neutral donors (e.g. CO) at the metal in planar phosphido complexes. In addition, the planar phosphido complex can undergo [2+2] cycloaddition reactions with unsaturated molecules (both activated and simple alkenes and alkynes).

1.3 Project overview

1.3.1 Background

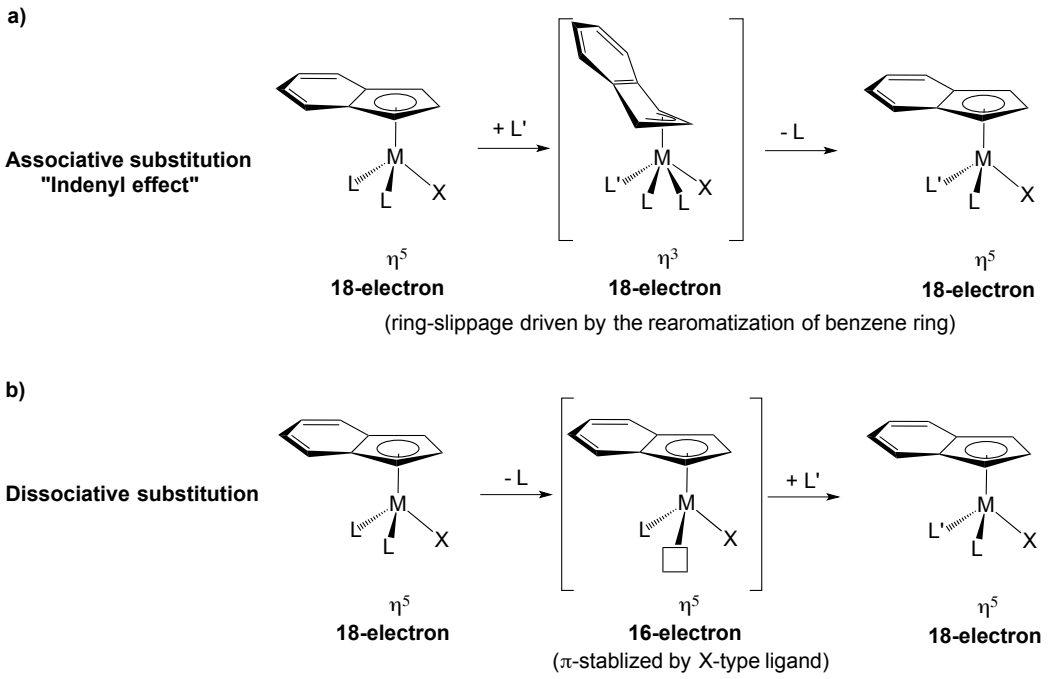

Figure 1.12 a) Indenyl effect: an associative mechanism for ligand substitution by a L-type ligand proceeding *via* an η^3-indenyl intermediate. **b)** A dissociative mechanism for ligand substitution by a L-type ligand proceeding *via* π-stabilization of X-type ligand in 16-electron intermediate.

Throughout our studies of the reactivity of the indenyl complexes Ru(η^5-indenyl)(PR_2)(PPh_3) shown in Figure 1.11, especially the apparent [2+2]-cycloaddition of alkenes and alkynes, the question has arisen whether the chemistry exhibited by this complex relies on the potential indenyl ring-slippage from an η^5 to an η^3 structure, to allow coordination of, for example, η^2-alkenes or alkynes, or η^2-H_2. It is well known that an increase in rates of substitution *via* associative mechanism is

observed for some indenyl complexes in substitution reactions relative to their Cp (or Cp*) analogues (Figure 1.12a).[6] This feature is termed as "indenyl effect", and is usually explained by variable hapticity.[59]

1.3.2 Some evidence for no "indenyl effect" in our system

Some indirect evidence suggests that there is no hapticity change in our indenyl system. Previous kinetic studies carried out by Gamasa et al. probing the mechanisms of phosphine substitution at the saturated Ru indenyl precursor Ru(η^5-indenyl)Cl(PPh_3)$_2$ provide evidence for dissociative pathways (Figure 1.12b), as opposed to the associative routes driven by facile ring-slippage.[60] Careful MS analysis done by our group with variable collision-induced energies of activation show relatively facile PR_3 dissociation and a remarkably stable Ru(η^5-indenyl) fragment.[61] All of these experimental results are in contrast to the literature most commonly cited in explanation of an "indenyl effect", which mostly includes Rh,[62,63] not Ru, indenyl complexes. We have explored computationally the trajectories of reaction of both H_2 and ethylene to our phosphido complexes, and have found no minima containing η^3-indenyl complexes: relatively stable η^2-adducts of both ethylene and H_2 instead exhibit a loss in the Ru-P double bond order. In these cases, the planar PR_2 fragment quite easily becomes pyramidal with a lone pair at P center, which generates the "vacant" coordination site at Ru.[31,64] The η^2-adduct of ethylene was observed at low temperature both visually and by VT-NMR spectroscopy.[64]

1.3.3 Goals and scope of this thesis

To gain further insight into the possible importance of variable hapticity in our indenyl half-sandwich Ru system, the chemistry of the analogous Cp* complexes is explored, which should not have the same proclivity to form η^3 structures as the

indenyl system. The ultimate goals of this project are: 1) synthesis of secondary phosphine complexes $Ru(\eta^5\text{-Cp*})Cl(PR_2H)(PPh_3)$ (R = alkyl or aryl) that are analogous to $Ru(\eta^5\text{-indenyl})Cl(PR_2H)(PPh_3)$, 2) formation of Cp* phosphido complexes $Ru(\eta^5\text{-Cp*})(PR_2)(PPh_3)$ *via* the dehydrohalogenation of these secondary phosphine complexes, 3) Investigation of reactivity of Cp* phosphido complexes with selected reagents (e.g. ethylene) to show whether or not the same reactivity as that observed for the indenyl is possible for the Cp* system.

Chapter 2 describes the synthesis of Cp* secondary phosphine complexes and cationic benzonitrile (PhCN) complexes $[Ru(\eta^5\text{-Cp*})(NCPh)(PPh_3)_2][B(C_6F_5)_4]$ from $Ru(\eta^5\text{-Cp*})Cl(PPh_3)_2$ and $[Ru(\eta^5\text{-Cp*})(NCPh)(PTol^p{}_2H)(PPh_3)][B(C_6F_5)_4]$ from synthesized $Ru(\eta^5\text{-Cp*})Cl(PTol^p{}_2H)(PPh_3)$. Chapter 3 describes the preparation of Cp* phosphido complexes $Ru(\eta^5\text{-Cp*})(PR_2)(PPh_3)$ containing a Ru-P double bond by dehydrohalogenation of secondary complexes synthesized in Chapter 2. The ease and rates of formation of orthometallated complex $Ru(\eta^5\text{-Cp*})\{\kappa^2\text{-}(o\text{-}C_6H_4)PPh_2\}(PR_2H)$ and also solution stability of base are assessed by using NMR monitoring in Chapter 3. In Chapter 4 and Chapter 5, the reactivity of these Cp* phosphido complexes with selected reagents (H_2, CO, PhCN, alkenes and alkynes) in NMR-scale reactions is presented. Throughout the whole thesis, my results are discussed in the context of comparison with prior results obtained for the indenyl analogues. In the final chapter of this thesis (Chapter 6), some future work is proposed.

As I will show, these studies of Cp* analogues indicate a higher phosphine lability for the Cp* systems (a sort of "inverse indenyl effect") that provides another indirect evidence for the absence of ring-slippage in the indenyl systems. The Cp* phosphido complexes resulting from this project are more sterically crowded than the

analogous indenyl complexes, but are also more nucleophilic/basic, which leads to some interesting chemistry for some reagents.

1.4 References

[1] Albers, M.; Robinson, D.; Singleton, E. *Coord. Chem. Rev.* **1987**, *79*, 1.

[2] Consiglio, G.; Morandini, F. *Chem. Rev.* **1987**, *87 (4)*, 761.

[3] Coville, N. J.; du Plooy, K. E.; Pickl, W. *Coord. Chem. Rev.* **1992**, *116*, 1.

[4] Cucullu, M. E.; Luo, L.; Nolan, S. P.; Fagan, P. J.; Jones, N. L.; Calabrese J. C. *Organometallics* **1995**, *14*, 289.

[5] Luo, L.; Nolan, S. P. *Organometallics* **1993**,*12*, 4305.

[6] Cadierno, V.; Diez, J.; Gamasa, M. P.; Gimeno, J.; Lastra, E. *Coord. Chem. Rev.* **1999**, *147*, 193.

[7] Trost, B. M. *Acc. Chem. Res.* **2002**, *35*, 695.

[8] Trost, B. M.; Toste, F. D.; Pinkerton, A. B. *Chem. Rev.* **2001**, *101*, 2067.

[9] Jazzar, R. F. R.; Kundig, E. P. *Ruthenium in Organic Synthesis*; Murahashi, S. -I., Ed.; WILEY-VCH: Weinheim, 2004.

[10] Wilczewski, T. *J. Organomet. Chem.* **1982**, *224*, C1-C4.

[11] Albers, M.; Robinson, D. J.; Shaver, A.; Singleton, E. *Organometallics* **1986**, *5*, 2199.

[12] Torres-Lubián, R.; Paz-Sandoval, M. A. *J. Organomet. Chem.* **1997**, *532*, 17.

[13] Torres-Lubián, R.; Rosales-Hoz, M. J.; Arif, A. M.; Ernst, R. D.; Paz-Sandoval, M. A. *J. Organomet. Chem.* **1999**, *585*, 68.

[14] Derrah, E. J.; Marlinga, J. C.; Mitra, D.; Friesen, D. M.; Hall, S. A.; McDonald, R.; Rosenberg, L. *Organometallics* **2005,** *24*, 5817.

[15] Derrah, E. J.; Pantazis, D. A.; McDonald, R.; Rosenberg, L.; *Organometallics* **2007,** *26,* 1473.

[16] Derrah, E. J.; Pantazis, D. A.; McDonald, R.; Rosenberg, L. *Angew. Chem. Int. Ed.* **2010**, *49*, 3367.

[17] Belli, R. G.; Burton, K. M. E.; Rufh, S. A.; McDonald, R.; Rosenberg, L. *Organometallics* **2015**, *34*, 5637.

[18] Esteban, M.; Pequerul, A.; Carmona, D.; Lahoz, F. J.; Martín, A.; Oro, L. A. *J. Organomet. Chem.* **1991**, *204*, 421.

[19] Paris, S. I. M.; Lemke, F. R.; Sommer, R.; Lönnecke, P.; Hey-Hawkins, E. *J. Organomet. Chem.* **2005**, *690*, 1807.

[20] Paris, S. I.; Petersen, J. L.; Hey-Hawkins, E.; Jensen, M. P. *Inorg. Chem.* **2006**, *45*, 5561.

[21] Guy Orpen, A.; Connelly, N. G. *Organometallics* **1990**, *9 (4)*, 1206.

[22] Hartwig, J. *Organotransition Metal Chemistry;* University Science Books: Sausalito, Calif., **2010**.

[23] Spessard, G. O.; Miessler, G. L. *Organometallic Chemistry*; Prentice-Hall Inc.: Toronto, **1997**.

[24] Orpen, A. G.; Connelly, N. G. *Organometallics* **1990**, *9*, 1206.

[25] Tolman, C. A. *Chem. Rev.* **1977**, *77*, 313.

[26] Brown, T. L.; Lee, K. J. *Coord. Chem. Rev.* **1993**, *128*, 89.

[27] Li, J.; Liu, L.; Fu, Y.; Guo, Q. *Tetrahedron* **2006**, *62*, 4453.

[28] Sues, P. E.; Lough, A. J.; Morris, R. H. *J. Am. Chem. Soc.* **2014**, *136*, 4746.

[29] Issleib, K.; Kummel, R. *J. Organomet. Chem.* **1965**, *3*, 84.

[30] Storhoff, B. N.; Lewis, H. C. *Coord. Chem. Rev.* **1977**, *23*, 1.

[31] Hoyle, M. M.; Pantazis, D. A.; Burton, H. M.; McDonald, R.; Rosenberg, L. *Organometallics* **2011**, *30*, 6458.

[32] Boni, G.; Blacque, O.; Sauvageot, P.; Poujaud, N.; Moise, C.; Kubicki, M. M. *Polyhedron* **2002**, *21*, 371.

[33] Buhro, W. E.; Zwick, B. D.; Georgiou, S.; Hutchinson, J. P.; Gladysz, J. A. *J. Am. Chem. Soc.***1988**, *110*, 2427

[34] Planas, J. G.; Hampel, F.; Gladysz, J. A. *Chem. Eur. J.* **2005**, *11*, 1402.

[35] Mastrorilli, P. *Eur. J. Inorg. Chem.* **2008**, 4835.

[36] Barre, C.; Boudot, P.; Kubicki, M. M.; Moise, C. *Inorg. Chem.* **1995**, *34*, 384.

[37] Chan, V. S.; Stewart, I. C.; Bergman, R. G.; Toste, F. D. *J. Am. Chem. Soc.* **2006**, *128*, 2786.

[38] Stephan, D. W. *Coord. Chem. Rev*. **1989**, *95*, 41.

[39] Wang, W. B.; Low, P. J.; Carty, A. J.; Sappa, E.; Gervasio, G.; Mealli, C.; Ienco, A.; Perez-Carreno, E. *Inorg. Chem.* **2000**, *39*, 998.

[40] Jimenez-Tenorio, M.; Puerta, M. C.; Valerga, P. *Eur. J. Inorg. Chem.* **2004**, 17.

[41] Rosenberg, L. *Coord. Chem. Rev.* **2012**, *256*, 606.

[42] Crimmin, M. R.; Barrett, A. G. M.; Hill, M. S.; Hitchcock, P. B.; Procopiou, P. A. *Organometallic* **2007**, *26*, 2953.

[43] Vanlinthoudt, J. P.; Vandenberghe, E. V.; Vanderkelen, G. P. *Spectroc. Acta A* **1980**, *36*, 315.

[44] Roddick, D. M.; Santarsiero, B. D.; Bercaw, J. E. *J. Am. Chem. Soc.* **1985**, *107*, 4670.

[45] Baker, R. T.; Calabrese, J. C.; Harlow, R. L.; Williams, I. D. *Organometallics* **1993**, *12*, 830.

[46] Kovacik, I.; Wicht, D. K.; Grewal, N. S.; Glueck, D. S.; Incarvito, C. D.; Guzei, I. A.; Rheingold, A. L. *Organometallics* **2000**, *19*, 950.

[47] Scriban, C.; Glueck, D. S.; DiPasquale, A. G.; Rheingold, A. L. *Organometallics* **2006**, *25*, 5435.

[48] Kazankova, M. A.; Shulyupin, M. O.; Borisenko, A. A.; Beletskaya,. I. P. *Russ. J. Org. Chem.* **2002**, 38, 1479.

[49] Planas, J. G.; Hampel, F.; Gladysz, J. A. *Chem. Eur. J.* **2005**, *11*, 1402.

[50] Xu, C.; Kennard, G. J. H. Hennersdorf, F.; Li, Y. X.; Pullarkat, S. A.; Leung, P. H. *Organometallic* **2012**, 31, 3022.

[51] Glueck, D. S.; Wicht, D. K. In *Catalytic Heterofunctionalization*; Togni, A., Grutzmacher, H., Eds.; Wiley-VCH: Toronto, **2001**.

[52] Scriban, C.; Kovacik, I.; Glueck, D. S. *Organometallics* **2005**, *24*, 4871.

[53] Wicht, D. K.; Kourkine, I. V.; Kovacik, I.; Glueck, D. S.; Concolino, T. E.; Yap, G. P. A.; Incarvito, C. D.; Rheingold, A. L. *Organometallics* **1999**, *18*, 5381.

[54] Pullarkat, S. A.; Leung, P. H. *Top. Organomet. Chem.* **2013**, *43*, 145

[55] Chan, V. S.; Stewart, I. C.; Bergman, R. G.; Toste, F. D. *J. Am. Chem. Soc.* **2006**, *128*, 2786.

[56] Chan, V. S.; Chiu, M.; Bergman, R. G.; Toste, F. D. *J. Am. Chem. Soc.* **2009**, *131*, 6021.

[57] Eichele, K.; Wasylishen, R. E.; Corrigan, J. F.; Taylor, N. J.; Carty, A. J.; Feindel, K. W.; Bernard, G. M. *J. Am. Chem. Soc.* **2002**, *124*, 1541.

[58] Derrah, E. J.; Giesbrecht, K. E.; McDonald, R.; Rosenberg, L. *Organometallics* **2008**, *27*, 5025.

[59] Jordan, R. B. *Reaction Mechanisms of Inorganic and Organometallic Systems,* 3rd edition*,* Oxford University Press, New York, 2007, p.156.

[60] Gamasa, M. P.; Gimeno, J.; Gonzalez-Bernardo, C.; Martin-Vaca, B. M. *Organometallics* **1996**, *15*, 302.

[61] Westmore, J. B.; Rosenberg, L.; Hooper, T. S. *Organometallics* **2002**, *21*, 5688.

[62] Rerek, M. E.; Basolo, F. *J. Am. Chem. Soc.* **1984**, *106*, 5908.

[63] Rerek, M. E.; Ji, L. N.; Basolo, F. *J. Chem. Soc. Chem. Commun.* **1983**, 1208.

[64] Burton, K. M. E. *Phosphorus-Containing Ruthenacycles: Exploring Their Potential in Processes Relevant to Hydrophosphination.* MSc. thesis, University of Victoria, **2010**.

Chapter 2 Ligand substitution reactions of $Ru(\eta^5\text{-}Cp^*)Cl(PPh_3)_2$ (1)

2.1 Introduction

In this chapter, the substitution reactions of secondary phosphines at $Ru(\eta^5\text{-}Cp^*)Cl(PPh_3)_2$ (**1**) to give monosubstituted secondary phosphine complexes $Ru(\eta^5\text{-}Cp^*)Cl(PR_2H)(PPh_3)$ (**2a-d**) and disubstituted $Ru(\eta^5\text{-}Cp^*)Cl(PR_2H)_2$ (**3a-d**) are described. Monosubstituted **2a-d** were successfully isolated. Two new cationic complexes $[Ru(\eta^5\text{-}Cp^*)(NCPh)(PPh_3)_2][B(C_6F_5)_4]$ (**4**) and $[Ru(\eta^5\text{-}Cp^*)(NCPh)(PTol^p{}_2H)(PPh_3)][B(C_6F_5)_4]$ (**5d**) were also synthesized through the addition of benzonitrile (PhCN) and $K[B(C_6F_5)_4]$ to the corresponding neutral chloride complexes **1** and **2d**.

2.1.1 Synthesis of Cp* ruthenium monosubstituted complexes

Ligand substitution is a common and important step in the synthesis of transition metal complexes. Ligand substitution is usually the first step of many stoichiometric and catalytic reactions of organometallic compounds.[1] For example, the replacement of a coordinated ligand or solvent by an incoming secondary phosphine (PR_2H) is important in metal-catalyzed hydrophosphination. Some half-sandwich ruthenium (Ru) secondary phosphine complexes have been reported in the literature *via* ligand substitution.[2,3,4,5,6] Most notably, Paz-Sandoval has reported the synthesis of Cp and Cp* ruthenium diphenylphosphine complexes from different starting materials.[6] The addition of 1.2-2 equivalents of PPh_2H to these starting materials afforded the monosubstituted $Ru(\eta^5\text{-}Cp)Cl(PPh_2H)(PPh_3)$ and $Ru(\eta^5\text{-}Cp^*)Cl(PPh_2H)(PPh_3)$ (**2c**). By increasing the number of equivalents of PPh_2H and refluxing, the substitution reactions eventually gave disubstituted complexes $Ru(\eta^5\text{-}Cp)Cl(PPh_2H)_2$ and $Ru(\eta^5\text{-}Cp^*)Cl(PPh_2H)_2$ (**3c**). (Scheme 2.1)

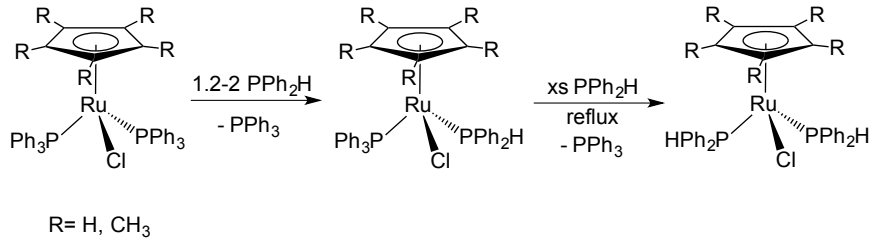

Scheme 2.1 Ligand substitutions to give monosubstituted and disubstituted secondary phosphine complexes with η^5-Cp/Cp* ligand.

In addition, previous graduate student Eric Derrah synthesized indenyl Ru complexes of different PR_2H.[7,8] Two equivalents of PR_2H (R = Cy, Et, Ph, Tol^p or Pr^i) were needed to replace one PPh_3 in Ru(η^5-indenyl)Cl(PPh_3)$_2$ (**1**$^{\boldsymbol{i}}$) in CH_2Cl_2 (the extra equivalent is needed to drive the equilibrium to product). These reactions need 3h refluxing and result in the formation of the monosubstituted complexes Ru(η^5-indenyl)Cl(PR_2H)(PPh_3) (**2**$^{\boldsymbol{i}}$**a-e**).[8]

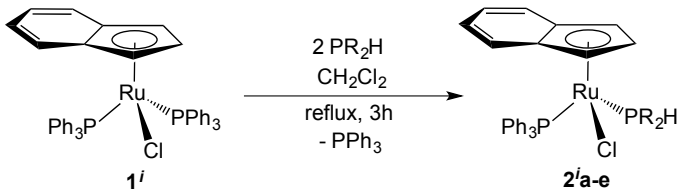

Scheme 2.2 Ligand substitutions to give monosubstituted secondary phosphine complexes with η^5-indenyl ligand.

I tried similar ligand substitution of Ru(η^5-Cp*)Cl(PPh_3)$_2$ (**1**) to make the Cp* analogues Ru(η^5-Cp*)Cl(PR_2H)(PPh_3) (**2a-d**). Different reaction conditions were tried to give an optimum synthetic method.

2.2.Triphenylphosphine ligand substitution reaction with secondary phosphine at Ru(η^5-Cp*)Cl(PPh_3)$_2$ (1)

This section describes how Ru(η^5-Cp*)Cl(PPh_3)$_2$ (**1**) was synthesized using literature methods and used as the starting material for ligand substitution reaction. Ligand substitution reactions of **1** were performed by using PR_2H containing both

alkyl (R = Cy (**a**), Et (**b**)) and aryl (R = Ph (**c**), Tol^p (**d**)) substituents. This allowed direct analysis of how the substitution chemistry at **1** is affected by different size and electronic character of the phosphine ligand. In addition, successful isolation of Ru(η^5-Cp*)Cl(PR_2H)(PPh_3) (**2a-d**) allowed us to assess how changes at the metal center due to the Cp* (relative to indenyl) affect the reactivity of half-sandwich complexes (Chapter 3).

2.2.1 Synthesis of Ru(η^5-Cp*)Cl(PPh_3)$_2$ (1)

Since the bis(triphenylphosphine) complex **1** can be used as a catalyst for other reactions, such as olefination of carbonyl compounds,[9] several methods for its synthesis have been reported.[10,11,12] Two of these methods were tried by Sophie Langis-Barsetti (a previous undergraduate student in the Rosenberg group) and me. Both of them gave the desired product, although Method A (Sophie's work, see Scheme 2.3) gave much lower yields than those reported in the literature.[10] However, Sophie did not try to further optimize the conditions for Method A. The Method B (my work, see Scheme 2.3) reported by Fokin was slightly modified to afford slightly higher yields than those reported in the literature (83%).[11]

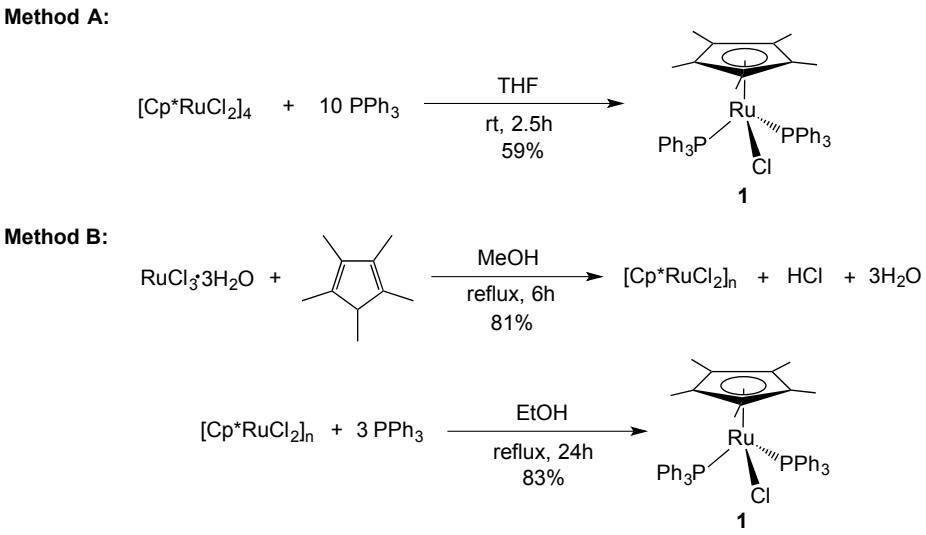

Scheme 2.3 Two methods to synthesize Ru(η^5-Cp*)Cl(PPh_3)$_2$ (**1**).

2.2.2 Synthesis of Ru(η^5-Cp*)Cl(PR_2H)(PPh_3) (2a-d)

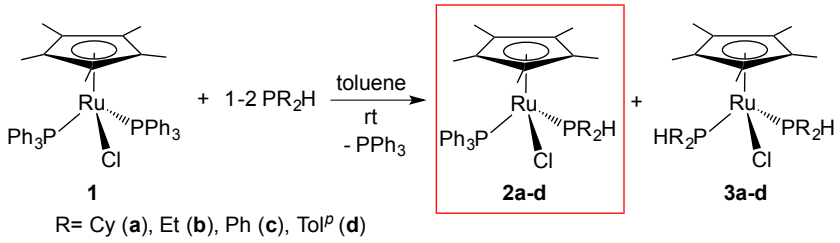

Scheme 2.4 Synthesis of Ru(η^5-Cp*)Cl(PR_2H)(PPh_3) (**2a-d**).

Complex **1** was used in substitution reaction with different PR_2H to give monosubstituted **2a-d** at room temperature (see Scheme 2.4). The cone angle of PPh_3 is 145°, while those of PR_2H ligands have various cone angles respectively (117°-142°), so these substitution reactions are favoured by a decrease in steric bulk of the phosphine (Table 1.1 in Chapter 1).[13] Due to high reactivity of complex **1**, it takes less time than for the indenyl analogue to form the product. Both of indenyl and Cp* complexes are consistent with a dissociative substitution mechanism.[14] Faster substitution of Cp* complexes relative to indenyl ones is attributed to an increase of electron density at the Ru center and steric influence of the methyl groups in Cp*Ru complex which facilitates the rate-determining loss of PPh_3.[15,16] For each of these phosphine substitution reactions, the $^{31}P\{^1H\}$ NMR spectrum always shows the formation of a significant amount of extra product, even when careful 1:1 stoichiometry is employed. This product is not isolated due to its high solubility, but the peak multiplicities (^1H, $^{31}P\{^1H\}$ and ^{31}P NMR) suggest that it is the disubstituted product **3a-d**, Ru(η^5-Cp*)Cl(HPR_2)$_2$ (see Scheme 2.4). As mentioned in Section 2.1.1, Paz-Sandoval reported the ease of formation of disubstituted product during the synthesis of the complex **2c** from **1**.[6] Different from Cp* complex **1**, this type of oversubstitution of PR_2H in the indenyl analogue was only observed when the secondary phosphine is PEt_2H (small phosphine).[7]

Cp* complexes are often highly soluble in most common solvents,[17] which makes the separation of monosubstituted **2** and disubstituted **3** difficult. Monosubstituted **2a-d** can be isolated and purified by recrystallization from toluene layered with pentane (1:5) to remove disubstituted complexes **3**. Because there are minor differences between each of these syntheses of complexes **2**, each of the synthesis will be mentioned below.

For complex **2a**, complex **1** is completely consumed after 2h. The red crystal of complex **2a** is isolated and washed by pentane. However, I prepared more than one batch of this crystalline product, and the $^{31}P\{^{1}H\}$ NMR spectrum of this crystal **2a** (R = Cy) always showed the formation of the same amount (~ 1.3%) of disubstituted complex **3a** and complex **1** relative to **2a**. The upfield doublet is identified as the signal due to the PCy_2H by a large $^{1}J_{PH}$ coupling in the ^{31}P NMR spectrum (see Figure 2.1). It seems that complex **2a** exists in equilibrium with **3a** and **1**. Small amount of complex **2a** will redistribute to complex **1** and complex **3a** when it dissolves in solvent. The solid dissolved to make the NMR sample is analytically pure (see Experimental in Section 2.6.3.1), which is further support for equilibrium redistribution rather than simple contamination. This redistribution was not observed for analogous indenyl complex Ru(η^5-indenyl)Cl(PCy_2H)(PPh_3) (**2^{i}a**). This difference again shows that the phosphine ligand is more labile in Cp* complex relative to indenyl analogue. In addition, the comparable size of the $HPCy_2$ and PPh_3 has an impact on the overall equilibrium at this crowded Ru center.

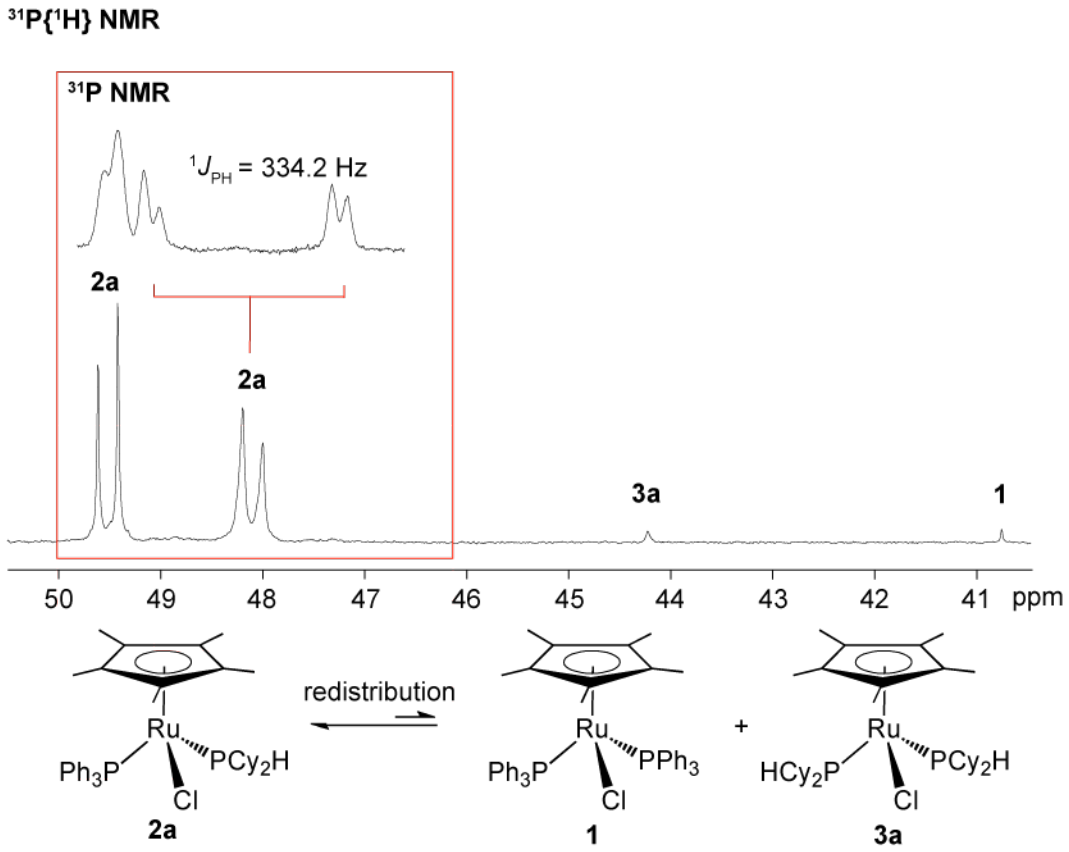

Figure 2.1 $^{31}P\{^{1}H\}$ NMR and ^{31}P NMR (inset) spectra (202.51 MHz, C_6D_6) of red crystal Ru(η^5-Cp*)Cl(PCy_2H)(PPh_3) (**2a**) showing the redistribution of pure crystal in solvent.

Attempts to make complex **2b** (R = Et) also inevitably give a mixture of the desired product and significant amounts of complex **3b** (up to 50%) (Scheme 2.4). Complex **1** can't be consumed completely with carefully controlled addition of only 1 equivalent of PEt_2H to it. A second equivalent of PEt_2H need to be added to force 100% conversion of complex **1**. The cone angle of PEt_2H is 117°, which is smaller than PPh_3 (145°) and the other PR_2H (R = Cy (142°); Ph (126°); Tol^p (126°)).[13] Relative to the ligand substitution reactions with these large PR_2H (R= Cy, Ph and Tol^p), the formation of the disubstituted complex **3b** is easy because coordination of PEt_2H to the Ru centre relieves steric crowding at **1** significantly. This results in the low yield of **2b** (see Experimental in Section 2.6.3.2). Work by previous group members showed the indenyl analogue can form the [Ru(η^5-indenyl)(PEt_2H)$_2$(PPh_3)]Cl.[7]

However, the formation of this analogous cationic disubstituted secondary phosphine complex during the synthesis of **2b** was not observed. Substitution of the chloride in the Cp* complex by incoming phosphine seems to be difficult. The lack of chloride substitution might be sterically driven. Cp* ligand makes Ru center more bulky than indenyl analogous and the chloride ligand is smaller than the PEt_2H ligand. However, facile displacement of either chloride or phosphine ligand may depend on the solvent and reaction conditions.[18]

Complex **1** can be used in a phosphine substitution reaction with PPh_2H to give monosubstituted **2c** mixed with a small amount of disubstituted **3c**. The cone angle of PPh_2H is 126°, which is less bulky ligand than PPh_3. Due to the similar solubility of **2c** and **3c**, as previously reported by Paz-Sandoval, isolation of pure monosubstituted complex **2c** is more challenging than other complexes **2**.[6] Although the mixed product is recrystallized twice from toluene-pentane at low temperature, complex **2c** is still contaminated with approximately 5% **3c** according to the ^1H NMR spectrum. This 5% of **3c** doesn't result from the redistribution of **2c** because signals due to **1** were not observed in the ^1H and $^{31}P\{^1H\}$ NMR spectra of isolated crystalline product.

Ligand substitution at **1** with $PTol^p_2H$ gives a monosubstituted **2d**. Different from **2c**, the solubility of **2d** is different from that of **3d**. This allowed the isolation of pure monosubstituted complex **2d** by recrystallization.

2.2.3 Detailed characterization of $Ru(\eta^5\text{-}Cp^*)Cl(PR_2H)(PPh_3)$ (2a-d)

All complexes **2a-d** were characterized by using 1D NMR (^1H, $^{31}P\{^1H\}$, ^{31}P, $^{13}C\{^1H\}$ and ^{13}C DEPT 135) and 2D NMR ($^1H/^{31}P\{^1H\}$-HSQC, $^1H/^{31}P\{^1H\}$-HMBC, $^1H/^{13}C\{^1H\}$-HSQC, $^1H/^{13}C\{^1H\}$-HMBC and ^1H-COSY), as described below. The disubstituted complexes **3a-d** can't be obtained sufficiently pure for complete characterization.

The $^{31}P\{^{1}H\}$ NMR spectra for these complexes **2a-d** show two doublets of identical $^{2}J_{PP}$ values (40 - 43 Hz) similar to indenyl analogues **2^{i}a-d** (42 - 49 Hz). Different from indenyl analogues, the most upfield peaks (δ: 34 - 48 ppm) for Cp* complex **2a-d** are assigned to coordinated PR_2H due to its large $^{1}J_{PH}$ coupling (334 - 365 Hz) in the ^{31}P NMR spectra. The relatively downfield peaks (δ: 45 - 51 ppm) are assigned to the coordinated PPh_3. In ^{1}H NMR spectra (Figure 2.2), the ^{1}H signals due to CH_3 in Cp* behave as a triplet (e.g., **2b** δ: 1.44 ppm, $^{4}J_{HP}$ = 1.5 Hz) because of their coupling to phosphorus (P) in both PR_2H and PPh_3. However, this coupling constant is usually very small, which is difficult to be observed even on the 500 MHz instrument. The ^{1}H signals of **2a, c, d** due to the PPh_3 ligand appear as broad peaks, even when the spectra are obtained on the 500 MHz instrument. This broadening isn't observed for **2b** that contains the much smaller PEt_2H. We have observed similarly broad PPh_3 signals for the indenyl analogues **2^{i}**, and have shown *via* VT-NMR studies that the broadening is a consequence of slow rotation on the NMR timescale around the Ru-PPh_3 bond in these relatively sterically congested complexes.[7] The protons on the phenyl rings have a wide range of chemical shift environment, in particular for H_o on these phenyl rings. The presence of a doublet with large $^{1}J_{PH}$ values (similar to the $^{1}J_{PH}$ values observed in the ^{31}P NMR spectra) in the ^{1}H NMR spectra of **2a-d** again confirms the coordination of PR_2H without P-H bond activation. In addition, the ^{1}H and $^{13}C\{^{1}H\}$ NMR spectra for **2a-d** show distinct signals for each of PR_2H substituents (R) because chirality of Ru center in **2a-d** makes each substituent diastereotopic.

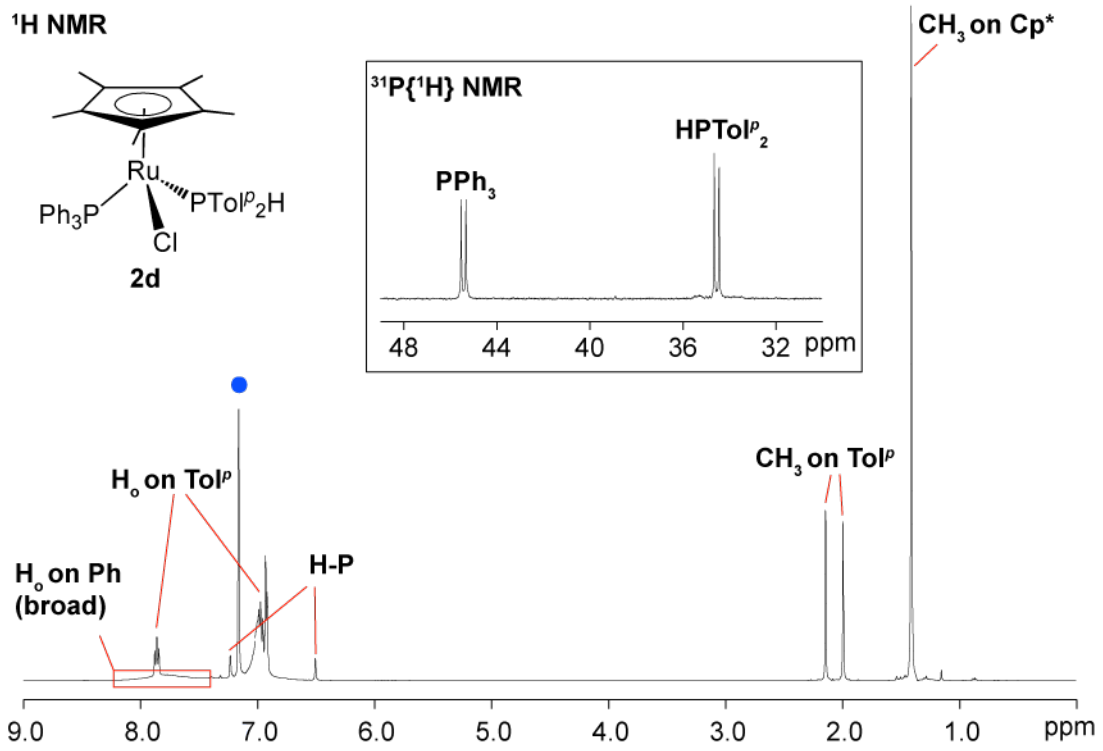

Figure 2.2 $^{31}P\{^{1}H\}$ NMR (202.51 MHz, C_6D_6, inset) and ^{1}H NMR (500.27 MHz, C_6D_6) spectra of Ru(η^5-Cp*)Cl(PTol$^p_2$H)(PPh_3) (**2d**). Solvent residual signal is labeled as blue dot. These spectra are typical of those observed for **2a-d**.

Single crystals of **2a,b** were obtained and X-ray diffraction analysis was performed. The resulting molecular structures are shown in Figures 2.3 and 2.4. Both of the structures show that the geometry of the complex is *pseudo*-octahedral. Selected bond distances and angles of **2a,b** are listed in Table 2.1. All the bond angles (83.5-92.5°) and bond lengths (2.29-2.44 Å) of these three-legged piano-stool Cp* complexes, which are not associated with the Cp* ligand, are within the normal range observed for η^5-Cp-derived Ru phosphine complexes.[19]

The structures of Cp* complex **2a** and **2b** were investigated carefully for the influence of different phosphine size on the Cp* Ru complex. The methyl groups on the Cp ring may affect steric crowding at the Ru center. Relative to **2a**, the stronger Cp*-Ru bonding interaction (shorter Cp*-Ru bond length) in **2b** leads to all of the inter-ligand (*trans* to the Cp* ligand) angles being further slightly compressed (~1°). There is no significant difference in Ru-Cl bond lengths between **2a** and **2b**. The

distance between the centroid of Cp* ring and Ru (Ru-C_{cent}) in **2b** is slightly shorter than in **2a**. The Ru-PPh_3 bond length in **2a**, 2.3146(5) Å, is slightly longer than the corresponding bond length in **2b**, 2.3071(8) Å. The Ru-PCy_2H bond length in **2a**, 2.3334(5) Å, is significantly longer than the corresponding bond length in **2b**, 2.2915(8) Å. These difference can be explained by the steric bulk of different substituents (R) on the PR_2H. Overall, it shows that P-substituents in the phosphine ligand and methyl groups in Cp* ligand are "fighting" for space in these complexes. The smaller phosphine bonds to the metal center stronger than the large phosphine does.

Table 2.1 Selected Interatomic Distances (Å) and Bond Angles (°) in the Structures of Ru(η^5-Cp*)Cl(PCy_2H)(PPh_3) (**2a**) and Ru(η^5-Cp*)Cl(PEt_2H)(PPh_3) (**2b**)[a]

	2a	**2b**
	Interatomic Distances	
Ru-P1	2.3334(5)	2.2915(8)
Ru-P2	2.3146(5)	2.3071(8)
Ru-Cl	2.4445(5)	2.4437(9)
Ru-C_{cent}	1.872	1.859
P1-H1P	1.29(2)	1.32(4)
	Bond Angles	
C_{cent}-Ru-P1	129.8	127.5
C_{cent}-Ru-P2	127.4	129.7
C_{cent}-Ru-Cl	120.6	121.6
P1-Ru-P2	92.51(2)	91.90(3)
P1-Ru-Cl	84.75(2)	83.54(3)
P2-Ru-Cl	88.29(2)	88.78(3)

[a] C_{cent} denotes the centroid of the least-squares plane defined by C1–C2–C3–C4–C5.

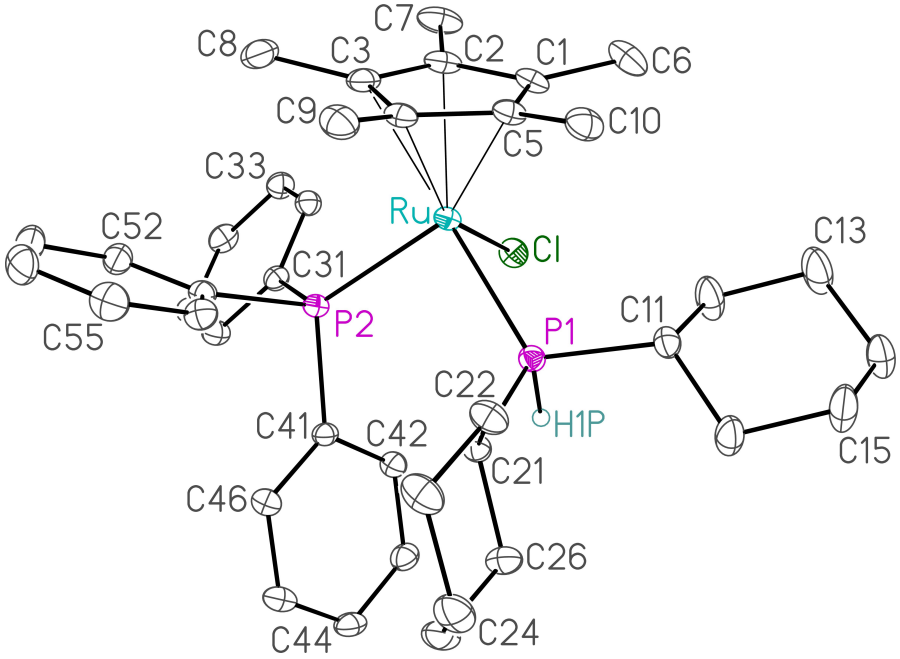

Figure 2.3 Perspective view of the Ru(η^5-Cp*)Cl(PCy_2H)(PPh_3) (**2a**) showing the atom-labeling scheme. Non-hydrogen atoms are represented by Gaussian ellipsoids at the 30% probability level. The hydrogen atom attached to P1 is shown with arbitrarily small thermal parameters; cyclohexyl- and phenyl-group hydrogens are not shown.

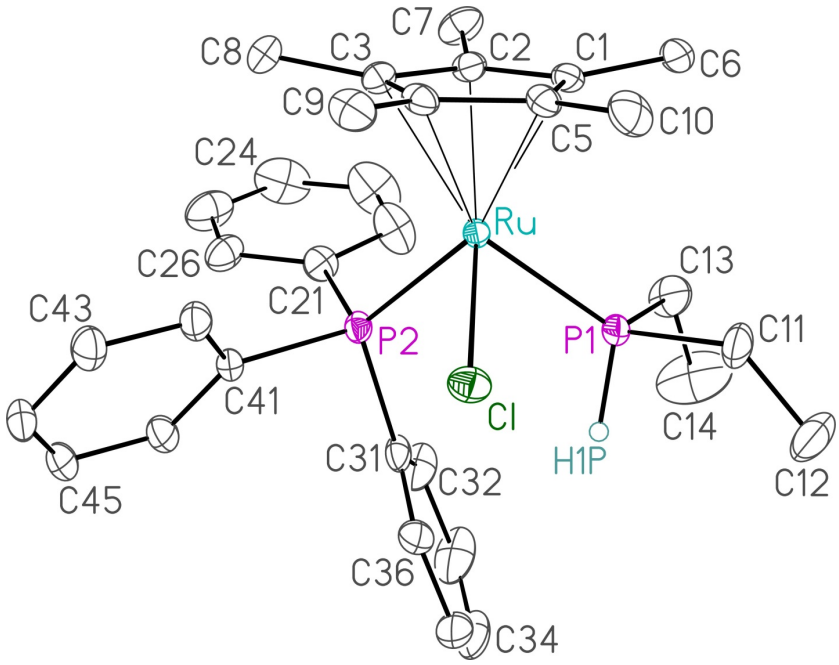

Figure 2.4 Perspective view of the Ru(η^5-Cp*)Cl(PEt_2H)(PPh_3) (**2b)** molecule showing the atom labeling scheme. Non-hydrogen atoms are represented by Gaussian ellipsoids at the 30% probability level. The hydrogen atom attached to P1 is shown with an arbitrarily small thermal parameter; all other hydrogens are not shown.

2.3 Comparison of Ru(η^5-Cp*)Cl(PCy_2H)(PPh_3) (2a) and its analogue Ru(η^5-indenyl)Cl(PCy_2H)(PPh_3) (2^{i}a)

In the previous section, experimental observation showed some difference of solution behaviour between the Cp* complexes and their indenyl analogues. In this section, the solid state structures of Cp* complex **2a** and indenyl analogue **2^{i}a,** as studied *via* X-ray crystallography and IR spectroscopy, are compared, to further understand the difference between the Cp* and indenyl system.

The crystal structures of Cp* complex **2a** and its indenyl analogue **2^{i}a** show some differences (Table 2.2). For the Ru-Cl bond lengths, there is no significant difference between **2a** and **2^{i}a**. However, the calculated distance between Ru and centroid of η^5-ligand (Ru-C_{cent}) in **2a** (1.872 Å) is slightly shorter than that in **2^{i}a** (1.883 Å), which indicates the Cp* ligand is closer to the Ru than indenyl ligand. This apparent stronger bond interaction causes greater steric crowding in **2a** relative to **2^{i}a** (methyl groups effect) and may also indicate greater electron density at Ru in the Cp* complex. The Ru-PPh_3 bond length in **2a**, 2.3146(5) Å, is slightly longer than the corresponding bond length in **2^{i}a**, 2.3099(9) Å. The Ru-PCy_2H bond length in **2a**, 2.3334(5) Å, is significantly longer than the corresponding bond length in **2^{i}a**, 2.2642(10) Å. Both of these longer bond lengths (Ru-P1 and Ru-P2) indicate the weaker Ru-P bonds in the Cp* complex relative to indenyl analogue. In addition, all of the inter-ligand angles of **2a**, P1-Ru-P2, P1-Ru-Cl, and P2-Ru-Cl, are approximately 2° smaller than corresponding bond angles of **2^{i}a**. In summary, the longer Ru-PCy_2H and Ru-PPh_3 distance and more compressed inter-ligand angles found in **2a** relative to **2^{i}a** shows higher steric congestion in the Cp* complex in comparison to the indenyl analogue.

The ν_{PH} stretch in the IR spectrum is an indirect indicator of the electron density at the metal center (see Figure 2.5). In the IR spectrum, the energy of the bond stretch is directly proportional to bond strength.[20] The comparison between Cp* complexes and their indenyl analogues shows that the indenyl analogues have slightly lower ν_{PH} frequencies (e.g., **2^{i}a**: 2319 cm^{-1}) than that for Cp* complexes (e.g, **2a**: 2329 cm^{-1}), which indicates that the indenyl analogues have relatively weaker P-H bonds. This observation can be explained by difference in electron density at the Ru center and steric crowding arising from the methyl groups in Cp* complex (as described in Section 2.2.2).

Table 2.2 Selected Interatomic Distances (Å) and Bond Angles (°) in the Structures of Ru(η^5-Cp*)Cl(PCy_2H)(PPh_3) (**2a**) and Ru(η^5-indenyl)Cl(PCy_2H)(PPh_3) (**2^{i}a**)[a]

	2a	**2^{i}a**
	Interatomic Distances	
Ru-P1	2.3334(5)	2.2642(10)
Ru-P2	2.3146(5)	2.3099(9)
Ru-Cl	2.4445(5)	2.4446(9)
Ru-C_{cent}	1.872	1.883
P1-H1P	1.29(2)	1.23(4)
	Bond Angles	
C_{cent}-Ru-P1	129.8	126.2
C_{cent}-Ru-P2	127.4	123.5
C_{cent}-Ru-Cl	120.6	124.0
P1-Ru-P2	92.51(2)	94.75(3)
P1-Ru-Cl	84.75(2)	86.25(3)
P2-Ru-Cl	88.29(2)	91.71(3)

[a] C_{cent} denotes the centroid of the least-squares plane defined by C1–C2–C3–C4–C5 [P1 = PCy_2H and P2 = PPh_3].

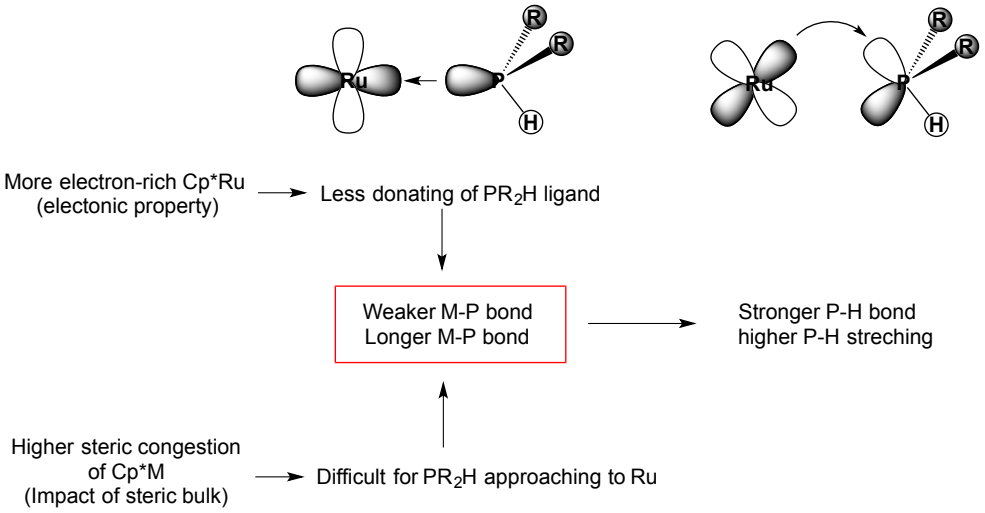

Figure 2.5 Bonding interactions between a metal and a PR_2H ligand affect the P-H bond stretching in Cp* complex.

2.4 Synthesis and characterization of cationic benzonitrile complexes 4 and 5d

In this section, I describe the synthesis of the cationic complexes $[Ru(\eta^5\text{-}Cp^*)(NCPh)(PPh_3)_2][B(C_6F_5)_4]$ (**4**) and $[Ru(\eta^5\text{-}Cp^*)(NCPh)(PTol^p{}_2H)(PPh_3)][B(C_6F_5)_4]$ (**5d**), for future use (see Chapter 6) as precursor for metal-catalyzed hydrophosphination. As mention in Chapter 1, the benefit of making these complexes was that they have a labile nitrile ligand (good for catalysis) instead of a chloride ligand. In addition, the P-H activation of cationic secondary phosphine complexes is easier relative to its corresponding neutral chloride complexes, since the P-H bond in a phosphine bound to a cationic centre will be more acidic, which will make it easier to remove by deprotonation.[21]

2.4.1 Synthesis of cationic complexes $[Ru(\eta^5\text{-}Cp^*)(NCPh)(PPh_3)_2][B(C_6F_5)_4]$ (4) and $[Ru(\eta^5\text{-}Cp^*)(NCPh)(PTol^p{}_2H)(PPh_3)][B(C_6F_5)_4]$ (5d)

The addition of excess benzonitrile and 1.2 equivalent $KB(C_6F_5)_4$ to a suspension of complex **1** or **2d** in MeOH gives the cationic benzonitrile complex **4**/**5d**. The $^{31}P\{^1H\}$ NMR spectrum of complex **4** always shows the contamination by a small amount of extra product $[Ru(\eta^5\text{-}Cp^*)(NCPh)_2(PPh_3)][B(C_6F_5)_4]$ (Scheme 2.5). For

complex **5d**, this byproduct does not form. These products **4** (+ bis(nitrile impurity) and **5d** were characterized by using 1D and 2D NMR spectroscopy as described below, similar to complexes **2a-d** (*vide supra*).

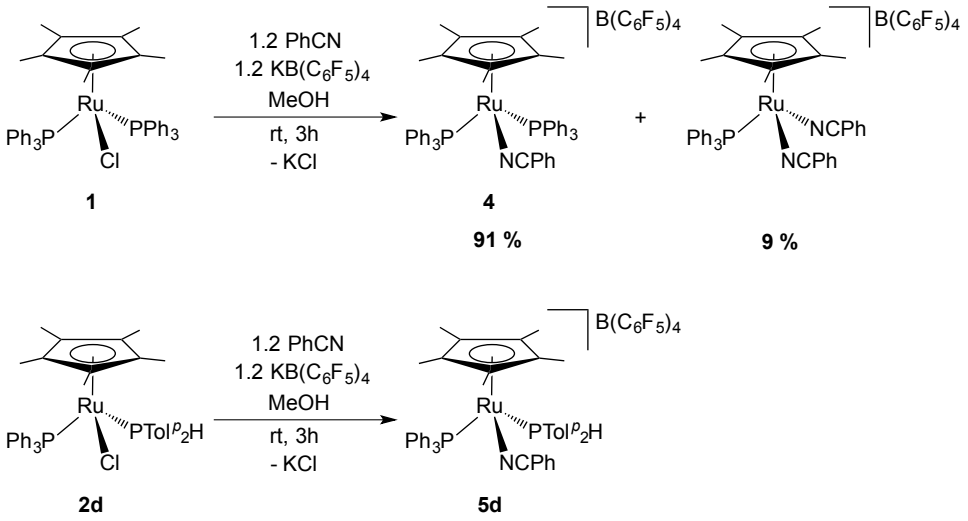

Scheme 2.5 Synthesis of $[Ru(\eta^5\text{-}Cp^*)(NCPh)(PPh_3)_2][B(C_6F_5)_4]$ (**4**) and $[Ru(\eta^5\text{-}Cp^*)(NCPh)(PTol^p{}_2H)(PPh_3)][B(C_6F_5)_4]$ (**5d**)

2.4.2 Detailed characterization of $[Ru(\eta^5\text{-}Cp^*)(NCPh)(PPh_3)_2][B(C_6F_5)_4]$ (4)

Complex **4** shows a $^{31}P\{^1H\}$ NMR signal as a singlet for PPh_3 ligand (δ: 41.7 ppm), which is similar to the ^{31}P shift of complex **1**. In the ^1H NMR spectrum, the ^1H signal due to the CH_3 in Cp* appears as a singlet (δ: 1.56 ppm). The H_o in PPh_3 can be identified by correlation between P in the PPh_3 ligand and the methyl protons in Cp* in the $^1H/^{31}P\{^1H\}$-HMBC spectrum. The remaining protons and carbons in PPh_3 can be identified by their correlations in $^1H/^{13}C\{^1H\}$-HSQC and HMBC spectra. For the PhCN ligand, the $^{13}C\{^1H\}$ NMR spectrum shows a diagnostic ^{13}C signal due to the sp carbon of coordinated nitrile (δ: 133.5 ppm). The ^{13}C signal due to the aromatic C_{ipso} in PhCN is distinctly upfield from the other aromatic carbons (δ: 111.4 ppm), which is similar to the indenyl analogue $[Ru(\eta^5\text{-indenyl})(NCPh)(PPh_3)_2][B(C_6F_5)_4]$.[22] The H_m in PhCN are identified by correlation with C_{ipso} in PhCN in the $^1H/^{13}C\{^1H\}$-HMBC spectrum (Figure 2.6). The signal due to H_m is then used to identify the

remaining protons and carbons in PhCN by correlations in the $^{1}H/^{13}C\{^{1}H\}$-HSQC and HMBC spectra. In addition, the *m/z* and isotope pattern of **4** obtained using ESI-mass spectrometry support its identity (see Experimental in Section 2.6.4).

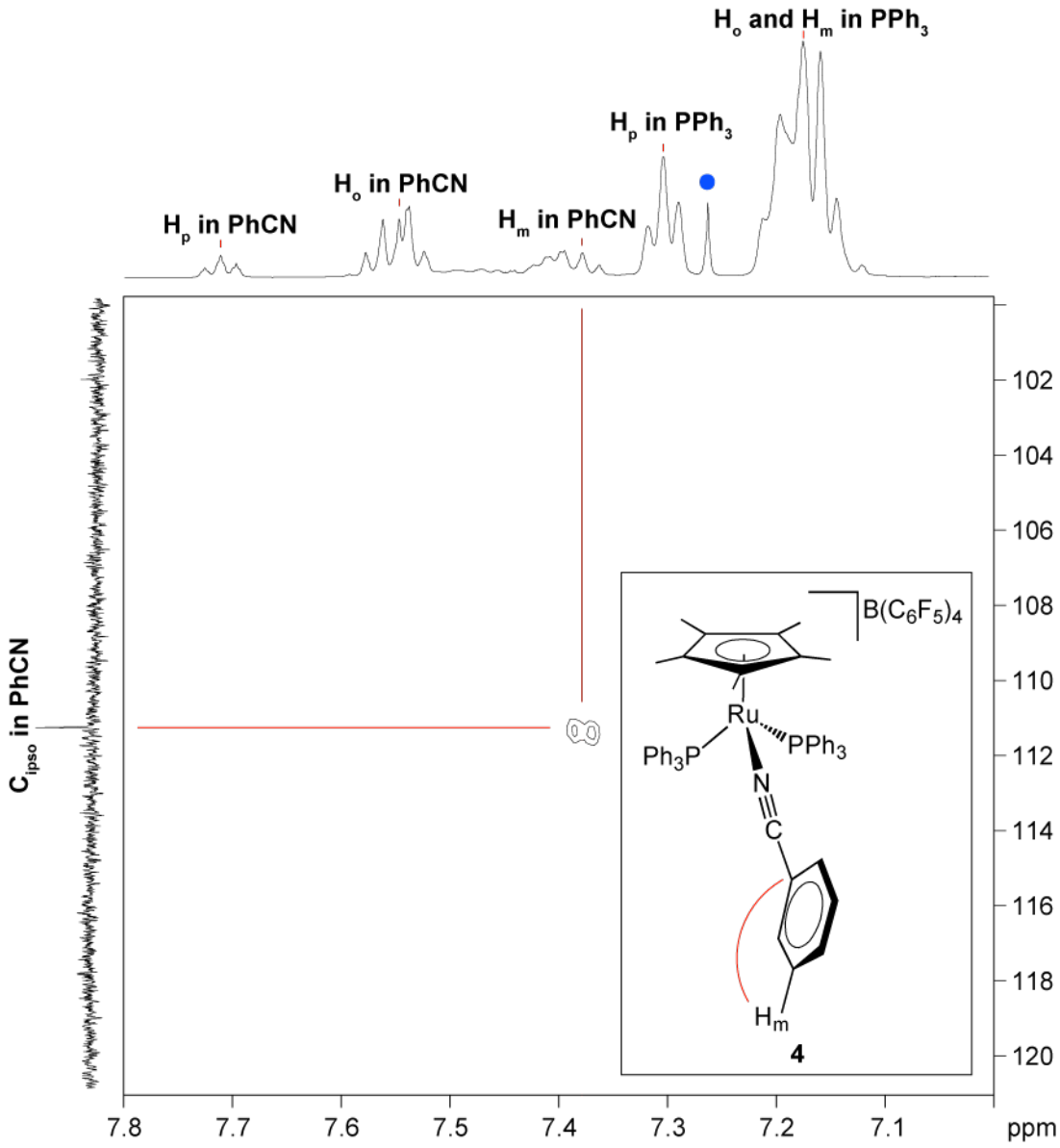

Figure 2.6 $^{1}H/^{13}C\{^{1}H\}$-HMBC NMR spectrum (500.27 MHz, $CDCl_3$) of cationic complex $[Ru(\eta^5\text{-Cp*})(NCPh)(PPh_3)_2][B(C_6F_5)_4]$ (**4**) highlighting the correlation between H_m and C_{ipso} in coordinated PhCN. Residual proteo solvent signal is labeled as blue dot.

For the byproduct $[Ru(\eta^5\text{-Cp*})(NCPh)_2(PPh_3)][B(C_6F_5)_4]$, it shows a ^{31}P signal due to P in PPh_3 ligand as a singlet (δ: 47.9 ppm) and a ^{1}H signal due to CH_3 in Cp* ligand as a doublet (δ: 1.41 ppm, $^{4}J_{PH}$ = 1.5 Hz). The $^{1}H/^{31}P\{^{1}H\}$-HMBC spectrum

also shows the correlation between these two signals. However, most of signals due to this disubstituted cationic complex can't be identified because it is the minor product. However, its *m/z* and isotope pattern obtained using ESI-mass spectrometry support its identity (see Experimental in Section 2.6.4).

2.4.3 Detailed characterization of [Ru(η^5-Cp*)(NCPh)(PTol$^p_2$H)(PPh$_3$)][B(C$_6$F$_5$)$_4$] (5d)

For complex **5d**, the $^{31}P\{^1H\}$ NMR spectrum shows two doublets of similar $^2J_{PP}$ value (40 Hz) relative to complex **2a-d**. The upfield peak (δ: 27.6 ppm) is identified as being the coordinated PTol$^p_2$H by a large $^1J_{PH}$ coupling (350 Hz) in the ^{31}P NMR spectrum. A doublet with similarly large $^1J_{PH}$ value is also observed in the P-H region of ^1H NMR spectrum. In the ^1H NMR spectrum, the ^1H signal due to the CH_3 in Cp* appears as a singlet (δ: 1.16 ppm). The H_o in PPh_3 is identified by correlation with the phosphorus in PPh_3 ligand in the $^1H/^{31}P\{^1H\}$-HMBC spectrum (Figure 2.7). The remaining protons and carbons in PPh_3 can be identified by their correlations in $^1H/^{13}C\{^1H\}$-HSQC and HMBC spectra. The ^1H, ^{13}C and ^{31}P signals due to PTol$^p_2$H can be identified by the same strategy as the assignment of PPh_3. For PhCN ligand, the ^{13}C signal due to C_{ipso} in PhCN is distinctly upfield from the other aromatic carbons (δ: 111.3 ppm), which is similar to complex **4** (*vide supra*) and indenyl analogues.[22] The H_m in PhCN are identified by its correlation with C_{ipso} in PhCN in the $^1H/^{13}C\{^1H\}$-HMBC spectrum. The ^1H signal due to H_m is then used to identify the remaining protons and carbons in PhCN by correlations in the $^1H/^{13}C\{^1H\}$-HSQC and HMBC spectra. However, the ^{13}C signal due to sp carbon of the nitrile functionality can't be observed in $^{13}C\{^1H\}$ NMR spectrum. In addition, its *m/z* and isotope pattern obtained using ESI-mass spectrometry support its identity (see Experimental in Section 2.6.5).

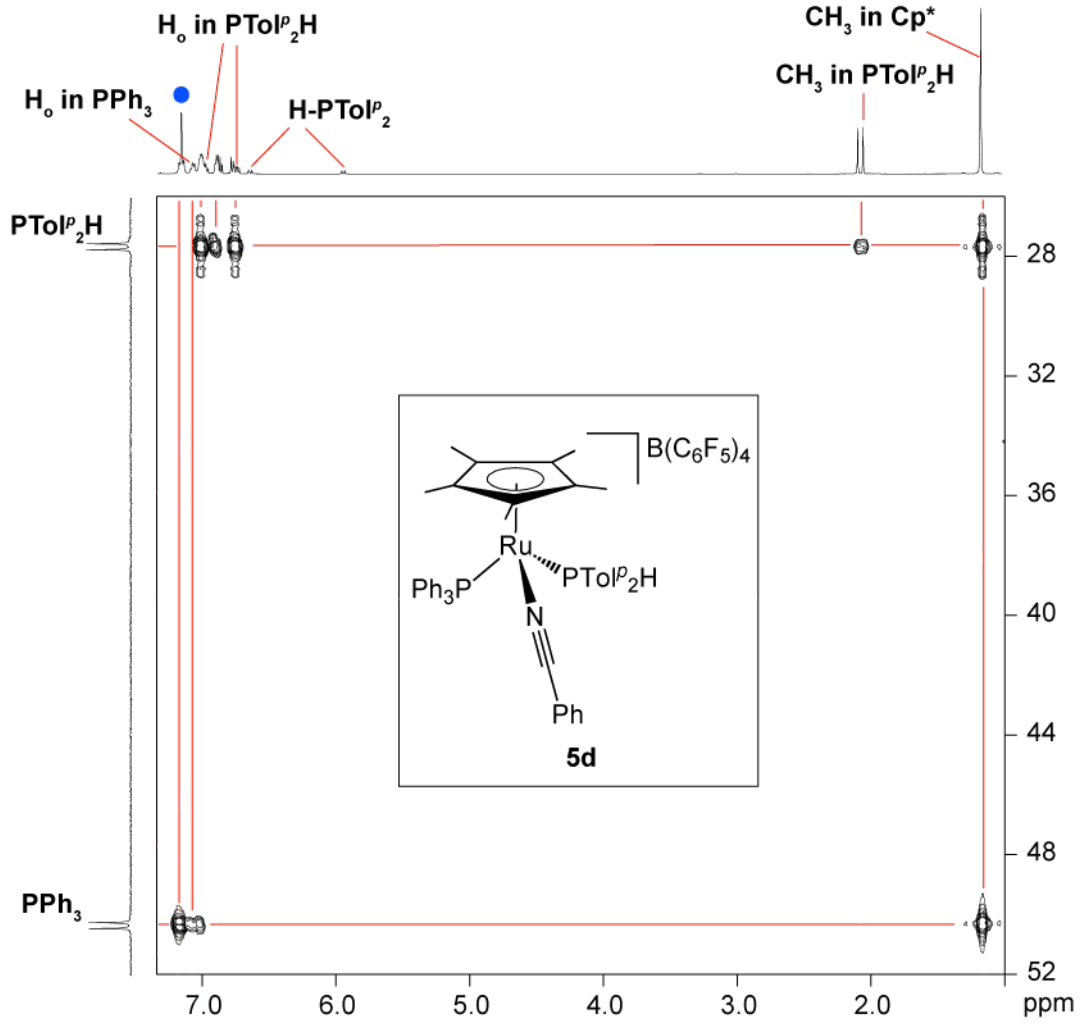

Figure 2.7 ^{1}H/^{31}P{^{1}H}-HMBC NMR spectrum (500.27 MHz, C_6D_6) of cationic complex [Ru(η^5-Cp*)(NCPh)(PTol$^p_2$H)(PPh$_3$)][B(C$_6$F$_5$)$_4$] (**5d**) highlighting the correlation between methyl protons and P in PPh$_3$ and PTol$^p_2$H and the correlations between H$_o$ and these P. Solvent residual signal is labeled as blue dot.

2.5 Conclusion

Monosubstituted complexes Ru(η^5-Cp*)Cl(PR$_2$H)(PPh$_3$) (**2a-d**) have been synthesized by ligand substitution of PPh$_3$ at Ru(η^5-Cp*)Cl(PPh$_3$)$_2$ (**1**) by both dialkylphosphines (R = Cy (**a**), Et (**b**)) and diarylphosphines (R = Ph (**c**), Tol^p (**d**)). The PPh$_3$ ligands in complex **1** are found to be more labile relative to the indenyl analogue Ru(η^5-indenyl)Cl(PPh$_3$)$_2$ (**1^i**). The phosphine size is also found to have an important influence on the degree of substitution in the Cp* complexes **2a-d**. In addition, two new cationic benzonitrile complexes [Ru(η^5-

Cp*)(NCPh)(PPh_3)$_2$][$B(C_6F_5)_4$] (**4**) and [Ru(η^5-Cp*)(NCPh)($PTol^p{}_2H$)(PPh_3)][$B(C_6F_5)_4$] (**5d**) have been synthesized as potential precursors for hydrophosphination.

Comparisons between the Cp* complex and indenyl analogue provide information that will be useful in making strategies for dehydrohalogenation of Cp* complexes (described in Chapter 3). The Cp* complex has higher steric congestion and an increase of electron density relative to the indenyl analogue, which is supported by X-ray crystallography and IR spectroscopy.

2.6 Experimental

2.6.1 General Experimental Details

All reactions and manipulations were performed under a nitrogen atmosphere in an MBraun Unilab 1200/780 glovebox or using conventional Schlenk techniques. All solvents were dried using an MBraun Solvent Purification System (SPS) after being purged with nitrogen for 25 min. (C_6D_6, $CDCl_3$) were purchased from Canadian Isotope Labs (CIL), degassed using at least three freeze-pump-thaw cycles, and vacuum-transferred from sodium/ benzophenone before use. Triphenylphosphine (PPh_3) was purchased from Aldrich Chemical Co. and used as received without further purification. All secondary phosphines were purchased from Strem Chemicals as 10 wt % solutions in hexanes (concentrations checked against a known quantity of triphenylphosphine oxide by $^{31}P\{^1H\}$ NMR before use). NMR spectra were recorded on a Bruker AVANCE 500 instrument operating at 500.27 MHz for ^1H, 125.79 MHz for ^{13}C and 202.51 MHz for ^{31}P or on a Bruker AVANCE 300 operating at 300.27 MHz for ^1H and 121.55 MHz for ^{31}P. Chemical shifts are reported in ppm at ambient temperature. ^1H chemical shifts are referenced to residual protonated solvent peaks at

7.26 ($CHCl_3$) and 7.16 (C_6D_5H). ^{13}C chemical shifts are referenced to $CDCl_3$ at 77.16 ppm and C_6D_6 at 128.4 ppm. All ^{1}H and ^{13}C shifts are reported relative to $Si(CH_3)_4$, and ^{31}P chemical shifts are reported relative to 85% H_3PO_4 (aq). Melting temperatures were recorded using a Gallenkamp apparatus for capillary samples. Microanalysis was performed by Canadian Microanalytical Service Ltd., Delta, BC, Canada. IR spectra were recorded on Perkin-Elmer FTIR Spectrum One spectrophotometer using KBr pellets under a nitrogen atmosphere. X-ray crystallography was performed by Dr. Robert McDonald from the X-ray Crystallography Laboratory at the University of Alberta. ESI-MS of synthetic products was collected by Jane Zhu in the McIndoe group at the University of Victoria in the positive ion mode on a Waters Micromass Q-TOF *micro* mass spectrometer using solutions prepared in CH_2Cl_2.

2.6.2 Synthesis of Ru(η^5-Cp*)Cl(PPh_3)$_2$ (1)

Multiple methods for the synthesis of this complex were previously reported in the literature.[10,11,12] Two methods were tried.

Method A (work of undergraduate student Sophie Langis-Barsetti):

The literature method reported by Moret was slightly modified.[10] PPh_3 (2.2 g, 8.4 mmol) was dissolved in THF (20 mL) and was transferred by cannula to a flask containing $[Cp^*RuCl]_4$ (0.90 g, 0.82 mmol); a brown-orange precipitate formed instantly. The solution was stirred for 1h after which THF (50 mL) was added to the reaction mixture and then transferred by cannula filtration into a clean flask. The solvent was then removed from the combined washings under vacuum. The solid was washed with hexane (5 x 15mL) and dried under vacuum to give an orange solid Ru(η^5-Cp*)Cl(PPh_3)$_2$ (**1**, 1.53 g, 1.9 mmol, 59% yield).

Method B (my work):

The literature method reported by Fokin was slightly modified.[11] The authors did not report full NMR characterization or microanalysis since Ru(η^5-Cp*)Cl(PPh_3)$_2$ is a well-known complex.

$RuCl_3$•3(H_2O) (6.05 g, 23.2 mmol) and MeOH (70 mL) were added to a 250 mL Schlenk flask. The flask was fitted with a reflux condenser and the mixture was refluxed under nitrogen for 1h to degas the MeOH. Pentamethylcyclopentadiene (Cp*H) (8.0 mL, 51.1 mmol) was added to the Schlenk flask *via* syringe. The brown suspension was refluxed for 6h and allowed to cool to room temperature. The resulting brown-black microcrystals were filtered and washed with ethanol (20 mL) and hexanes (3 x 20 mL) to afford 5.76 g (81% yield) of [Cp*$RuCl_2$]$_n$. [Cp*$RuCl_2$]$_n$ (1.19 g, 3.84 mmol) was placed into a 100 mL Schlenk flask fitted with a reflux condenser. The flask was purged with nitrogen and absolute ethanol (70 mL, degassed for 2h by nitrogen purge) was added. Triphenylphosphine (4.04 g, 15.4 mmol) was added as a solid under nitrogen. The mixture was refluxed for at least 24h and allowed to cool to room temperature. The orange reaction mixture was filtered and the solid was washed with ethanol (20mL) and hexanes (5 x 10 mL) to afford 2.54 g (83 % yield) of Ru(η^5-Cp*)Cl(PPh_3)$_2$ as orange microcrystals. ^{1}H NMR (C_6D_6, 300.27 MHz) δ ppm: 8.20-7.44 (m, 12H, P(C_6H_5)$_3$), 7.10-6.47 (m, 18H, P(C_6H_5)$_3$) 1.14 (t, 15H, $^4J_{PH}$ = 1.5 Hz, C_5(CH_3)$_5$). ^{31}P NMR (C_6D_6, 121.5 MHz) δ ppm: 40.8 (s, *P*Ph_3). (Literature NMR data reported for the sample in $CDCl_3$ were similar to ours.[23])

2.6.3 General method for synthesis of Ru(η^5-Cp*)Cl(PR_2H)(PPh_3) (2a-d)

This method is adapted slightly from a procedure previously reported for the synthesis of **2c**.[6] Toluene (20 mL) was added to a flask containing Ru(η^5-Cp*)Cl(PPh_3)$_2$ (approximately 500 mg, see details below) and a solution of PR_2H in

hexane (variable molar ratios relative to starting material). The suspension was stirred for 1-2.5h at RT until the mixture became homogeneous and $^{31}P\{^{1}H\}$ NMR of an aliquot removed from the solution showed no signals due to **1**. The solvent was removed under vacuum. The residue was dissolved in a minimum volume of toluene (~2-3 mL), layered with pentane (~10-15 mL), and left to stand overnight. The supernatant was decanted from the resulting red crystalline product, which was washed with pentane (at least 3 x 10 mL) and dried under vacuum. Red-orange microcrystals were obtained (1st crop). The solvent was removed under vacuum from the supernatant. This residue was dissolved in minimum volume of toluene and layered with pentane (1:5 ratio again), which usually gave a 2nd crop of product. $^{31}P\{^{1}H\}$ NMR data for **2a-d** and **3a-d** are reported in Table 2.3 and Table 2.4. ^{1}H, $^{13}C\{^{1}H\}$, and $^{31}P\{^{1}H\}$ spectra of isolated compounds can be found in Appendix C.

2.6.3.1 Synthesis of Ru(η^5-Cp*)Cl(PCy_2H)(PPh_3) (2a)

Complex **1** (0.52g, 0.65 mmol) and PCy_2H in hexane (0.33M, 2.3 mL, 0.78 mmol) were used. Reaction was stirred for 2.5h. Red-orange microcrystals were obtained (0.24 g, 0.33 mmol, 50% yield). Melting point: 199-201 °C. IR (KBr, cm^{-1}): 2329 (w, ν_{PH}). Anal. found (calc'd for $C_{40}H_{53}P_2ClRu$): C, 65.65 (65.60); H, 7.72 (7.30).

2.6.3.2 Synthesis of Ru(η^5-Cp*)Cl(PEt_2H)(PPh_3) (2b)

Complex **1** (0.52g, 0.65 mmol) and PEt_2H in hexane (0.75M, 2.0 mL, 1.49 mmol) were used. The suspension was stirred for 2h. Red-orange microcrystals were obtained (0.11 g, 0.18 mmol, 27% yield). Melting point: 196-198 °C. IR (KBr, cm^{-1}): 2327 (w, ν_{PH}). Anal. found (calc'd for $C_{32}H_{41}P_2ClRu$): C, 59.20 (61.58); H, 6.26

(6.62).The %C is low that probably arises from the contamination of grease (see in ^{1}H NMR) in analyzed sample.

2.6.3.3 Synthesis of Ru(η^5-Cp*)Cl(PPh_2H)(PPh_3) (2c)

We obtained similar yield and purity (relative amounts of mono and di-substituted product) for this synthesis to that reported by Paz-Sandoval.[6] As described below, we also carried out this reaction in CH_2Cl_2 (one time only, Method B), obtaining a slightly higher yield (77%) and similar purity. We have not yet repeated this preparation to ensure reproducibility. Note: using CH_2Cl_2 as solvent gave messier product mixtures for the dialkylphosphine complexes.

Method A:

We prepared the complex using the general method described above: complex **1** (0.50 g, 0.63 mmol) and PPh_2H in hexanes (0.54 M, 1.4 mL, 0.76 mmol) were used. Reaction was stirred for 1h. The residue was recrystallized at -4 °C instead of RT. The product was washed with pentane (3 x 10 mL) and dried under vacuum. Red-orange microcrystals were obtained (0.31 g, 0.43 mmol, 68% yield). The product contained an impurity of ~4% of the disusbstituted product Ru(η^5-Cp*)Cl(PPh_2H)$_2$ (**3c**). Melting point: 217-219 °C. IR (KBr, cm^{-1}): 2343 (w, ν_{PH}).

Method B:

The following method gave a higher yield of **2c**. CH_2Cl_2 (20 mL) was added to a flask containing complex **1** (0.50 g, 0.63 mmol) and a solution of PPh_2H in hexane (0.54 M, 1.4 mL, 0.76 mmol). The solution was stirred for 40 min after which the solvent was removed under vacuum. The product was washed with hexane (5 x 10mL) and dried under vacuum to give an orange-red microcrystalline product (0.35 g, 0.48

mmol, 77% yield). The product contained an impurity of ~4% of the disusbstituted product Ru(η^5-Cp*)Cl(PPh_2H)$_2$ (**3c**).

2.6.3.4 Synthesis of Ru(η^5-Cp*)Cl($PTol^p_2H$)(PPh_3) (2d)

This complex was prepared using the general method described above. Complex **1** (0.61 g, 0.77 mmol) and $HPTol^p_2$ in hexanes (0.45 M, 3.5 mL, 1.6 mmol) were used. The solution was stirred for 1h. The red residue was recrystallized at -4 °C instead of RT. Red-orange microcrystals were obtained (0.38 g, 0.51 mmol, 66% yield). Melting point: 218-220 °C. IR (KBr, cm^{-1}): 2339 (w, ν_{PH}). Anal. found (calc'd for $C_{42}H_{45}P_2ClRu$): C, 67.12 (67.41); H, 6.07 (6.06).

Table 2.3 202.51 MHz $^{31}P\{^1H\}$ NMR data for Cp* complex **2a-d** in C_6D_6 at 300 K: δ (ppm) (multiplicity, $^2J_{PP}$ (Hz)).

Complex		PR_2H	PPh_3
Ru(η^5-Cp*)Cl(PCy_2H)(PPh_3)	**2a**	48.2 (d, 40)	49.6 (d)
Ru(η^5-Cp*)Cl(PEt_2H)(PPh_3)	**2b**	38.7 (d, 43)	50.5 (d)
Ru(η^5-Cp*)Cl(PPh_2H)(PPh_3)	**2c**	36.5 (d, 42)	45.3 (d)
Ru(η^5-Cp*)Cl($PTol^p_2H$)(PPh_3)	**2d**	34.6 (d, 42)	45.5 (d)

Table 2.4 121.55 MHz $^{31}P\{^1H\}$ NMR data for Cp* complex **3a-d** in C_6D_6 at 300 K: δ (ppm)).

Complex		PR_2H
Ru(η^5-Cp*)Cl(PCy_2H)$_2$	**3a**	44.3 (s)
Ru(η^5-Cp*)Cl(PEt_2H)$_2$	**3b**	34.4 (s)
Ru(η^5-Cp*)Cl(PPh_2H)$_2$	**3c**	36.9 (s)
Ru(η^5-Cp*)Cl($PTol^p_2H$)$_2$	**3d**	34.9 (s)

2.6.4 Synthesis of [Ru(η^5-Cp*)(NCPh)(PPh_3)$_2$][$B(C_6F_5)_4$] (4)

MeOH (20 mL) was added to a Schlenk flask containing complex **1** (0.31 g, 0.39 mmol), benzonitrile (0.047 mL, 0.80 mmol) and $KB(C_6F_5)_4$ (0.33 g, 0.46 mmol). The resulting orange mixture was stirred for 3h, during which time it turned yellow with a pale precipitate. The solvent was removed under vacuum. The residue was then

dissolved in CH_2Cl_2 and filtered to remove KCl. The CH_2Cl_2 was then removed under vacuum and the resulting residue was washed with pentane (at least 3 x 10 mL), which gave a pale yellow solid (0.32 g, 0.21 mmol, 53% yield). $^{31}P\{^1H\}$ NMR (202.51 MHz, $CDCl_3$) δ ppm: 41.7 (s, *P*Ph_3). Melting point: 158 - 160 °C. IR (KBr, cm^{-1}): 2216 (w, ν_{CN}). LR-ESI-MS (CH_2Cl_2, *m/z*): 864.26 (M^+, 62%), 761.08 ([M – NCPh]$^+$, 100%), 602.18 ([M – PPh_3]$^+$, 78%). The product contained an impurity of ~9% of the disusbstituted benzonitrile product $[Ru(\eta^5\text{-Cp*})(NCPh)_2(PPh_3)][B(C_6F_5)_4]$ as determined by ^1H NMR spectrum. $^{31}P\{^1H\}$ NMR (202.51 MHz, $CDCl_3$) δ ppm: 47.9 (s, *P*Ph_3). LR-ESI-MS (CH_2Cl_2, *m/z*): 705.27 (M^+, 21%), 602.18 ([M – NCPh]$^+$, 78%).

2.6.5 Synthesis of $[Ru(\eta^5\text{-Cp*})(NCPh)(PTol^p{}_2H)(PPh_3)][B(C_6F_5)_4]$ (5d)

MeOH (20 mL) was added to a Schlenk flask containing complex containing complex **1** (0.11 g, 0.15 mmol), benzonitrile (0.011 mL, 0.18 mmol) and $KB(C_6F_5)_4$ (0.13 g, 0.18 mmol). The resulting orange mixture was stirred for 3h, during which time it turned yellow. The solvent was removed under vacuum. The residue was then dissolved in CH_2Cl_2 and filtered to remove KCl. The CH_2Cl_2 was then removed under vacuum and trituration of the resulting residue with MeOH (10 mL) gave a bright yellow solid (0.083 g, 0. 055 mmol, 38% yield). $^{31}P\{^1H\}$ NMR (202.51 MHz, C_6D_6) δ ppm: 50.3 (d, $^2J_{PP}$ = 40 Hz, *P*Ph_3), 27.6 (d, *P*$Tol^p{}_2H$). Melting point: 88 - 90 °C. IR (KBr, cm^{-1}): 2343 (w, ν_{PH}), 2221 (w, ν_{CN}). LR-ESI-MS (CH_2Cl_2, *m/z*): 816.62 (M^+, 100%). The complex **5d** is contaminated with grease (see in ^1H NMR), and grease can't be washed out by pentane because **5d** is also soluble in pentane. This is why no microanalysis is reported.

Table 2.5 500.27 MHz ^{1}H NMR data for Ru(η^5-Cp*)Cl(PR_2H)(PPh_3) **2a-d** in C_6D_6 at 300 K: δ in ppm (multiplicity, RI, J_{avg} or $\omega_{1/2}$ in Hz, assignment).[a]

	η^5-Cp*	PPh_3	HPR_2
2a	1.50 (s, 15H)	**H_o** 8.13-7.43 (br s, 6H, $\omega_{1/2}$ 35.9) **$H_{m,p}$** 7.30- 6.80 (m, H_m and H_p overlapping, 9H)	**H-PCy$_2$** 4.07 (dm, 1H, $^1J_{PH}$ 334.2) **Cy:** **CH** 2.42-2.33 (m, 1H), 1.93-1.83 (m, 1H) **CH_2** 2.33-2.25 (m, 1H), 2.09-2.00(m, 2H), 1.80-1.74 (m, 1H), 1.74-1.66 (m, 2H), 1.66-1.63 (m, 1H), 1.61-1.56 (m, 1H), 1.44-1.19 (m, 9H), 1.18-1.01 (m, 3H)
2b	1.44 (t, 15H, $^4J_{PH}$ 1.6)	**H_o** 8.00-7.60 (br s, 6H, $\omega_{1/2}$ 24.1) **H_m** 7.14- 7.06 (m, 6H) **H_p** 7.06- 6.99 (m, 3H)	**H-PEt$_2$** 4.06 (dm, 1H, $^1J_{PH}$ 334.1) **Et:** **CH_2 (A)** 2.13-1.92 (m, 1H), 1.60-1.50 (m, 1H) **CH_2 (B)** 1.80-1.68 (m, 1H), 1.50-1.39 (m, 1H) **CH_3 (A)** 1.05 (dt, 3H, $^3J_{PH}$ 13.9, $^3J_{HH}$ 7.5) **CH_3 (B)** 0.92 (dt, 3H, $^3J_{PH}$ 14.0, $^3J_{HH}$ 7.6)
2c	1.36 (s, 15H)	**H_o** 8.34-7.26 (m, overlaps H_o in $HPPh_2$, 6H) **$H_{m,p}$** 7.11- 6.58 [m, H_m and H_p overlapping, 9H (also overlaps with $H_{o,m,p}$ in $HPPh_2$)]	**H-PPh$_2$** 6.86 (d, 1H, $^1J_{PH}$ 364.9) **Ph:** **H_o** 7.89 (dd, 2H, $^3J_{PH}$ 10.8, $^3J_{HH}$ 7.9), 7.00 (m, overlaps $H_{m,p}$ in $HPPh_2$ and PPh_3, 2H) **$H_{m,p}$** 7.11- 6.58 [m, H_m and H_p overlapping, 6H (*also overlaps with $H_{m,p}$ in PPh_3)]
2d	1.41 (s, 15H)	**H_o** 8.39-7.42 (br s, overlaps with H_o in $HPTol^p_2$, 6H, $\omega_{1/2}$ 170.1) **$H_{m,p}$** 7.10- 6.80 [m, H_m and H_p overlapping, 9H (*also overlaps with $H_{o,m}$ signals in $HPTol^p_2$)]	**H-PTol$^p_2$** 6.87 (d, 1H, $^1J_{PH}$ 363.5) **H_o** 7.86 (dd, 2H, $^3J_{PH}$ 10.5, $^3J_{HH}$ 8.1), 6.96 (dd, 2H, $^3J_{PH}$ 10.5, $^3J_{HH}$ 8.1) **H_m** 6.94-6.90 (m, overlaps with $H_{m,p}$ in PPh_3, 4H) **CH_3** 1.99 (s, 3H), 2.14 (s, 3H)

[a] PR_2H [R= Cy(**a**), Et (**b**), Ph (**c**), Tol^p (**d**)].

Table 2.6 125.79 MHz $^{13}C\{^1H\}$ NMR data for Ru(η^5-Cp*)Cl(PR_2H)(PPh_3) **2a-d** in C_6D_6 at 300 K: δ in ppm (multiplicity, RI, J_{avg} or $\omega_{1/2}$ in Hz, assignment).[a]

	η^5-Cp*	**PPh_3**	**HPR_2**
2a	C_{ring} 88.7 (s) C_{methyl} 11.1 (s)	C_{ipso} not observed C_{ortho} 137.9 (br s, $\omega_{1/2}$ 44), 135.6 (br s, $\omega_{1/2}$ 44), 134.4 (br s, $\omega_{1/2}$ 43) C_{para} 129.9 (s) C_{meta} 128.1 (br s, $\omega_{1/2}$ 23)	CH 38.6 (d, $^1J_{PC}$ 19), 36.9 (dd, $^1J_{PC}$ 20, 4) CH_2 35.6 (d, 2), 34.8 (d, 3), 32.3 (d, 4), 31.4 (s), 28.8-28.4 (five different C overlapping), 27.1 (d, 17)
2b	C_{ring} 88.7 (t, $^2J_{PC}$ 2) C_{methyl} 10.1 (s)	C_{ipso} 137.5 (br s, $\omega_{1/2}$ 72) C_{ortho} 135.2 (br s, $\omega_{1/2}$ 34) C_{para} 129.0 (s) C_{meta} 127.7 (d, $^4J_{PC}$ 9)	CH_2 (A) 18.9 (dd, $^1J_{PC}$ 23, $^3J_{PC}$ 2) CH_2 (B) 18.8 (dd, $^1J_{PC}$ 23, $^3J_{PC}$ 2) CH_3 (A) 14.1 (d, $^2J_{PC}$ 8), CH_3 (B) 13.6 (d, $^2J_{PC}$ 6)
2c	C_{ring} 89.4 (s) C_{methyl} 10.0 (s)	C_{ipso}, C_{ortho}, C_{para} not observed C_{meta} 127.6 (d, $^4J_{PC}$ 8)	C_{ipso} not observed C_{ortho} 134.5 (d, $^2J_{PC}$ 9), 133.1 (d, $^2J_{PC}$ 9) C_{para} 129.5 (s, $^4J_{PC}$ 2), 129.0 (d, $^4J_{PC}$ 2) C_{meta} 128.2 (d, $^3J_{PC}$ 9), 127.7 (d, $^3J_{PC}$ 9)
2d	C_{ring} 89.3 (s) C_{methyl} 10.0 (s)	C_{ipso}, C_{ortho}, C_{para} not observed C_{meta} 127.6 (d, $^4J_{PC}$ 8)	C_{para} 139.4 (d, $^4J_{PC}$ 2), 138.8 (d, $^4J_{PC}$ 2) C_{ortho} 134.6 (d, $^2J_{PC}$ 9), 133.3 (d, $^2J_{PC}$ 9) C_{ipso} 132.9 (dd, $^1J_{PC}$ 36, 7), 131.5 (d, $^1J_{PC}$ 42) C_{meta} 128.9 (d, $^3J_{PC}$ 9), 128.6 (d, $^3J_{PC}$ 9) CH_3 21.3 (s), 21.2 (s)

[a] PR_2H [R= Cy(**a**), Et (**b**), Ph (**c**), Tol^p (**d**)].

Table 2.7 500.27 MHz ^{1}H NMR data for [Ru(η^5-Cp*)(NCPh)(PPh_3)$_2$][B(C_6F_5)$_4$] **4** and [Ru(η^5-Cp*)(NCPh)(PTol$^p_2$H)(PPh_3)][B(C_6F_5)$_4$] **5d** at 300 K: δ in ppm (multiplicity, RI, J_{avg} or $\omega_{1/2}$ in Hz, assignment).

	η^5-Cp*	**PPh_3**	**Other**
4[a]	1.56 (s, 15H)	**H_p** 7.30 (t, 6H, $^3J_{HH}$ 7.1) **$H_{o,m}$** 7.23-7.10 (m, H_o and H_m overlapping, 12H)	**H_o** 7.58-7.51 (m, 2H) **H_m** 7.43-7.35 (m, 2H) **H_p** 7.71 (t, 1H, $^3J_{HH}$ 7.1)
5d[b]	1.16 (s)	**H_o** 7.21-7.12 (m, overlap with solvent signal and H_p in NCPh, 6H) **H_m** 7.05-6.95 (m, overlap with H_o in HPTol$^p_2$, 6H) **H_p** 7.08 (t, $^3J_{HH}$ 7.1, 3H)	**PTol$^p_2$H:** **H-PTol$^p_2$** 6.29 (dd, 1H, $^1J_{PH}$ 350.4, $^3J_{PH}$ 11) **H_o** 7.05-6.95 (m, overlap with H_m in PPh_3, 2H), 6.74 (dd, 2H, $^3J_{PH}$ 11, $^3J_{HH}$ 7.8) **H_m** 6.92-6.86 (m, overlap with H_m in NCPh, 4H) **CH_3** 2.08 (s), 2.04 (s) **NCPh:** **H_p** 7.16 (m, overlaps with solvent signal and H_o in PPh_3) **H_m** 6.86 (d, 2H, $^3J_{HH}$ 7.7) **H_o** 6.77 (d, 2H, $^3J_{HH}$ 7.7)

[a] in $CDCl_3$. [b] in C_6D_6.

Table 2.8 125.79 MHz $^{13}C\{^1H\}$ NMR data for $[Ru(\eta^5\text{-Cp*})(NCPh)(PPh_3)_2][B(C_6F_5)_4]$ **4** and $[Ru(\eta^5\text{-Cp*})(NCPh)(PTol^p{}_2H)(PPh_3)][B(C_6F_5)_4]$ **5d** at 300 K: δ in ppm (multiplicity, RI, J_{avg} or $\omega_{1/2}$ in Hz, assignment).

	η^5-Cp*	**PPh_3**	**Other**
4[a]	C_{ring} 93.7 (s) C_{methyl} 9.35 (s)	C_{ipso} 133.5 (d, $^1J_{PC}$ 40) C_{ortho} 133.9 (t, $^2J_{PC}$ 5) C_{para} 130.2 (s) C_{meta} 128.1 (t, $^3J_{PC}$ 5)	**PhCN:** C_{para} 134.4 (s), CN 133. 5 (d, $^3J_{PC}$ 2), C_{ortho} 132.0 (s), C_{meta} 129.6 (s), C_{ipso} 111.4 (s) **$B(C_6F_5)_4$:** 149.3 (s), 147.4 (s), 139.3 (s), 137.3 (s), 135.4 (s)
5d[b]	C_{ring} 93.3 (s) C_{methyl} 9.26 (s)	C_{ipso} not observed C_{ortho} 134.0 (d, $^2J_{PC}$ 11) C_{para} 130.7 (s) C_{meta} 128.6 (d, $^3J_{PC}$ 9)	**$PTol^p{}_2H$:** C_{ipso} not observed C_{ortho} 133.4 (d, $^2J_{PC}$ 10), 132.9 (d, $^2J_{PC}$ 10) C_{para} 141.3 (s), 141.2 (s) C_{meta} 129.8 (d, $^3J_{PC}$ 9), 129.5 (d, $^3J_{PC}$ 9) CH_3 21.1 (s), 21.0 (s) **NCPh:** C_{para} 133.9 (s), C_{ortho} 131.5 (s), C_{meta} 129.5 (s), C_{ipso} 111.3 (s), CN not observed **$B(C_6F_5)_4$:** 150.2 (s), 148.3 (s), 138.1 (s), 136.1 (s)

[a] in $CDCl_3$. [b] in C_6D_6.

2.7 References

[1] Hartwig, J. *Organotransition Metal Chemistry;* University Science Books: Sausalito, Calif., 2010.

[2] Nell, B. P.; Tyler, D. R. *Coord. Chem. Rev.* **2014**, *279*, 23.

[3]. Gibson, G. L.; Morrow, K. M. E.; McDonald, R.; Rosenberg, L. *Inorg. Chim. Acta* **2011**, *369*, 133.

[4] Paris, S. I. M.; Lemke, F.R.; Sommer, R.; Lönnecke, P.; Hey-Hawkins, E.; *J. Organomet. Chem.* **2005**, *690*, 1807.

[5] Paris, S. I. M.; Petersen, J. L.; Hey-Hawkins, E.; Jensen, M. P. *Inorg. Chem.* **2006**, *45*, 5561.

[6] Torres-Lubián, R.; Paz-Sandoval, M. A. *J. Organomet. Chem.* **1997**, *532*, 17.

[7] Derrah, E. J.; Marlinga, J. C.; Mitra, D.; Friesen, D. M.; Hall, S. A.; McDonald, R.; Rosenberg, L. *Organometallics* **2005,** *24*, 5817.

[8] Derrah, E. *Probing the Reactivity of Ruthenium Indenyl Complexes in P-C Bond Forming Reactions.* Ph.D thesis, University of Victoria, **2009**.

[9] Pedro, F. M.; Santos, A. M.; Baratta, W.; Kühn, F. E. *Organometallics* **2007**, *26*, 302.

[10] Morandini, F.; Dondana, A.; Munari, I.; Pilloni, G.; Consiglio, G.; Sironi, A.; Moret, M. *Inorg. Chim. Acta* **1998**, *282*, 163.

[11] Boren, B.C.; Narayan, S.; Rasmussen, L.K.; Zhang, L.; Zhao, H.; Lin, Z.; Jia, G.; Fokin, V. V. *J. Am. Chem. Soc.*, **2008**, *130*, 8923.

[12] Yoda, H.; Nakatani, K.; Terashima, T.; Ouchi, M.; Sawamoto, M.; *Macromolecules* **2010**, *43*, 5595.

[13] Tolman, C. A. *Chem. Rev.* **1977**, *77 (3)*, 313.

[14] Gamasa, M. P.; Gimeno, J.; Godefroy, I.; Gonzalez-Bernardo, C.; Martion-Alvarez, J. M.; Monti, D; Basseti, M. *Organometallics* **1996**, *15*, 302.

[15] Davies, S. G.; McNally, J. P.; Smallridge, A. J. *Adv. Organomet. Chem.* **1990**, *30*, 1.

[16] Bordwell, F. G.; Bausch, M. J. *J. Am. Chem. Soc.*, **1983**, *105*, 6188.

[17] Crabtree, R. *The Organometallic Chemistry of the Transition Metals*; Wiley: New York, 1988.

[18] Ashby, G. S.; Bruce, M. I.; Tomkins, I. B.; Wallis, R. C.; *Austr. J. Chem.* **1979**, *32*, 1003.

[19] For X-ray data on Ru indenyl complexes see: Derrah, E. J.; Marlinga, J. C.; Mitra, D.; Friesen, D. M.; Hall, S. A.; R. McDonald, L. Rosenberg, *Organometallics* **2005**, 24, 5817 and references therein. For X-ray data on Ru Cp and Cp* complexes see: Torres-Lubáin, R.; Angeles Paz-Sandoval, M. *J. Organomet. Chem.* **1997**, *532*, 17.

[20] Silverstein, R. M.; Bassler, G. C.; Morrill, T. C. *Spectrometric Identification of Organic Compounds*; Fifth ed.; John Wiley & Sons, Inc.: Toronto, 1991.

[21] Planas, J. G.; Hampel, F.; Gladysz, J. A. *Chem. Eur. J.* **2005**, *11*, 1402.

[22] Belli, R. G.; Burton, K. M. E.; Rufh, S. A.; McDonald, R.; Rosenberg, L. *Organometallics* **2015**, *34*, 5637.

[23] Pedro, F.; Santos, A.; Baratta, W.; Kühn, F. *Organometallics* **2007**, *26*, 302.

Chapter 3 Investigation of Cp* ruthenium phosphido complexes containing a Ru=P

3.1 Introduction

This chapter describes the generation of phosphido complexes Ru(η^5-Cp*)(PR_2)(PPh_3) (**6a-d**) from the secondary phosphine complexes Ru(η^5-Cp*)Cl(PR_2H)(PPh_3) (**2a-d**) introduced in Chapter 2. Cp* phosphido **6a-d** are compared to the indenyl analogues to better understand reactivity in η^5-Cp* derivative half-sandwich complexes.

3.1.1 Diagnostic spectroscopic evidence for transition metal phosphido complexes

As described in Chapter 1 (Section 1.2), there are three types of phosphido bonding modes in transition metal complexes: terminal phosphido, planar phosphido and bridging phosphido (see Figure 3.1).[1] These different binding modes for phosphido can be diagnosed by $^{31}P\{^1H\}$ NMR spectroscopy. The chemical shifts observed for these three types of phosphido ligand vary widely, taking into account factors such as the metal type[2,3,4] and different substituents (R) at phosphorus (P).[4,5] The ^{31}P shifts for the pyramidal terminal phosphido (sp^3 P) ligand in half-sandwich ruthenium (Ru) complexes are approximately from 83 to 23 ppm.[4, 5, 6, 7] The planar phosphido (sp^2 P) ligand exhibits a huge downfield shift (400 to 130 ppm) compared to a pyramidal terminal phosphido ligand.[1] The bridging phosphido complexes have even wider range of chemical shifts of approximately 461 to -181 ppm.[8] The bridging and planar terminal phosphido ligands tend to have more downfield ^{31}P shifts than pyramidal terminal phosphido ligands with analogous substituents, which can be explained by the greater donation of the bridging and planar terminal phosphido ligands to the metal center (s).[9]

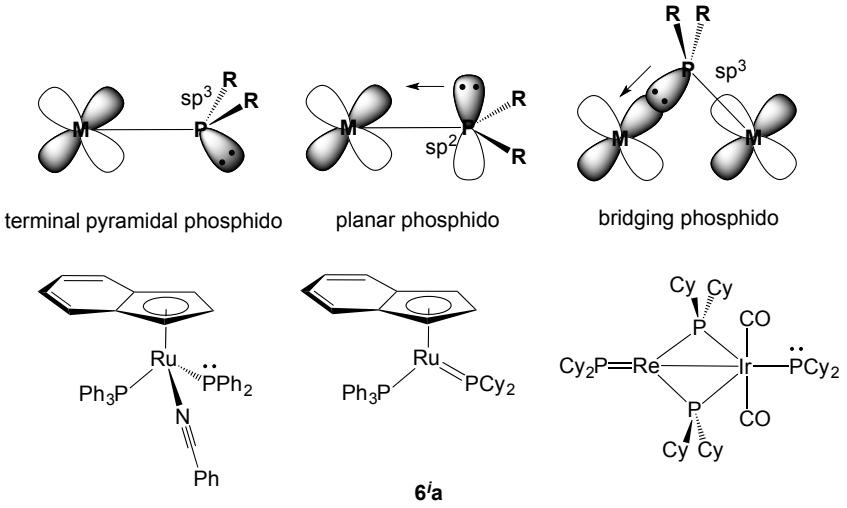

Figure 3.1 Three bonding modes of phosphido ligands in transition metal complexes.

Also, the different bonding modes of phosphido ligand can be assigned in X-ray crystallography. Ru(η^5-indenyl)(PPh_2)(NCPh)(PPh_3) and Ru(η^5-indenyl)(PCy_2)(PPh_3) (**6^{i}a**) shown in Figure 3.1 can be examples to assign the geometry at the phosphorus center by using their X-ray crystallography data. The sum of three bond angles around P (Ru-P-R, Ru-P-R, R-P-R; R = Ph or Cy) in Ru(η^5-indenyl)(PPh_2)(NCPh)(PPh_3) (pyramidal terminal phosphido) is 315.41°,[7] while the sum of these three bond angles in planar phosphido **6^{i}a** is 358.18°.[4] In addition, Ru-P bond length can indicate the geometry of P center (see Section 1.2, Chapter 1). All these results above are strong evidence for assignment of the geometry at P (sp^3 or sp^2).

3.1.2 Dehydrohalogenation of coordinated secondary phosphine (PR_2H)

As mentioned in Chapter 1 (Section 1.2.1), the base-induced P-H bond activation is widely used in formation of the phosphido complexes.[4,11-17] A lot of bases have been used for the formation of phosphido complexes by deprotonating the coordinated PR_2H, including: KOBu^t,[4,10] $LiN(SMe_3)_2$,[11,12] $NaOSiMe_3$,[13] *n*-BuLi,[14] and DBU[15,16] (diaza(1,3)bicycle[5.4.0]undecane). KOBu^t is well behaved in dehydrohalogenation of the indenyl analogues of the Cp*Ru secondary phosphine complexes studied in this

thesis, Ru(η^5-indenyl)Cl(PR_2H)(PPh_3) (**2*i***).[4] There are several reasons for choosing $KOBu^t$ as the appropriate base for generating the indenyl phosphido complexes Ru(η^5-indenyl)(PR_2)(PPh_3) (**6*i***). Firstly, $KOBu^t$ is a sufficiently strong base (the pK_a of the conjugate acid of *t*-butoxide, $HOBu^t$, is 19.2[17]), to deprotonate the P-H bond of coordinated PR_2H ligands. Secondly, the potassium cation facilitates abstraction of the Ru-Cl bond to give an open coordination site at Ru for π-donation of the lone pair of electrons from phosphido ligand. This π-donation gives an "operationally" unsaturated phosphido complex (18 e^-, 5-coordinate) instead of "coordinatively" unsaturated one (16 e^-, 5-coordinate), which is helpful for isolation of phosphido complexes.[18,19,20] In addition, the butoxide anion is bulky, which should discourage formation of such an intermediate containing Ru-OBu^t. If it does form, the absence of β-protons will avoid the β-elimination from a possible Ru-alkoxy intermediate. According to all the reasons above, using $KOBu^t$ for dehydrohalogenation of Cp* secondary phosphine complexes **2a-d** seems to be a good strategy to generate the Cp* phosphido complexes **6a-d** (Scheme 3.1).

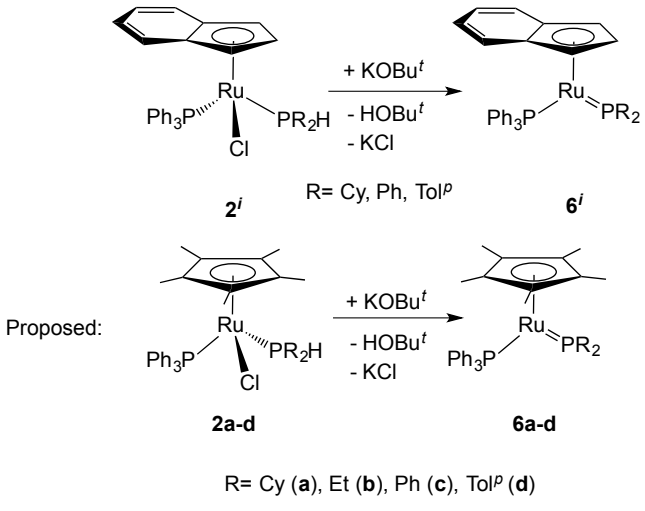

Scheme 3.1 Proposed dehydrohalogenation of the Cp* secondary phosphine complexes **2a-d**.

3.2 Dehydrohalogenation of Ru(η^5-Cp*)Cl(PR_2H)(PPh_3) (2a-d) by $KOBu^t$

The reactions of **2a-d** with $KOBu^t$, as described in detail below, can give planar phosphido complexes **6a-d**. However, dehydrohalogenation of Cp* complexes **2a-d** is relatively slower than that of indenyl analogues. Also, extra complications result from the orthometallation in phosphido complexes **6a-d** (Scheme 3.2), since H_o in a PPh_3 ligand have the potential to reprotonate the phosphido moiety. Although this orthometallation was previously observed for the indenyl analogues,[4] it is much faster for Cp* complexes. The orthometallation reaction can be seen as a simple acid-base reaction. As will be described in detail below, this difference between indenyl and Cp* complexes arises from the more basic phosphido ligand in the Cp* complexes **6a-d** and compression of the ligands around Ru in the Cp* complex. The isolation of Cp* phosphido complexes **6a-d** is difficult because they are too reactive to withstand orthometallation during the dehydrohalogenations.

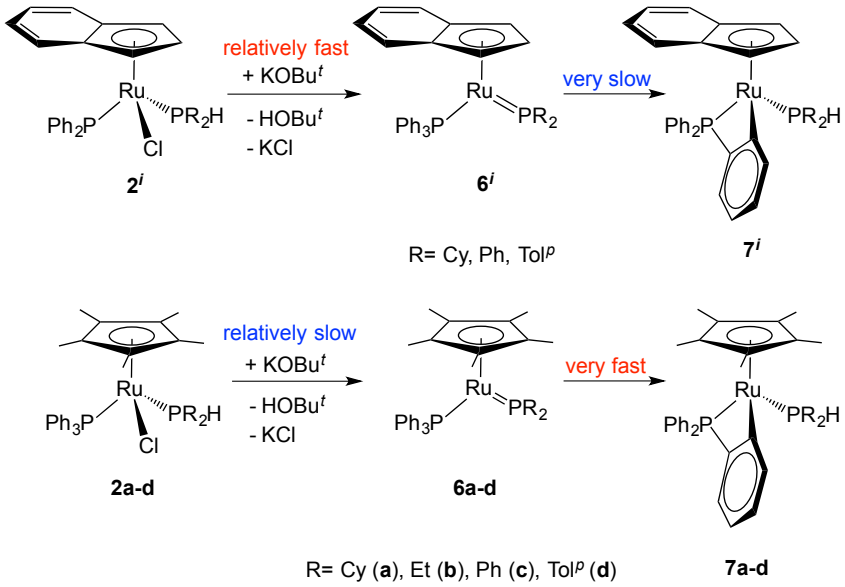

Scheme 3.2 Different dehydrohalogenations between the Cp* secondary phosphine complexes **2a-d** and their indenyl analogues.

3.2.1 Preliminary attempts at dehydrohalogenation in complexes 2a-d

In an NMR-scale reaction, 1 equivalent of $KOBu^t$ was added to a C_6D_6 solution of complexes **2a-d**, and the reaction was monitored by ^1H and $^{31}P\{^1H\}$ NMR spectroscopy. The reaction mixture initially maintained the orange colour of **2a-d** but showed a slight dark red colour (for **2a,b**) or dark blue (for **2c,d**) at the bottom of the NMR tube along with the undissolved $KOBu^t$ (this white powder is slow to dissolve in benzene and toluene that are typically used as the solvents in this chemistry). Shaking the NMR tube caused the entire solution to turn dark red (for **2a,b**) or dark blue (for **2c,d**), indicating the formation of **6a-d**. In the ^1H NMR spectrum, the decrease of signal due to H-P can be a strong evidence to support the successful deprotonation of complexes **2a-d**. In addition, two new doublets (e.g., **6a** δ: 210.8 ppm and 62.8 ppm) start to show in the $^{31}P\{^1H\}$ NMR spectrum. In Figure 3.2, the extreme downfield signal (e.g., **6a** δ: 210.8 ppm) are assigned to the phosphido (PR_2^-) ligand and the signal (**6a** δ: 62.8 ppm), which is in the range expected for coordinated PR_3, is assigned to the PPh_3 ligand. In addition, the coupling constant of phosphido complex **6a** ($^2J_{PP}$ = 72 Hz) is significantly bigger than that of secondary phosphine complex **2a** ($^2J_{PP}$ = 40 Hz), which can be explained by the shorter Ru-P bond caused by π-stabilization of phosphido complexes.[9] The ^{31}P signal due to PR_2 in **6a** appears ~50 ppm upfield from corresponding signal in the $^{31}P\{^1H\}$ NMR spectrum of its indenyl analogue **6*i*a**. For the ^{31}P signal due to PPh_3 ligand, in **6a** this only appears ~6 ppm upfield from **6*i*a**.[21] The more shielded ^{31}P shifts in complex **6a** might be explained by its more electron rich Ru center relative to its indenyl analogue.[9]

However, complexes **6a-d** converted to orthometallated complexes **7a-d**, which have the formula $Ru(\eta^5\text{-Cp*})\{\kappa^2\text{-}(o\text{-}C_6H_4)PPh_2\}(HPR_2)$. In addition to ^{31}P signals due to complexes **6a-d**, two new doublets (e.g., **7a** δ: 58.6 ppm and -18.5 ppm) also show

in the $^{31}P\{^{1}H\}$ NMR spectra. The upfield signal (e.g., **7a** δ: -18.5 ppm) is assigned to the P in the P(*o*-C_6H_4)Ph_2 fragment and the other signal (**7a** δ: 58.6 ppm) is assigned to the PR_2H ligand. These Cp* orthometallated complexes **7a-d** have similar chemical shifts and coupling constants compared to indenyl analogues.[4, 7] In addition, the presence of orthometallated PPh_3 is diagnosed in **7a-d** by an upfield shift of 84 ppm for ^{31}P shifts relative to **2a-d**.[22]

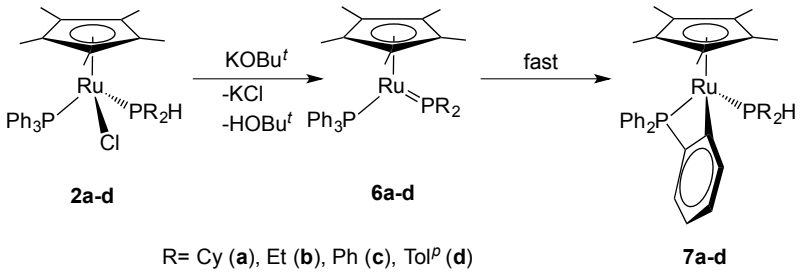

Scheme 3.3 Dehydrohalogenation reactions of complexes **2a-d**.

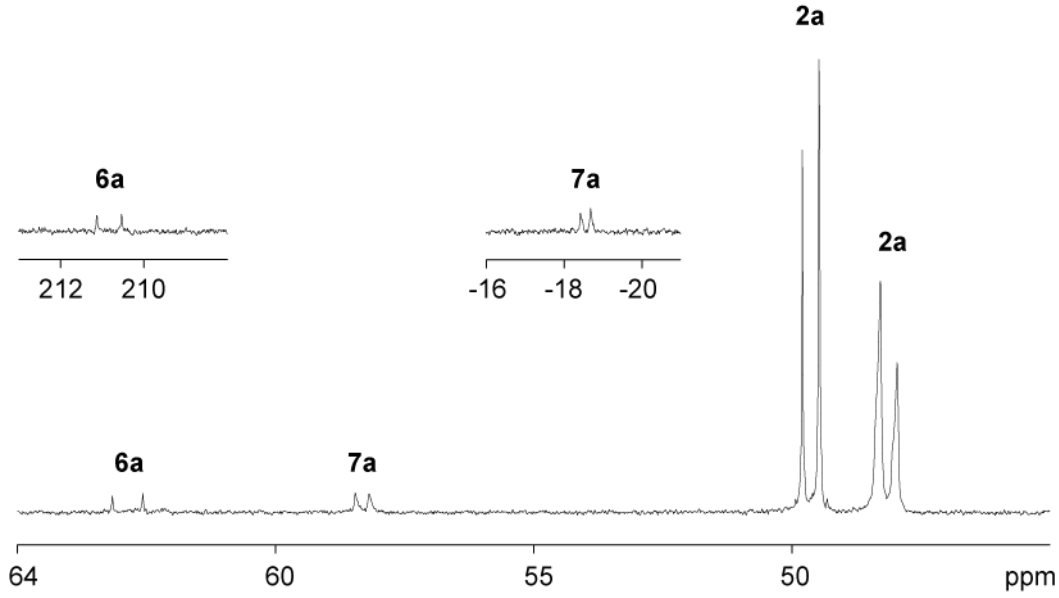

Figure 3.2 $^{31}P\{^{1}H\}$ NMR spectrum (121.55 MHz, C_6D_6) showing the attempted dehydrohalogenation of complex **2a** by KOBu^t in 0.5 h.

In addition, KOBu^t is found to be dissolved slowly in benzene/toluene, the usual solvent used for synthesis of the indenyl phosphido complexes. The reason of using benzene or toluene as the usual solvent for metal phosphido complexes is that these nonpolar solvents are inert to highly reactive phosphido complexes.[23,24] This slow

dissolving issue of KOBu^t in benzene or toluene can affect dehydrohalogenation of complex **2a-d** (*vide infra*). In order to scrupulously investigate the dehydrohalogenation of Cp* complex in NMR scale reactions, it is necessary to allow KOBu^t to completely dissolve in C_6D_6 before adding this mixture to complexes **2a-d**. All subsequent experiments described in this chapter used the method of pre-dissolving the solid base.

3.2.2 Comparison of dehydrohalogenation between Cp* complex 2a and indenyl analogue 2^{i}a

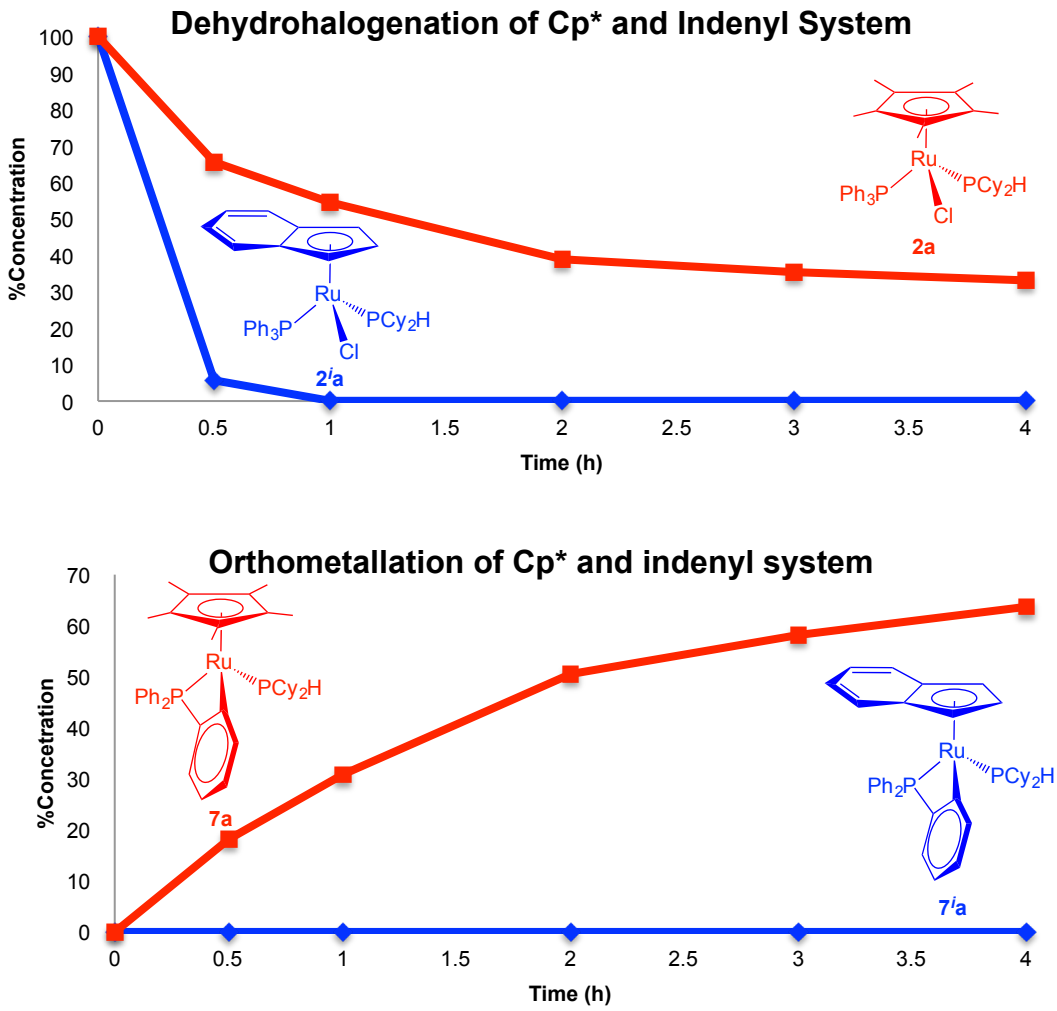

Figure 3.3 The difference in rates of dehydrohalogenation and orthometallation between indenyl complex (**2^{i}a**) and Cp* complex (**2a**) as monitored by ^{1}H NMR spectroscopy.

The reaction of Ru(η^5-indenyl)Cl(PR_2H)(PPh_3) (**2a^i**) with KOBu^t was monitored in order to show the difference of dehydrohalogenations between Cp* secondary phosphine complex **2a** and its indenyl analogue **2^{i}a**. 1.2 equivalent of KOBu^t relative to the complex **2a** and **2^{i}a** was used for their corresponding dehydrohalogenation. The relative concentrations of species in these reactions, as determined by ^{1}H NMR integrations, were plotted vs. reaction time to show the progress of reaction.

Figure 3.3 shows that the rate of dehydrohalogenation for indenyl complex **2^{i}a** is significantly greater than that for Cp* complex **2a**. After 30 min, 93% of **2^{i}a** is consumed, giving only phosphido product **6^{i}a**. The phosphido **6^{i}a** generated from indenyl complex **2a^i** is stable in the solvent, there is no orthometallated complex observed even after 24h. Compared to indenyl analogue, only 34% of **2a** is consumed in 30 min and 53% of the phosphido **6a** formed has already converted to **7a** during this time.

In conclusion, indenyl complex **2^{i}a** appears to have a more acidic P-H relative to the Cp* analogue **2a** because the rate of its deprotonation is faster than **2a** (as described in Chapter 2). On the other hand, the basicity of Cp* phosphido **6a** is much greater than that of indenyl analogous phosphido **6^{i}a**. These different acidities and basicities in these systems may arise from different electronic properties of the Ru center. The CH_3 on Cp* are electron donors, resulting in more electron density at the metal than for the analogous indenyl complex.[25]

3.2.3 Monitoring of the formation of Ru(η^5-Cp*)(PR_2)(PPh_3) (6a-d)

In the previous section, the difference of dehydrohalogenation between the Cp* complex and indenyl analogue was described. I also monitored carefully the dehydrohalogenations of complexes **2a-d** by ^{1}H NMR and ^{31}P{^{1}H} NMR spectroscopy to investigate the effects of different PR_2H ligands on

dehydrohalogenation in the Cp* system. In these experiments, 1.2 equivalent of $KOBu^t$ relative to the complexes **2a-d** was predissolved in C_6D_6, and this mixture was added to complexes **2a-d**. The relative concentrations of species in these reactions, as determined by ^1H NMR integrations, were plotted vs. reaction time to qualitatively show the progress of reaction.

3.2.3.1 The reaction of complex 2a with $KOBu^t$

Complex **2a** (R= Cy) shows the most complicated product mixture of the four reactions studied (Scheme 3.4). 30 min after the $KOBu^t/C_6D_6$ solution is added to complex **2a**, the ^{31}P $\{^1H\}$ NMR spectrum shows the formation of phosphido complex **6a**. In addition to complex **6a**, ^{31}P signals due to orthometallated **7a** are observed (δ: 58.6 ppm and -18.5 ppm) in the $^{31}P\{^1H\}$ NMR spectrum (see Figure 3.4). As mentioned above, the formation of **7a** (18 e^-, 6-coordinate) is because of the PCy_2 basicity and functional unsaturation of phosphido complex **6a** (16 e^-, 5-coordinate). In addition to irreversible orthometallation, the isomerization (i.e. β-H elimination) of **6a** to a phosphaalkene $Ru(\eta^5\text{-Cp*})H(P\{=C(\text{-}C_5H_{10}\text{-})\}Cy)(PPh_3)$ is observed during the reaction. This kind of metallaphosphaalkene was also previously observed for the analogous indenyl phosphido system.[4] Different from orthometallation, this isomerization of the phosphaalkene is reversible. As complex **6a** is consumed by the orthometallation, its phosphaalkene isomer will isomerize to **6a** to maintain the equilibrium of isomerization, which is confirmed by final disappearance of phosphaalkene signal after 8h in $^{31}P\{^1H\}$ NMR spectrum. Interestingly, the phosphaalkene isomer existed longer than phosphido **6a** in the solution. It seems to indicate that the phosphaalkene isomer has low reactivity relative to phosphido complex **6a** and the orthometallation occurs at a greater rate than that of isomerization of phosphaalkene isomer to its phosphido complex **6a**.

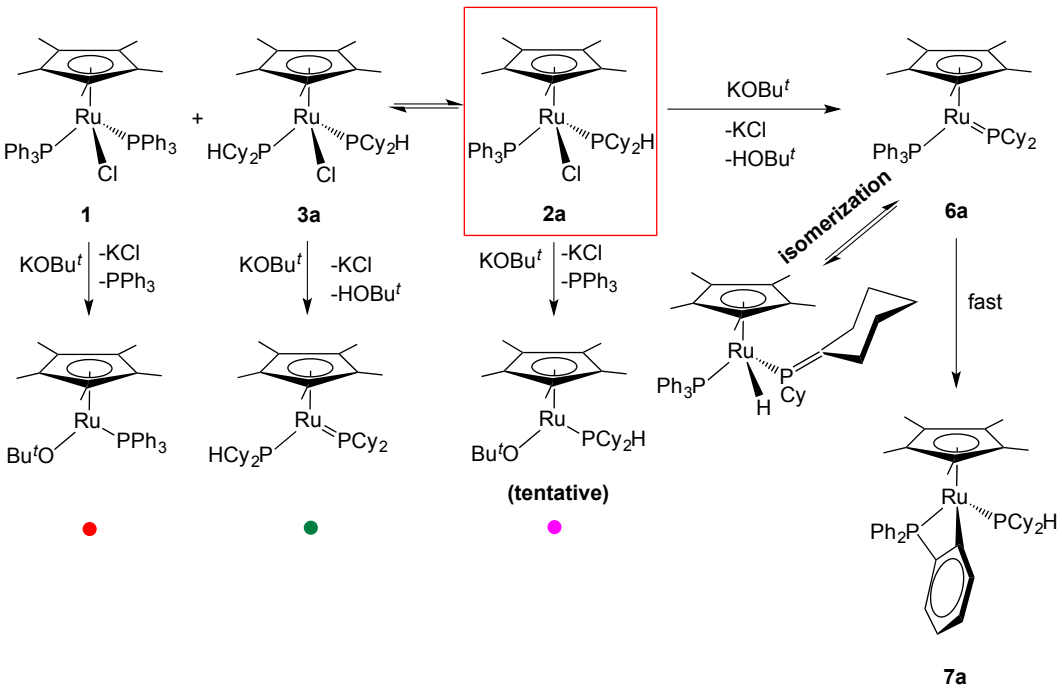

Scheme 3.4 Possible products in NMR scale reaction of complex **2a** with KOBu^t. Coloured dots are used to correlate structures with spectroscopic assignments shown in Figure 3.4.

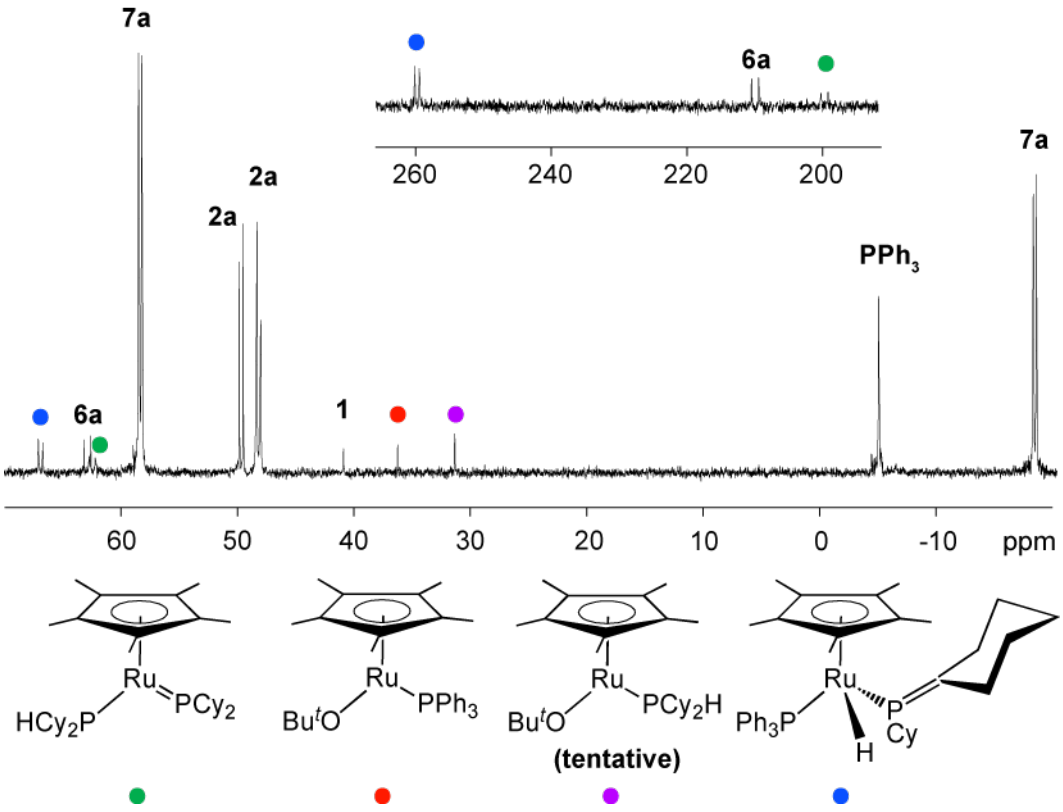

Figure 3.4 The $^{31}P\{^1H\}$ NMR spectrum (121.5 MHz, C_6D_6) showing the reaction of complex **2a** with KOBu^t after 3h.

Different from dehydrohalogenation of indenyl analogue **2*i*a**, the extra complication in this reaction of Cp* complex **2a** arises from its redistribution to Ru(η^5-Cp*)Cl(PPh_3)$_2$ (**1**) and Ru(η^5-Cp*)Cl(PCy_2H)$_2$ (**3a**) (as described in Chapter 2). Both of complex **1** and **3a** can react with KOBu^t to form some extra products. I carried out a control experiment of complex **1** with KOBu^t. The $^{31}P\{^1H\}$ NMR spectrum shows various resulting products. The major product gives a singlet (δ: 36.2 ppm) in the $^{31}P\{^1H\}$ NMR spectrum, as well as a doublet (δ: 1.48 ppm, $^4J_{PH}$ = 1.2 Hz) in the ^1H NMR spectrum, which is assigned to a Cp* Ru alkoxy phosphine complex Ru(η^5-Cp*)(OBu^t)(PPh_3) (red dot in Scheme 3.4). This doublet is the ^1H signal due to CH_3 in Cp*, which shows a small coupling constant to P in the PPh_3 ligand. Some analogous alkoxy complexes were reported by Caulton and coworkers.[26] This 16 e$^-$ complex is stabilized by donation of π-electrons from the X-type ligand (OBu^t) to the metal center (Ru).[18] This Cp* Ru alkoxy complex is soluble in non-polar solvents and can't be isolated. The ^{31}P signal (δ: 31.3 ppm) in the reaction of **2a** is due to another extra product. One possibility for this product is that complex **2a** undergoes substitution to form a secondary phosphine alkoxy complex Ru(η^5-Cp*)(OBu^t)(PCy_2H) (purple dot in Scheme 3.4). However, there is no further evidence to confirm this structure. In addition, since there are two P-H bonds in the complex **3a**, one of the P-H bonds could be deprotonated by KOBu^t to give a new phosphido complex Ru(η^5-Cp*)(PCy_2)(PCy_2H) (green dot in Scheme 3.4). This phosphido complex shows diagnostic ^{31}P signals for Ru-P double bond (δ: 198.5 ppm and $^2J_{PP}$ = 67 Hz), which is slightly different from those of phosphido **6a**. The ^{31}P shift for the PCy_2H ligand in this proposed product (δ: 62.7 ppm) is very similar to that for PPh_3 ligand (δ: 62.8 ppm) in complex **6a**. This ^{31}P signal (δ: 62.7 ppm) also splits in two signals in the ^{31}P NMR spectrum (^1H coupled), which is a strong

evidence for the existence of a P-H bond ($^1J_{PH}$ = ~310 Hz). The isomerization to phosphaalkene is not observed for this new phosphido complex Ru(η^5-Cp*)(PCy_2)(PCy_2H).

Due to the complexity of the reaction of **2a**, only complex **2a**, phosphido **6a**, its phosphaalkene Ru(η^5-Cp*)H(P{=C(-C_5H_{10}-)}Cy)(PPh_3) and orthometallated **7a** are used to make a plot that roughly shows the relation between their relative concentration and reaction time (Figure 3.5). The rate of dehydrohalogenation for **2a** is very slow. The orthometallation is fast for **6a**. For complex **6a**, the rate of orthometallation is much faster relative to its isomerization to phosphaalkene. Although complex **6a** has a basic phosphido PCy_2, the overall orthometallation is slowed down because of the competitive phosphaalkene isomerization of **6a** and slow dehydrohalogenation of **2a**. The overall conversion to orthometallated **7a** is 63 % over 5h. The orthometallation continues to proceed after 5h.

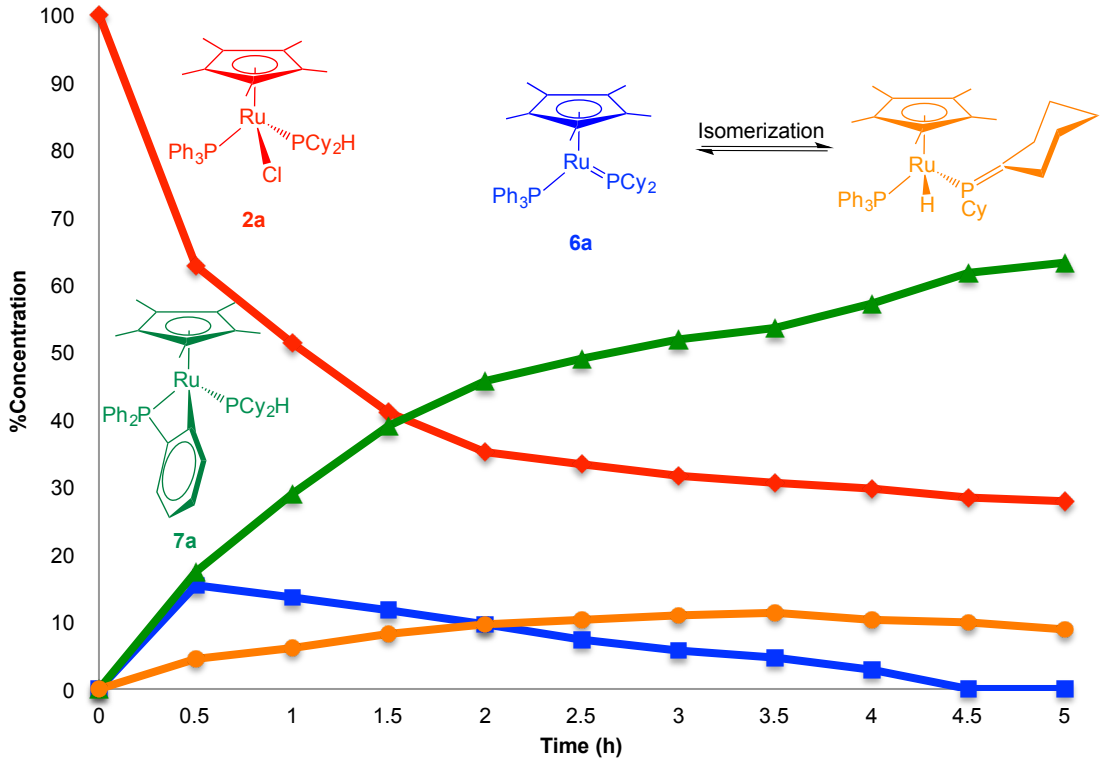

Figure 3.5 The dehydrohalogenation of complex **2a** by $KOBu^t$ monitored by ^1H NMR spectroscopy.

3.2.3.2 The reaction of complex 2b with KOBu^t

Similar to complex **2a**, the complex **2b** (R= Et) reacted with KOBu^t resulting in the formation of the phosphido **6b**. Meanwhile, **6b** irreversibly transformed into orthometallated **7b**. Phosphido **6b** shows diagnostic ^{31}P signal for planar phosphido ligand (PEt$_2$ δ: 183.5 ppm and $^2J_{PP}$ = 72 Hz) and orthometallated **7b** shows diagnostic ^{31}P{^{1}H} NMR signal for metallacycle (P(o-C$_6$H$_4$)Ph$_2$ δ: -10.0 ppm and $^2J_{PP}$ = 33 Hz).[27] The isomerization of phosphido **6b** to its phosphaalkene isomer is not observed during the reaction.

Figure 3.6 shows that the rate of dehydrohalogenation for **2b** is greater than that for **2a** and all **2b** is consumed in 2h. The **2b** has slightly more acidic P-H bond relative to **2a** due to the effect of the substituents of their PR$_2$H ligands.[28] The PEt$_2$H ligand also reduces the steric congestion in **2b**, and the base can easily approach and deprotonate the P-H bond. Similar to **2a**, the orthometallation of **2b** is also fast. The overall conversion to orthometallated **7b** is 95 % over 5h. The orthometallation continues to proceed after 5h.

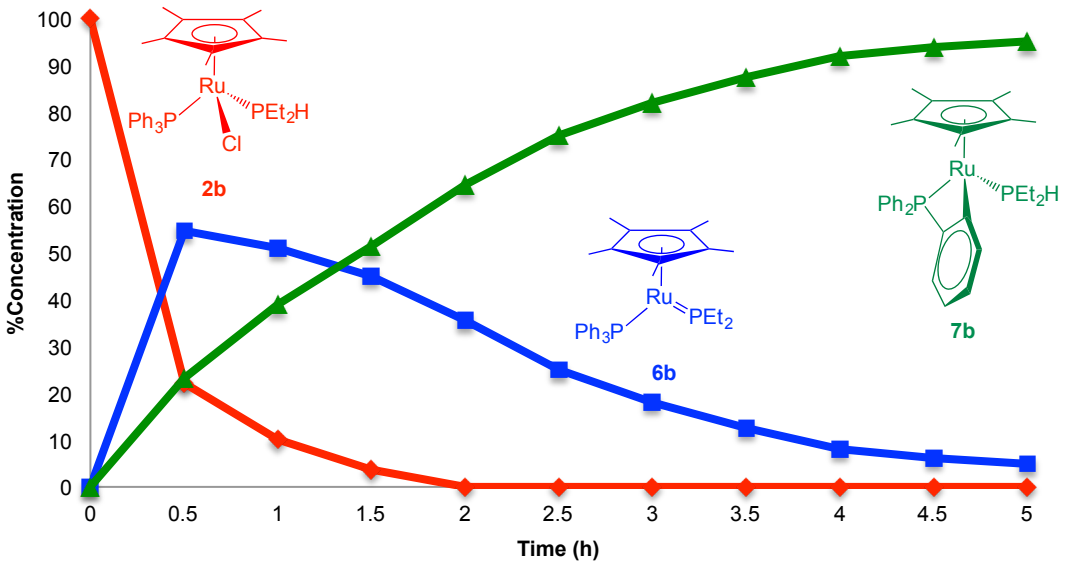

Figure 3.6 The dehydrohalogenation of complex **2b** by KOBu^t monitored by ^{1}H NMR spectroscopy.

3.2.3.3 The reaction of complex 2c with KOBu^t

Different from the dialkylphosphine complexes **2a,b**, the dehydrohalogenation for complex **2c** (R = Ph) gives much faster formation of the phosphido complex **6c**. Similar to dialkyl **2a,b**, diarylphosphido **6c** is also unstable with respect to irreversible isomerization to orthometallated **7c**. Complex **6c** shows diagnostic ^{31}P signal for sp^2 phosphido ligand (PPh$_2$ δ: 156.8 ppm and $^2J_{PP}$ = 67 Hz), which has more upfield shift relative to dialkylphosphido **2a,b**. The complex **7c** also shows diagnostic ^{31}P signal for metallacycle (P(o-C$_6$H$_4$)Ph$_2$ δ: - 13.3 ppm and $^2J_{PP}$ = 32 Hz).

Figure 3.7 shows that the rate of dehydrohalogenation for complex **2c** is greater than that for dialkylphosphine complexes **2a,b** and all complex **2c** is consumed in 0.5h. The orthometallation of **6c** is significantly slower than that of dialkylphosphido complex **6a,b**. The diarylphosphido **6c** converts to orthometallated **7c** over 5h (60 % conversion). The orthometallation continues to proceed after 5h.

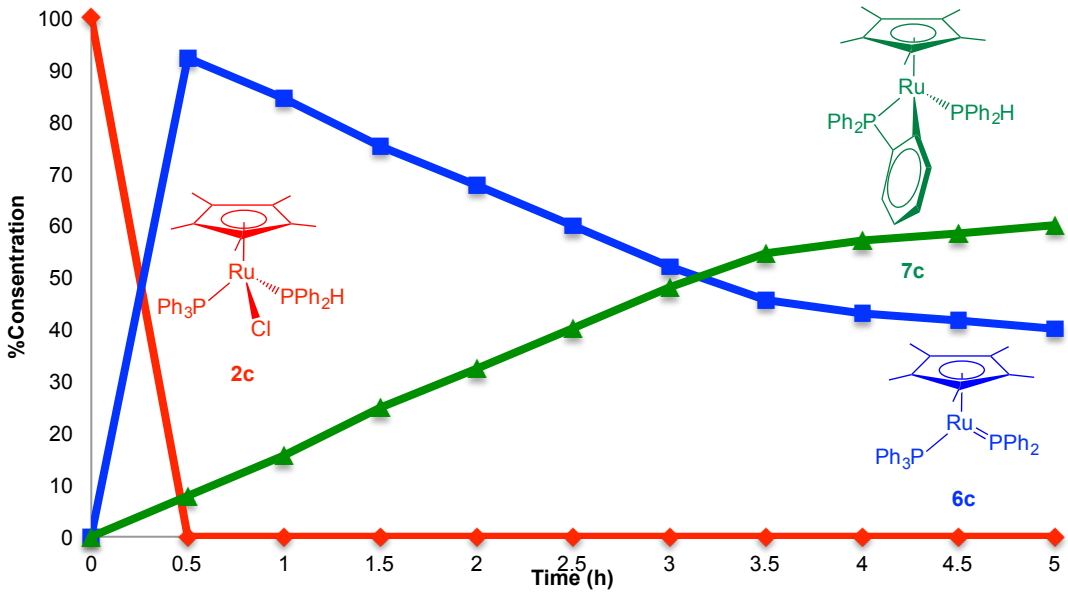

Figure 3.7 The dehydrohalogenation of complex **2c** by KOBu^t monitored by ^{1}H NMR spectroscopy.

3.2.3.4 The reaction of complex 2d with KOBu^t

Similar to the complex **2c**, the complex **2d** is also well behaved in the formation of its phosphido complex **6d**, and then phosphido **6d** converts to orthometallated **7d**. Complex **6d** shows a diagnostic ^{31}P signal for a planar phosphido ligand (PPh$_2$ δ: 159.0 ppm and $^2J_{PP}$ = 67 Hz) and complex **7d** shows diagnostic ^{31}P{^{1}H} NMR signal for metallacycle (P(o-C$_6$H$_4$)Ph$_2$ δ: -13.2 ppm and $^2J_{PP}$ = 32 Hz). All ^{31}P chemical shifts are very similar to those observed in the **2c** reaction.

As illustrated in Figure 3.8, the rate of dehydrohalogenation for complex **2d** is also greater than those for dialkylphosphine complexes **2a,b** and all complex **2d** is consumed in 0.5h. The rate of dehydrohalogenation of complex **2d** is similar to that of complex **2c** and the orthometallation of diarylphosphido complex **6d** is significantly slower than that of dialkylphosphido complexes **6a,b**. The orthometallation of phosphido **6d** is slightly faster relative to phosphido derivative **6c**, which can be explained by the slightly higher basicity of PTol$^p_2$$^-$ in **6d** compared with PPh$_2^-$ in **6c** (Table 1.3 in Chapter 1).[29] The reaction reached 70 % conversion of orthometallated complex **7d** in 5h. The orthometallation continues to proceed after 5h.

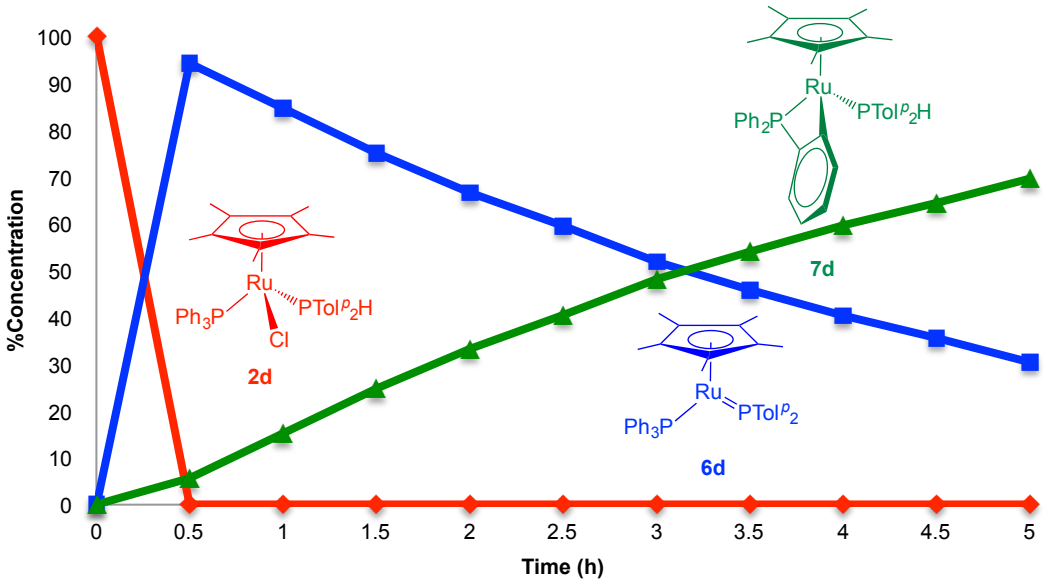

Figure 3.8 The dehydrohalogenation of complex **2d** by $KOBu^t$ monitored by ^1H NMR spectroscopy.

3.2.4 Discussion

The comparison of the dehydrohalogenation/orthometallation of Cp* phosphine/phosphido complexes with their indenyl analogues show that the P-H bond is less acidic and the phosphido ligand is more basic in the Cp* system. Using a stronger base than $KOBu^t$ might result in faster dehydrohalogenation and give a "clean" phosphido complex without before forming orthometallated isomer. In the Cp* system, the dialkyl (**2a,b**) and diaryl (**2c,d**) complexes exhibit different behaviors in dehydrohalogenation and orthometallation. These difference correlate with the acidity of these four PR_2H ligands in the order $PPh_2H > PTol^p_2H > PEt_2H \approx PCy_2H$ (see Section 1.1.1, Chapter 1). [28, 29] The basicity of dialkylphosphido complexes is higher than that of diarylphosphido complexes (slower orthometallation of **6c,d**), which can be explained by the presence of the electron-donating alkyl derivatives.

3.3 Dehydrohalogenation of 2a-d by other base reagents

I also explored the use of some bases other than $KOBu^t$ in dehydrohalogenation of complexes **2a-d**, including DBU (diaza(1,3)bicycle[5.4.0]undecane), $NaOCH_2C(CH_3)_3$ (sodium *tert*-pentoxide) and *n*-BuLi. All these reactions can be helpful to investigate the acidity of the P-H bond in complexes **2a-d** and the Brønsted basicities of phosphido complexes **6a-d**.

In an NMR-scale reaction, 1 equivalent of DBU was added to complexes **2a-d** in C_6D_6, and the reactions were monitored by $^{31}P\{^1H\}$ NMR spectroscopy. The mixture maintains the original orange colour of **2a-d** and the $^{31}P\{^1H\}$ NMR spectrum only shows the presence of **2a-d**. No change is observed after 48h, both visually and by $^{31}P\{^1H\}$ NMR spectroscopy. This observation indicates that DBU (pK_a ($HDBU^+$)

11.5)[30] is not basic enough to deprotonate the P-H bond of secondary phosphine complexes **2a-d**.

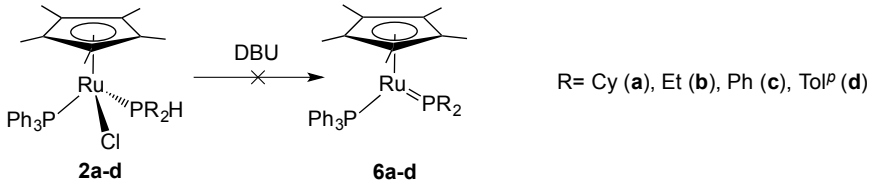

Scheme 3.5 The NMR scale reactions of complex **2a** with 1 equivalent of DBU.

$NaOCH_2C(CH_3)_3$, which is fast to dissolve in benzene and has similar basicity to $KOBu^t$,[31] was used as a reagent for dehydrohalogenation of diarylphosphine complex **2c**. $NaOCH_2C(CH_3)_3$ is well behaved in dehydrohalogenation of **2c**, giving the results that are similar to that by using $KOBu^t$. This base might be a good basic reagent in large synthetic scale reactions. However, for reactions monitored spectroscopically, the signal due to the *tert*-pentoxide anion can overlap with some signals due to alkyl protons in the resulting product(s), especially for the reactions of **2a,b**. The $KOBu^t$ is the better choice for studying the Cp* complexes **2a-d** in NMR-scale reaction.

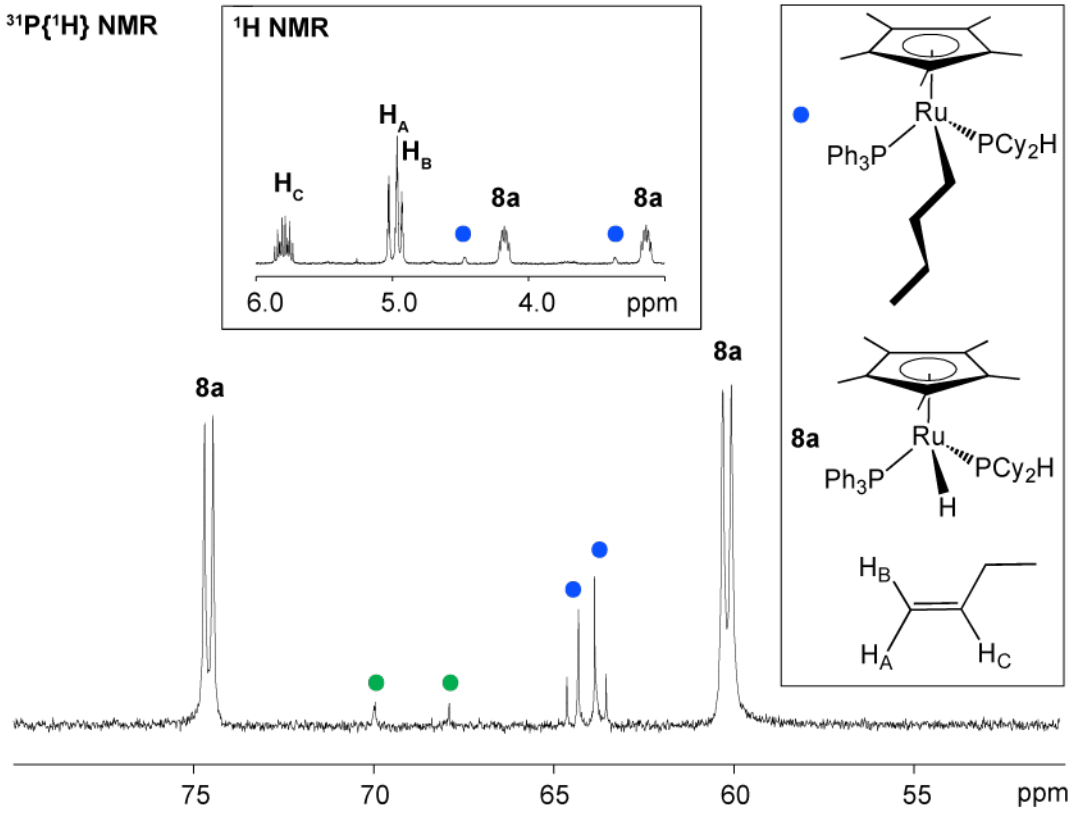

Figure 3.9 The $^{31}P\{^{1}H\}$ NMR spectrum (121.55 MHz, C_6D_6) and partial ^{1}H NMR spectrum (300.27 MHz, C_6D_6, inset) showing the reaction of complex **2a** with *n*-BuLi after 0.5 h. The signals due to unidentified products are labeled as green dot.

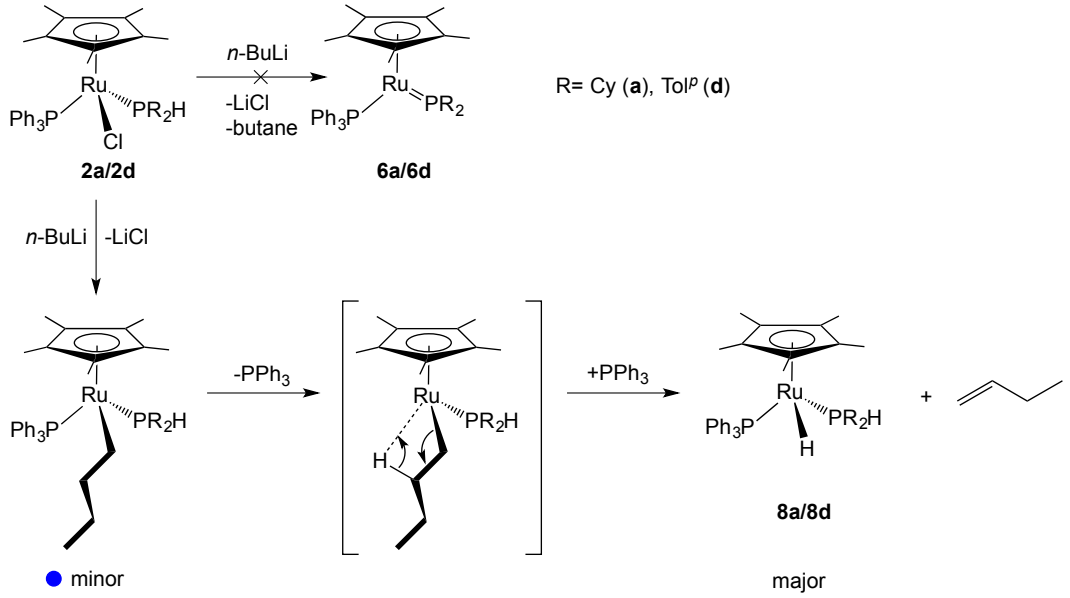

Scheme 3.6 Possible NMR scale reactions of complexes **2a/2d** with 1 equivalent of *n*-BuLi.

1 equivalent of *n*-BuLi (pK_a (BuH) ~50)[32] was added to dialkylphosphine complex **2a** and diarylphosphine complex **2d** in NMR tubes containing C_6D_6. The mixture changed from the original orange colour of **2a/2d** to a bright red colour immediately, but the $^{31}P\{^{1}H\}$ NMR showed no formation of phosphido complexes **6a/6d**. Instead, hydride complex Ru(η^5-Cp*)H(PR_2H)(PPh_3) (**8a/8d**) are observed as major products in both the ^{1}H and $^{31}P\{^{1}H\}$ NMR spectra (Figure 3.9). These complexes show diagnostic upfield ^{1}H NMR signals as a triplet due to H-Ru coupled to two P in PR_2H and PPh_3 (e.g., **8d** δ: -12.50 ppm) and $^{31}P\{^{1}H\}$ NMR signals as two doublet (**8d** δ: 74.6 ppm and 42.9 ppm, $^{2}J_{PP}$ = 33 Hz). The NMR characterizations of the hydride complexes **8a-d** are described in Chapter 4. In addition, two other doublet signals (e.g., for **2d** δ: 49.3 ppm and 61.8 ppm, $^{2}J_{PP}$ = 41 Hz) are observed in the $^{31}P\{^{1}H\}$ NMR spectra as well, which are tentatively assigned to alkyl complexes Ru(η^5-Cp*)($CH_2CH_2CH_2CH_3$)(PR_2H)(PPh_3) (blue dot in Scheme 3.6). Visually, some

white precipitate is present at the bottom of the NMR tube，indicative of the formation of solid LiCl. It seems that these alkyl complexes result from chloride substitution by *n*-BuLi. The free PPh_3 signal was observed at the beginning of the reaction, but disappeared later. The signal due to the alkyl complex also eventually disappeared. All these observations suggest a possible mechanism for reactions of complexes **2a/2d** with *n*-BuLi (Scheme 3.6): the chloride ligand is substituted by *n*-BuLi to give alkyl complexes $Ru(\eta^5\text{-}Cp^*)(CH_2CH_2CH_2CH_3)(PR_2H)(PPh_3)$ and LiCl. The PPh_3 ligand on this alkyl complex is labile and dissociates to give a coordination site that allows β-elimination of alkyl group to eventually form the major product hydride complexes **8a/8d**. In addition, the ^1H NMR spectrum shows the signals of vinyl protons on 1-butene, the formation of 1-butene is strong evidence for the formation of alkyl complexes. *n*-BuLi shows completely different reactivity relative to $KOBu^t$ due to its much high basicity. Katritzky et al. reported a competing reaction in 4-bromoimidazole between N-H bond deprotonation and dehalogenation using *n*-BuLi, which shows that dehalogenation is easier than deprotonation for *n*-BuLi in that situation.[33]

3.3 Synthesis and detailed characterization of orthometallated complex $Ru(\eta^5\text{-}Cp^*)\{\kappa^2\text{-}(o\text{-}C_6H_4)PPh_2\}(PR_2H)$ (7a-d)

All orthometallated complexes **7a-c** (generated in NMR scale reactions) and **7d** (isolated) were characterized by using 1D NMR and 2D NMR spectroscopy as described below.

3.3.1 Synthesis of orthometallated complex 7d

As mention above (Section 3.2.4), diarylphosphido complexes **6c,d** are relatively stable. Since complex **2c** always contains some disubstituted complex **3c** and both of

them undergo the dehydrohalogenation, complex **2d** might be a good starting material to synthesize and isolate Cp* phosphido **6**. We attempted to isolate phosphido complex **6d**, but the resulting product was always mixed with the orthometallated **7d**. Therefore the orthometallated **7d** was deliberately prepared on a synthetic scale to allow the full characterization by NMR spectroscopy (reactions see Scheme 3.3). The mixture was stirred for approximately 24h to make sure 100% conversion to orthometallated complex before the isolation.

3.3.2 Detailed characterization of Ru(η^5-Cp*){κ^2-(*o*-C_6H_4)PPh_2}(PR_2H) (7a-d)

As describe above, these complexes show diagnostic ^{31}P NMR signals for P in 4-membered metallacycle (e.g., **7b** *P*(*o*-C_6H_4)Ph_2 δ: -10.0 ppm, $^2J_{PP}$ = 33Hz) and PR_2H (e.g., **7b** *P*Et_2H δ: 43.5 ppm). Signals due to all protons and carbons on the *o*-C_6H_4 fragment attached to Ru and P in complexes **7a-d** have been assigned in the ^1H and $^{13}C\{^1H\}$ NMR spectra. The orthometallated complexes with dialkylphosphine (**7a,b**) have less complicated aromatic signals relative to diaryl complexes **7c,d**. In addition, as described above (Section 3.2.3.1), complex **7a** is not the only product in the reaction. As a result, the characterization of complex **7b** is used as a starting point to show how each proton and carbon on the *o*-C_6H_4 fragment is assigned. The assignment for protons and carbons on the *o*-C_6H_4 fragment in the rest of orthometallated complexes (**7a,c,d**) is based on the characterization of orthometallated **7b**. The H_D (δ: 7.60-7.54 ppm) is assigned by its nOe interactions with the protons of Cp* ligand and PEt_2H ligand shown in the ^1H-NOESY spectrum (Figure 3.10). The C_D signal (δ: 136.5 ppm) is identified by correlation with H_D in the $^1H/^{13}C\{^1H\}$-HSQC spectrum. The rest of the protons and carbons on the *o*-C_6H_4 fragment can be identified by their correlation with H_D and C_D in the $^1H/^{13}C$-HSQC and HMBC spectra. The other protons and carbons are easily identified by the

$^{1}H/^{13}C\{^{1}H\}$-HSQC and HMBC spectrum. Both of the ^{1}H and $^{13}C\{^{1}H\}$ NMR spectra for **7b** show distinct signals for each of the Et groups in PEt_2H and each of Ph groups in P(*o*-C_6H_4)Ph_2 fragment, since all these groups are diastereotopic because of the chirality at Ru.

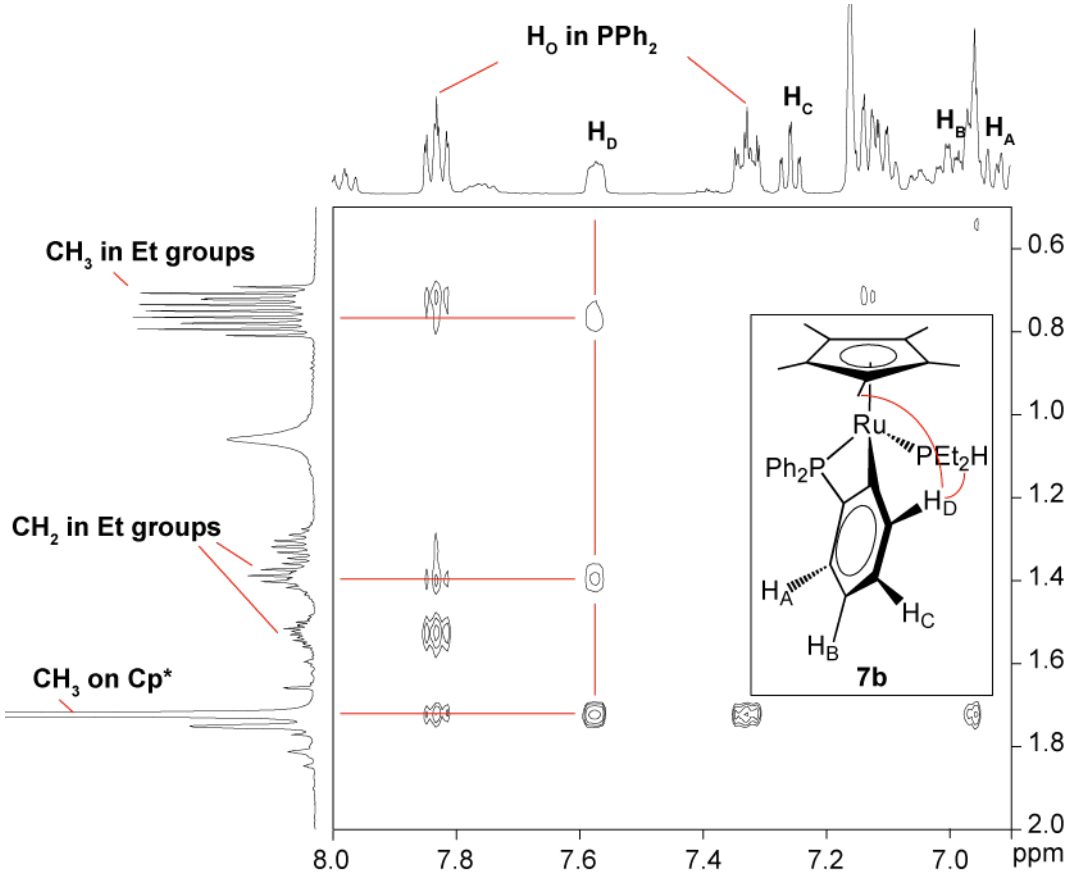

Figure 3.10 Partial ^{1}H-NOESY NMR spectrum (500.27 MHz, C_6D_6) of reaction of [**2b** + $KOBu^t$] after 24h highlighting the interactions between H_D and protons on ethyl group/methyl protons on Cp* ligand in orthometallated **7b**.

3.4 Effects on dehydrohalogenation of 2a-d caused by slow dissolving of $KOBu^t$

As stated in the Section 3.2.1, the $KOBu^t$ is slow to dissolve in benzene/toluene, which will affect the dehydrohalogenation of complexes **2a-d**. In this section, two experimental methods are investigated to show the effect on dehydrohalogenation caused by slow dissolving of $KOBu^t$ in benzene.

Due to the relatively fast dehydrohalogenation of diarylphosphine complexes, the complex **2c** was used to compare the difference between these two methods:

Method 1 is to add the C_6D_6 as a solvent to the solid mixture of the complex **2c** and base, and Method 2 is to allow the base to completely dissolve in C_6D_6 24h before adding this mixture to solid **2c**. Since complex **2c** is readily soluble in C_6D_6, while the base dissolves very slowly, Method 1 provides a slow delivery of low concentrations of base to the reaction, while Method 2 ensure a high initial concentration of base. Both of the methods are monitored by ^1H and $^{31}P\{^1H\}$ NMR spectrum over 4h. The relative concentrations of species in these reactions, as determined by ^1H NMR, were plotted vs. reaction time to roughly show the progress of reaction (Figure 3.11).

There is a significant difference between two methods (Figure 3.11). Due to the slow dissolving of $KOBu^t$ in benzene, the rate of dehydrohalogenation for Method 1 is much slower than that for Method 2. Correspondingly, the rate of orthometallation for Method 1 is slower than that for Method 2.

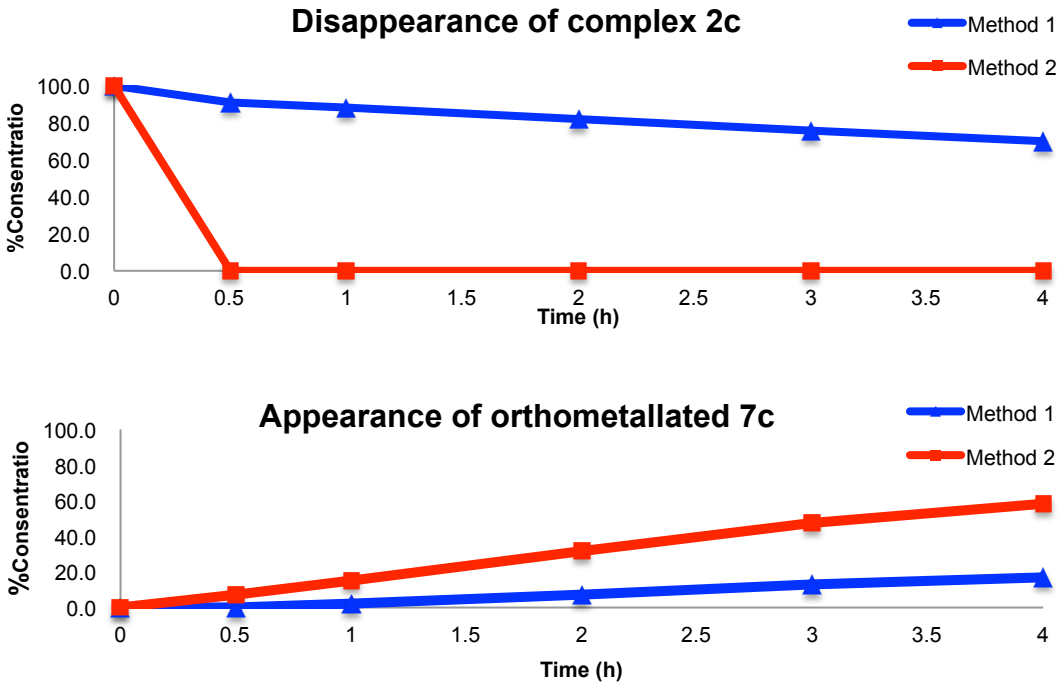

Figure 3.11 Comparison of relative rates of dehydrohalogenation and orthometallation using Methods 1 and 2 in the reaction of [**2c** + $KOBu^t$].

In conclusion, both of these methods can be useful in the study of Cp* complexes **2a-d**. Method 2 is a better method for monitoring the dehydrohalogenation of complexes **2a-d** by KOBu^t and obtaining a maximum (early) conversion to the phosphido complexes **6a-d**. Method 1 should be a better method for exploring the reactivity of **6a-d** with various trapping reagents (see Chapter 4), since it slows down and minimizes the competing orthometallation reaction.

3.5 Conclusion

In this Chapter, I show that complexes **2a-d** undergo dehydrohalogenation by using KOBu^t to form phosphido complexes **6a-d**, similar to their indenyl analogues. Several experimental methods for these dehydrohalogenations and the use of some other bases are tried to optimize the formation of phosphido complexes **6a-d**. According to the monitoring of the formation of the phosphido **6a-d**, the results show that dialkylphosphine complexes **2a,b** have less acidic P-H bond than that in diarylphosphine complexes **2c,d**, and their corresponding dialkylphosphido **6a,d** have more basic phosphido ligand than those of the diarylphosphido complexes **6c,d**. Decomposition *via* orthometallation occurs fast in Cp* phosphido complexes **6a-d**.

The Cp* complex **2a** shows a less acidic P-H bond relative to its indenyl analogue **2^{i}a**, and Cp* phosphido **6a** has a more basic phosphido ligand compared with the indenyl phosphido **6^{i}a**. Due to these difference, it is challenging to generate and isolate the Cp* phosphido complexes **6a-d**. In order to investigate the reactivity of Cp* phosphido complexes **6a-d**, trapping the phosphido *via* Method 1 can be a good strategy, since it allows the slow generation of **6a-d** *in situ* while minimizing the competing orthometallation.

3.6 Experimental

See Chapter 2, Section 2.6.1 for general experimental detail. NMR samples monitoring the progress of reaction were prepared in J. Young tubes. Complexes $Ru(\eta^5\text{-}Cp^*)Cl(PR_2H)(PPh_3)$ (**2a-d**) were prepared as described in Chapter 2 (Section 2.6.3). Potassium *tert*-butoxide ($KOBu^t$), sodium *tert*-pentoxide ($NaOCH_2C(CH_3)_3$), *n*-butyl lithium (*n*-BuLi) and diaza(1,3)bicycle[5.4.0]undecane (DBU) were purchased from Aldrich Chemical Co. and used as received without further purification. The spectroscopic data is available for most major species identified in the NMR-tube reactions performed in this chapter. The ^1H and ^{13}C NMR data can be found in Tables 3.3 - 3.4.

3.6.1 Preliminary attempts at dehydrohalogenation of 2a-d

1 mL of C_6D_6 was added to the mixture of solid base and metal complex in a small vial. This mixture was transferred to an NMR tube. The reaction was monitored by ^1H and $^{31}P\{^1H\}$ NMR (Method 1 as described in Section 3.4).

3.6.2 General method for monitoring the dehydrohalogenation of 2a-d

1 mL of C_6D_6 was added to the solid base in a small vial, to allow it to completely dissolve. After 24h, the metal complex was added to this solution and the mixture was transferred to an NMR tube. Solid (**2a:** 12 mg, 0.016 mmol; **2b:** 10 mg, 0.016 mmol; **2c:** 10 mg, 0.016 mmol; **2d:** 12 mg, 0.016 mmol) and an excess of $KOBu^t$ (2 mg, 0.018 mmol) were used. The initially orange solution turned dark red (for **2a,b**) or blue (for **2c,d**) quickly, and eventually turned orange again. The reaction was monitored over 5h. The reaction was monitored by ^1H and $^{31}P\{^1H\}$ NMR spectroscopy (Method 2 as described in Section 3.4). The tube was shaken between

each measurement. $^{31}P\{^{1}H\}$ NMR spectra for the period of monitoring are in Appendix C.

3.6.2.1 Reaction of 2a with KOBu^t

After 0.5h unreacted complex **2a** (63%), phosphido **6a** (15%), orthometallated **7a** (17%) and phosphaalkene isomer Ru(η^5-Cp*)H(P{=C(-C_5H_{10}-)}Cy)(PPh_3) (5%) were observed. $^{31}P\{^{1}H\}$ NMR data are reported in Table 3.1 (for **6a**) and Table 3.2 (for **7a**). Some other products are described in Chapter 3, Section 3.2.3.1.

3.6.2.2 Reaction of 2b with KOBu^t

After 0.5h unreacted complex **2b** (22%), phosphido **6b** (55%) and orthometallated **7b** (23%) were observed. $^{31}P\{^{1}H\}$ NMR data are reported in Table 3.1 (for **6b**) and Table 3.2 (for **7b**).

3.6.2.3 Reaction of 2c with KOBu^t

After 0.5h, phosphido **6c** (92%) and orthometallated **7c** (8%) were observed. $^{31}P\{^{1}H\}$ NMR data are reported in Table 3.1 (for **6c**) and Table 3.2 (for **7c**).

3.6.2.4 Reaction of 2d with KOBu^t

After 0.5h, phosphido **6d** (94%) and orthometallated **7d** (6%) were observed. $^{31}P\{^{1}H\}$ NMR data are reported in Table 3.1 (for **6d**) and Table 3.2 (for **7d**).

Table 3.1 121.55 MHz $^{31}P\{^{1}H\}$ NMR data for Cp* phosphido complex **6a-d** in C_6D_6 at 300 K: δ (ppm) (multiplicity, $^{2}J_{PP}$ (Hz))

Complex		PR_2	PPh_3
Ru(η^5-Cp*)(PCy_2)(PPh_3)	**6a**	210.8 (d, 22)	62.9 (d)
Ru(η^5-Cp*)(PEt_2)(PPh_3)	**6b**	183.6 (d, 72)	61.5 (d)
Ru(η^5-Cp*)(PPh_2)(PPh_3)	**6c**	156.5 (d, 67)	56.2 (d)
Ru(η^5-Cp*)($PTol^p_2$)(PPh_3)	**6d**	158.8 (d, 68)	56.6 (d)

Table 3.2 202.47 MHz $^{31}P\{^{1}H\}$ NMR data for Cp* orthometallated complex **7a-d** in C_6D_6 at 300 K: δ (ppm) (multiplicity, $^{2}J_{PP}$ (Hz)).

Complex		-(*o*-C_6H_4)Ph_2P-	PR_2H
[Ru(η^5-Cp*){κ^2-(*o*-C_6H_4)PPh_2}(PCy_2H)]	**7a**	-18.5 (d, 32)	58.3 (d)
[Ru(η^5-Cp*){κ^2-(*o*-C_6H_4)PPh_2}(PEt_2H)]	**7b**	-9.8 (d, 34)	43.6 (d)
[Ru(η^5-Cp*){κ^2-(*o*-C_6H_4)PPh_2}(PPh_2H)]	**7c**	-13.6 (d, 31)	48.6 (d)
[Ru(η^5-Cp*){κ^2-(*o*-C_6H_4)PPh_2}($PTol^p_2H$)]	**7d**	-13.3 (d, 33)	46.9 (d)

3.6.2.5 Reaction of Ru(η^5-indenyl)Cl(PCy_2H)(PPh_3) (2^i**a**) with $KOBu^t$

Solid **2^{i}a** (12 mg, 0.017 mmol) and an excess of $KOBu^t$ (2 mg, 0.018 mmol) were used. The initially orange solution turned deep blue immediately. After 0.5h, phosphido **6a^i** and phosphaalkene Ru(η^5-indenyl)H(P{=C(-C_5H_{10}-)}Cy)(PPh_3) were observed. $^{31}P\{^{1}H\}$ NMR (C_6D_6, 121.55 MHz) δ ppm: 275.8 (d, $^{2}J_{PP}$ = 66 Hz, phosphido, *P*Cy_2), 242.9 (d, $^{2}J_{PP}$ = 36 Hz, phosphaalkene, *P*=C(-C_5H_{10}-)Cy), 62.9 (d, phosphido, *P*Ph_3), 61.8 (d, phosphaalkene, *P*Ph_3)

3.6.3 Reaction of 2a-d with DBU

Solid **2** (**2a:** 12 mg, 0.016 mmol; **2b:** 10 mg, 0.016 mmol; **2c:** 12 mg, 0.017 mmol; **2d:** 12 mg, 0.016 mmol) and an excess of DBU (3mg, 0.020 mmol) were used. The initially orange solution kept the same colour over 48h. Only signals due to complex **2a-d** were observed over 48 h.

3.6.4 Reaction of 2a-d with $NaOCH_2C(CH_3)_3$

Solid **2** (**2a:** 12 mg, 0.016 mmol; **2b:** 10 mg, 0.016 mmol; **2c:** 12 mg, 0.017 mmol; **2d:** 12 mg, 0.016 mmol) and an excess of $NaOCH_2C(CH_3)_3$ (3mg, 0.020 mmol) were used. The initially orange solution turned dark red (for **2a,b**)/deep blue (for **2c,d**), and eventually turned orange again. The products are similar to that by using

$KOBu^t$. $^{31}P\{^1H\}$ NMR data is reported in Table 3.1 (for **6a-d**) and Table 3.2 (for **7a-d**).

3.6.5 Reaction of dialkylphosphine complex 2a/2d with *n*-BuLi

1 mL of C_6D_6 was added to solid **2** (**2a**: 12 mg, 0.016 mmol; **2d**: 12 mg, 0.016 mmol) in a J. Young NMR tube, and then a slight excess of *n*-BuLi (8 μL, 0.020 mmol, 2.5 M) was added to this mixture by syringe. The reaction was monitored by ^1H and $^{31}P\{^1H\}$ NMR. The tube was shaken before the measurement. The initially orange solution turned dark red, and eventually turned yellow. For 0.5h reactions, hydride complexes **8** are observed as major products. $^{31}P\{^1H\}$ NMR data are reported in Table 4.1. Some other products are described in Chapter 3, Section 3.3.

3.6.6 Attempted isolation of Ru(η^5-Cp*)(PTol$^p_2$)(PPh$_3$) (6d)

10 mL of benzene was added to a flask containing **2d** (139 mg, 0.19 mmol) and an excess of $KOBu^t$ (23mg, 0.21 mmol), which caused the orange solution to turn deep blue. The mixture was stirred for 5h at RT, and then the solution was filtered through Celite to remove solid and gelationous byproduct KCl and $HOBu^t$. The benzene was removed under vacuum. Trituration of the resulting blue oily residue with pentane (2 x 10 mL) gave a tacky blue solid (crude yield 42 mg, 0.059 mmol, 31%). The resulting product contains a major product of ~79% phosphido **6d** and an impurity of ~21% of orthometallated **7d**.

3.6.7 Synthesis of Ru(η^5-Cp*){κ^2-(*o*-C$_6$H$_4$)PPh$_2$}(PTol$^p_2$H) (7d)

10 mL of benzene was added to a Schlenk flask containing complex **2d** (0.10 g, 0.13 mmol) and $KOBu^t$ (0.018 g, 0.16 mmol). The solution was stirred for 24h. The resulting brown solution was filtered through Celite to remove solid and gelatinous byproducts KCl and $HOBu^t$. The benzene was removed under vacuum, and the

resulting brown paste was dissolved in 10 mL of pentane. The pentane was removed under vacuum to give a yellow powder (0.030 g, 0.042 mmol, yield 32%). $^{31}P\{^{1}H\}$ NMR data is in Table 3.2. Dec. point: 178-180 °C. IR (KBr, cm^{-1}): 2304 (w, ν_{PH}). The complex **7d** is contaminated with grease (see in ^{1}H NMR), and grease can't be washed out by pentane because **7d** is also soluble in pentane. This is why no microanalysis reported.

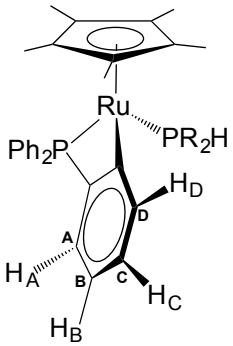

Figure 3.12 Structure of orthometallated **7** showing locations of *o*-C_6H_4 protons $H_{A\text{-}D}$ and corresponding carbons $C_{A\text{-}D}$.

Table 3.3 500.27 MHz ^{1}H NMR data for Ru(η^5-Cp*)\{κ^2-(*o*-C_6H_4)PPh_2\}(PR_2H) **7a-d** in C_6D_6 at 300 K: δ in ppm (multiplicity, RI, J_{avg} or $\omega_{1/2}$ in Hz, assignment).[a]

	η^5-Cp*	**κ^2-(*o*-C_6H_4)PPh_2**	**PR_2H**
7a	1.67 (s, 15H)	**Ph:** **H_o** 7.81 (dd, 2H, $^{3}J_{PH}$ 10.0, $^{3}J_{HH}$ 7.9), 7.50 (dd, 2H, $^{3}J_{PH}$ 10.2, $^{3}J_{HH}$ 7.7) **$H_{m,p}$** 7.14-6.94 [m, H_m and H_p overlapping,6H (also overlap with H_B in -C_6H_4-)] **κ^2-(*o*-C_6H_4):** **H_D** 7.67-7.61 (m, 1H) **H_C** 7.26 (t, 1H, $^{3}J_{HH}$ 7.4) **H_B** 7.03-7.01 (m, overlaps with H_m and H_p on Ph ring, 1H) **H_A** 6.87 (dd, 1H, $^{3}J_{PH}$ 10.7, $^{3}J_{HH}$ 7.7)	**H-PCy_2** 4.08 (d, 1H, $^{1}J_{PH}$ 309.2) **Cy:** 1.92-1.71 (m, 5H), 1.63-1.26 (m, 9H), 1.12-0.88 (m, 8H)
7b	1.72 (t, $^{4}J_{PH}$ 1.6 Hz)	**Ph:** **H_o** 7.83 (ddd, 2H, $^{3}J_{PH}$ 10.0, $^{3}J_{HH}$ 7.7, $^{5}J_{PH}$ 1.5), 7.36-7.29 (m, 2H) **$H_{m,p}$** 7.15-7.07 (m, H_m and H_p overlapping, 4H) **H_m** 6.98-6.94 (m, 2H) **κ^2-(*o*-C_6H_4):**	**H-PEt_2** 3.95 (d, 1H, $^{1}J_{PH}$ 316.8) **CH_2** 1.58-1.47 (m, 1H), 1.45-1.25 (m, 3H) **CH_3** 0.82-0.66 (m, 6H)

		H_D 7.60-7.54 (m, 1H) **H_C** 7.25 (td, 1H, $^3J_{HH}$ 7.4, $^4J_{PH}$ 1.3) **H_B** 7.02-6.98 (m, 1H) **H_A** 6.92 (dd, 1H, $^3J_{PH}$ 10.7, $^3J_{HH}$ 7.3)	
7c	1.59 (s, 15H)	**Ph:** **H_o** 7.55-7.42 (m, 4H) **$H_{m,p}$** 7.10-6.99 [m, H_m and H_p overlapping, 3H (*also overlap with H_B in -C_6H_4- and H_o in PPh_2H)] **H_p** 6.91-6.85 (m, overlaps with H_m and H_p in PPh_2H, 1H) **H_m** 6.85-6.78 (m, 2H) **κ^2-(*o*-C_6H_4):** **H_D** 7.76-7.68 (m, 1H) **H_C** 7.40-7.29 (m, overlaps with H_o in PPh_2H, 1H) **H_B** 7.10-6.99 [m, overlaps with H_m and H_p on Ph ring of metallacycle, 1H (*also overlaps with H_o in PPh_2H)] **H_A** 6.98-6.92 (m, overlaps with H_m and H_p in PPh_2H, 1H)	**H-PPh_2** 6.36 (d, 1H, $^1J_{PH}$ 337.8, $^3J_{PH}$ 5.1) **H_o** 7.40-7.29 (m, overlaps with H_C in -C_6H_4-, 2H), 7.10-6.99 [m, overlaps with H_B in -C_6H_4-, 2H (*also overlaps with H_m and H_p on Ph ring of metallacycle)] **H_m** 6.98-6.92 (m, overlaps with H_A in -C_6H_4- and H_p in PPh_2H, 2H), 6.91-6.85 (m, overlaps with H_p on Ph ring of metallacycle and H_p in PPh_2H, 2H) **H_p** 6.98-6.92 (m, overlaps with H_A in -C_6H_4- and H_m in PPh_2H, 1H), 6.91-6.85 (m, overlaps with H_p on Ph ring of metallacycle and H_m in PPh_2H, 1H)
7d	1.64 (s, 15H)	**Ph:** **H_o** 7.55 (dd, 2H, $^3J_{PH}$ 10.1, $^3J_{HH}$ 7.7), 7.36-7.30 (m, overlap with H_C in -C_6H_4-, 2H) **$H_{m,p}$** 6.99-6.92 [m, H_m and H_p overlapping, 3H (*also overlap with H_A in -C_6H_4-)] **H_p** 6.92-6.89 (m, 1H) **H_m** 6.86-6.81 (m, 2H) **κ^2-(*o*-C_6H_4):** **H_D** 7.77-7.73 (m, 1H) **H_C** 7.39-7.36 (m, overlaps with H_o in $PTol^p{}_2H$ and H_o on Ph ring of	**H-$PTol^p{}_2$** 6.37 (d, 1H, $^1J_{PH}$ 337.5, $^3J_{PH}$ 5.7) **H_o** 7.45-7.39 (m, overlap with H_C in -C_6H_4-, 2H), 7.02 (dd, 2H, $^3J_{PH}$ 10.3, $^3J_{HH}$ 7.8) **H_m** 6.87 (d, 2H, $^3J_{HH}$ 7.8), 6.76 (d, 2H, $^3J_{HH}$ 7.6) **CH_3** 2.12 (s, 3H), 1.98 (s, 3H)

metallacycle, 1H)
H_B 7.10-7.05 (m, 1H)
H_A 6.99-6.92 (m, overlaps with H_m and H_p on Ph ring of metallacycle, 1H)

[a] Structure illustrating locations of *o*-C_6H_4 protons H_{A-D} [R= Cy(**a**), Et (**b**), Ph (**c**), Tol^p (**d**)] in Figure 3.12.

Table 3.4 125.79 MHz $^{13}C\{^1H\}$ NMR data for Ru(η^5-Cp*){κ^2-(*o*-C_6H_4)PPh_2}(PR_2H) **7a-d** in C_6D_6 at 300 K: δ in ppm (multiplicity, RI, J_{avg} or $\omega_{1/2}$ in Hz, assignment).[a]

	η^5-Cp*	**κ^2-(*o*-C_6H_4)PPh_2**	**PR_2H**
7a	C_{ring} 89.1 (s) C_{methyl} 11.0 (s)	**Ph:** C_{ipso} 138.1 (d, $^1J_{PC}$ 32), 137.2 (d, $^1J_{PC}$ 21) C_{ortho} 132.3 (d, $^2J_{PC}$ 10), 132.2 (d, $^2J_{PC}$ 10) C_{para} 128.9 (d, $^4J_{PC}$ 2), 128.5 (d, $^4J_{PC}$ 2) C_{meta} 128.3 (d, $^3J_{PC}$ 8), 128.0 (d, $^3J_{PC}$ 8) **κ^2-(*o*-C_6H_4):** C_{ipso}-Ru 173.1 (dd, $^2J_{PC}$ 22, $^2J_{PC}$ 16) C_{ipso}-P 154.8 (dd, $^1J_{PC}$ 47, $^3J_{PC}$ 2) C_D 138.3 (dd, $^3J_{PC}$ 20, $^3J_{PC}$ 2), C_C 129.4 (d, $^4J_{PC}$ 4), C_A 125.7 (s), C_B 120.6 (d, $^3J_{PC}$ 8)	CH 36.0 (d, $^1J_{PC}$ 22), 34.6 (dd, $^1J_{PC}$ 20, $^3J_{PC}$ 6) CH_2 33.2 (s), 32.7 (d, $^3J_{PC}$ 6), 31.6 (s), 30.3 (s), 28.2 (d, $^2J_{PC}$ 11), 28.1 (d, $^3J_{PC}$ 7), 28.0 (d, $^2J_{PC}$ 10), 27.6 (d, $^2J_{PC}$ 11), 26.8 (s), 26.4 (s)
7b	C_{ring} 89.5 (s) C_{methyl} 11.1 (s)	**Ph:** C_{ipso} 138.1 (d, $^1J_{PC}$ 32), 137.2 (d, $^1J_{PC}$ 21) C_{ortho} 132.7 (d, $^2J_{PC}$ 12), 132.0 (d, $^2J_{PC}$ 9) C_{para} 129.1 (s), 128.2 (d, $^4J_{PC}$ 2) C_{meta} 128.1 (d, $^3J_{PC}$ 8), 128.0 (d, $^3J_{PC}$ 8) **κ^2-(*o*-C_6H_4):** C_{ipso}-Ru 172.6 (d, $^2J_{PC}$ 21) C_{ipso}-P 154.8 (d, $^1J_{PC}$ 47) C_D 136.5 (dd, $^3J_{PC}$ 20, $^3J_{PC}$ 2), C_C 129.6 (dd, $^4J_{PC}$ 4, $^4J_{PC}$ 2), C_A 125.7 (s), C_B 120.8 (dd, $^3J_{PC}$ 8, $^5J_{PC}$ 2)	CH_3 13.0 (d, $^2J_{PC}$ 6), 12.5 (d, $^2J_{PC}$ 5) CH_2 19.4 (d, $^1J_{PC}$ 23), 18.9 (dd, $^1J_{PC}$ 25, $^3J_{PC}$ 6)

7c	C_{ring} 90.2 (s) C_{methyl} 10.7 (s)	**Ph:** C_{ipso} 136.3 (dd, $^{1}J_{PC}$ 37, $^{3}J_{PC}$ 2), 135.4 (d, $^{1}J_{PC}$ 24) C_{ortho} 132.4 (d, $^{2}J_{PC}$ 11), 132.7 (d, $^{2}J_{PC}$ 11) C_{para} 128.7 (s), 128.5 (d, $^{4}J_{PC}$ 2) C_{meta}, 127.8 (d, $^{3}J_{PC}$ 9), 127.6 (d, $^{3}J_{PC}$ 9, overlaps with C_{meta} in PPh_2H) **κ^2-(*o*-C_6H_4):** C_{ipso}-Ru 172.6 (dd, $^{2}J_{PC}$ 24, $^{2}J_{PC}$ 18) C_{ipso}-P 154.2 (dd, $^{1}J_{PC}$ 47, $^{2}J_{PC}$ 2) C_D 137.3 (dd, $^{3}J_{PC}$ 19, $^{3}J_{PC}$ 2), C_C 129.9 (d, $^{4}J_{PC}$ 4), C_A 126.6 (s), C_B 121.3 (d, $^{3}J_{PC}$ 8)	C_{ipso} 137.8 (d, $^{1}J_{PC}$ 33), 137.6(dd, $^{1}J_{PC}$ 37, $^{3}J_{PC}$ 6) C_{ortho} 132.2 (d, $^{2}J_{PC}$ 9), 132.1 (d, $^{2}J_{PC}$ 9) C_{para} 128.3 (d, $^{4}J_{PC}$ 2), 128.0 (s) C_{meta} 128.1 (d, $^{3}J_{PC}$ 8), 127.6 (d, $^{3}J_{PC}$ 9, overlaps with C_{meta} on the Ph ring of metallacycle)
7d	C_{ring} 90.3 (s) C_{methyl} 10.8 (s)	**Ph:** C_{ipso} 138.1 (d, $^{1}J_{PC}$ 32), 137.2 (d, $^{1}J_{PC}$ 19, $^{3}J_{PC}$ 2) C_{ortho} 132.8 (d, $^{2}J_{PC}$ 11), 132.1 (d, $^{2}J_{PC}$ 10) C_{para} 128.5 (s, overlaps with C_{meta} in $PTol^{p}_2H$), 128.3 (s, overlaps with C_{meta} in $PTol^{p}_2H$) C_{meta} 128.1 (d, $^{3}J_{PC}$ 9), 127.5 (d, $^{3}J_{PC}$ 9) **κ^2-(*o*-C_6H_4):** C_{ipso}-Ru 172.2 (d, $^{2}J_{PC}$ 17) C_{ipso}-P 154.4 (d, $^{1}J_{PC}$ 47) C_D 137.3 (d, $^{3}J_{PC}$ 19, $^{3}J_{PC}$ 2), C_C 129.8 (d, $^{4}J_{PC}$ 4) C_A 126.5 (s), C_B 121.2 (d, $^{3}J_{PC}$ 8)	C_{para} 138.4 (s), 137.5 (s) C_{ortho} 134.5 (d, $^{2}J_{PC}$ 11), 132.4 (d, $^{2}J_{PC}$ 10) C_{ipso} 134.4 (dd, $^{1}J_{PC}$ 38, $^{3}J_{PC}$ 6), 133.3 (d, $^{1}J_{PC}$ 39) C_{meta} 128.5 (d, $^{3}J_{PC}$ 8), 128.4 (d, $^{3}J_{PC}$ 8) CH_3 21.2 (s), 21.1 (s)

[a] Structure illustrating locations of *o*-C_6H_4 carbons $C_{A\text{-}D}$ [R= Cy(**a**), Et (**b**), Ph (**c**), Tol^{p} (**d**)] in Figure 3.12.

3.7 References

[1] Rosenberg, L. *Coord. Chem. Rev*, **2012**, *256*, 606

[2] Bonnet, G.; Kubicki, M. M.; Moise, C.; Lazzaroni, R.; Salvadori, P.; Vitulli, G. *Organometallics* **1992**, *11*, 964.

[3] Baker, R. T.; Whitney, J. F.; Wreford, S. S. *Organometallics* **1983**, 2, 1049.

[4] Derrah, E. J.; Pantazis, D. A.; McDonald, R.; Rosenberg, L. *Organometallics* **2007,** *26,* 1473

[5] Derrah, E. J.; Giesbrecht, K. E.; McDonald, R.; Rosenberg, L. *Organometallics* **2008**, 27, 5025

[6] Planas, J. G.; Hampel, F.; Gladysz, J. A. *Chem. Eur. J.* **2005**, *11*, 1402

[7] Hoyle, M. A. M.; Pantazis, D. A.; Burton, H. M.; McDonald, R.; L. Rosenberg, L. *Organometallics* **2011**, *30*, 6458

[8] Verkade, J. G.; Quin, L. D. *Phosphorus-31 NMR Spectroscopy in Stereochemical Analysis*; VCH Publishers, Inc.: Deerfield Beach, Fl, **1987**; Vol.8

[9] Quin, L. D. *A Guide to Organophosphorus Chemistry*; Wiley-Interscience: Toronto, **2000**.

[10] Sues, P. E.; Lough, A. J.; Morris, R. H. *J. Am. Chem. Soc.* **2014**, *136*, 4746.

[11] Findlay, A. E.; Leelasubcharoen, S.; Kuzmina, L. G.; Howard, J. A. K.; Nikonov, G. I. *Dalton Trans.* **2010**, *39*, 9264.

[12] Zhuravel, M. A.; Glueck, D. S. *Organometallics* **2002**, *21*, 3208.

[13] Cain, M. F.; Hughes, R. P.; Glueck, D. S.; Golen, J. A.; Moore, C. E.; Rheingold, A. L. *Inorg. Chem.* **2010**, *49*, 7650.

[14] Altenhoff, G.; Bredeau, S.; Erker, G.; Kehr, G.; Kataeva, O.; Fröhlich, R. *Organometallics* **2002**, *21*, 4084

[15] Belli, R. G.; Burton, K. M. E.; Rufh, S. A.; McDonald, R.; Rosenberg, L. *Organometallics* **2015**, *34*, 5637

[16] Alvarez, M. A.; Anaya, Y.; García, M. E.; Riera, V.; Ruiz, M. A. *Organometallics* **2004,** *23,* 433

[17] Stewart, R. *The Proton: Applications to Organic Chemistry*, Academic Press: Orlando, **1985**

[18] Jiménez-Tenorio, M.; Puerta, M. C.; Valerga, P. *Eur. J. Inorg. Chem.* **2004**, 17

[19] Johnson, T. J.; Folting, K.; Streib, W. E.; Martin, J. D.; Huff- man, J. C.; Jackson, S. A.; Eisenstein, O.; Caulton, K. G.; *Inorg. Chem.* **1995**, *34*, 488

[20] Caulton, K. G. *New J. Chem.* **1994**, *18*, 25

[21] NMR data of indenyl phosphido complexes see: Derrah, E. J.; Pantazis, D. A.; McDonald, R.; Rosenberg, L.; *Organometallics* **2007,** *26,* 1473.

[22] Garrou, P. E. *Chem. Rev.* **1981**, *81*, 229.

[23] E. J. Derrah, K. E. Giesbrecht, R. McDonald, L. Rosenberg, *Organometallics* **2008**, 27, 5025–5032

[24] R. Torres-Lubián, M. J. Rosales-Hoz, A. M. Arif, R. D. Ernst, M. A. Paz-Sandoval, *J. Organomet. Chem.* **1999**, 585, 68

[25] Hartwig, J. *Organotransition Metal Chemistry.* Sausalito, Calif.: University Science Books, **2010**.

[26] Johnson, T. J.; Folting, K.; Streib, W. E.; Martin, J. D.; Huffman, J. C.; Jackson, S. A.; Eisenstein, O.; Caulton, K. G. *Inorg. Chem.* **1995**, *34*, 488.

[27] Derrah, E. J.; Pantazis, D. A.; McDonald, R.; Rosenberg, L. *Angew. Chem. Int. Ed.* **2010**, *49*, 3367.

[28] Support for the proposed increase in acidity of $HPEt_2$ relative to $HPCy_2$ comes from evaluation by Morris of pK_a values for tertiary phosphine cationic acids: pK_a($HPEt_3^+$) (8.9) < pK_a($HPCy_3^+$) (9.7). Abdur-Rashid, K.; Fong, T. P.; Greaves, B.; Gusev, D. G.; Hinman, J. G.; Landau, S. E.; Lough, A. J.; Morris, R. H. *J. Am. Chem. Soc.* **2000**, *122*, 9155.

[29] Support for the proposed basicity: $PTol^p_2$ > PPh_2 comes from evaluation by Morris of pK_a values for acidity of correspond secondary: pK_a($HPTol^p_2$) > pK_a($HPPh_2$).Also, pK_a values for acidity of Cp*Ru-PR2: pK_a(Cp*Ru-$PTol^p_2$) > pK_a(Cp*Ru-PPh_2). Sues, P. E.; Lough, A. J.; Morris, R. H. *J. Am. Chem. Soc.* **2014**, *136*, 4746

[30] Kaupmees, K.; Trummal, A.; Leito, I. *Croat. Chem. Acta* **2014**, *87*, 385

[31] Support for similar basicity of $NaOCH_2C(CH_3)_3$ to $KOBu^t$ comes from evaluation of acidities of simple alcohols in dimethyl sulfoxide solution by Bordwell. Olmstead, W. N.; Margolin, Z.; Bordwell, F. G. *J. Org. Chem.* **1980**, *45*, 3295.

[32] Schlosser, M. *Organometallics in Organic Synthesis*, Wiley: New York, **1994**.

[33] Katritzky, A. R.; Slawinski, J. J.; Brunner, F. *J. Chem. Soc. Perkin Trans. I* **1989**, 1139.

Chapter 4 Similar reactivity of Cp* ruthenium phosphido complexes to their indenyl analogues

4.1 Introduction

As described in Chapter 3, Ru(η^5-Cp*)Cl(PR_2H)(PPh_3) (**2a-d)** and $KOBu^t$ can be used to generate the Cp* phosphido complexes Ru(η^5-Cp*)(PR_2)(PPh_3) (**6a-d**) *in situ* ("Method 1"). This allowed us to explore the reactivity of **6a-d** with various trapping reagents (different trapping reagents will be described in Chapter 4 and 5). This Chapter presents the reactions of the Cp* phosphido **6a-d** with some gas reagents (H_2, CO and ethylene) to show their similar reactivity to indenyl analogues Ru(η^5-indenyl)(PR_2)(PPh_3) (**6^i**). In addition, lability of PPh_3 ligand in Cp* system (see Chapter 2) results in the formation of some new species, which will also be described in this Chapter.

4.1.1 High reactivity of indenyl ruthenium phosphido complex exhibiting Ru-P π Bonding with H_2, CO and Ethylene

As described in Chapter 1, the reactivity of indenyl phosphido **6^i** (5-coordinate) was previously studied by Rosenberg group in a series of reactions (e.g. H_2, CO and ethylene in Scheme 4.1).[1,2,3,4] H_2 adds across the Ru-P double bond of indenyl phosphido complexes, which results in delivery of the electrophilic proton (H^+) to the phosphido ligand while the nucleophilic hydride (H^-) coordinates to the metal center. The L-type ligand CO can bind to the Ru center of the 5-coordinate indenyl phosphido complexes to disrupt the Ru-P double bond and give 6-coordinate terminal phosphido complexes Ru(η^5-indenyl)(PR_2)(CO)(PPh_3) (**9^i**). Current graduate student Roman Belli is now studying catalytic hydrophosphination of activated alkenes by this 6-coordinate phosphido species that are important reactive intermediates in

catalytic P-C bond formation. In addition, the indenyl phosphido **6**^{i} can undergo a [2+2] cycloaddition with non-activated simple alkene ethylene to give metallacyclic species. These metallacycles also have potential to be important intermediate for metal catalyzed hydrophosphination.[5]

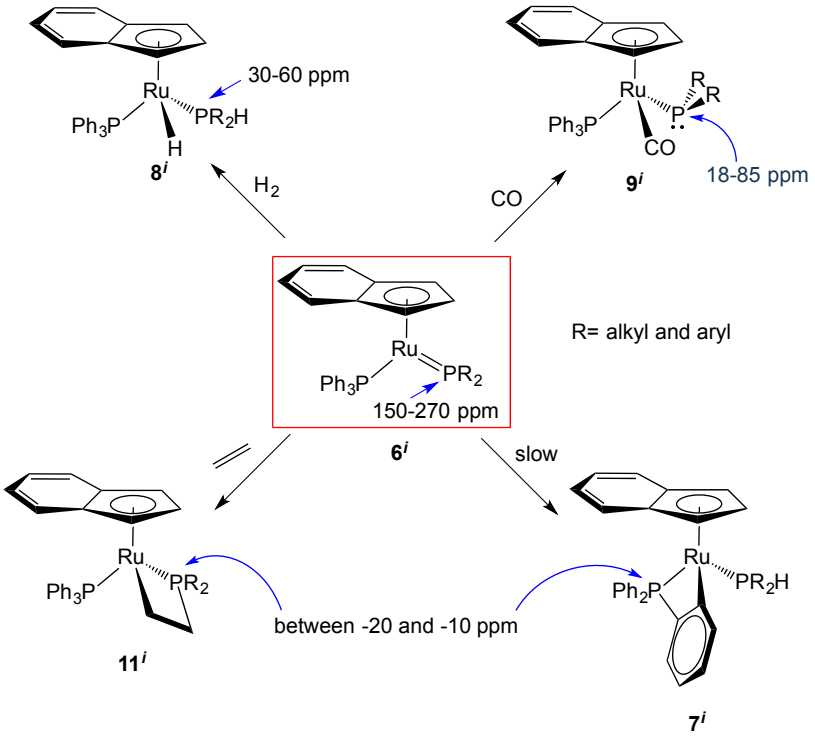

Scheme 4.1 The reactivity of indenyl phosphido complexes and diagnostic ^{31}P chemical shifts for resulting products.

All of these products from reactions of **6**^{i} show diagnostic ^{31}P chemical shifts (Scheme 4.1). As previously described (see Section 3.1.1, Chapter 3), planar phosphido complexes have a huge downfield ^{31}P shift (for **6**^{i} δ: 150-270 ppm).[1] The ^{31}P chemical shifts observed for indenyl hydride complexes **8**^{i} are in the typical coordinated phosphine range (δ: 30-60 ppm).[6] For terminal phosphido complexes, the phosphido ligand exhibits relatively downfield shifts (18-85 ppm) compared to the original planar phosphido complexes. [1,7] The 4-membered metallacycles have more upfield ^{31}P shifts (from -10 to -20 ppm for **7**^{i} and **11**^{i}) than other resulting products.[4]

All these $^{31}P\{^{1}H\}$ NMR spectroscopic data can be useful to study and identify Cp* analogues.

4.1.2 Exploring the possibility of variable hapicity in indenyl complexes

The indenyl ligand is a Cp derivative and it typically coordinates to the metal center through all five carbons (η^5) like other Cp derivatives (e.g, Cp and Cp*) do. However, as described in Chapter 1, the indenyl ligand is different from Cp and Cp* because of the ring slippage from 5-coordinate mode (η^5) to 3-coordinate mode (η^3). For example, this hapticity change of the indenyl ligand might be an important part of the mechanism by which ethylene undergo cycloaddition at the Ru center in the indenyl systems studied by the Rosenberg group. There are two possible mechanisms for this cycloaddition shown in Scheme 4.2. Like ethylene, the addition of H_2 or CO to indenyl phosphido complexes may undergo the same mechanism that changes the hapticity of indenyl group without disrupting the Ru-P double bond.

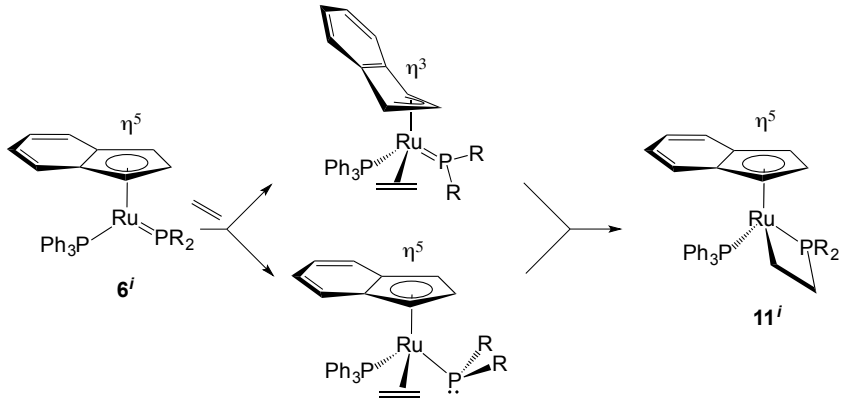

Scheme 4.2 Two possible mechanisms of ethylene cycloaddition at indenyl phosphido complexes Ru(η^5-indenyl)(PR_2)(PPh_3) (**6^i**).

As described in Chapter 1 (Section 1.3.1), if Cp* phosphido **6a-d** react with H_2, CO and ethylene like the indenyl analogues **6^i** does, it will provide evidence that the changing hapticity in indenyl phosphido complex is not necessary for these reaction to take place. As a result, the reactions of Cp* phosphido **6a-d** with H_2, CO and

ethylene were investigated carefully to elucidate the possible importance of variable hapticity for indenyl analogues.

4.2 Dihydrogen (H_2) addition to Cp* phosphido Ru(η^5-Cp*)(PR_2)(PPh_3) (6a-d)

Cp* phosphido complexes **6a-d** (complex **2a-d** + $KOBu^t$) were generate *in situ* in sealed NMR tubes (see Chapter 3), and 0.9 atm H_2 was added to these degassed solutions. The reactions were monitored by NMR spectroscopy and the NMR tubes were shaken to mix the samples between experiments.

4.2.1 Products resulting from addition of H_2

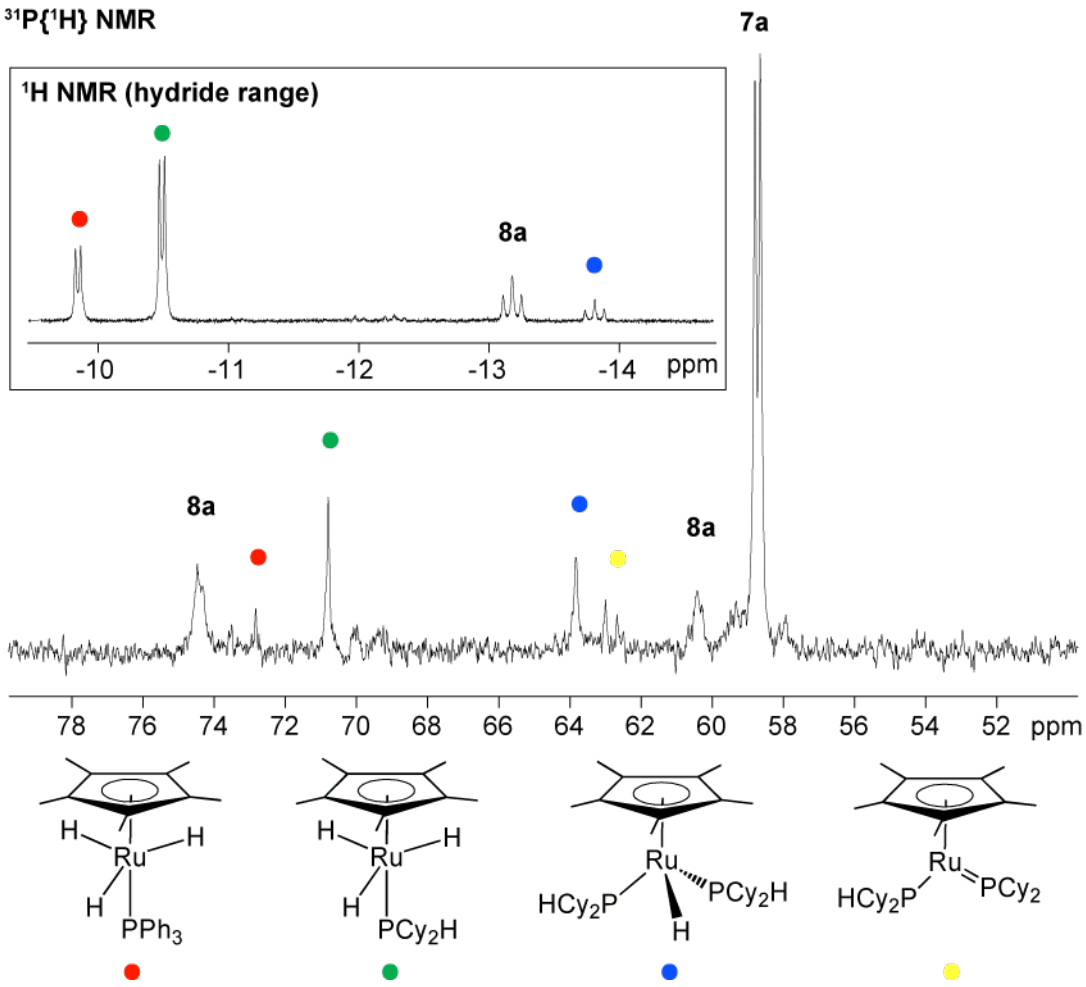

Figure 4.1 Partial $^{31}P\{^1H\}$ NMR (202.51 MHz, C_7D_8) spectrum of [**2a** + $KOBu^t$] with 0.9 atm H_2. Inset shows partial ^1H NMR (500.27 MHz, C_7D_8) spectrum showing Ru-H signals.

Complex **6a** shows the most complicated product mixture of the four reactions studied (see Scheme 4.3). In Figure 4.1, $^{31}P\{^{1}H\}$ NMR spectrum shows orthometallated Ru(η^5-Cp*)\{κ^2-(*o*-C_6H_4)PPh_2\}(PCy_2H) (**7a**) as the major product, hydride complex Ru(η^5-Cp*)H(PCy_2H)(PPh_3) (**8a**) (*P*Ph_3 δ: 74.3 ppm and *P*Cy_2H δ: 60.2 ppm) and other minor products. Peaks due to four hydride-containing complexes are observed in the ^{1}H NMR spectrum (two doublets and two triplets). In the $^{31}P\{^{1}H\}$ NMR spectrum, due to the increase of the free PPh_3 signal, the ^{31}P signal (δ: 70.7 ppm) is attributed to a product that arises from ligand substitution of PPh_3 by H_2 to an η^2-H_2 adduct Ru(η^5-Cp*)H(η^2-H_2)(PCy_2H) and then oxidative addition of H_2 to give a trihydride complex Ru(η^5-Cp*)H_3(PCy_2H) (green dot in Figure 4.1). In addition, this ^{31}P signal (singlet) splits into two broad singlets ($^{1}J_{PH}$ = ~310 Hz, $\omega_{1/2}$ = ~50 Hz) in the ^{31}P NMR spectrum, which supports the coordination of a PCy_2H ligand. Due to the redistribution of complex **2a** (see Chapter 2, Section 2.2.2), the complex **1** and **3a** can also react with KOBu^t and H_2 to give a corresponding complex Ru(η^5-Cp*)H_3(PPh_3) ($^{31}P\{^{1}H\}$ δ: 72.8 ppm and ^{1}H for Ru-H δ: -9.82 ppm; red dot in Figure 4.3) and Ru(η^5-Cp*)(H)(PCy_2H)$_2$ ($^{31}P\{^{1}H\}$ δ: 63.7 ppm and ^{1}H for Ru-H δ: -13.82 ppm; blue dot in Figure 4.3). Suzuki et al. reported the similar trihydrides Ru(η^5-Cp*)H_3(PR_3) (PR_3 = PMe_3, PEt_3, $P(CHMe_2)_3$, PCy_3, PPh_2Me and PPh_3).[8] All of these minor products can not be characterized furher because of their low intensity in the NMR spectrum.

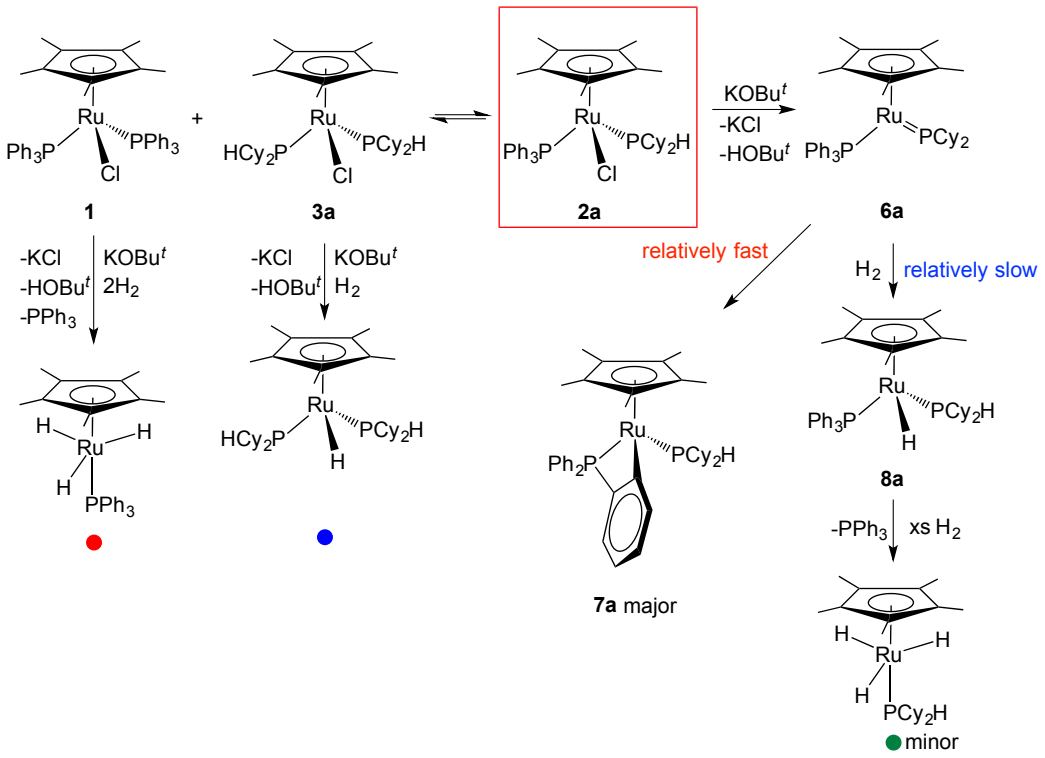

Scheme 4.3 Possible reactions in NMR scale reaction of [**2a** + $KOBu^t$] with 0.9 atm H_2.

For both $Ru(\eta^5\text{-}Cp^*)H_3(PPh_3)$ and $Ru(\eta^5\text{-}Cp^*)H_3(PCy_2H)$, the ^1H NMR spectrum shows ^1H signals due to the CH_3 in Cp* (δ: ~2 ppm) and the three hydrides (H-Ru) as sharp doublets (δ: ~-10 ppm, $^2J_{PH}$ = ~20 Hz) and the integration ratio corresponds to one Cp*and three hydrides. All the protons (Cp* and hydride) are assigned by correlation with the corresponding P in phosphine ligands (PPh_3 or PCy_2H) in the $^1H/^{31}P\{^1H\}$-HMBC spectrum. Interestingly, the $^{31}P\{^1H\}$ NMR spectrum (see Figure 4.2a) also shows extra signals close to the major signals due to $Ru(\eta^5\text{-}Cp^*)H_3(PPh_3)$ and $Ru(\eta^5\text{-}Cp^*)H_3(PCy_2H)$, which suggests the other structural isomers.[9] The major signals are assigned to a trigonal bipyramidal structure (all three hydride ligands are equivalent) and minor signals are assigned to the square based pyramidal structure (three hydride assuming slow exchange, two are *cis* and one is *trans* to phosphine ligand). The ^1H VT-NMR spectrum (see Figure 4.2b) provided evidence for both structural isomers. At RT, sharp doublets are observed with

diagnostic coupling constant ($^2J_{PH}$ = ~20 Hz) to confirm the major isomers are the trigonal bipyramidal structure of the trihydride complexes.[10] The broad signals overlapping with the sharp doublets are assigned to the minor isomers, which are the square based pyramidal structure. One of these broad signals is separated from the sharp doublets and can be observed at -80 °C. Graham reported that the Os(η^5-Cp*)H_3(CO) exhibits a separate doublet and triplet in the ration (1:2) for the hydride complex at -50 °C but a broad singlet at 25 °C.[11] Based on the VT-NMR spectrum, the trihydride complexes, Ru(η^5-Cp*)H_3(PPh_3) and Ru(η^5-Cp*)H_3(PCy_2H), presumably favor the trigonal bipyramidal structure, which can also be explained by the steric requirement of the bulky phosphine ligand.

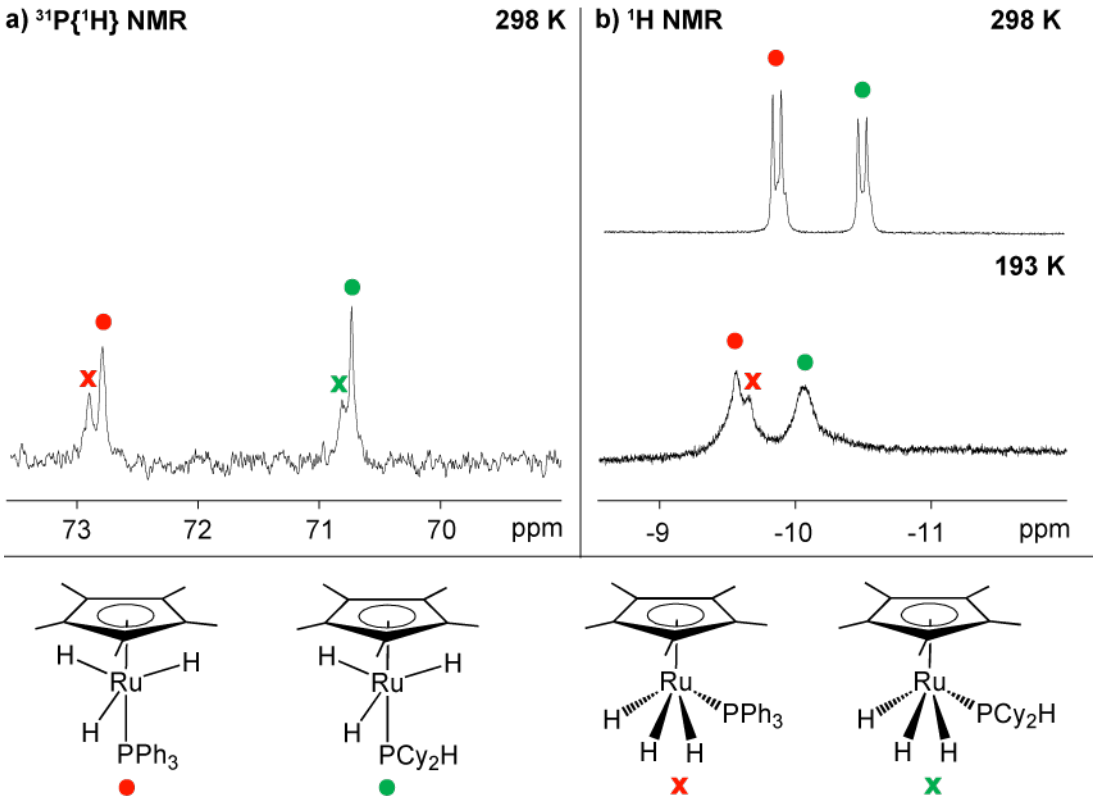

Figure 4.2 a) Partial $^{31}P\{^1H\}$ NMR spectrum (121.55 MHz, C_6D_6) of [**2a** + KOBu^t] with 0.9 atm H_2 highlighting trihydride complexes Ru(η^5-Cp*)H_3(PPh_3) (red) and Ru(η^5-Cp*)H_3(PCy_2H) (green) with their structural isomers. **b)** ^1H VT-NMR spectrum (360.28 MHz, C_7D_8) of [**2a** + KOBu^t] with 0.9 atm H_2 highlighting Ru(η^5-Cp*)H_3(PPh_3) (red) and Ru(η^5-Cp*)H_3(PCy_2H) (green)**.**

The reactions of **6b-d** with H_2 are much cleaner relative to **6a** (Scheme 4.4a). After 3h, all three reactions gives hydride Ru(η^5-Cp*)H(PR_2H)(PPh_3) (**8b-d**) as the major product (94-96%) and orthometallated **7b-d** as a minor product (4-5%), and that the reaction of **6c** also shows ~2% of another hydride product, assigned as Ru(η^5-Cp*)H(PPh_2H)$_2$ (Scheme 4.4b), which forms from the impurity of disubstituted complex **3c** (see Chapter 2, Section 2.2.2). All major hydride species **8b-d** are characterized by using 1D NMR and 2D NMR spectroscopy, as described below.

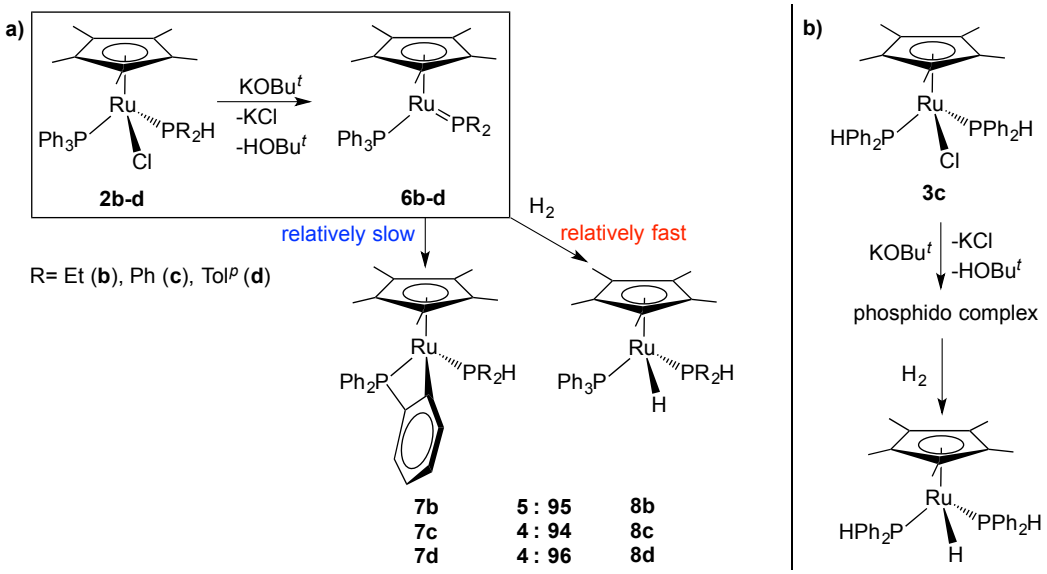

Scheme 4.4 a) Products of NMR scale reactions of [**2b-d** + KOBu^t] with 0.9 atm H_2 after 3h. **b)** Product of NMR scale reaction of [**3c** + KOBu^t] with 0.9 atm H_2.

4.2.2 Detailed characterization of Ru(η^5-Cp*)H(PR_2H)(PPh_3) (8b-d)

For the reactions of **6b-d** with H_2, **8b-d** are the major products in a mixture, so most of the signals can be observed in their NMR spectra as described here for **8d** (R = Tol^p). The Ru(η^5-indenyl)H(PR_2H)(PPh_3) (R = Ph ,Tol^p) are also used as analogues to identify and compare with complex **8b-d**.[12] These complexes show diagnostic upfield ^{1}H signals due to the hydride at the Ru (e.g., **8d** δ: -12.50 ppm) in the ^{1}H NMR spectra. The Cp* and hydride protons can be identified by correlations with P in both the PPh_3 and the PR_2H ligand in the ^{1}H/^{31}P{^{1}H}-HMBC spectrum (Figure 4.3)

and relative integration confirms a ratio of one Cp* to one hydride ligand. The ^{1}H signal due to H-Ru in **8d** appears as a triplet ($^{2}J_{PH}$ = 34.7 Hz), which is similar to the corresponding signal of the indenyl analogue **8**^{i}. The $^{31}P\{^{1}H\}$ NMR signals (**8d** δ: 74.6 ppm and 42.9 ppm, $^{2}J_{PP}$ = 33 Hz) due to P in PR_2H and PPh_3 are observed as two doublets, which is also similar to those of the indenyl analogue. The rest of the protons and all the carbon signals can be identified by using the $^{1}H/^{13}C$-HSQC and HMBC spectra.

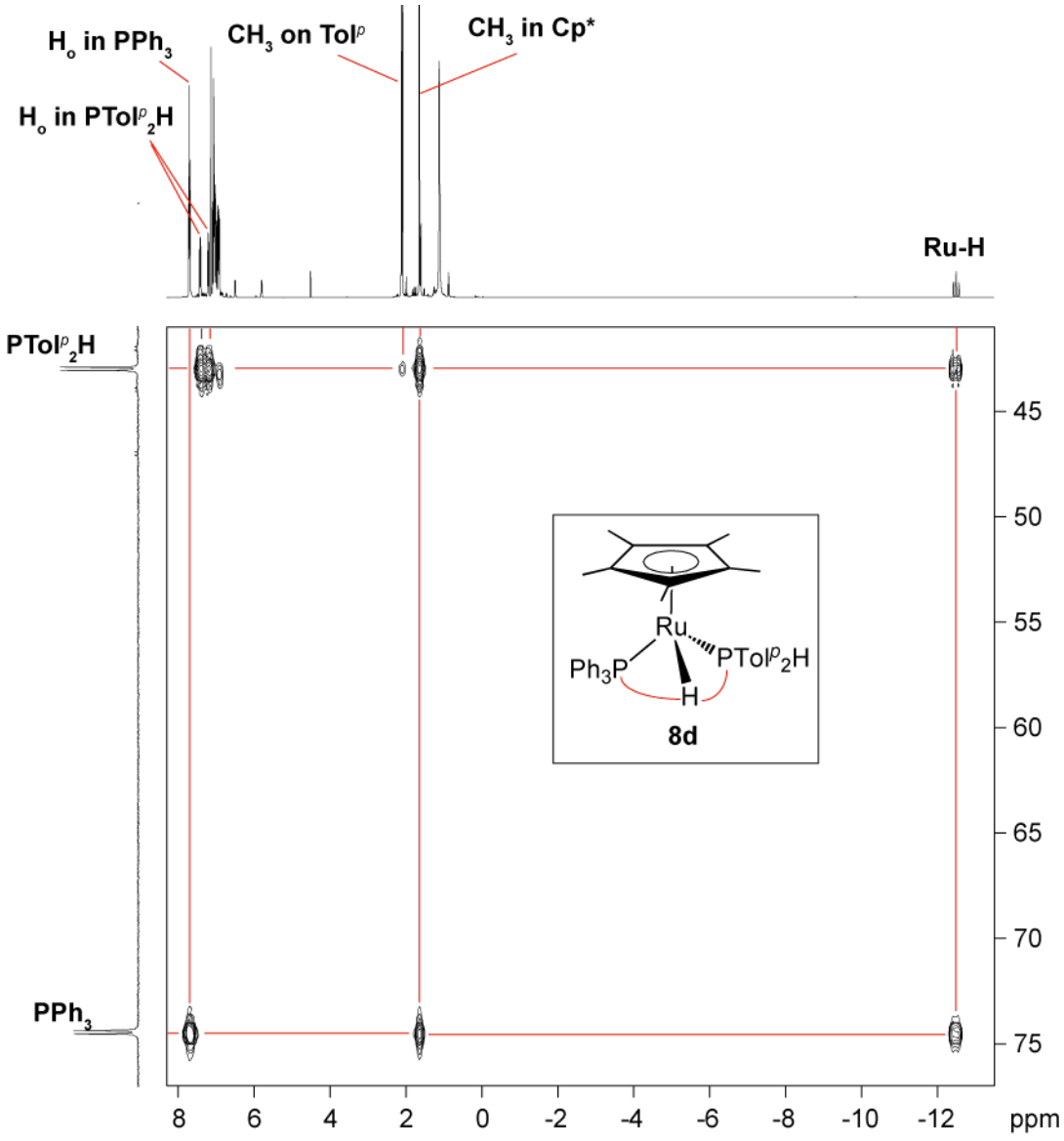

Figure 4.3 $^{1}H/^{31}P\{^{1}H\}$-HMBC NMR spectrum (500.27 MHz, C_7D_8) of reaction of [**2d** + KOBu^{t}] with 0.9 atm H_2 highlighting all correlations between H and P in hydride complex **8d**.

4.2.3 Comparison of the reactivity of Cp* phosphido complexes 6a-d and indenyl analogues in the reactions with H_2

1,2-addition of H_2 occurs quickly at Cp* phosphido complexes **6a-d** generated *in situ*. Both the Cp* phosphido **6a-d** and indenyl analogues **6^i** react completely with H_2 within seconds visually as determined by the colour change from dark red (**6a,b**) or dark blue (**6c,d**) to yellow. The formation of these Cp* hydride complexes **8a-d** is a possible indication that the variable hapticity of the indenyl ligand is not important for indenyl half-sandwich complexes in the mechanism of these 1,2-addition reactions.

DFT (PBE/DKH2-TZVP) calculations were carried out to find the trajectory of H_2 addition for a simplified indenyl dialkylphosphido Ru complex.[12] The H_2 bonds first to the Ru phosphido complex to form an η^2-H_2 intermediate which then allows the phosphido to nucleophilicly attack or deprotonate this η^2-H_2 intermediate. These computational studies highlight the importance of ready access to a vacant coordination site at the Ru center through a variable phosphido binding mode, instead of hapticity changes of the indenyl ligand.

However, in spite of giving hydride complex **8a-d**, Cp* phosphido **6a-d** will also convert to orthometallated complexes **7a-d**, indicative of a competition between 1,2-addition of H_2 and orthometallation. The complex **6a** (R = Cy) prefers orthometallation, and the other **6b-d** prefer the addition of H_2. For dicyclohexylphosphido **6a**, it is difficult for H_2 to bind to Ru center to form an η^2-H_2 intermediate, which would inhibit the formation of hydride complex **8a**. The formation of the trihydride complex Ru(η^5-Cp*)H_3(PCy_2H) also indicated the steric congestion in the Cp* complexes. This competition was never observed in indenyl analogues, in which H_2 addition occurs much faster than orthometallation.

4.3 The Trapping of Cp* phosphido Ru(η^5-Cp*)(PR_2)(PPh_3) (6a-d) with carbon monoxide (CO)

Cp* phosphido **6a-d** (complexes **2a-d** + KOBu^t) were generated *in situ* in sealed NMR tubes. After degassed, the mixed solution was exposed to 0.9 atm CO. The reactions were monitored by NMR spectroscopy.

4.3.1 Products resulting from addition of CO

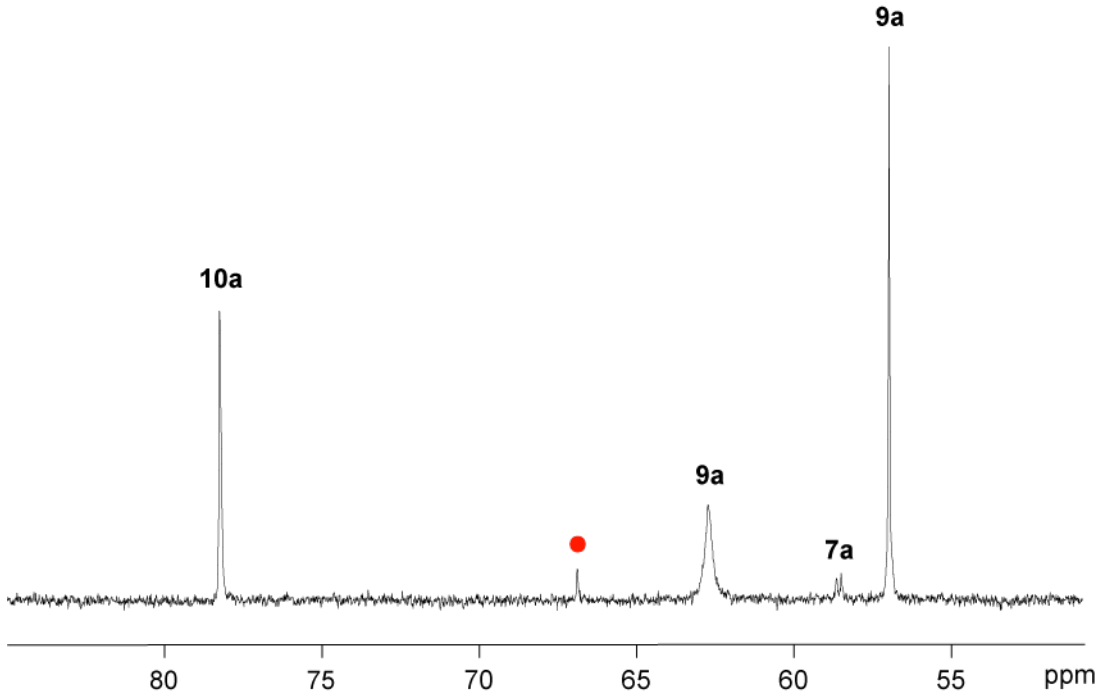

Figure 4.4 Partial $^{31}P\{^1H\}$ NMR spectrum (121.55 MHz, C_7D_8) of the reaction of [**2a** + KOBu^t] with 0.9 atm CO after 0.5h. The signal due to unidentified product is labeled as red dot.

The $^{31}P\{^1H\}$ NMR spectra (e.g. Figure 4.4) show carbonyl phosphido Ru(η^5-Cp*)(PR_2)(CO)(PPh_3) (**9a-d**) (e.g., **9a** *P*Cy_2 δ: 62.7 ppm and *P*Ph_3 δ: 57.0 ppm) as the major product in 0.5h. Under an excess of CO gas in sealed NMR tube samples, carbonyl phosphido **9a-d** are found to undergo PPh_3 ligand substitution with CO and form dicarbonyl complexes Ru(η^5-Cp*)(PR_2)$(CO)_2$ (**10a-d**) (Scheme 4.5). This type of oversubstitution of CO was previously observed in indenyl carbonyl analogues **9*i***.[13]

The Ru(η^5-Cp*)(PCy_2)(CO)(PPh_3) (**9a**) converts completely to the dicarbonyl complex Ru(η^5-Cp*)(PCy_2)$(CO)_2$ (**10a**) in 3h, but the same reaction for indenyl analogue Ru(η^5-indenyl)(PCy_2)(CO)(PPh_3) (**9^{i}a**) needs approximately 17 days to get 100% conversion.[13] Both the ^1H and $^{31}P\{^1H\}$ NMR spectra (after 3h) show dicarbonyl **10a** (~85%) as the major products and orthometallated **7a** (~7%) as one of the minor products. The other minor products are not identified (~8%). The formation of dicarbonyl **10a** (R = Cy) from **9a** is faster relative to the rest of the Cp* carbonyl complexes **9b-d**, which suggests this substitution is driven by relief of the steric crowding at the Ru center.

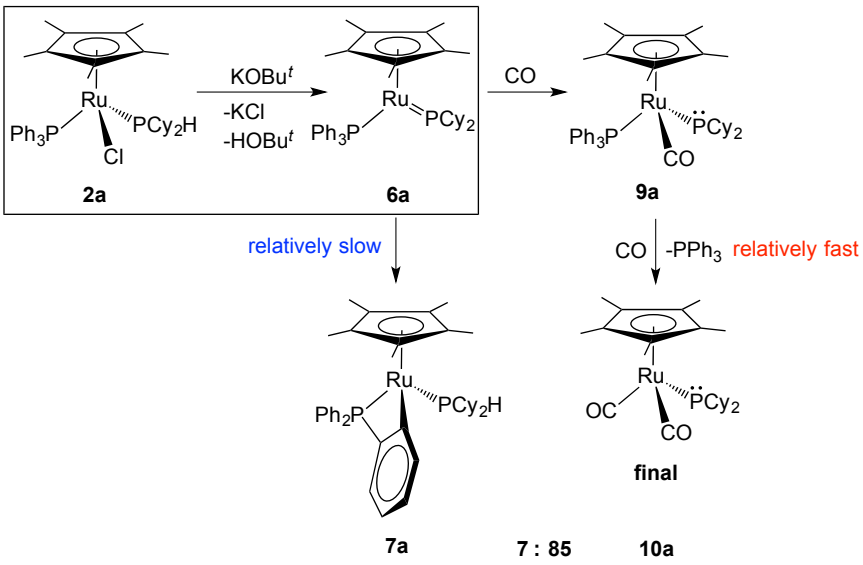

Scheme 4.5 Products of NMR scale reactions of [**2a** + KOBu^t] with 0.9 atm CO after 3h.

For **6b-d**, both the ^1H and $^{31}P\{^1H\}$ NMR spectra (after 3h) show carbonyl complex **9** (87-95%) as the major product, dicarbonyl complex **10** (5-13%) as the only minor product. Interestingly, the ^{13}C signal due to the CH_3 of the Cp* in the $^{13}C\{^1H\}$ NMR spectra shows as a doublet for both of **9** and **10**, which may arise from $^3J_{PC}$ coupling (5~8 Hz) to P in PR_2. In addition, for the reaction of complex **6d**, over time (~15 d) carbonyl **9d** is found to react with dicarbonyl complex **10d**, giving a bridging phosphido complex tentatively identified as $Ru_2(\eta^5$-Cp*$)_2(\mu$-$CO)_2(\mu$-

PTol$^p_2$)(PTol$^p_2$)(CO) (blue dot in Scheme 4.7). The $^{31}P\{^1H\}$ NMR spectrum shows two doublet (δ: 113.8 ppm and 55.7 ppm, $^2J_{PP}$ = 31 Hz). The downfield signal in the $^{31}P\{^1H\}$ spectrum (δ: 113.8 ppm) is assigned to the bridging phosphido (μ-PTol$^p_2$) due its diagnostic ^{31}P shift.[14,15,16,17,18] The other ^{31}P peak (δ: 55.7 ppm) is assigned to terminal phosphido (PTol$^p_2$).[1,7] In ^1H NMR spectrum, it shows two distinct ^1H signals (δ: 1.53 ppm and 1.30 ppm) due to CH_3 in two different Cp*. These methyl protons in two Cp* group have correlations with P in the bridging (μ-PTol$^p_2$) in the $^1H/^{31}P\{^1H\}$-HMBC NMR spectrum (Figure 4.5). Unexpectedly, these methyl protons in two Cp* group also have correlations with P in the terminal PTol$^p_2$ in the $^1H/^{31}P\{^1H\}$-HMBC NMR spectrum, which may result from the fluxionality**.** In $^{13}C\{^1H\}$ NMR spectrum, two distinct ^{13}C peaks (δ: 207.2 ppm and 205.0 ppm) are assigned to the bridging CO and terminal CO due to correlations with H in Cp* ligands in the $^1H/^{13}C\{^1H\}$-HMBC spectrum. However, because this bridging phosphido complex is the minor product in the mixture, some signals could not be observed in the ^1H and $^{13}C\{^1H\}$ NMR spectra.

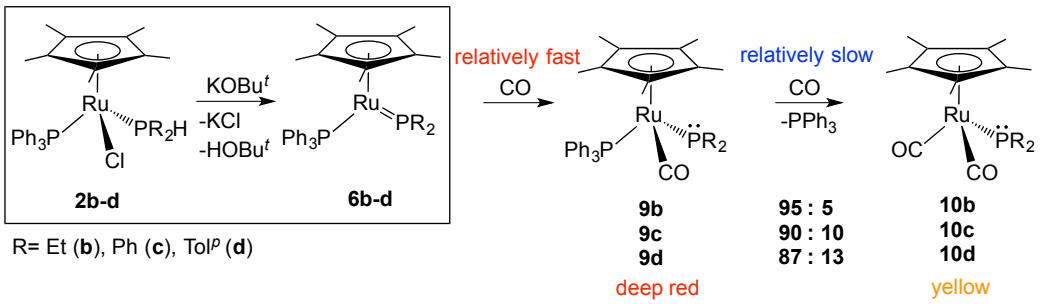

Scheme 4.6 Products of NMR scale reactions of [**2b-d** + KOBu^t] with 0.9 atm CO after 3h.

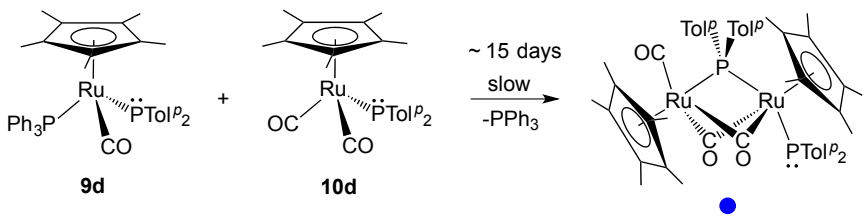

Scheme 4.7 Possible reaction of carbonyl **9d** with dicarbonyl **10d** after 15 d.

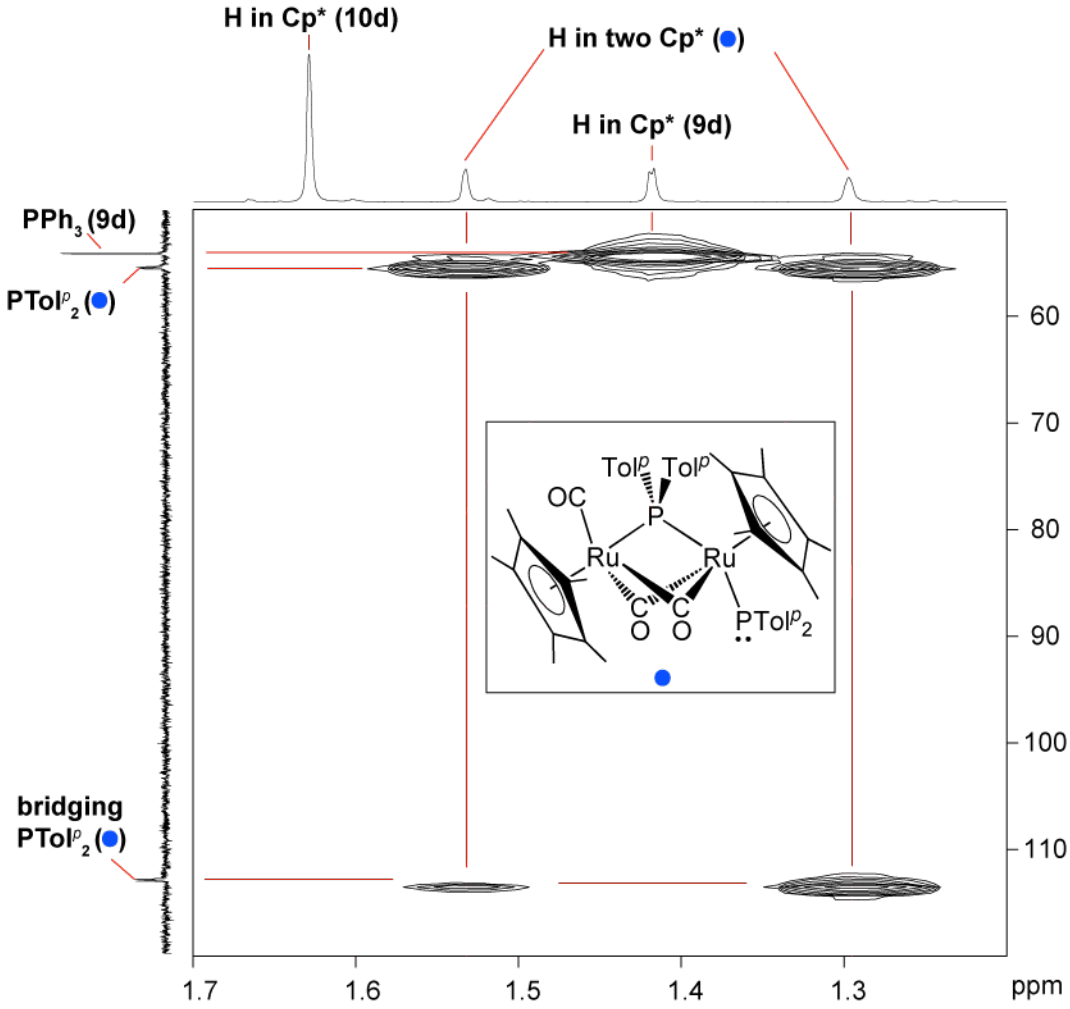

Figure 4.5 Partial $^{1}H/^{31}P\{^{1}H\}$-HMBC NMR spectrum (500.27 MHz, C_7D_8) of [**2d** + $KOBu^t$] with 0.9 atm CO after 15 d highlighting the correlations between H of Cp* and P in different phosphido ligands in μ-phosphido complex (blue dot).

4.3.2 Detailed characterization of Ru(η^5-Cp*)(PR_2)(CO)(PPh_3) (9b-d)

The major species in these reactions were characterized by using 1D NMR and 2D NMR spectroscopy (*vide infra*). As mentioned above, for the reaction of complex **2a** (R = Cy) with CO, the resulting carbonyl **9a** is unstable and easy to react with another equivalent CO to give a dicarbonyl **10a**. This oversubstitution is very fast, so I could not obtain the $^{13}C\{^{1}H\}$ NMR data for **9a**. For **9a**, only ^{1}H and $^{31}P\{^{1}H\}$ NMR data are reported. The carbonyl complexes **9b-d** are more stable relative to **9a**. Thus, **9c** is used here as an example to show the characterization of these carbonyl

complexes. ^{1}H and $^{13}C\{^{1}H\}$ assignments for **9b** and **9d** are reported in the Experimental (Section 4.6.2).

For **9c**, the $^{31}P\{^{1}H\}$ NMR spectrum shows two broad singlets (δ: 53.9 ppm and 15.6 ppm, $\omega_{1/2}$ = 15 Hz) instead of two doublets. These two broad singlets are actually two doublets containing a small $^{2}J_{PP}$ coupling constant and this coupling constant is too small to be observed in $^{31}P\{^{1}H\}$ NMR spectrum. The similar small $^{2}J_{PP}$ coupling was also observed in indenyl analogues ***9^i^***.[1,12] This conspicuously small $^{2}J_{PP}$ coupling for pyramidal phosphido complexes is attributed to the p character of the atomic orbital contribution from phosphorus to the M-P bond (long M-P bond).[7,19,20,21] The upfield singlet in the $^{31}P\{^{1}H\}$ NMR spectrum (δ: 15.6 ppm) is assigned to PPh_2 due to correlation with H_o in the phenyl group of the $^{1}H/^{31}P\{^{1}H\}$-HMBC spectrum (Figure 4.6). The downfield ^{31}P shift (δ: 53.9 ppm) is assigned to the PPh_3 ligand. The distinct ^{1}H signals due to H_o in PPh_3 and PPh_2 can be used to identify the other phenyl protons in these two ligands. The assignment of all carbons is confirmed by correlation with identified protons in $^{1}H/^{13}C\{^{1}H\}$-HMBC and -HSQC spectra.

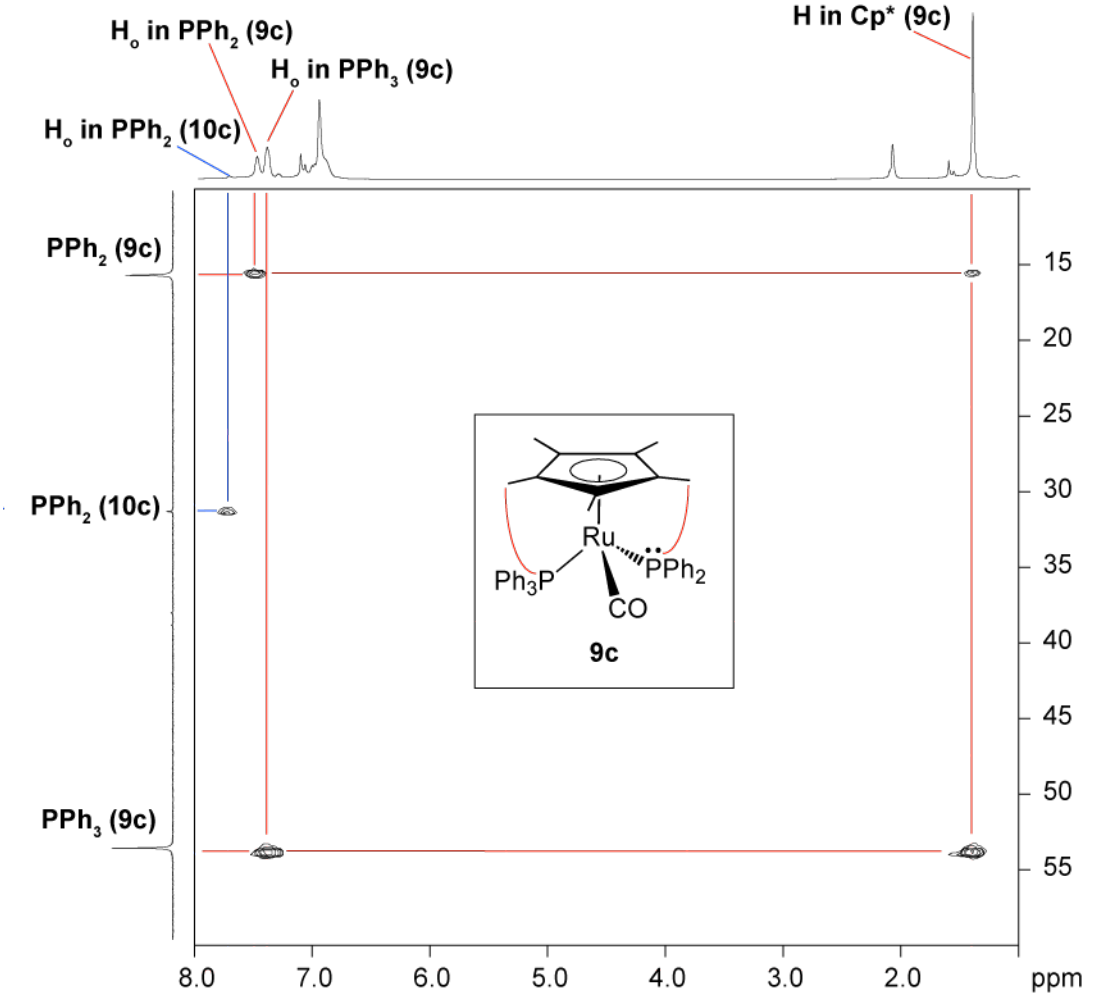

Figure 4.6 Partial $^{1}H/^{31}P\{^{1}H\}$-HMBC NMR spectrum (500.27 MHz, C_7D_8) of reaction of [**2c** + KOBu^t] with 0.9 atm CO highlighting the correlations between H of Cp* and P in PPh_3/PPh_2 ligand in carbonyl complex **9c**.

4.3.3 Detailed characterization of Ru(η^5-Cp*)(PCy$_2$)(CO)$_2$ (10a)

Since **10a** is the major product in the mixture for the dicyclohexylphosphido precursor **6a**, it is used as an example to show the characterization of the dicarbonyl complexes. Full NMR characterization of the other complexes **10b-d** were not reported because they are the minor products in the mixtures. The $^{31}P\{^{1}H\}$ NMR spectrum shows a singlet (δ: 78.2 ppm) and signal due to free PPh_3. The singlet signal is assigned to the P of PCy_2 in **10a** due to its correlations with the alkyl protons on the Cp* and Cy groups in the $^{1}H/^{31}P\{^{1}H\}$-HMBC NMR spectrum. A ^{13}C peak at 206.1

ppm in the $^{13}C\{^1H\}$ NMR spectrum is assigned to the coordinated CO by correlation with H in Cp* ligand in the $^1H/^{13}C\{^1H\}$-HMBC NMR spectrum (Figure 4.7).

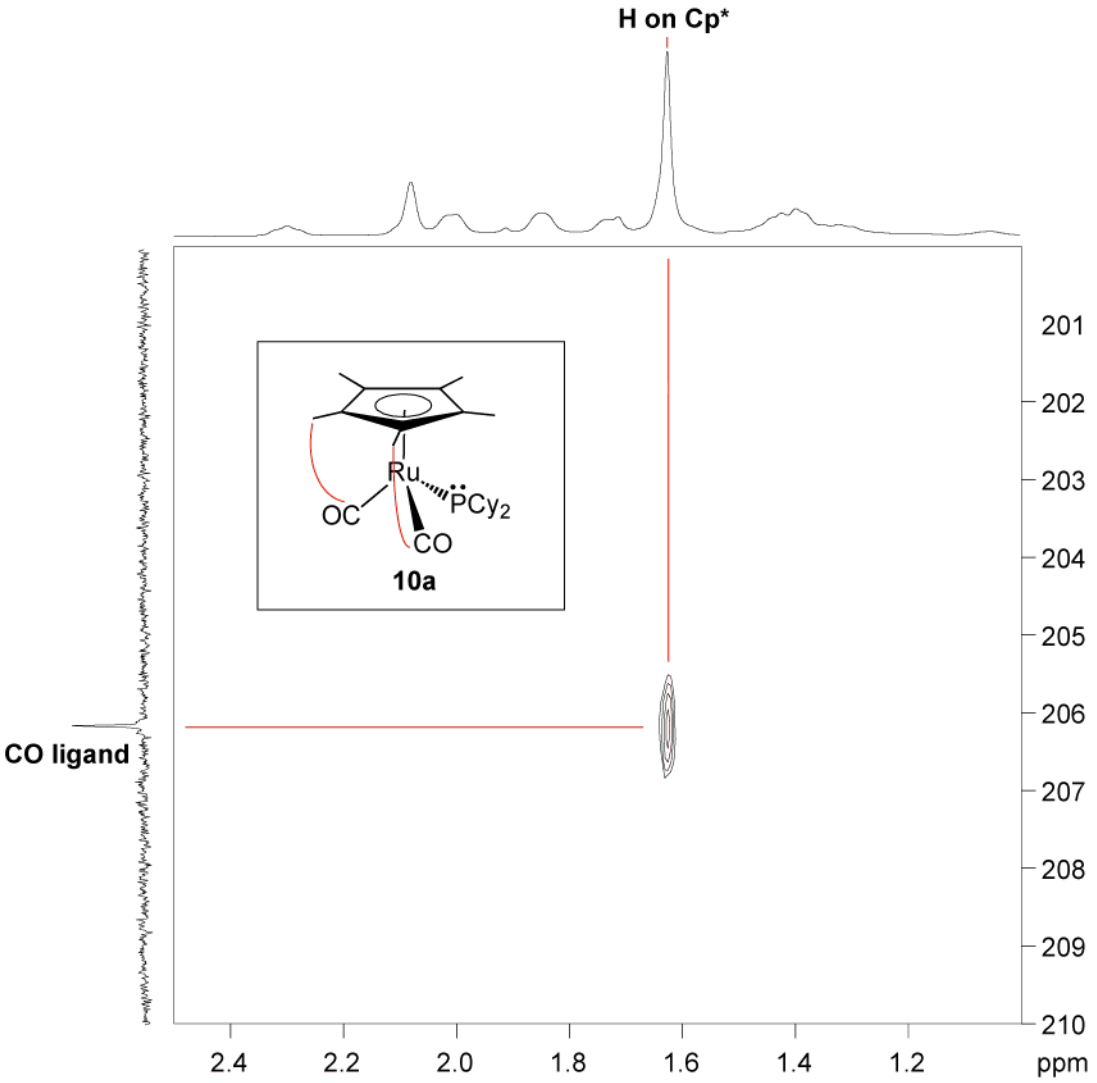

Figure 4.7 Partial $^1H/^{13}C\{^1H\}$-HMBC NMR spectrum (500.27 MHz, C_7D_8) of reaction of [**2a** + KOBu^t] with 0.9 atm CO highlighting the correlation between H of Cp* and C in coordinated CO ligand in dicarbonyl complex **10a**.

4.3.4 Comparison of the reactivity of Cp* phosphido complexes 6a-d and indenyl analogues in the reactions with CO

Similar to their indenyl analogues, CO binds irreversibly to the Ru center of the coordinatively unsaturated complexes **6a-d** to give coordinatively saturated products **9a-d**. The formation of **9a-d** is another indication that the variable hapticity of the indenyl ligand is not necessary for the reactivity of the indenyl half-sandwich

complexes. However, the formation of dicarbonyl **10a-d** indicates **9a-d** are not stable relative to indenyl analogues **9**^{i}.

4.4 [2+2] Cycloaddition reactions of ethylene at Cp* phosphido complexes 6a-d

Similar to the reactions with H_2 and CO, phosphido **6a-d** were generated in sealed NMR tubes. The mixed solutions were then exposed to 0.9 atm ethylene, prior to the tube being placed in the NMR spectrometer.

4.4.1 Products resulting from addition of ethylene

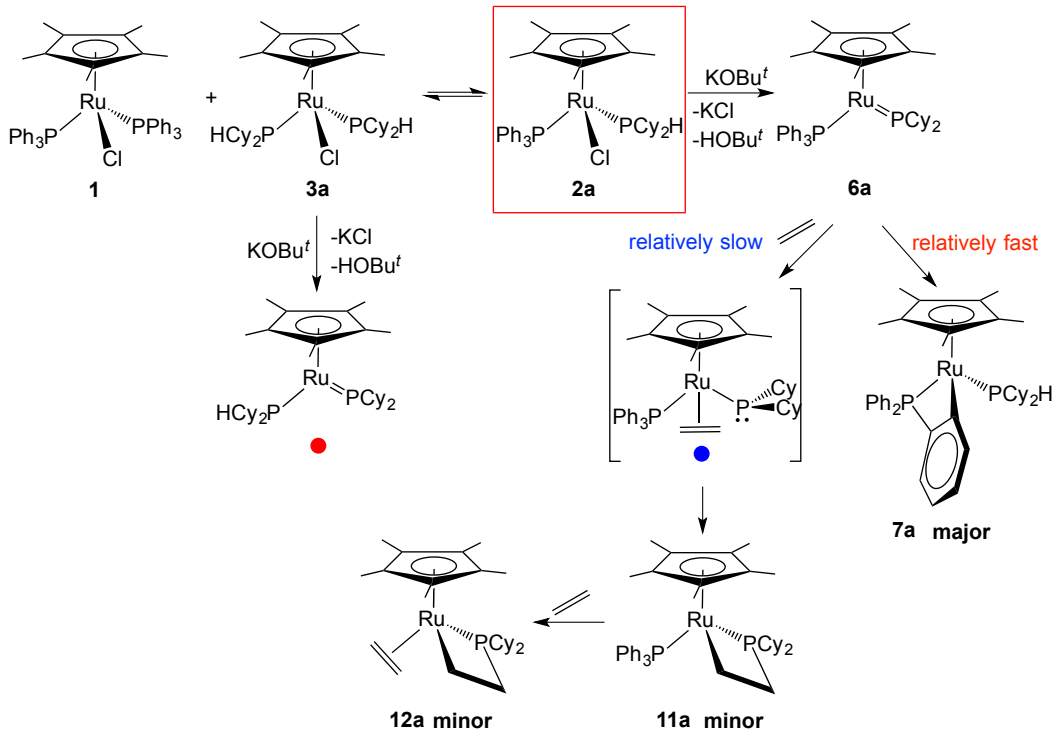

Scheme 4.8 Possible products in the NMR scale reaction of [**2a** + KOBu^{t}] with 0.9 atm ethylene.

Complex **2a** shows the most complicated product mixture of the four reactions studied (see Scheme 4.8). The $^{31}P\{^{1}H\}$ NMR spectrum (Figure 4.8) shows orthometallated complex **7a** (PPh$_3$ δ: 58.6 ppm and PCy$_2$ δ: -18.5 ppm) as the major product, metallacycle **11a** (PPh$_3$ δ: 63.1 ppm and PCy$_2$ δ: -13.0 ppm) and another metallacycle **12a**, in which the PPh$_3$ ligand has been displaced by an η^2-ethylene

ligand (PCy_2 δ: -15.3 ppm), as the minor products. In addition, some other products, unreacted **2a** and free PPh_3 are observed. Among these products, a possible assignment for the ^{31}P signals at 75.0 ppm and 3.0 ppm is Ru(η^5-Cp*)(PCy_2)(η^2-CH_2CH_2)(PPh_3) (blue dot in Figure 4.10), because the indenyl analogue has similar chemical shifts was observed at low temperature in the $^{31}P\{^1H\}$ NMR spectrum.[22] The singlet ^{31}P signal at 53.1 ppm may result from ligand substitution: ethylene exchanges for the PPh_3 ligand in unreacted **2a** to give an η^2-ethylene adduct Ru(η^5-Cp*)Cl(η^2-CH_2CH_2)(PCy_2H). The two doublet ^{31}P signals (δ: 198.6 ppm and δ: 62.7 ppm) have similar chemical shifts and coupling constant ($^2J_{PP}$ = 67 Hz) to the parent phosphido complex **6a**, so are tentatively assigned to a phosphido complex Ru(η^5-Cp*)(PCy_2)(PCy_2H) (red dot in Figure 4.8) due to the redistribution of **2a** (detail in Chapter 2, Section 2.2.2). The ^{31}P signal at 62.7 ppm also splits in the ^{31}P NMR (^1H coupled) spectrum, which supports the presence of coordinated PCy_2H. These minor products could not be fully characterized by NMR spectroscopy because of their low intensity in the NMR spectrum.

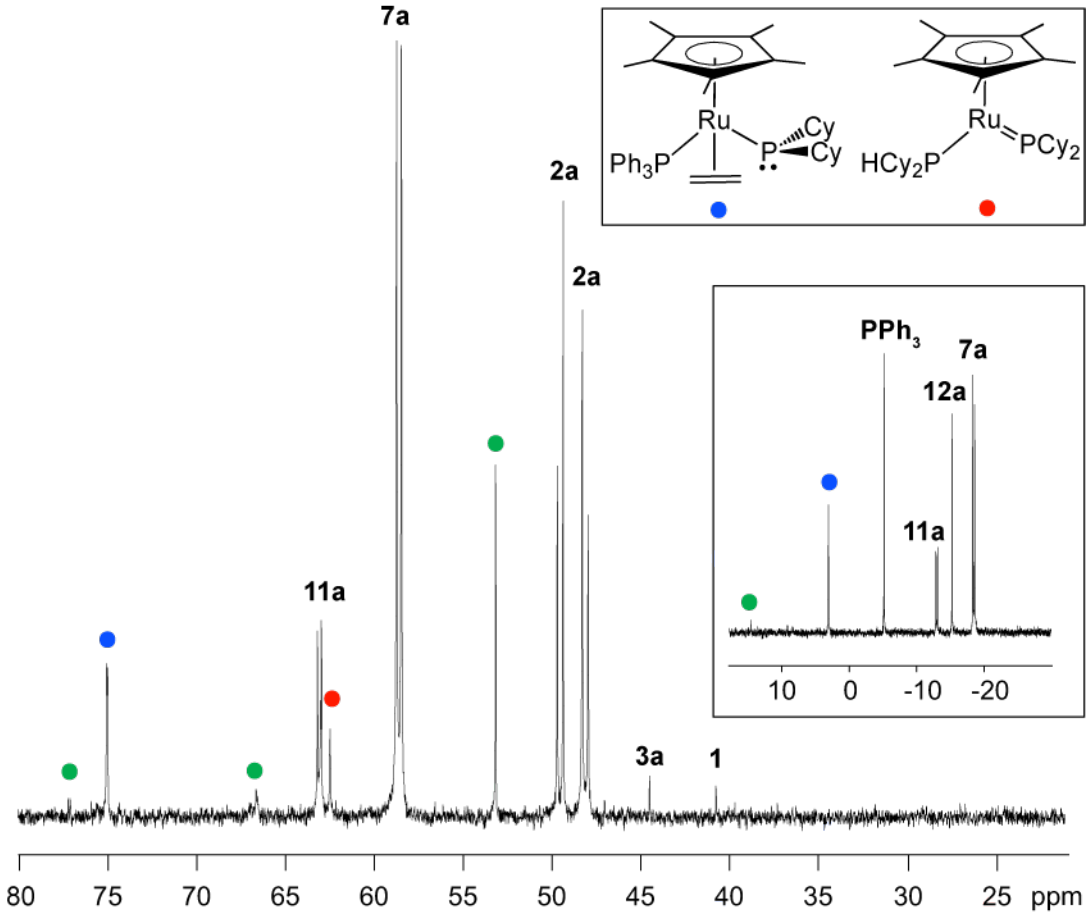

Figure 4.8 Partial $^{31}P\{^{1}H\}$ NMR spectrum (121.55 MHz, C_7D_8) of the reaction of [**2a** + $KOBu^t$] with 0.9 atm ethylene after 0.5 h. The green dot marks signals due to multiple unidentified products.

The reactions of **6b-d** with ethylene are much cleaner than that of **6a** (Scheme 4.9). The $^{31}P\{^{1}H\}$ NMR spectra (after 3h reaction) shows metallacycle **11b-d** (14-82%), orthometallated **7b-d** (1-7%) and another metallacycle **12b-d** (11-83%). The metallacyclic products, the major species in these three reactions are relatively straightforward to characterize using 1D NMR and 2D NMR spectroscopy, as described below.

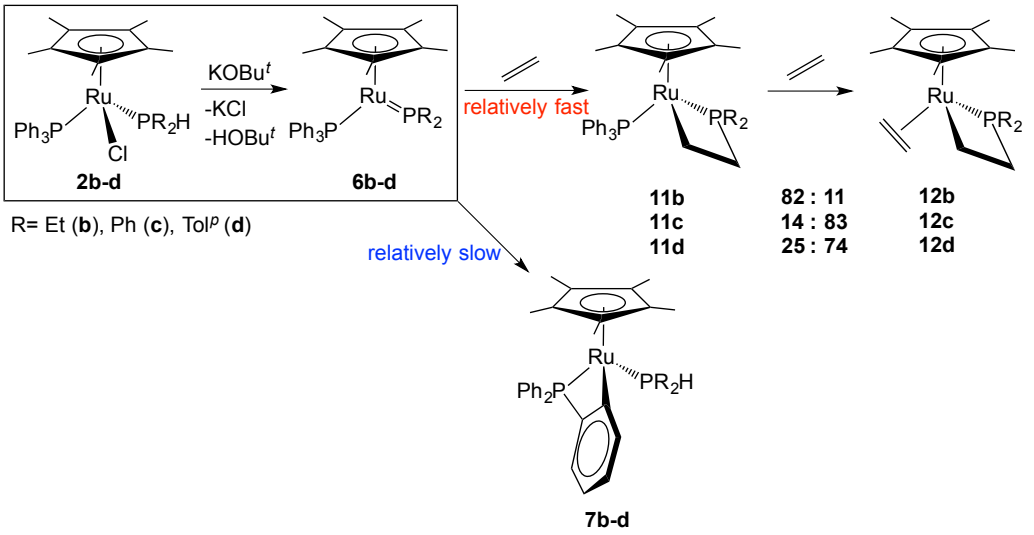

Scheme 4.9 Products of NMR scale reactions of [**2b-d** + KOBu^t] and 0.9 atm ethylene after 3h.

4.4.2 Detailed characterization of Ru(η^5-Cp*)(κ^2-CH$_2$CH$_2$PR$_2$)(PPh$_3$) (11b)

For the reaction of phosphido **6b** with ethylene, the metallacycle **11b** is the major product in a mixture, so most of the signals can be observed in the NMR spectra. Since **11c,d** are the minor products in the mixture, some of their signals can not be observed in the NMR spectra. Thus, **11b** is used here as an example to show the characterization of metallacycles **11b-d**.

Complex **11b** shows a diagnostic ^{31}P signal for the metallacycle (*P*Et$_2$ δ: -22.0 ppm), a downfield ^{13}C signal for the β-carbon atom attached to P (δ: 36.3 ppm) and an upfield signal for the α-carbon atom attached to Ru (δ: -16.1 ppm). These signals are similar to the shifts previously observed for the indenyl metallacycles Ru(η^5-indenyl)(κ^2-CH$_2$CH$_2$PR$_2$)(PPh$_3$) (11^i).[4] For PPh$_3$ ligand, H$_o$ can be identified by its correlation with P in PPh$_3$ in the ^{1}H/^{31}P{^{1}H}-HMBC spectrum. The rest of the protons and carbons can be identified by their correlations with H$_o$ in the phenyl groups in the ^{1}H/^{13}C{^{1}H}-HSQC and HMBC spectra. For the metallacycle protons, H$_D$ (δ: 3.26-3.15 ppm) is distinctly downfield from the other metallacycle protons, and its assignment is confirmed by an nOe interaction with ^{1}H signals due to the CH$_3$ on the -

PEt_2- fragment and the Cp* ligand in the ^{1}H-NOESY spectrum. The assignment of H_B is also confirmed by an nOe interaction with signals due to H_o in PPh_3 relative to other metallacycle protons in ^{1}H-NOESY spectrum (Figure 4.9). The remaining protons attached to the β- (H_C) and α-carbons (H_A) can be identified by their correlations with the β- and α-carbon in the ^{1}H/^{13}C{^{1}H}-HSQC spectrum. The other ^{13}C signals due to ethyl groups on PEt_2 fragment are assigned in ^{13}C DEPT 135 NMR spectrum. All the protons on the PEt_2 fragment of the metallacycle can be identified by correlation with these carbons on the Et groups in the ^{1}H/^{13}C{^{1}H}-HSQC spectrum.

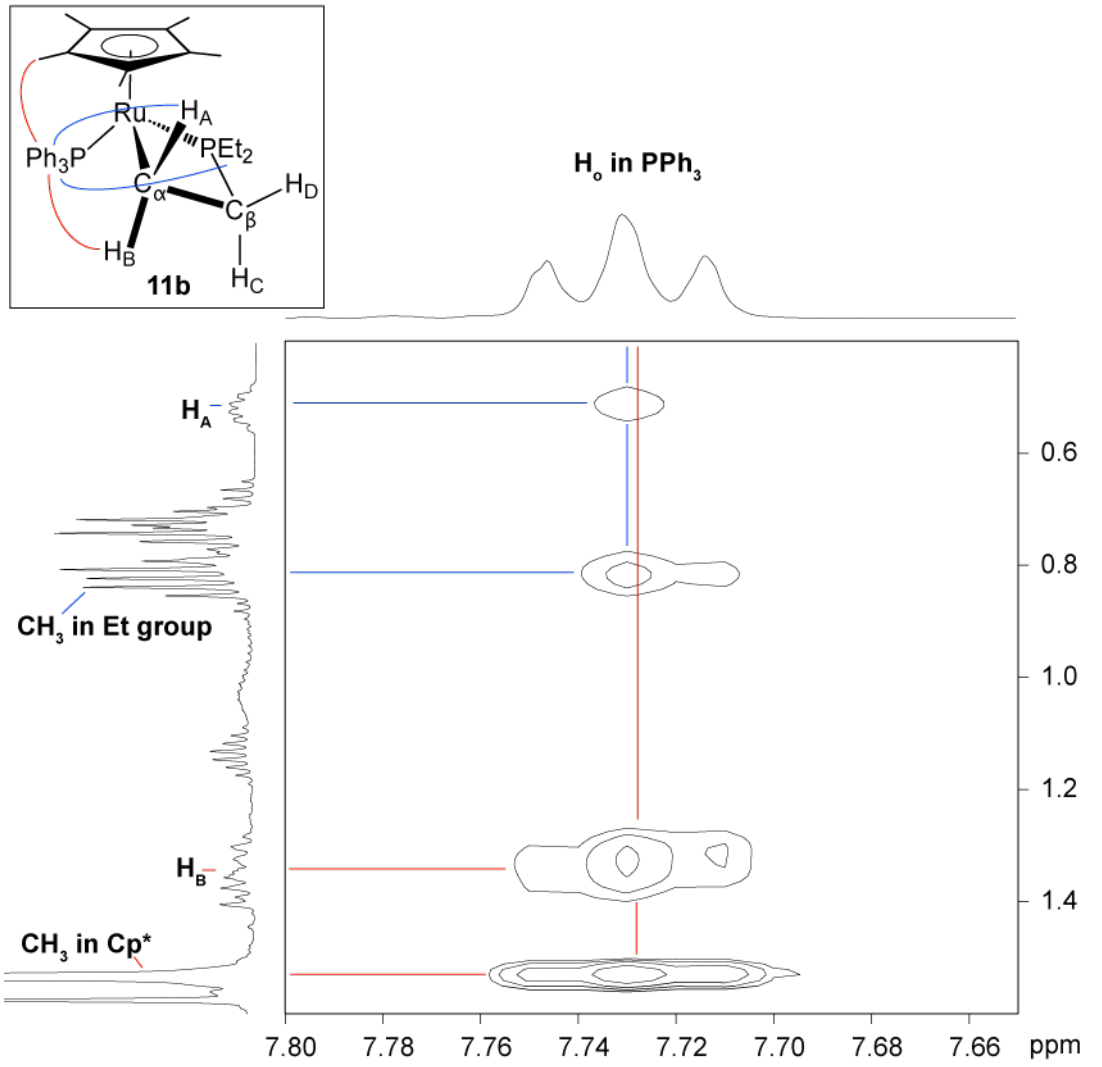

Figure 4.9 Partial ^{1}H-NOESY NMR spectrum (500.27 MHz, C_7D_8) of [**2b** + $KOBu^t$] with 0.9 atm ethylene highlighting the interactions of H_o in PPh_3 with H_B/methyl protons in Cp* ligand (relatively strong in red line) and H_A/methyl protons in ethyl group (relatively weak in blue line) in metallacycle **11b**.

4.4.3 Detailed characterization of Ru(η^5-Cp*)(κ^2-CH_2CH_2PR_2)(η^2-CH_2CH_2) (12c,d)

For the reactions of **6c,d** with ethylene, **12c,d** are the major products in a mixture, so most of the signals can be observed in their NMR spectra. As for **11b**, these complexes show diagnostic upfield ^{31}P signals due to the phosphorus atom in the metallacycle (e.g., **12d** *P*Tol$^p_2$ δ: -10.8 ppm), downfield ^{13}C signals for the β-carbon atom attached to P (e.g., **12d** δ: 36.3 ppm) and upfield signals for the α-carbon atom attached to Ru (e.g., **12d** δ: -9.2 ppm). All four distinct protons on the ethylene fragment of the 4-membered metallacycle in complex (**12c,d**) have been identified and assigned in the ^{1}H NMR spectrum. The protons attached to the β- (H_C/H_D) and α-carbons (H_A/H_B) can be identified by their correlations with the β- and α-carbons in the ^{1}H/^{13}C{^{1}H}-HSQC and HMBC spectra. The ^{1}H shift for H_D (e.g., **12d** δ: 4.07-3.94 ppm) is distinctly downfield from the other metallacycle protons. Its assignment is confirmed by an nOe interaction with signals due to the H_o on the -PAr_2- fragment and the methyl-protons of the Cp* ligand in the ^{1}H-NOESY NMR spectra. For **12d**, in a 1D-selective ^{1}H NOESY NMR spectrum (Figure 4.10), the nOe interactions between H_C (irradiated) and other metallacycle protons can be used to identify the rest of the metallacycle protons. In addition, the nOe interactions between H_C and two broad signals (e.g., **12d** δ: 2.06-1.97 and 1.89-1.79 ppm) are observed. These broad signals are assigned as the coordinated η^2-CH_2CH_2 ligand due to their correlation with P on the PAr_2 fragment of the metallacycle in the ^{1}H/^{31}P{^{1}H}-HMBC spectra and nOe interaction with protons on the metallacycle. In the 2D ^{1}H/^{1}H TOCSY NMR spectra (see example for **12c** in Figure 4.11), these two broad signals also correlate to each other, which is an evidence to support the coordination of ethylene. As for broadening

of signals of PPh_3 ligand (Chapter 2, Section 2.2.2), these broad signals of η^2-CH_2CH_2 may arise from slowed rotation around the bond from Ru to η^2-CH_2CH_2 ligand.

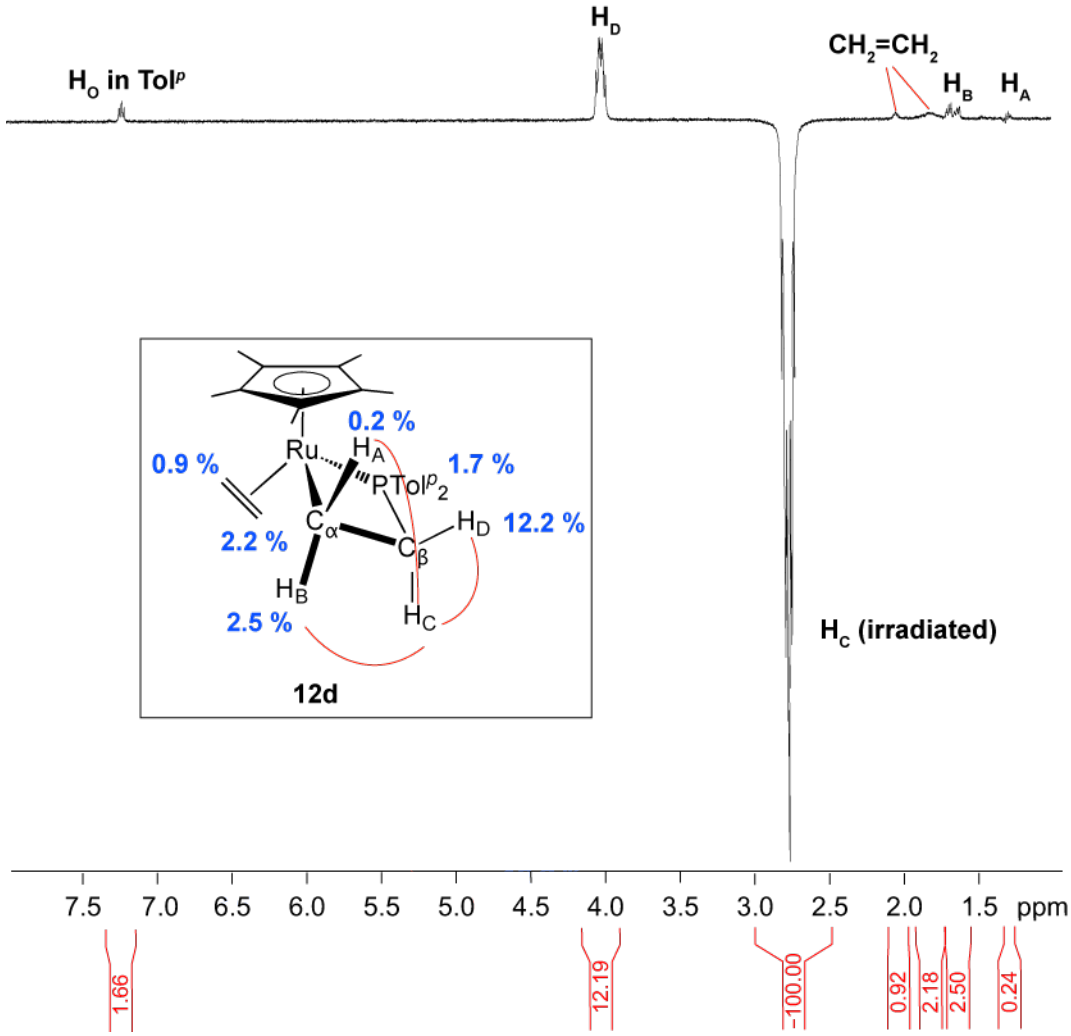

Figure 4.10 1D-selective ^{1}H-NOESY NMR spectrum (500.27 MHz, C_7D_8) of [**2d** + KOBu^t] with 0.9 atm ethylene, showing the percentage of nOe interaction between H_C (irradiated) and other protons in metallacycle **12d**.

For the reaction of **6b** with ethylene, because **12b** is the minor product in the mixture, some signals could not be observed in the NMR spectrum. All observed signals for **12b** have been carefully identified by using the same strategies as for complexes **12c,d**. However, neither proton nor carbon signals for coordinated η^2-ethylene ligand in **12b** are observed.

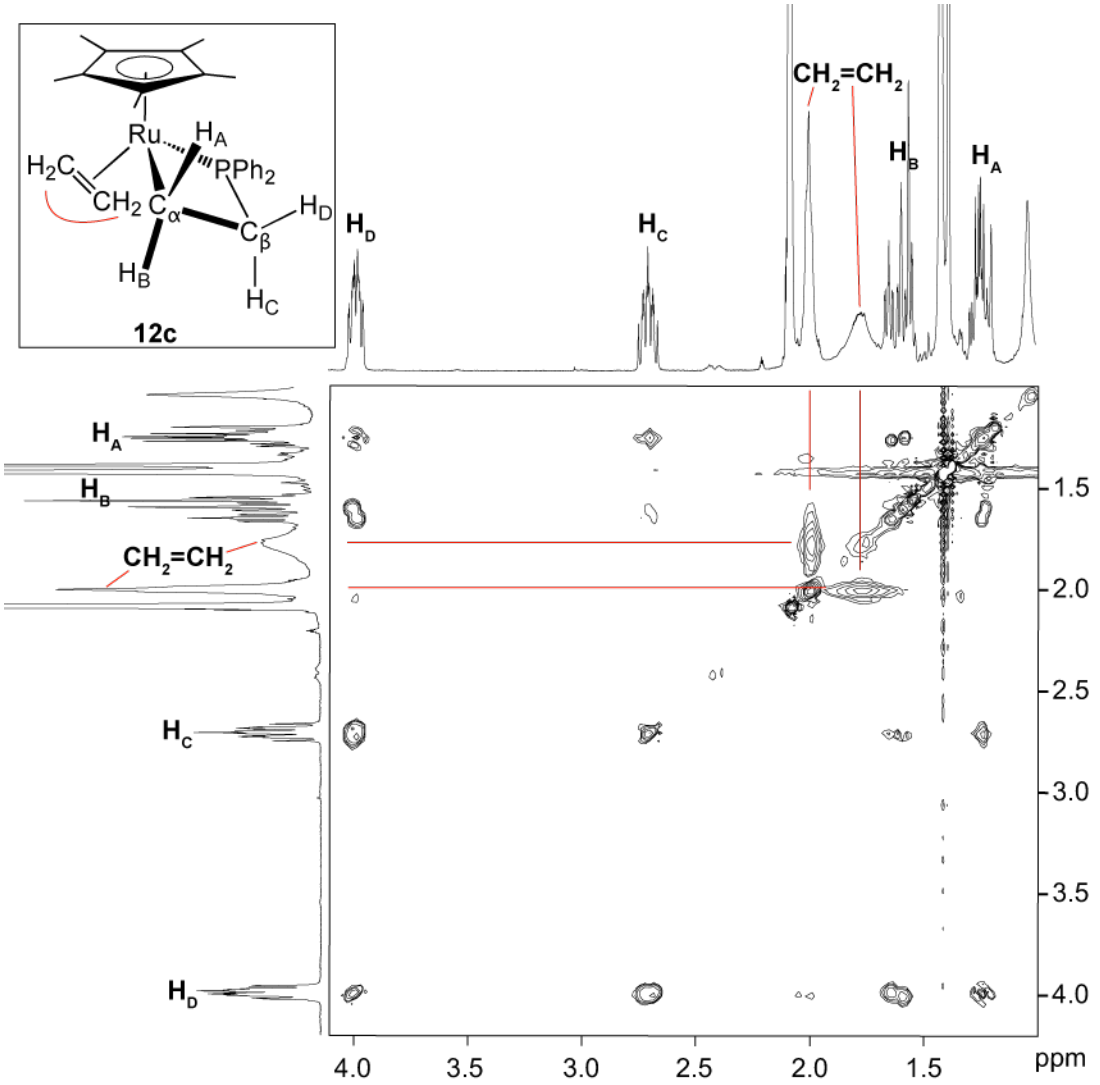

Figure 4.11 Partial 2D $^{1}H/^{1}H$ TOCSY NMR (500.27 MHz, C_7D_8) of [**2c** + KOBu^t] with 0.9 atm ethylene highlighting the interactions between protons on coordinated η^2-ethylene ligand in metallacycle **12c**.

4.4.4 Comparison of the reactivity of Cp* phosphido complexes 6a-d and indenyl analogues in the reactions with ethylene

The cycloaddition of ethylene occurs at phosphido complexes **6a-d** generated *in situ*. As for the reactions of H_2 and CO, the formation of these Cp* metallacycle **11a-d** provides strong proof that variable hapticity of the indenyl ligand is not essential for the alkene cycloaddition reactions to occur for the indenyl half-sandwich analogues.

In support of this conclusion, our collaborator, Dimitrios Pantazis, has performed DFT (PBE/DKH2-TZVP) calculations that found two possible reaction trajectories for the reaction of indenyl phosphido complexes with ethylene.[22] The lower energy

pathway shows that the approach of ethylene to the phosphido complex can prompt some disruption of the Ru=PR_2 double bond, which opens a coordination site at Ru and allows the ethylene to bind to the Ru prior to the cycloaddition. In this case, no formal hapticity change occurs along the reaction trajectory.

In addition, the formation of the η^2-ethylene coordinated indenyl intermediate Ru(η^5-indenyl)(PCy_2)(η^2-CH_2CH_2)(PPh_3) was observed at low temperature, both visually (deep red solution) and by $^{31}P\{^1H\}$ NMR sepctrum (PPh_3 δ: 55.3 ppm and PCy_2 δ: 27.6 ppm) by previous graduate student Krista Morrow.[22] The same observations are found in the reactions of complexes **6b-d** and ethylene. After the NMR tubes, containing complexes **6b-d** generated *in situ* and ethylene, were sealed by flame, they were kept in the ice bath without inversion and then placed in spectrometer as soon as possible. The colour of solution in NMR tube was deep red, and $^{31}P\{^1H\}$ NMR spectrum shows two similar broad signals (e.g., PPh_3 δ: 55.3 ppm and PEt_2 δ: -0.5 ppm in **6b** reaction, red dot in Figure 4.12 bottom), which is presumably the intermediate Ru(η^5-Cp*)(PR_2)(η^2-CH_2CH_2)(PPh_3). When warming up to room temperature, these signals disappeared over time. The colour of the samples also turned to the orange/yellow, indicative of formation of the cycloadduct **11b-d** (see Figure 4.12 top).

However, similar to the reactions of other trapping reagents (H_2 and CO), all Cp* metallacycle **11a-d** will easily form complexes **12a-d** by exchanging the "large" PPh_3. This confirms that increased steric congestion of the Cp* metallacycle fragments Ru(η^5-Cp*)(κ^2-$\underline{C}H_2CH_2\underline{P}R_2$), relative to the indenyl metallacycles.

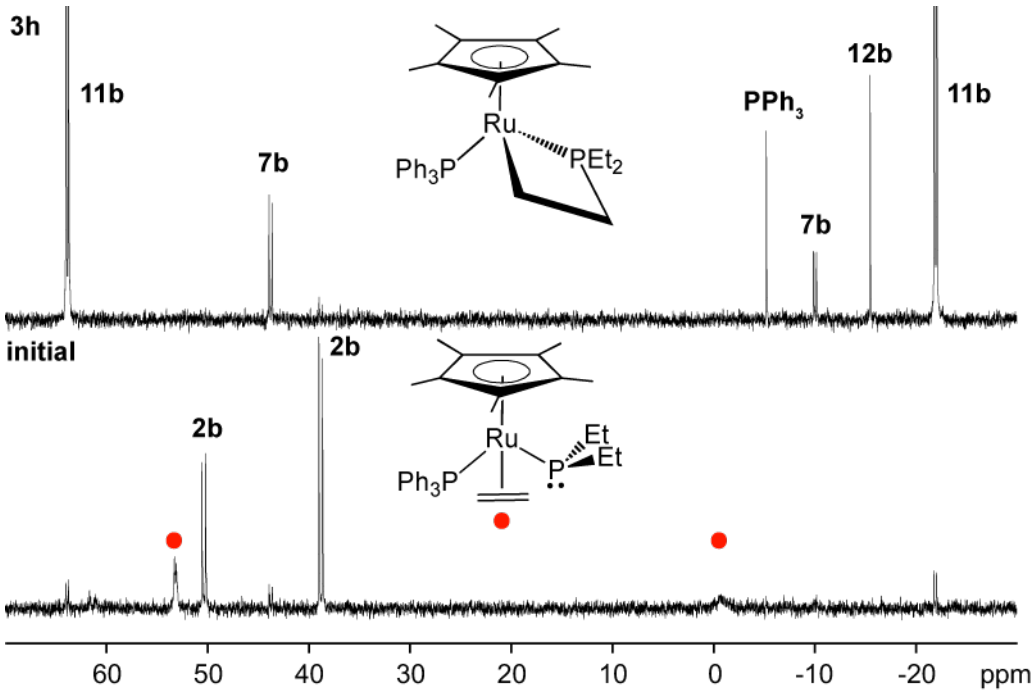

Figure 4.12 $^{31}P\{^{1}H\}$ NMR (202.51 MHz, C_7D_8) of the reaction of [**2b** + KOBu^t] with ethylene showing the formation of intermediate at 0 °C (initial, top), and its subsequent conversion to the metallacyclic product 11b upon warming to room temperature after 3h (bottom)**.**

4.5 Conclusion

In this Chapter, Cp* phosphido **6a-d** are generated *in situ* and their reactivity is explored in a series of NMR-scale reactions with H_2, CO and ethylene. The products of these reactions are mostly identified and characterized. Similar to analogous indenyl complexes, Cp* phosphido **6a-d** can form the hydride complexes **8a-d**, carbonyl complexes **9a-d** and metallacycles **11a-d**, which indicates that the variable hapticity of indenyl group is not necessary for these reactions to occur.

However, as mentioned in Chapter 2, Cp* complexes are not as stable as the indenyl analogues, because of increased steric congestion. H_2 can displace the PPh_3 ligand in hydride complex **8a**. The PPh_3 ligand in the carbonyl complexes **9a-d** is also easy to substitute by CO to give dicarbonyl complexes **10a-d**. Metallacycles **11a-d** also pefer the substitution of PPh_3 ligand by ethylene to form η^2-ethylene adducts **12a-d**.

4.6 Experimental

See Chapter 2, Section 2.6.1 for general experimental details. C_7D_8 was purchased from Canadian Isotope Labs (CIL), degassed using at least three freeze-pump-thaw cycles, and vacuum-transferred from sodium/ benzophenone before use. Complexes Ru(η^5-Cp*)Cl(PR_2H)(PPh_3) (**2a-d**) were prepared as described in Chapter 2 (Section 2.6.3). Potassium *tert*-butoxide ($KOBu^t$) was purchased from Aldrich Chemical Co. and used as received without further purification. Carbon monoxide (CO), ethylene and hydrogen gas (H_2) were purchased from Praxair Canada Inc. Variable temperature NMR spectra were recorded on a Bruker AVANCE 360 operating at 360.28 MHz for ^{1}H, 90.63 MHz for ^{13}C and 145.84 MHz for ^{31}P. NMR spectra were recorded ^{1}H chemical shifts are referenced to residual proteo-solvent peaks at 2.08 (C_7D_7H). ^{13}C chemical shifts are referenced to C_7D_8 at 20.43 ppm. The spectroscopic data is available for most major species identified in the NMR-tube reactions performed in this chapter. The ^{1}H and ^{13}C NMR data can be found in Tables 4.4 - 4.9.

4.6.1 General method for NMR scale reactions with H_2, CO and ethylene

1 mL of C_6D_6 was added to the mixture of solid base (2 mg, 0.018 mmol) and metal complex (**2a**: 12 mg, 0.016 mmol; **2b**: 10 mg, 0.016 mmol; **2c**: 12 mg, 0.017 mmol; **2d**: 12 mg, 0.016 mmol) in a small vial. The initially orange solutions turned dark red (for **2a,b**) or dark blue (for **2c,d**) quickly.

This mixture was transferred to a flame-sealable NMR tube. The sample was degassed by three freeze-pump-thaw cycles before approximately 0.9 atm of gas (H_2, CO or ethylene) was introduced. The sealed sample was inverted five times, and

content were then analyzed by NMR spectroscopy. NMR tubes were also shaken between acquiring each spectrum.

4.6.1.1 Reactions of [complex 2a-d + KOBu^t] with 0.9 atm H_2

These solutions turned to yellow/orange after the samples were inverted. The $^{31}P\{^1H\}$ NMR data and relative amounts of **8** observed after 3h reaction are reported in Table 4.1 (for **8a-d**). The other product is orthometallated **7a-d**. Some extra minor products for reaction of complex **2a** are described in Section 4.2.1.

Table 4.1 202.51 MHz $^{31}P\{^1H\}$ NMR data for hydride complex **8a-d** and their relative amounts after 3h in C_7D_8 at 300 K: δ (ppm) (multiplicity, $^2J_{PP}$ (Hz)).

Complex		PR_2H	PPh_3	% Conversion
Ru(η^5-Cp*)H(PCy_2H)(PPh_3)	**8a**	60.1 (d, 30)	74.5 (d)	0
Ru(η^5-Cp*)H(PEt_2H)(PPh_3)	**8b**	43.9 (d, 32)	74.6 (d)	95
Ru(η^5-Cp*)H(PPh_2H)(PPh_3)	**8c**	44.9 (d, 32)	74.3 (d)	94
Ru(η^5-Cp*)H($PTol^p{}_2H$)(PPh_3)	**8d**	42.9 (d, 32)	74.5 (d)	96

4.6.1.2 Reactions of [complex 2a-d + KOBu^t] with 0.9 atm CO

These solutions turned to red after the samples were inverted, and eventually turned to yellow. The $^{31}P\{^1H\}$ NMR data and relative amounts of **9** and **10** observed after 3h reaction are reported in Table 4.2. The other products are described in Section 4.3.1.

Table 4.2 202.51 MHz $^{31}P\{^1H\}$ NMR data for carbonyl complexes **9a-d** and dcarbonyl complexes **10a-d** and their relative amounts after 3h in C_7D_8 at 300 K: δ (ppm) (multiplicity, $^2J_{PP}$ (Hz)).

Complex		PR_2	PPh_3	%Conversion
Ru(η^5-Cp*)(PCy_2)(CO)(PPh_3)	**9a**	62.7 (s, 58)	57.0 (s)	0
Ru(η^5-Cp*)(PEt_2)(CO)(PPh_3)	**9b**	30.0 (s)	61.4 (s)	95
Ru(η^5-Cp*)(PPh_2)(CO)(PPh_3)	**9c**	15.6 (s)	53.9 (s)	90
Ru(η^5-Cp*)($PTol^p{}_2$)(CO)(PPh_3)	**9d**	19.6 (s)	54.5 (d, 3)	87
Ru(η^5-Cp*)(PCy_2)$(CO)_2$	**10a**	78.3 (s)	N/A	85
Ru(η^5-Cp*)(PEt_2)$(CO)_2$	**10b**	40.2 (s)	N/A	5

$Ru(\eta^5\text{-}Cp^*)(PPh_2)(CO)_2$	**10c**	31.4 (s)	N/A	10
$Ru(\eta^5\text{-}Cp^*)(PTol^p{}_2)(CO)_2$	**10d**	30.3 (s)	N/A	13

4.6.1.3 Reactions of [complex 2a-d + $KOBu^t$] with 0.9 atm ethylene

These solutions turned to orange after the samples were inverted. The $^{31}P\{^1H\}$ NMR data relative amounts of **11** and **12** observed after 3h reaction are reported in Table 4.3. The other products are described in Section 4.4.1.

Table 4.3 202.51 MHz $^{31}P\{^1H\}$ NMR data for metallacycles **11a-d** and **12a-d** and their relative amounts after 3h in C_7D_8 at 300 K: δ (ppm) (multiplicity, $^2J_{PP}$ (Hz)).

Complex		$-PR_2-$	PPh_3	%Conversion
$Ru(\eta^5\text{-}Cp^*)(\kappa^2\text{-}\underline{C}H_2CH_2\underline{P}Cy_2)(PPh_3)$	**11a**	-13.1 (d, 29)	63.0 (d)	14
$Ru(\eta^5\text{-}Cp^*)(\kappa^2\text{-}\underline{C}H_2CH_2\underline{P}Et_2)(PPh_3)$	**11b**	-22.0 (d, 30)	63.8 (d)	82
$Ru(\eta^5\text{-}Cp^*)(\kappa^2\text{-}\underline{C}H_2CH_2\underline{P}Ph_2)(PPh_3)$	**11c**	-13.9 (d, 29)	63.6 (d)	14
$Ru(\eta^5\text{-}Cp^*)(\kappa^2\text{-}\underline{C}H_2CH_2\underline{P}Tol^p{}_2)(PPh_3)$	**11d**	-16.0 (d, 29)	63.7 (d)	25
$Ru(\eta^5\text{-}Cp^*)(\kappa^2\text{-}\underline{C}H_2CH_2\underline{P}Cy_2)(\eta^2\text{-}CH_2CH_2)$	**12a**	-15.4 (s)	N/A	5
$Ru(\eta^5\text{-}Cp^*)(\kappa^2\text{-}\underline{C}H_2CH_2\underline{P}Et_2)(\eta^2\text{-}CH_2CH_2)$	**12b**	-15.6 (s)	N/A	11
$Ru(\eta^5\text{-}Cp^*)(\kappa^2\text{-}\underline{C}H_2CH_2\underline{P}Ph_2)(\eta^2\text{-}CH_2CH_2)$	**12c**	-9.0 (s)	N/A	83
$Ru(\eta^5\text{-}Cp^*)(\kappa^2\text{-}\underline{C}H_2CH_2\underline{P}Tol^p{}_2)(\eta^2\text{-}CH_2CH_2)$	**12d**	-10.8 (s)	N/A	74

Table 4.4 500.27 MHz ^{1}H NMR data for Ru(η^5-Cp*)H(PR_2H)(PPh_3) **8b-d** in C_7D_8 at 300 K: δ in ppm (multiplicity, RI, J_{avg} or $\omega_{1/2}$ in Hz, assignment).[a]

	η^5-Cp*	H-Ru	PPh_3	PR_2H
8b	1.72 (s, 15H)	-12.91 (t, 1H, $^{2}J_{PH}$ 34.5)	**H_o** (dd, 6H, $^{3}J_{PC}$ 10.4, $^{3}J_{HH}$ 8.7) **H_m** 7.12-7.06 (m, 6H) **H_p** 7.04-6.98 (m, 3H)	**H-PEt$_2$** 6.12 (dm, 1H, $^{1}J_{PH}$ 314.6) **CH_2** 1.46-1.34 (m, 2H), 1.19-1.09 (m, 1H), 1.04-0.94 (m, overlaps CH_3, 1H) **CH_3** 1.08-0.98 (m, overlaps CH_2, 3H), 0.94-0.84 (m, 3H)
8c	1.59 (s, 15H)	-12.50 (t, 1H, $^{2}J_{PH}$ 34.7 Hz)	**H_o** 7.72-7.59 (m, 6H) **$H_{m,p}$** 7.11- 6.95 [m, H_m and H_p overlapping, 9H (*also overlaps H_m and H_p in $HPPh_2$)]	**H-PPh$_2$** 6.12 (dd, 1H, $^{1}J_{PH}$ 348.2, $^{3}J_{PH}$ 8.3) **H_o** 7.43 (dd, 2H, $^{3}J_{PH}$ 11.0, $^{3}J_{HH}$ 7.9), 7.24 (dd, 2H, $^{3}J_{PH}$ 10.8, $^{3}J_{PH}$ 8.0) **$H_{m,p}$** 7.11- 6.95 [m, H_m and H_p overlapping, 6H(*also overlaps H_m and H_p in PPh_3)]
8d	1.63 (s, 15H)	-12.50 (t, 1H, $^{2}J_{PH}$ 34.7 Hz)	**H_o** 7.68 (dd, 6H, $^{3}J_{PH}$ 10.3, $^{3}J_{HH}$ 7.7) **H_m** 7.07- 7.02 (m, 9H) **H_p** 7.02-6.96 (m, 3H)	**H-PTol$^p_2$** 6.13 (dd, 1H, $^{1}J_{PH}$ 347.8, $^{3}J_{PH}$ 8.3) **H_o** 7.40 (dd, 2H, $^{3}J_{PH}$ 10.7, $^{3}J_{HH}$ 8.0), 7.19 (dd, 2H, $^{3}J_{PH}$ 10.2, $^{3}J_{PH}$ 8.0) **H_m** 6.95-6.90 (m, 4H) **CH_3** 2.11 (s, 3H), 2.09-2.06 (s, overlaps solvent signals, 3H)

[a] PR_2H [R= Et (**b**), Ph (**c**), Tol^p (**d**)].

Table 4.5 125.79 MHz $^{13}C\{^{1}H\}$ NMR data for Ru(η^5-Cp*)H(PR_2H)(PPh_3) **8b-d** in C_7D_8 at 300 K: δ in ppm (multiplicity, RI, J_{avg} or $\omega_{1/2}$ in Hz, assignment).[a]

	η^5-Cp*	PPh_3	PR_2H
8b	C_{ring} 90.6(s) C_{methyl} 11.6 (s)	C_{ipso} 140.6 (dd, $^{1}J_{PC}$ 36, $^{3}J_{PC}$ 2) C_{ortho} 134.5 (d, $^{2}J_{PC}$ 11) C_{para} 128.3 (s) C_{meta} 127.3 (d, $^{3}J_{PC}$ 9)	**Et:** CH_2 21.3 (d, $^{1}J_{PC}$ 25), 21.2 (dd, $^{1}J_{PC}$ 26, $^{3}J_{PC}$ 4) CH_3 12.5 (d, $^{2}J_{PC}$ 3), 12.0 (s)
8c	C_{ring} 91.5(s) C_{methyl} 11.3 (s)	C_{ipso} 139.4 (dd, $^{1}J_{PC}$ 37, 2) C_{ortho} 134.4 (d, $^{2}J_{PC}$ 11) C_{para} 128.3 (s) C_{meta} 127.3 (d, $^{3}J_{PC}$ 9)	**Ph:** C_{ipso} 136.9 (d, $^{1}J_{PC}$ 34) C_{ortho} 134.1 (d, $^{2}J_{PC}$ 11), 133.3 (d, $^{2}J_{PC}$ 11) C_{para} 128.6 (s), 128.2 (s) C_{meta} 127.7 (d, $^{3}J_{PC}$ 9), 127.6 (d, $^{3}J_{PC}$ 9)

8d	C_{ring} 91.4 (s) C_{methyl} 11.4 (s)	C_{ipso} 139.6 (dd, $^1J_{PC}$ 37, $^3J_{PC}$ 2) C_{ortho} 134.5 (d, $^2J_{PC}$ 11) C_{para} 128.3 (s) C_{meta} 127.3 (d, $^3J_{PC}$ 9)	**Tol^p:** C_{para} 138.2 (s), 137.7 (s) C_{ipso} 135.9 (d, $^1J_{PC}$ 41), 135.8 (d, $^1J_{PC}$ 41) C_{ortho} 134.2 (d, $^2J_{PC}$ 11), 133.4 (d, $^2J_{PC}$ 11) C_{meta} 128.5 (d, $^3J_{PC}$ 9), 128.4 (d, $^3J_{PC}$ 9) CH_3 21.2 (s), 21.1 (s)

[a] PR_2H [R= Cy(**a**), Et (**b**), Ph (**c**), Tol^p (**d**)].

Table 4.6 500.27 MHz ^{1}H NMR data for Ru(η^5-Cp*)(PR_2)(CO)(PPh_3) **9a-d** and Ru(η^5-Cp*)(PR_2)(CO)$_2$ **10a-d** in C_7D_8 at 300 K: δ in ppm (multiplicity, RI, J_{avg} or $\omega_{1/2}$ in Hz, assignment).[a]

	η^5-Cp*	**PPh_3**	**PR_2**
9a	1.52 (s, 15H)	**H_o** 7.56 (br s, 6H, $\omega_{1/2}$ 28.9) **$H_{m,p}$** 7.08- 6.99 (m, H_m and H_p overlapping, 9H)	**Cy (all signals overlap with 10a):** **CH** 2.37-2.23 (m, 2H) **CH_2** 2.05-1.96 (m, 4H), 1.90-1.68 (m, 8H), 1.49-1.35 (m, 8H)
9b	1.49 (s, 15H)	**H_o** 7.60-7.48 (t, 6H, $^3J_{PH}$ 8.6) **H_m** 7.07-7.02 (m, 6H) **H_p** 7.02-6.98 (m, 3H)	**Et:** **CH_2 (B)** 2.24-2.14 (m, 1H), 1.97-1.87 (m, 1H) **CH_2 (A)** 1.38-1.33 (m, 1H), 1.23-1.17 (m, 1H) **CH_3 (B)** 1.46-1.40 (m, 3H) **CH_3 (A)** 1.11-1.04 (m, 3H)
9c	1.40 (s, 15H)	**H_o** 7.41 (br s, 6H, $\omega_{1/2}$ 28.9) **$H_{m,p}$** 7.05-6.84 [m, H_m and H_p overlapping, 9H (*also overlap $H_{m,p}$ signals in PPh_2)]	**Ph:** **H_o** 7.50 (br s, 4H, $\omega_{1/2}$ 20.6) **$H_{m,p}$** 7.05-6.84 [m, H_m and H_p overlapping, 6H (*also overlap $H_{m,p}$ in PPh_3)]
9d	1.42 (d, 15H, $^4J_{PH}$ 1.4)	**H_o** 7.48-7.42 (m, overlaps H_o in PTol$^p_2$, 6H) **$H_{m,p}$** 7.00-6.93 [m, H_m and H_p overlapping, 9H (*also overlap with H_m signals in PTol$^p_2$)]	**Tol^p:** **H_o** 7.48-7.42 (m, overlaps H_o in PPh_3, 4H) **H_m** 7.00-6.42 (m, overlaps $H_{m,p}$ in PPh_3, 4H) **CH_3** 2.11(s, 3H), 2.06 (s, overlaps solvent residual signal, 3H)

10a	1.63 (s, 15H)	N/A	**Cy (all signals overlap with 9a):** **CH** 2.37-2.23 (m, 2H) **CH_2** 2.05-1.96 (m, 4H), 1.90-1.68 (m, 8H), 1.49-1.35 (m, 8H)
10b	1.62 (s, 15H)	N/A	Not observed.
10c	1.60 (s, 15H)	N/A	**Ph:** **H_o** 7.50 (br s, 4H, $\omega_{1/2}$ 20.6) **$H_{m,p}$** not observed, must overlap with signals in **9c**
10d	1.63 (s, 15H)	N/A	**Tol^p:** **H_o** 7.68 (dd, 4H, $^3J_{PH}$ 8.0, $^3J_{HH}$ 7.7) **H_m** 6.96 (d, 4H, $^3J_{HH}$ 7.7) **CH_3** 2.10 (s, 6H)

[a] PR_2 [R= Cy(**a**), Et (**b**), Ph (**c**), Tol^p (**d**)].

Table 4.7 125.79 MHz $^{13}C\{^1H\}$ NMR data for Ru(η^5-Cp*)(PR_2)(CO)(PPh_3) **9a-d** and Ru(η^5-Cp*)(PR_2)$(CO)_2$ **10a-d** in C_7D_8 at 300 K: δ in ppm (multiplicity, RI, J_{avg} or $\omega_{1/2}$ in Hz, assignment).[a]

	η^5-Cp*	**CO**	**PPh_3**	**PR_2**
9b	C_{ring} 97.7 (s) C_{methyl} 9.4 (d, $^3J_{PC}$ 8)	210.9 (s)	C_{ipso} 136.9 (d, $^1J_{PC}$ 43) C_{ortho} 134.5 (d, $^2J_{PC}$ 11) C_{para} 129.5 (s) C_{meta} 127.9 (d, $^3J_{PC}$ 10)	**Et:** CH_2 (A) 25.8 (d, $^1J_{PC}$ 29) CH_2 (B) 23.0 (d, $^1J_{PC}$ 33) CH_3 (A) 17.1 (d, $^2J_{PC}$ 25), CH_3 (B) 16.3 (d, $^2J_{PC}$ 17)
9c	C_{ring} 97.9 (s) C_{methyl} 9.6 (d, $^3J_{PC}$ 4)	Not observed	C_{ipso} 135.6 (d, $^1J_{PC}$ 40) C_{ortho} 134.6 (d, $^2J_{PC}$ 10, $^4J_{PC}$ 2) C_{para} 129.5 (s) C_{meta} 127.2 (d, $^3J_{PC}$ 5)	**Ph:** C_{ipso} 148.8 (d, $^1J_{PC}$ 40) C_{ortho} 135.9 (d, $^2J_{PC}$ 20) C_{meta} 127.8 (d, $^3J_{PC}$ 9) C_{para} 125.4 (s)
9d	C_{ring} 97.9 (s) C_{methyl} 9.6 (d, $^3J_{PC}$ 5)	211.3 (s)[b]	C_{ortho} 134.6 (d, $^2J_{PC}$ 11, $^4J_{PC}$ 2) C_{meta} 127.8 (d, $^3J_{PC}$ 10) C_{meta} 129.3 (d, $^4J_{PC}$ 2)	**Tol^p:** C_{ipso} not observed C_{ortho} 136.1 (d, $^2J_{PC}$ 20) C_{meta} 128.1 (d, $^3J_{PC}$ 5) C_{para} not observed

10a	C_{ring} 100.5 (s) C_{methyl} 9.8 (d, $^3J_{PC}$ 8)	206.1(s)	N/A	**Cy:** CH 36.3 (d, $^1J_{PC}$ 31) CH_2 33.2 (d, 10), 32.6 (d, 14), 28.4 (d, 9), 28.3 (d, 12), 27.3 (s)
10b	C_{ring} not observed C_{methyl} 9.6 (d, $^3J_{PC}$ 6)	Not observed	N/A	Not observed
10c	C_{ring} 100.3 (s) C_{methyl} 9.5 (d, $^3J_{PC}$ 5)	203.2 (s)	N/A	**Ph:** C_{ipso} not observed C_{ortho} 134.2 (d, $^2J_{PC}$ 20) C_{meta} 128.7 (d, $^3J_{PC}$ 9) C_{para} 126.6 (s)
10d	C_{ring} 100.2 (s) C_{methyl} 9.6 (d, $^3J_{PC}$ 5)	203.5 (s)	N/A	**Tol^p:** C_{ipso} not observed C_{para} not observed C_{ortho} 134.2 (d, $^2J_{PC}$ 20) C_{meta} 128.7 (d, $^3J_{PC}$ 5) CH_3 21.1 (s)

[a] PR_2 [R= Cy(**a**), Et (**b**), Ph (**c**), Tol^p (**d**)].
[b]Not directly observed but tracked by $^1H/^{13}C\{^1H\}$-HMBC spectrum (CO <=> H in Cp*).

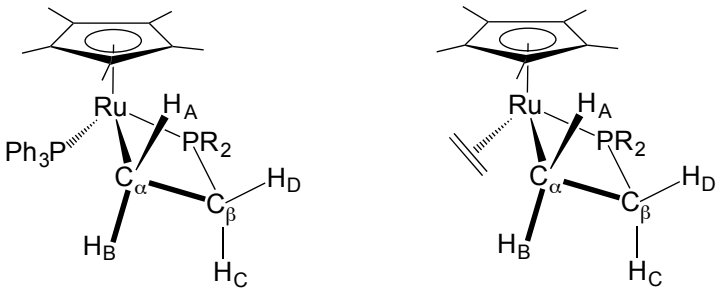

11 **12**

Figure 4.13 Structures of Ru(η^5-Cp*)(κ^2-CH_2CH_2PR_2)(PPh_3) **11** and Ru(η^5-Cp*)(κ^2-CH_2CH_2PR_2)(η^2-CH_2CH_2) **12** showing -CH_2CH_2- metallacycle protons H_{A-D} and carbons C_β and C_α.

Table 4.8 500.27 MHz ^{1}H NMR data for Ru(η^5-Cp*)(κ^2-CH_2CH_2PR_2)(PPh_3) **11b-d** and Ru(η^5-Cp*)(κ^2-CH_2CH_2PR_2)(η^2-CH_2CH_2) **12b-d** in C_7D_8 at 300 K: δ in ppm (multiplicity, RI, J_{avg} or $\omega_{1/2}$ in Hz, assignment).[a]

	η^5-Cp*	**κ^2-CH_2CH_2PR_2**	**Others**
11b	1.53 (s, 15H)	**CH_2CH_2:** **H_D** 3.26-3.15 (m, 1H), **H_C** 2.05-1.98 (m, 1H) **H_B** 1.36-1.27 (m, 1H), **H_A** 0.82-0.73 (m, 1H) **PEt_2:** **CH_2 (A)** 1.96-1.84 (m, 1H), 1.61-1.49 (m, 1H) **CH_2 (B)** 1.19-1.08 (m, 1H), 0.57-0.46 (m, 1H) **CH_3 (B)** 0.86-0.79 (m, 3H) **CH_3 (A)** 0.75-0.68 (m, 3H)	**PPh_3:** **H_o** 7.73 (dd, 6H, $^3J_{PH}$ 9.3, $^3J_{HH}$ 8.3) **$H_{m,p}$** 7.11-7.01 (m, H_m and H_p overlapping, 9H)
11c	1.38 (s, 15H)	**CH_2CH_2:** **H_D** 4.05-3.99 (m, 1H), **H_C** 2.04-1.95 (m, 1H) **H_B** 1.71-1.56 (m, 1H), **H_A** 1.39-1.29 (m, 1H) **PPh_2:** **H_o** 7.34-7.28 (m, overlaps with **12c**, 2H), 7.13-7.07 (m, overlaps with **12c**, 2H) **H_m** 7.05-6.97(m, overlaps with **12c**, 2H), 6.91-6.78 (m, 2H) **H_p** not observed	**PPh_3:** **H_o** 7.52 (br s, 6H, $\omega_{1/2}$ 28.7) **$H_{m,p}$** not observed
11d	1.42 (s, 15H)	**CH_2CH_2:** **H_D** 4.07-3.94 (m, 1H), **H_C** 2.12-2.05 (m, 1H) **H_B** 1.72-1.57 (m, 1H), **H_A** 1.42-1.34 (m, 1H) **$PTol^p_2$:** **H_o** 7.36-7.25 (m, 2H), 6.93-6.85 (m, 2H) **H_m** 7.11-7.07 (m, 2H), 6.73 (d, 2H, $^3J_{PH}$ 9.2), **CH_3** 2.06-2.00 (s, overlaps with **12d**, 3H), 1.98 (s, 3H)	**PPh_3:** **H_o** 7.57 (br s, 6H, $\omega_{1/2}$ 25.2) **$H_{m,p}$** not observed
12b	1.53 (s, 15H)	**CH_2CH_2:** **H_D** 3.07-2.98 (m, 1H), **H_C** 2.18-2.09 (m, 1H), **H_B** 1.61-1.52 (m, 1H), **H_A** 0.79-0.70 (m, 1H)	**η^2-CH_2CH_2:** Not observed

		PEt_2: **CH_2** 1.43-1.31 (m, 1H), 1.07-0.86 (m, 2H), 0.69-0.61 (m, 1H) **CH_3** 0.87-0.77 (m, 3H), 0.80-0.67 (m, 3H)	
12c	1.41 (d, $^4J_{PH}$ 1.5, 15H)	**CH_2CH_2:** **H_D** 4.05-3.99 (m, 1H), **H_C** 2.80-2.68 (m, 1H) **H_B** 1.71-1.60 (m, 1H), **H_A** 1.34-1.23 (m, 1H) **PPh_2:** **H_o** 7.36-7.29 (m, overlaps with **11c**, 2H), 7.26 (dd, 2H, $^3J_{PH}$ 9.2, $^3J_{HH}$ 8.0) **$H_{m,\,p}$** 7.07-6.97 (m, H_m and H_p overlapping, 6H)	**η^2-CH_2CH_2:** 2.04-1.95 (br s, 2H, $\omega_{1/2}$ 19.2) 1.91-1.63 (br s, 2H, $\omega_{1/2}$ 57.9)
12d	1.47 (s, 15H)	**CH_2CH_2:** H_D 4.07-3.94 (m, 1H), H_C 2.81-2.71 (m, 1H), H_B 1.72-1.57 (m, 1H), H_A 1.36-1.26 (m, 1H) **$PTol^p_2$:** **H_o** 7.34-7.25 (m, overlaps with **11d**, 2H), 7.22 (dd, 2H, $^3J_{PH}$ 9.8, $^3J_{HH}$ 8.2) **H_m** 6.93-6.85 (m, 4H) **CH_3** 2.04 (s, 3H), 2.02 (s, 3H)	**η^2-CH_2CH_2:** 2.06-1.97 (br s, overlaps with CH_3 on *p*-Tol, 2H), 1.89-1.71 (br s, 2H, $\omega_{1/2}$ 42.1)

[a] Structure illustrating locations of -CH_2CH_2- metallacycle protons H_{A-D} [R= Cy(**a**), Et (**b**), Ph (**c**), Tol^p (**d**)] in Figure 4.13.

Table 4.9 125.79 MHz $^{13}C\{^1H\}$ NMR data for Ru(η^5-Cp*)(κ^2-$\underline{C}H_2CH_2\underline{P}R_2$)($PPh_3$) **11b-d** and Ru($\eta^5$-Cp*)($\kappa^2$-$\underline{C}H_2CH_2\underline{P}R_2$)($\eta^2$-$CH_2CH_2$) **12b-d** in C_7D_8 at 300 K: δ in ppm (multiplicity, RI, J_{avg} or $\omega_{1/2}$ in Hz, assignment).[a]

	η^5-Cp*	**κ^2-$\underline{C}H_2CH_2\underline{P}R_2$**	**Others**
11b	C_{ring} 89.3 (s) C_{methyl} 10.6 (s)	**CH_2CH_2:** C_β 36.3 (d, $^1J_{PC}$ 31), C_α -16.1 (dd, $^2J_{PC}$ 42, $^2J_{PC}$ 12) **PEt_2:** CH_2 (A) 18.3 (dd, $^1J_{PC}$ 16, $^3J_{PC}$ 2), 6.9 (d, $^2J_{PC}$ 8) CH_2 (B) 16.5 (dd, $^1J_{PC}$ 4, $^3J_{PC}$ 2,), 8.2 (s)	**PPh_3:** C_{ortho} 140.6 (d, $^1J_{PC}$ 30), 135.2 (d, $^2J_{PC}$ 10) C_{para} 128.3 (d, $^4J_{PC}$ 2) C_{meta} 127.4 (d, $^3J_{PC}$ 8)
11c	C_{ring} 89.9 (s)	**CH_2CH_2:** C_β 41.8 (d, $^1J_{PC}$ 30), C_α not observed	**PPh_3:** C_o 135.3 (br s,

	C_{methyl} 10.6 (s)	**PPh_2:** C_{ortho} 132.0 (d, $^2J_{PC}$ 9) C_{meta} 127.7 (d, $^2J_{PC}$ 8), 127.2 (d, $^2J_{PC}$ 8) C_{para} and C_{ipso} not observed	$\omega_{1/2}$ 21) $C_{m,p}$ not observed.
11d	C_{ring} 89.8 (s) C_{methyl} 10.7 (s)	**CH_2CH_2:** 41.8 (d, $^1J_{PC}$ 30, C_β), C_α was not observed **$PTol^p_2$:** C_{ortho} 133.3 (d, $^2J_{PC}$ 9), 132.1 (d, $^2J_{PC}$ 9) C_{meta}, C_{para} and C_{ipso} not observed. CH_3 21.1 (s), 21.0 (s)	**PPh_3:** C_o 135.4 (d, $^2J_{PC}$ 10) $C_{m,p}$ not observed.
12b	C_{ring} 91.7 (s), C_{methyl} 9.6 (s)	**CH_2CH_2:** C_β 33.8 (d, $^1J_{PC}$ 30), C_α -10.0 (d, $^2J_{PC}$ 45) **PEt_2:** CH_2 16.1 (d, $^1J_{PC}$ 16), another CH_2 not observed, CH_3 7.5 (s), 7.1 (d, $^2J_{PC}$ 7)	**η^2-CH_2CH_2:** Not observed.
12c	C_{ring} 91.9 (d, $^2J_{PC}$ 2) C_{methyl} 9.2 (s)	**CH_2CH_2:** C_β 38.2 (d, $^1J_{PC}$ 30), C_α -9.3 (d, $^2J_{PC}$ 47) **PPh_2:** C_{ipso} 138.9 (d, $^1J_{PC}$ 31), 135.1 (d, $^1J_{PC}$ 23) C_{ortho} 132.7 (d, $^2J_{PC}$ 10), 131.3 (d, $^2J_{PC}$ 9) C_{para} 129.0 (d, $^4J_{PC}$ 2), 128.3 (d, $^4J_{PC}$ 2) C_{meta} 128.2 (d, $^3J_{PC}$ 9), 128.1 (d, $^3J_{PC}$ 9)	**η^2-CH_2CH_2:** Not observed.
12d	C_{ring} 91.9 (s) C_{methyl} 9.2 (s)	**CH_2CH_2:** C_β 38.2 (d, $^1J_{PC}$ 31), C_α -9.2 (d, $^2J_{PC}$ 47) **$PTol^p_2$:** C_{para} 138.8 (d, $^4J_{PC}$ 2), 137.7 (d, $^4J_{PC}$ 2) C_{ipso} 135.7 (d, $^1J_{PC}$ 33), 132.0 (d, $^1J_{PC}$ 25) C_{ortho} 132.7 (d, $^2J_{PC}$ 10), 131.4 (d, $^2J_{PC}$ 9) C_{meta} 129.0 (d, $^3J_{PC}$ 8), 128.8 (d, $^3J_{PC}$ 8) CH_3 21.2 (s), 21.1 (s)	**η^2-CH_2CH_2:** Not observed.

[a] Structure illustrating locations of -CH_2CH_2- metallacycle carbons C_β and C_α [R= Cy(**a**), Et (**b**), Ph (**c**), Tol^p (**d**)] in Figure 4.13.

4.7 References

[1] Derrah, E. J.; Pantazis, D. A.; McDonald, R.; Rosenberg, L. *Organometallics* **2007,** *26,* 1473.

[2] Derrah,E. J.; Giesbrecht, K. E.; McDonald, R.; Rosenberg, L. *Organometallics* **2008**, 27 , 5025.

[3] Derrah, E. J.; McDonald. R; Rosenberg, L. *Chem. Commun.* **2010**, *46*, 4592.

[4] Derrah, E. J.; Pantazis, D. A.; McDonald, R.; Rosenberg, L. *Angew. Chem. Int. Ed.* **2010**, *49*, 3367.

[5] Rosenberg, L. *ACS Catal.* **2013**, *3*, 2845.

[6] Derrah, E. J.; Marlinga, J. C.; Mitra, D.; Friesen, D. M.; Hall, S. A.; McDonald, R.; Rosenberg, L. *Organometallics* **2005,** *24*, 5817

[7] Planas, J. G.; Hampel, F.; Gladysz. J. A. *Chem. Eur. J.* **2005**, *11*, 1402.

[8] Comparable chemical shifts of $Ru(\eta^5\text{-}Cp^*)H_3(PR_3)$ see: Suzuki, H.; Lee, D. H.; Oshima, N.; Morooka, Y. *Organometallics*, **1987**, *6*, 1569. For $PR_3 = PPh_3$ ($^{31}P\{^1H\}$ δ: 79.3 ppm and ^1H for Ru-H δ: -9.72 ppm, $^2J_{PH} = 20.5$ Hz in C_6D_6)

[9] Davies, S. G.; Moon, S. D.; Simpson, S. J. *J. Chem. Soc., Chem. Commun.* **1983**, 1278

[10] For $^2J_{PH}$ coupling constant characteristic of *cis*- and *trans*- phosphine ruthenium hydrides see: J. B. Letts, T. J. Mazanek, D. W. Meek, *J. Am. Chem. Soc.*, **1982**, 104, 3898.

[11] J. K. Hoyano, W. A. G. Graham, *J. Am. Chem. Soc.,* **1982**, 104, 3722.

[12] Hoyle, M. M.; Pantazis, D. A.; Burton, H. M.; McDonald, R.; Rosenberg, L. *Organometallics* **2011**, *30*, 6458.

[13] Derrah, E. *Probing the Reactivity of Ruthenium Indenyl Complexes in P-C Bond forming Reactions.* Ph.D. Thesis, University of Victoria, **2009**.

[14] Baker, R. T.; Krusic, P. J.; Tulip, T. H.; Calabrese, J. C.; Wreford, S. S. *J. Am. Chem. Soc.* **1983**, 105, 6763.

[15] Baker, R. T.; Calabrese, J. C.; Glassman, T. E. *Organometallics* **1988**, *7*, 1889.

[16] Baker, R. T.; Tulip, T. H.; Wreford, S. S. *Inorg. Chem.* **1985**, *24*, 1379.

[17] Pangan, L. N.; Kawano, Y.; Shimoi, M. *Organometallics* **2000**, *19*, 5575.

[18] Verkade, J. G.; Quin,L. D. *Phosphorus-31 NMR Spectroscopy in Stereochemical Analysis*; VCH Publishers, Inc.: Deerfield Beach, Fl, **1987**; Vol.8

[19] Deeming, A. J.; Doherty, S.; Marshall, J. E.; Powell, J. L.; Senior, A. M. *J. Chem. Soc., Dalton Trans.* **1993**, 1093.

[20] Wicht, D. K.; Paisner, S. N.; Lew, B. M.; Glueck, D. S.; Yap, G. P. A.; Liable- Sands, L. M.; Rheingold, A. L.; Harr, C. M.; Nolan, S. P. *Organometallics* **1998**, *17*, 652

[21] Zhuravel, M. A.; Glueck, D. S.; Zakharov, L. N.; Rheingold, A. L. *Organometallics* **2002**, *21*, 3208.

[22] Burton, K. M. E. *Phosphorus-Containing Ruthenacycles: Exploring Their Potential in Processes Relevant to Hydrophosphination.* MSc. Thesis, University of Victoria, **2010**.

Chapter 5 Different reactivity of Cp* phosphido complexes Ru(η^5-Cp*)(PR_2)(PPh_3) (6a-d) from their indenyl analogues

5.1 Introduction

In Chapter 4, similar reactivity to indenyl analogues was demonstrated for Cp* phosphido Ru(η^5-Cp*)(PR_2)(PPh_3) (**6a-d**). However, some difference in reactivity of the Cp* and indenyl phosphido complexes is also revealed. This Chapter will present studies of the reactivity of Cp* phosphido **6a-d** generated *in situ* (see Chapter 3) with some alkyne and alkene reagents that is different relative to the indenyl analogues. Note: indenyl complexes discussed in this chapter were only given numbers if the Cp* analogues were prepared.

5.1.1 [2+2]-Cycloaddition reactions of substituted alkenes and alkynes at indenyl phosphido complexes Ru(η^5-indenyl)(PR_2)(PPh_3) (**6^i**)

The indenyl phosphido complexes Ru(η^5-indenyl)(PR_2)(PPh_3) (**6^i**, R= alkyl or aryl) have been found to undergo [2+2] cycloaddition reactions with both activated and simple alkynes and alkenes (Scheme 5.1).[1,2,3] The addition of alkyne to **6^i** results in the rapid formation of metallacycle **14^i** as a major product and alkynyl complex **13^i** as a minor product. For alkene (e.g., 1-hexene, acrylonitrile) reactions, the metallacycle is found to be the only product and the reaction is mostly highly stereoselective for the *syn*-isomer (>95%), where the R group on the Ru-bound α-carbon is oriented *syn* with respect to the Ru-indenyl bond (see Scheme 5.1). In addition, these reactions are found to be regioselective with the P-C bond forming at the terminal β-carbon of the substrate. This stereo- and regioselectivity of

cycloaddition may be used to design the desirable selectivity in metal-catalyzed hydrophosphination.

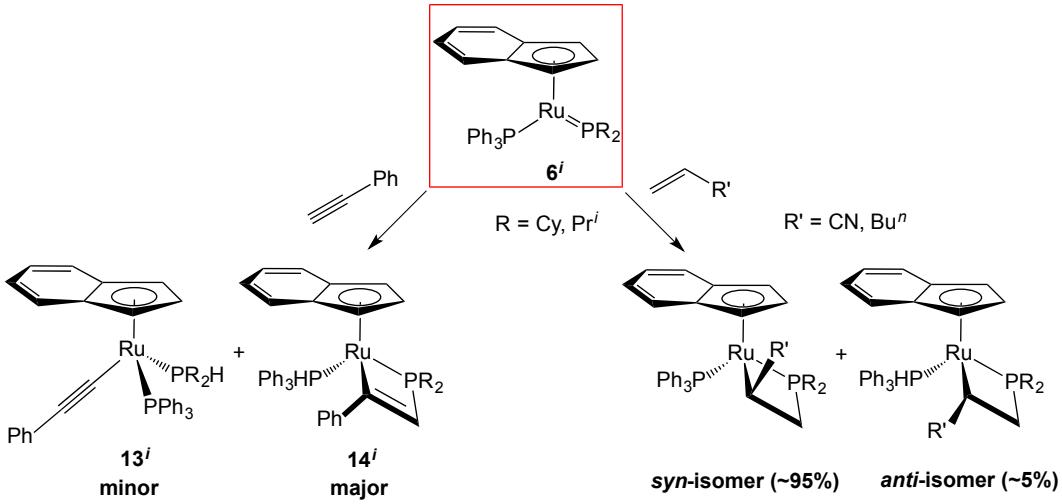

Scheme 5.1 [2+2] cycloaddition of both alkyne and alkenes at the indenyl phosphido complexes ***6****i*.

5.1.2 Benzonitrile adducts of terminal indenyl diarylphosphido complexes

Previous undergraduate student Marc-André Hoyle synthesized and isolated the benzonitrile-stabilized terminal diarylphosphido complexes Ru(η^5-indenyl)(NCPh)(PR_2)(PPh_3) (R= Ph, Tol^p, see Scheme 5.2).[3] The benzonitrile ligand was found to be more labile in these complexes relative to the CO-adducts Ru(η^5-indenyl)(CO)(PR_2)(PPh_3) (***9****i*, R= Ph, Tol^p). These six-coordinate phosphido complexes with pyramidal geometry at phosphorus (P) may be more nucleophilic relative to the planar phosphido complexes, since they contain a Ru-PR_2 single bond with the lone pair localized at P.[4] As a result, these terminal phosphido compounds with labile PhCN ligand are likely to be important reactive intermediates in catalytic P-C bond formation *via* a nucleophilic addition. Current graduate student Roman Belli is now studying their activity for the catalytic hydrophosphination of activated alkenes.[5]

In this Chapter, I have attempted to reproduce these reactivities (of alkynes, alkenes and nitrile) with Cp* phosphido **6**.

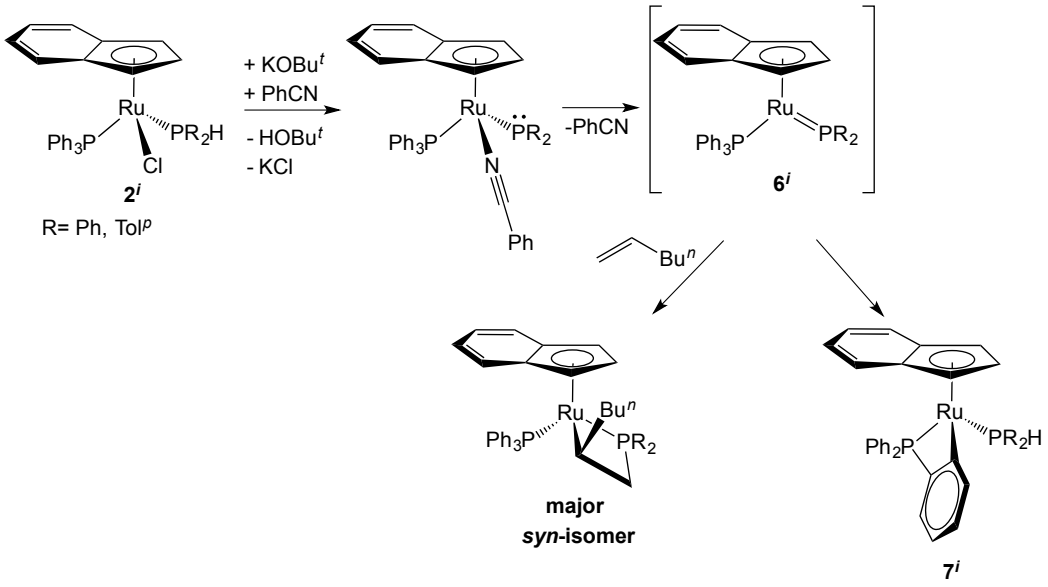

Scheme 5.2 Dehydrohalogenation of complexes **2^i** in the presence of benzonitrile gives benzonitrile adducts Ru(η^5-indenyl)(NCPh)(PR_2)(PPh_3) and reactions show the facile dissociation of benzonitrile ligand.

5.2 Reactions of phenylacetylene with Cp* phosphido complexes 6a-d

The phosphido **6a-d** were generated *in situ* as described previously in Chapter 3, and then phenylacetylene were added to the mixed solution. The reactions were monitored by NMR spectroscopy.

5.2.1 Products resulting from addition of phenylacetylene

As usual, complex **2a** (R= Cy) gave the most complicated product mixture of the four reactions studied (Scheme 5.3). The $^{31}P\{^1H\}$ NMR spectrum (Figure 5.1b) shows orthometallated complex Ru(η^5-Cp*)\{κ^2-(*o*-C_6H_4)PPh_2\}(PCy_2H) (**7a**, ~52 %), alkynyl complex Ru(η^5-Cp*)(C≡CPh)(PCy_2H)(PPh_3) (**13a**, ~20 %) and some other products

after 3h. No metallacyclic product is observed in this reaction, which is different from the reaction of the indenyl analogue with phenylacetylene (Scheme 5.1).

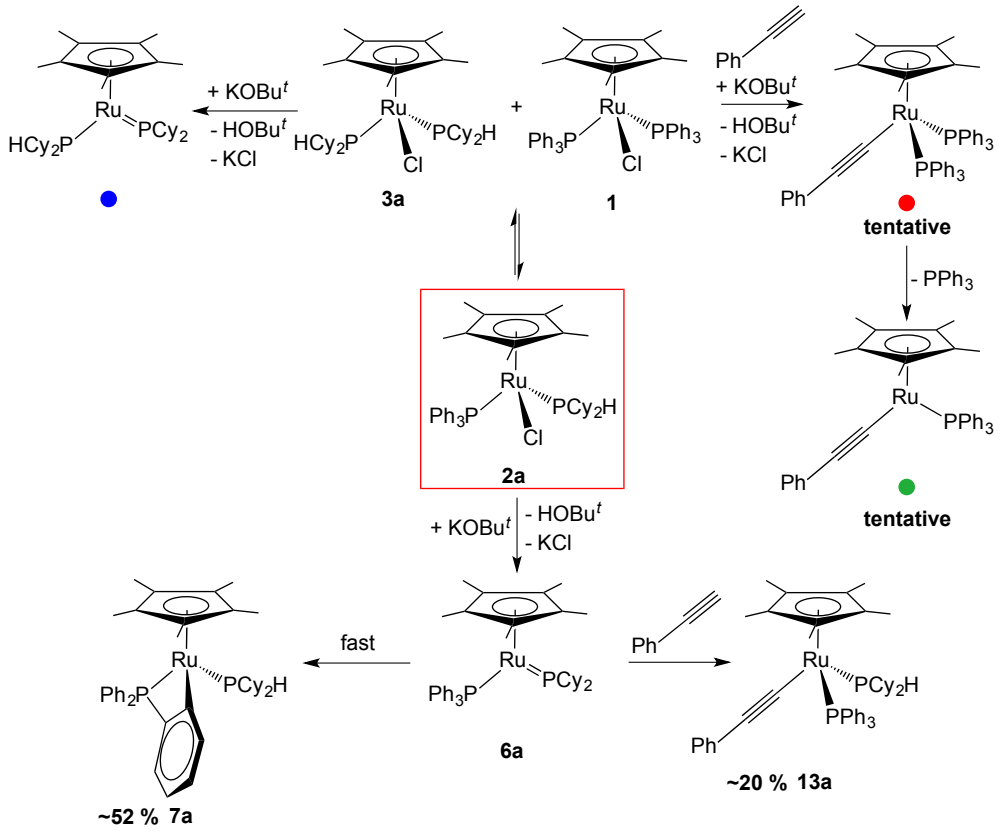

Scheme 5.3 Possible products in NMR scale reaction of [**2a** + KOBu^t] with phenylacetylene after 3h.

In addition, some minor products are observed due to the redistribution of **2a** to complex Ru(η^5-Cp*)Cl(PCy_2H)$_2$ (**3a**) and Ru(η^5-Cp*)Cl(PPh_3)$_2$ (**1**) in a solution (see Chapter 2, Section 2.2.2). Complex **3a** can be deprotonated by KOBu^t to give a phosphido complex Ru(η^5-Cp*)(PCy_2)(PCy_2H) (blue dot in Figure 5.1a, ~15%). Complex **1** also can react with KOBu^t and phenylacetylene to give a new alkynyl complex Ru(η^5-Cp*)(C≡CPh)(PPh_3)$_2$ (~10%), which is tentatively assigned to the singlet peak at 53.3 ppm (red dot in Figure 5.1a). Slattery and coworkers reported the synthesis and $^{31}P\{^1H\}$ NMR spectroscopic data (δ: 50.9 ppm in C_7D_8) for an analogue Ru(η^5-Cp)(C≡CPh)(PPh_3)$_2$, which supports the assignment of Ru(η^5-Cp*)(C≡CPh)(PPh_3)$_2$.[6] This Cp* alkynyl complex doesn't seems to be stable due to

the facile dissociation of the PPh_3 ligand, as previously seen in the ligand substitution reactions of complex **1** (see Chapter 2). It may lose one PPh_3 ligand to give an unsaturated complex $Ru(\eta^5\text{-}Cp^*)(C{\equiv}CPh)(PPh_3)$ (green dot in Figure 5.1b, ~3%), which explains the singlet at 60.4 ppm. These assignments are also supported by the control experiment (Figure 5.1b) in which complex **1** reacts with $KOBu^t$ and phenylacetylene. These minor products could not be fully characterized because of their low intensity in the NMR spectra.

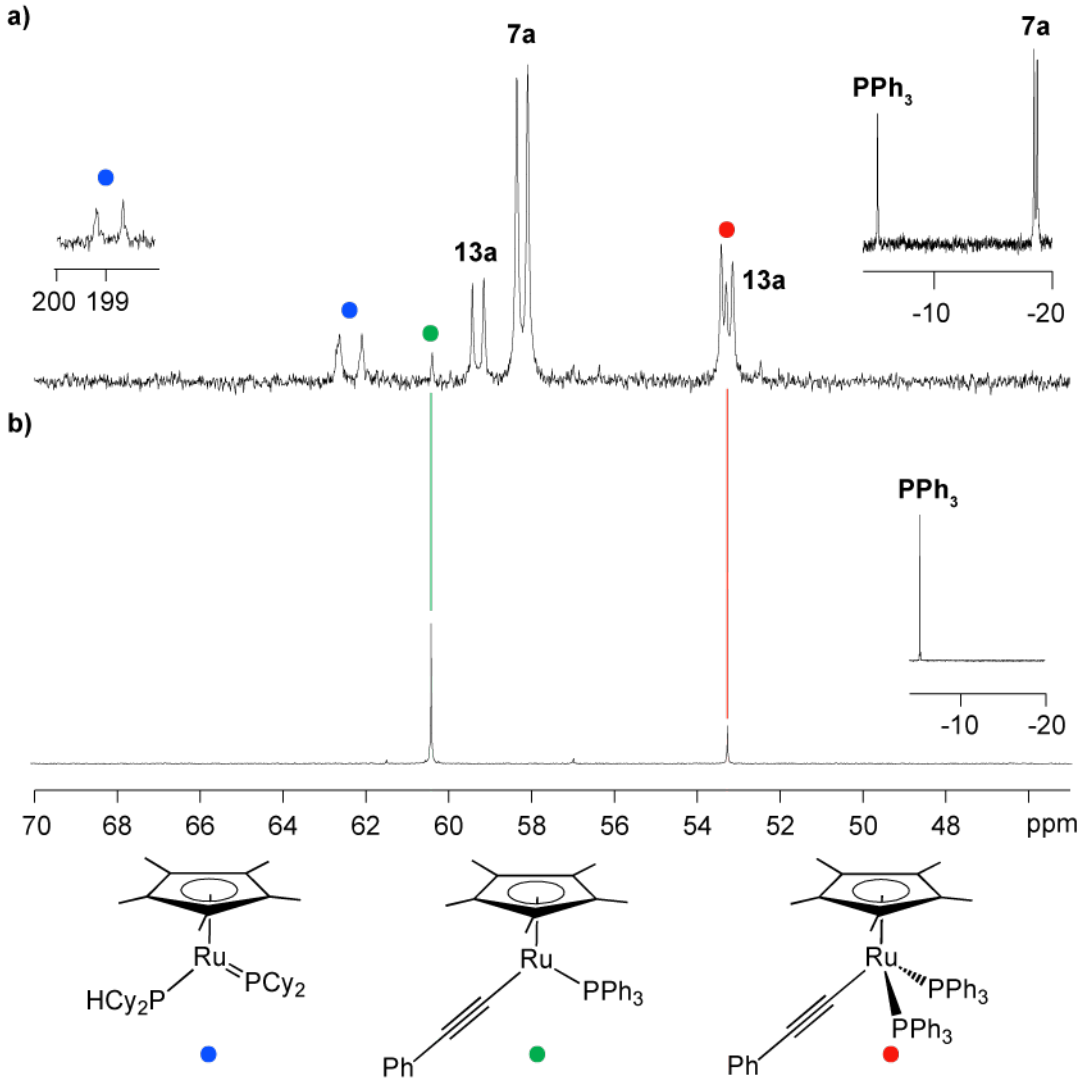

Figure 5.1 a) $^{31}P\{^1H\}$ NMR spectrum (202.51 Hz, C_6D_6) of the reaction of [**2a** + $KOBu^t$] with phenylacetylene after 3h. **b)** $^{31}P\{^1H\}$ NMR spectrum (202.51 Hz, C_6D_6) of the control reaction of [**1** + $KOBu^t$] with phenylacetylene after 3h.

The addition of phenylacetylene to **2b-d** resulted in the formation of two complexes (Scheme 5.4). After 3h, one product is identified as the alkynyl complex Ru(η^5-Cp*)(C≡CPh)(PR_2H)(PPh_3) (**13b-d**) (20-82%), and the other product is identified as an unsaturated metallacycle Ru(η^5-Cp*)(κ^2-PhC=CHPR_2)(PPh_3) (14b-d) (15-80%).

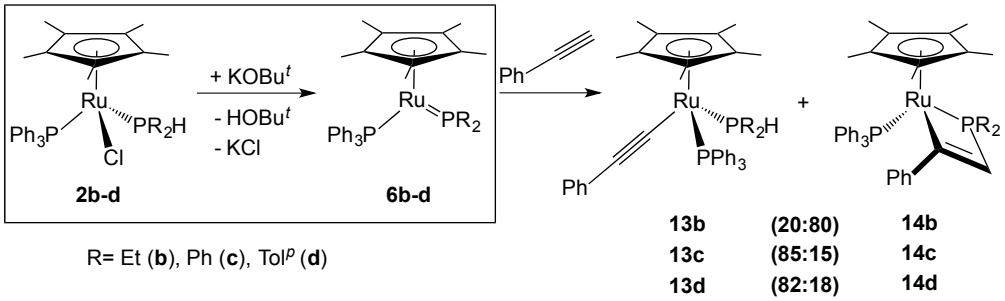

Scheme 5.4 Products of NMR scale reactions of [**2a-d** + KOBu^t] with phenylacetylene after 3h.

The alkynyl complexes **13a-d** resulting from the deprotonation of the terminal proton of phenylacetylene are identified in the $^{31}P\{^1H\}$ NMR spectra by the presence of two doublets (e.g. **13d** δ: 56.2 and 39.6 ppm, $^2J_{PP}$ = 37 Hz). The upfield doublet signals are assigned to PR_2H due to the presence of a large $^1J_{PH}$ coupling (e.g. **13d**: 377 Hz) in ^1H and ^{31}P NMR spectra.

The metallacyclic structure of **14b-d** is confirmed by the $^{31}P\{^1H\}$ NMR spectra which shows the diagnostic upfield signals (e.g. **14d** $P\text{Tol}^p_2$ δ: -40.8 ppm) for 4-membered metallacycles (see Section 4.1.1).[7,8] Relative to indenyl analogues Ru(η^5-indenyl)(κ^2-PhC=CHPR_2)(PPh_3) (**14^i**), these signals due to the P of the metallacycle for Cp* complex **14b-d** are further upfield.[8] This further upfield signals may arise from more electron-rich Ru in the Cp* complex which requires for less electron donation from P of the metallacycle. The ^1H signals (e.g. **14d** δ: 1.41 ppm) due to CH_3 in Cp* can be identified by correlation with both of the P on the 4-membered metallacycle and PPh_3 in the $^1H/^{31}P\{^1H\}$-HMBC spectrum.

The major products, alkynyl **13c,d** and metallacycle **14b,** are characterized by using 1D and 2D NMR spectroscopy, as described below. For the minor products **13a,b** and **14c,d**, attempts to gain more structural information from NMR spectra were unsuccessful because of their low abundance in the reaction mixture.

5.2.2 Detailed characterization of Ru(η^5-Cp*)(C≡CPh)(PR_2H)(PPh_3) (13c-d)

As described above, two doublets in the $^{31}P\{^1H\}$ NMR spectra are assigned to coordinated PR_2H and PPh_3 ligands in alkynyl complexes **13a-d**. The assignment of ^1H and ^{13}C signals for the major products **13c** and **13d** is carried out as follows. The H_o and H_m in PR_2H ligand can be identified by their correlation with P in the $^1H/^{31}P\{^1H\}$-HMBC NMR spectra, and then corresponding C_{ortho} and C_{meta} can be identified by the correlation with H_o and H_m in the $^1H/^{13}C\{^1H\}$-HSQC NMR spectra. The remaining protons and carbons in coordinated PR_2H can be found by the correlation with the C_{ortho} and C_{meta} in the $^1H/^{13}C\{^1H\}$-HMBC NMR spectra. Similar to the PR_2H ligand, most of signals due to the proton and carbon in PPh_3 ligand can be identified by their correlations in the $^1H/^{13}C\{^1H\}$-HSQC and HMBC NMR spectra. The signals due to H_o on the phenyl rings are very broad (e.g., **13d** δ: 7.91-7.47 ppm, $\omega_{1/2}$ = 145.8 Hz). For the alkynyl group, the ^{13}C shifts for the β-carbon (e.g., **13d** δ: 112.3 ppm) are distinctly downfield relative to free phenylacetylene (δ: 83.8 ppm) (Figure 5.2).[9] These assignments are confirmed by correlation with signals due to H_o in the coordinated phenylacetylene in the $^1H/^{13}C\{^1H\}$-HMBC NMR spectra (e.g., **13c** in Figure 5.2). The assignment of these ^{13}C shifts due to the β-carbon are also very similar to the analogue Ru(η^5-Cp)(C≡CPh)(PPh_3)$_2$ reported by Slattery and coworkers.[6] However, signals due to the α-carbon are not observed in $^{13}C\{^1H\}$ NMR spectra, which may arise from the low intensity of the quaternary carbon.

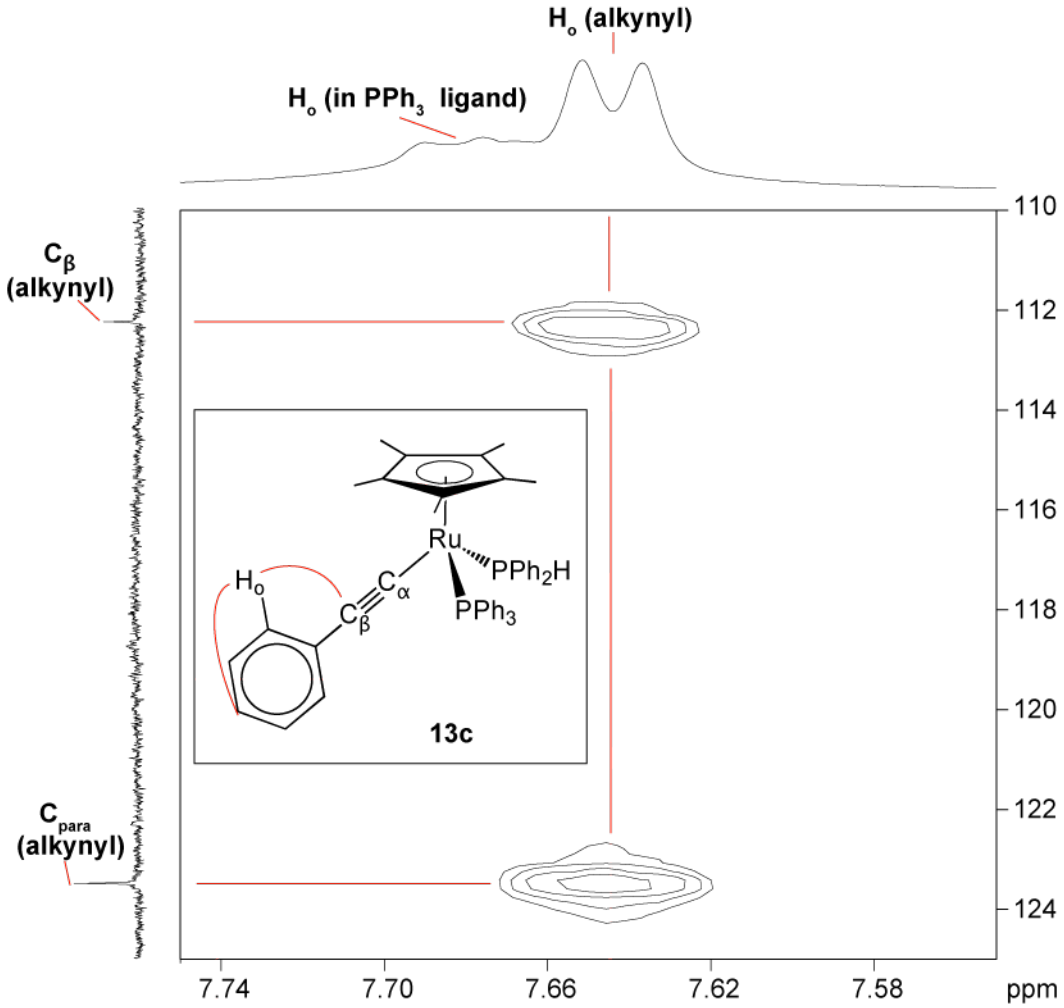

Figure 5.2 Partial $^{1}H/^{13}C\{^{1}H\}$-HMBC NMR spectrum (500.27 MHz, C_6D_6) of [**2c** + KOBu^t] with phenylacetylene, highlighting the correlation of H_o with Cβ and C_{para} in alkylnyl group in alkynyl complex **13c**.

5.2.3 Detailed characterization of Ru(η^5-Cp*)(κ^2-PhC=CHPEt$_2$)(PPh$_3$) (14b)

As described in Section 5.2.1, the $^{31}P\{^{1}H\}$ NMR spectra show diagnostic signals for the 4-membered metallacycles. For **14b**, this ^{31}P signal due to PEt_2 has a upfield shift (δ: -41.9 ppm) and the signal at δ 61.9 ppm is assigned to PPh_3 ligand. Signals due to all the protons and carbons on the PEt_2 fragment on the metallacycle can be identified by their correlations in the $^{1}H/^{13}C\{^{1}H\}$-HSQC and HMBC spectra. The ^{1}H signal due to the proton attached to β-carbon (see Figure 5.3 for labels) can be identified by its correlation with the P of PEt_2 in the $^{1}H/^{31}P\{^{1}H\}$-HMBC spectrum, which indicates the P-C bond connectivity. The ^{13}C peak at 125.0 ppm is assigned to

the β-carbon attached to the P in PEt_2 due to its correlation with the protons on the 4-membered metallacycle in the $^1H/^{13}C\{^1H\}$-HSQC spectrum. This regiochemistry is also supported by the ^{13}C signal due to the β-carbon which shows a large $^1J_{PC}$ coupling (43 Hz) to the P on the 4-membered metallacycle and a small $^3J_{PC}$ coupling (2 Hz) to P in the PPh_3 ligand. This is also consistent with coupling observed in the ^1H NMR spectrum which shows that the H attached to the β-carbon has a $^2J_{PH}$ coupling (9.4 Hz) to PEt_2 in the metallacycle and a $^3J_{PH}$ coupling (4.0 Hz) to the PPh_3 ligand. The signal due to the metallated α-carbon attached to the phenyl group on the metallacycle is not directly observed in the $^{13}C\{^1H\}$ NMR spectrum because of the low intensity of the quaternary carbon. However, approximate ^{13}C shift (δ: ~193.4 ppm) for the α-carbon can be found by its correlations with signals due to H_o of the phenyl group on the metallacycle and the H attached to the β-carbon in the $^1H/^{13}C\{^1H\}$-HMBC spectrum. Similar chemical shifts and coupling constants for α- and β-carbons were previously observed for indenyl analogues.[1] Signals due to the remaining protons and carbons on the metallacycle fragment can be identified by their correlations with assigned signals in the $^1H/^{13}C\{^1H\}$-HSQC and HMBC spectra. For the PPh_3 ligand, the signal due to H_o on the phenyl rings is very broad, which is similar to alkynyl complexes mentioned above.

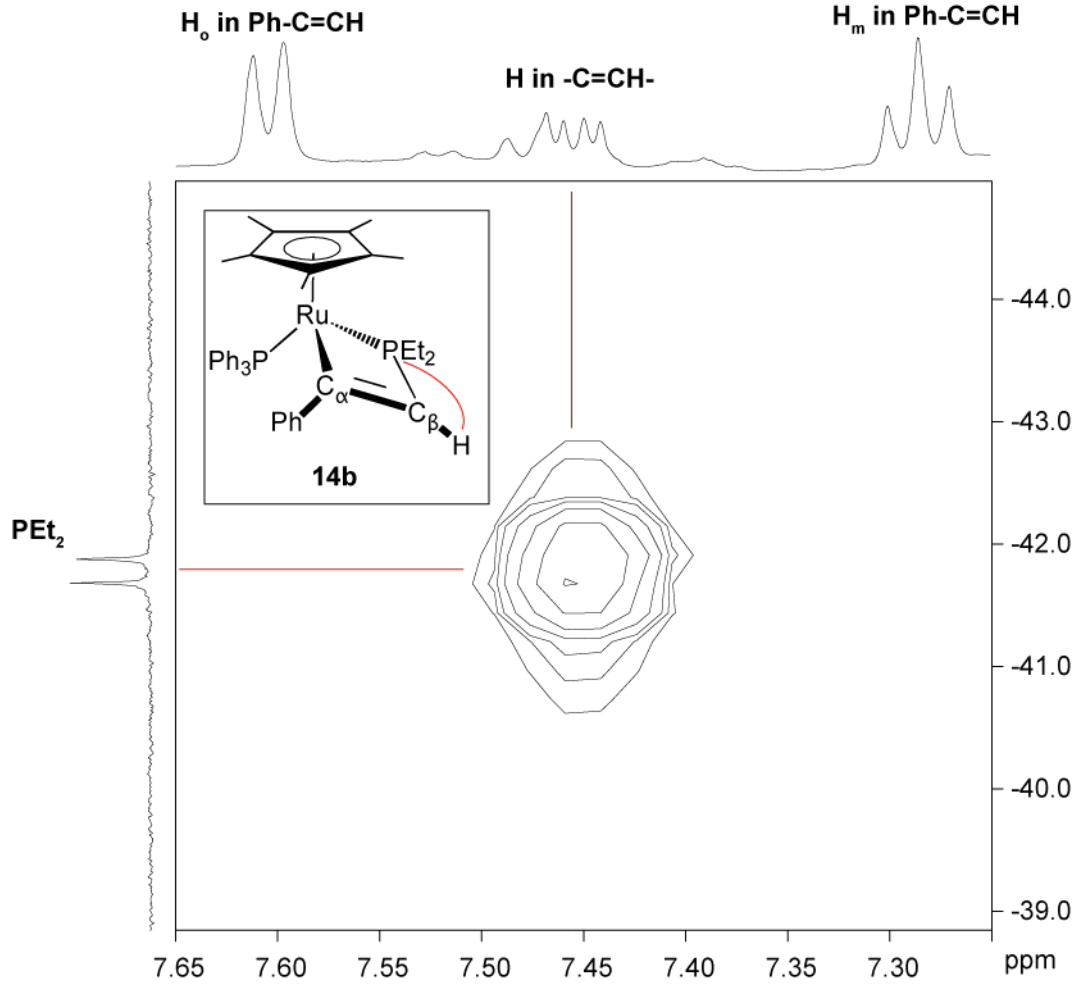

Figure 5.3 Partial $^{1}H/^{31}P\{^{1}H\}$-HMBC NMR spectrum (500.27 MHz, C_6D_6) of [**2b** + $KOBu^t$] with phenylacetylene, highlighting the correlations between H on β-carbon and P in -PEt_2- fragment in metallacycle **14b**.

5.2.4 Alkynyl complex Ru(η^5-Cp*)(C≡CPh)(PEt_2H)(PPh_3) (13b) as a potential catalyst for dimerization of phenylacetylene.

As described in Section 5.2.1, all phosphido **6a-d** can deprotonate the terminal proton of phenylacetylene to give alkynyl complexes **13a-d**. Interestingly, for the reaction of complex **2b** with $KOBu^t$ and excess phenylacetylene (~ 10 equivalent) at RT, the ^{1}H NMR spectrum shows, in addition to **13b** and **14b**, the formation of the dimer (*E*)-1,4-diphenyl-1-buten-3-yne and its *Z* isomer (*E* : *Z* = 63: 37, 30% conversion) after 24h. The structures of both of isomers are confirmed by correlations of their vinyl protons in the ^{1}H-COSY spectrum (Figure 5.4). Some examples of half-

sandwich Ru-catalyzed dimerization of terminal alkynes were reported in the literature.[10,11,12,13,14]

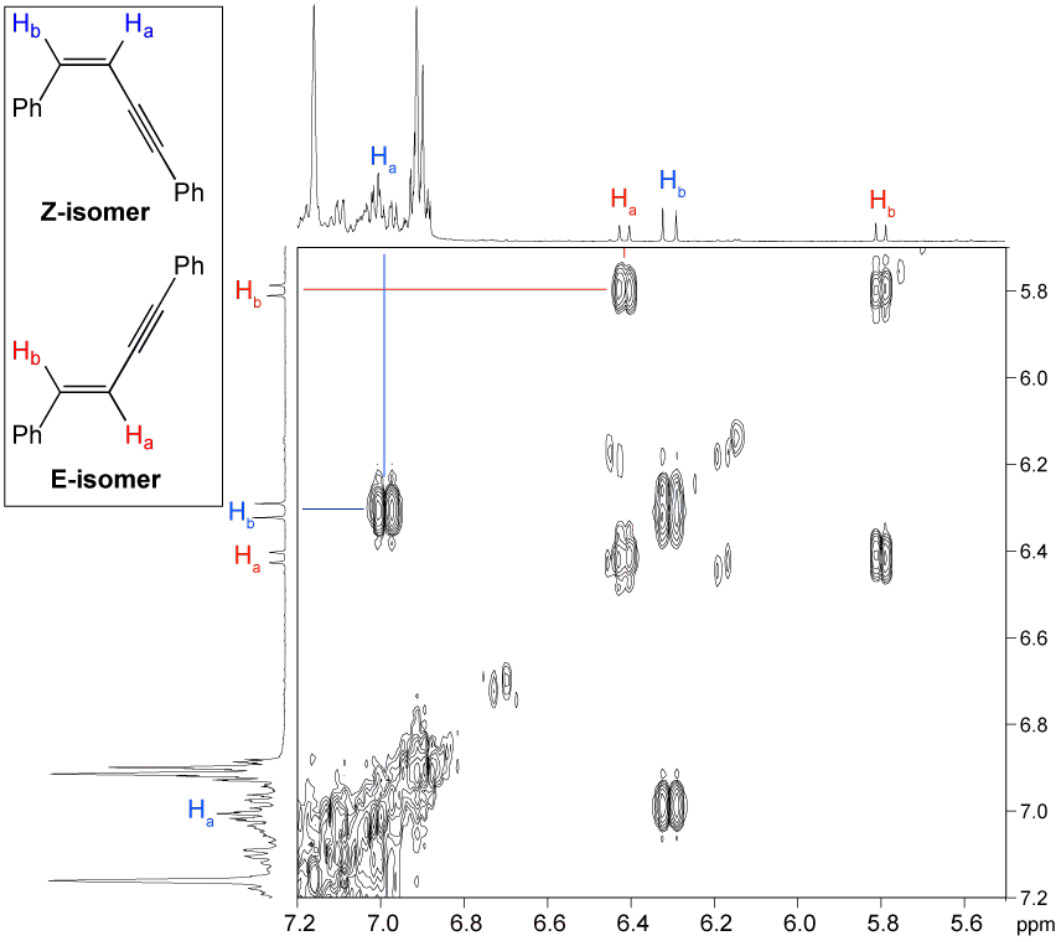

Figure 5.4 ^{1}H-COSY NMR spectrum (500.27 MHz, C_6D_6) of the reaction of [**2b** + KOBu^{t}] with excess phenylacetylene after 24h highlighting the correlations of vinyl protons in two resulting dimers.

Alkynyl complex **13b** may catalyze the dimerization of phenylacetylene. A proposed mechanism is shown in Scheme 5.5. Dissociation of PPh_3 ligand from alkynyl complex **13b** is necessary to open a coordination site for phenylacetylene, which is probably the initial step in catalytic reactions (Step A). The excess phenylacetylene can bond to coordinately unsaturated alkynyl complex Ru(η^5-Cp*)(C≡CPh)(PEt_2H) (Step B), and then acetylene-vinylidene isomerization[12] occurs to form a vinylidene complex Ru(η^5-Cp*)(=C=CPh)(η^2-HC≡CPh)(PEt_2H) (Step C). The key C–C bond forming step (Step D) is the migration of an alkynyl group to the

α-carbon of the Ru-coordinated vinylidene ligand. Regeneration of the alkynyl intermediate Ru(η^5-Cp*)(C≡CPh)(PEt_2H) can be achieved by the subsequent coordination of another phenylacetylene and the elimination of dimeric products (Step E). Another possible mechanism, which is direct insertion instead of vinylidene formation (Step C and Step D combined), is not favoured in my case because this mechanism can't give the *E* isomer as a product.

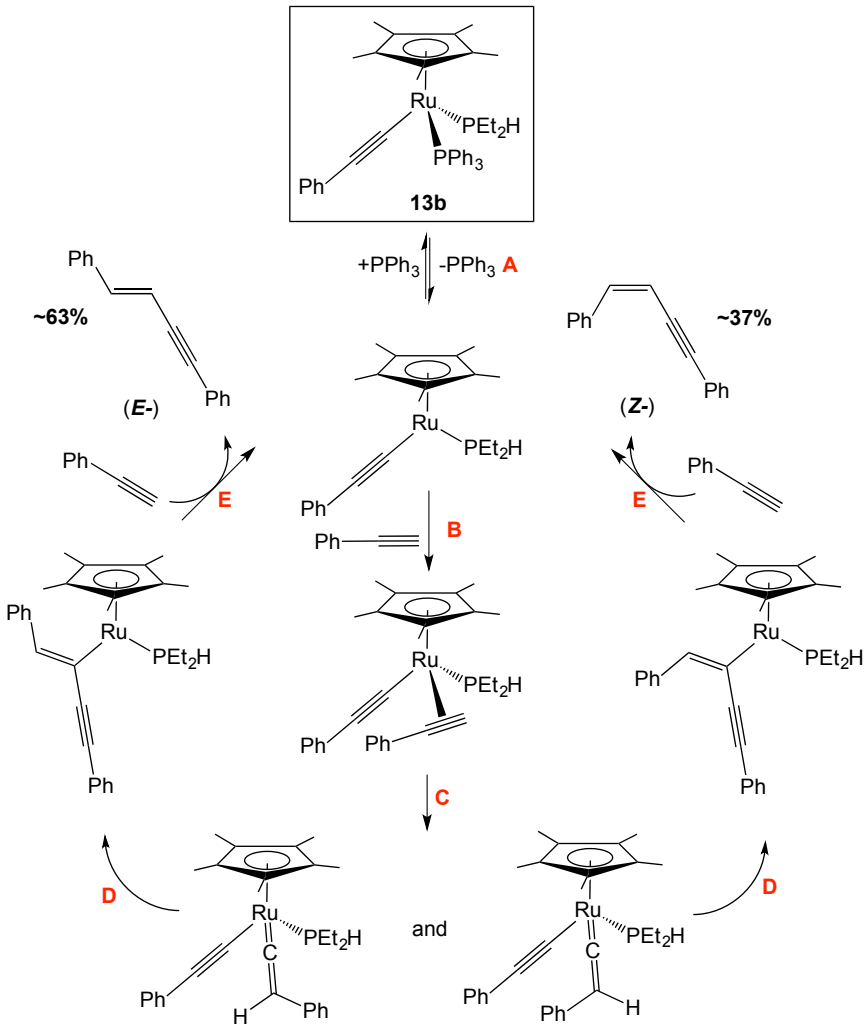

Scheme 5.5 Proposed mechanism of dimerization of phenylacetylene catalyzed by alkynyl **13b**.

The selectivity of resulting product (*E* or *Z* isomer) is proposed to arise from the two orientations for the vinylidene group. For Ru(η^5-Cp*)$H_3(PR_3)$ (R= Ph, Cy, Me), Liu and coworkers reported the Z isomer is increasingly favored over the *E* isomer as

the size of PR_3 ligand increases.[12] For the catalytic reaction of **13b**, the *Z*:*E* isomer ratio shows approximately 1 : 1.7, which is slightly in favor of the *E* isomer. This poor selectivity results from the small size of PEt_2H ligand. This dimerization reaction is not observed for complex **6c,d** and excess phenylacetylene, which may arise from their increased steric hindrance that prevents approach of the phenylacetylene to the Ru center.

5.2.5 Comparison of the reactivity of Cp* phosphido complexes 6a-d and indenyl analogues in the reactions with phenylacetylene

As Section 5.2.1 described, all reactions of Cp* complexes **2a-d** with alkynes give alkynyl complexes **13a-d** (20%-85%) and metallacycle **14b-d** (15-80 %). However, the same reaction of indenyl analogues $\mathbf{6}^{i}$ with phenylacetylene (see Scheme 5.1) shows metallacycle Ru(η^5-indenyl)(κ^2-Ph<u>C</u>=CH<u>P</u>R_2)(PPh_3) (R= Cy, Et) (~94%) as the major product and alkynyl complex Ru(η^5-indenyl)(C≡CPh)(PR_2H)(PPh_3) (~6%) as the minor product. These reactions of Cp* complexes **2a-d** show high conversion to alkynyl complex, which suggest high *P*-basicity in the Cp* phosphido complex **6a-d**. The pK_a of the terminal proton of phenylacetylene is 20.[15] The terminal proton is acidic enough to be deprotonated by Cp* phosphido **6a-d**. This high *P*-basicity of Cp* phosphido was already seen in Chapter 3 (see Section 3.2.2 for detail), based on the fast orthometallation of Cp* phosphido **6a-d**.

For phenylacetylene, Cp* phosphido **6a-d** prefer deprotonation of the terminal proton to nucleophilic attack in comparison with indenyl analogues $\mathbf{6}^{i}$. In addition, within the four Cp* complex **6a-d**, only the reaction of complex **6b** shows the metallacycle **14a** as the major product, which can be explained by its lower steric bulk at the Ru center (see Chapter 2, Section 2.2.2). For complex **6a**, **6c** and **6d**, their PR_2

(R = Cy, Ph and Tol^{p}) are more bulky relative to **6b**, which stops the phenylacetylene approaching their phosphido group. Deprotonation of the terminal proton of phenylacetylene does not require as close an approach to the Ru center.

These results shown in this section indicates the high basicity of Cp* phosphido complexes **6a-d**. Also, the differences in reactivity seems to correlate with the higher steric congestion in the Cp* system relative to indenyl analogues.

5.3 Attempted reactions of activated and simple terminal alkenes with Cp* phosphido complexes 6a-d

In this section, the Cp* phosphido **6a-d** were generated *in situ* (as described above), and then an activated alkene (acrylonitrile, styrene) or a simple alkene (1-hexene) was separately added to the mixed solution.

5.3.1 Reactions of activated alkenes with Cp* phosphido 6a-d

1 equiv of acrylonitrile was added to Cp* phosphido **6a-d** (complex **2a-d** + KOBu^{t}). After the addition of acrylonitrile, the dark red (for **6a,b**)/dark blue (for **6c,d**) solution turned orange and some pale yellow solid formed in these solution, which may result from the polymerization of acrylonitrile by the KOBu^{t} (Scheme 5.6). Although this reaction with in situ-generated **6** was anticipated, in this case both the KOBu^{t} and acrylonitrile were used up in polymerization. Zilkha reported acrylonitrile polymerization by metal alkoxide catalysts in 1961.[16] As a result, the $^{31}P\{^{1}H\}$ NMR spectra show the only presence of **2a-d**.

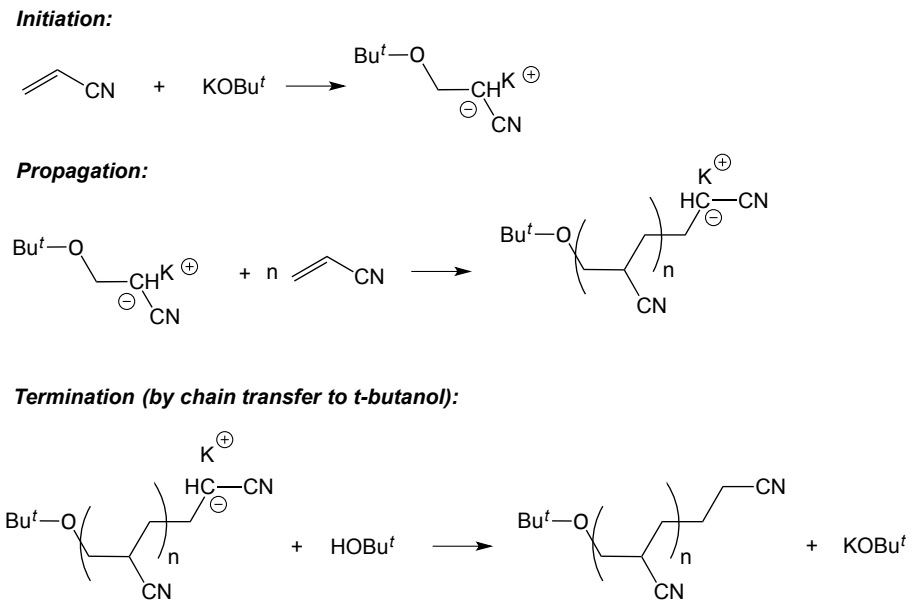

Scheme 5.6 Possible mechanism for KOBu^t participated in acrylonitrile polymerization.

The preliminary investigation of another activated alkene (styrene) with phosphido **6d** generated *in situ* (complex **2d** + KOBu^t) shows the formation of two new doublets in the $^{31}P\{^1H\}$ NMR spectrum (blue dot in Figure 5.5), along with unreacted **2d**. These two doublets (δ: 62.0 and 50.1 ppm, $^2J_{PP}$ = 39 Hz) were tentatively assigned to an alkenyl complex Ru(η^5-Cp*)(CH=CHPh)(PTol$^p{}_2$H)(PPh$_3$). The upfield doublet was assigned to PTol$^p{}_2$H ligand due to the presence of a large $^1J_{PH}$ coupling (355 Hz) in the ^{1}H and ^{31}P NMR spectra. The ^{1}H NMR spectrum shows a diagnostic shift (δ: 8.97 ppm, doublet of triplets $^3J_{HH}$ = 17.0 Hz, $^3J_{PH}$ = 3.0 Hz) due to H on the α-carbon in the alkenyl group (Figure 5.5).[17]

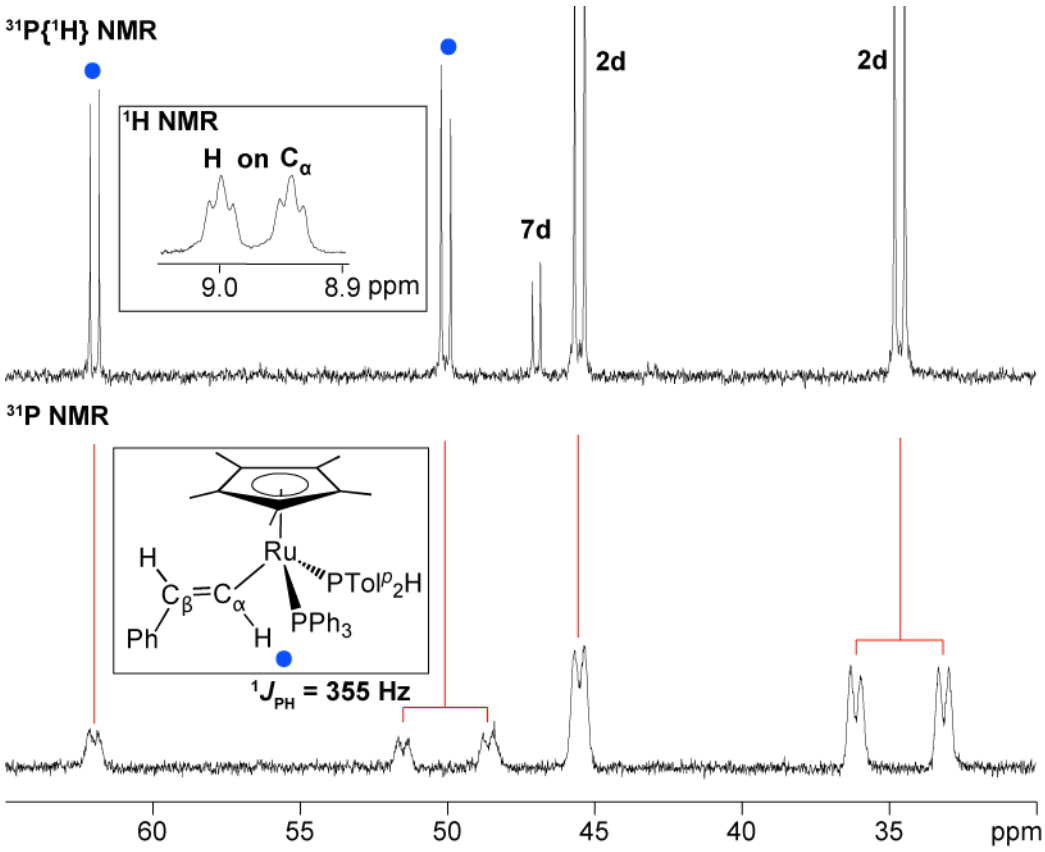

Figure 5.5 Partial $^{31}P\{^{1}H\}$ NMR (202.51 MHz, C_6D_6) spectrum of the preliminary reaction of [**2d** + KOBu^t] with styrene after 0.5 h stacked above the partial ^{31}P NMR (202.51 MHz, C_6D_6) spectrum. Inset shows partial ^{1}H NMR (500.27 MHz, C_6D_6) spectrum showing diagnostic signal due to H on the α-carbon in alkenyl group.

5.3.2 Reactions of 1-hexene with Cp* phosphido 6a-d

The Cp* phosphido **6a-d** (complexes **2a-d** + KOBu^t) were generated *in situ*, and then 5 equiv of 1-hexene was added to the mixed solution. For **6a**, the $^{31}P\{^{1}H\}$ NMR spectrum shows that dehydrohalogenation and orthometallation occurred in the mixture (see Chapter 3). The reaction of complex **6b** (after 0.5 h) shows unreacted **2b** (68%), phosphido **6b** (17%), the orthometallated **7b** (14%) and a new product showing as a singlet (δ: 57.0 ppm, 1%). This singlet is tentatively assigned to identified as an η^3-allyl complex Ru(η^5-Cp*)\{η^3-$CH_2CHCH(C_3H_7)$\}(PEt_2H) (**15b**). Since there is only a small amount of this new product in the mixture, most of signals can't be observed by NMR spectroscopy. For **6c,d**, the $^{31}P\{^{1}H\}$ NMR spectra show signals due to the proposed η^3-allyl complex (**15c**: 56%; **15d**: 52%) and

orthometallated complex (**7c**: 44%; **7d**: 48%). The formation of these allyl complexes results from the deprotonation of the allylic C-H bond in 1-hexene. As mentioned in Chapter 3 (Section 3.2.4), the orthometallation of dialkylphosphido **6a,b** is faster relative to diarylphosphido **6c,d**. The relatively slow orthometallation of **6c,d** allows them to deprotonate the most acidic proton in 1-hexene. In addition, for phosphido **6b** (R= Et), the $^{31}P\{^{1}H\}$ NMR spectrum (after 24h) shows two new doublets (δ: 63.0 and 49.5 ppm, $^{2}J_{PP}$ = 42 Hz), which are tentatively assigned to a branched η^1-alkyl complex Ru(η^5-Cp*)(CH(CH=CH$_2$)C$_3$H$_7$)(PEt$_2$H)(PPh$_3$) (red dot in Figure 5.6, ~2%). This alkyl complex is only observed for **6b**, which may be because it has the least bulky Ru center within complexes **6a-d** (Scheme 5.7). Detailed characterization of allyl complexes **15c,d** by 1D and 2D NMR spectroscopy, is described below.

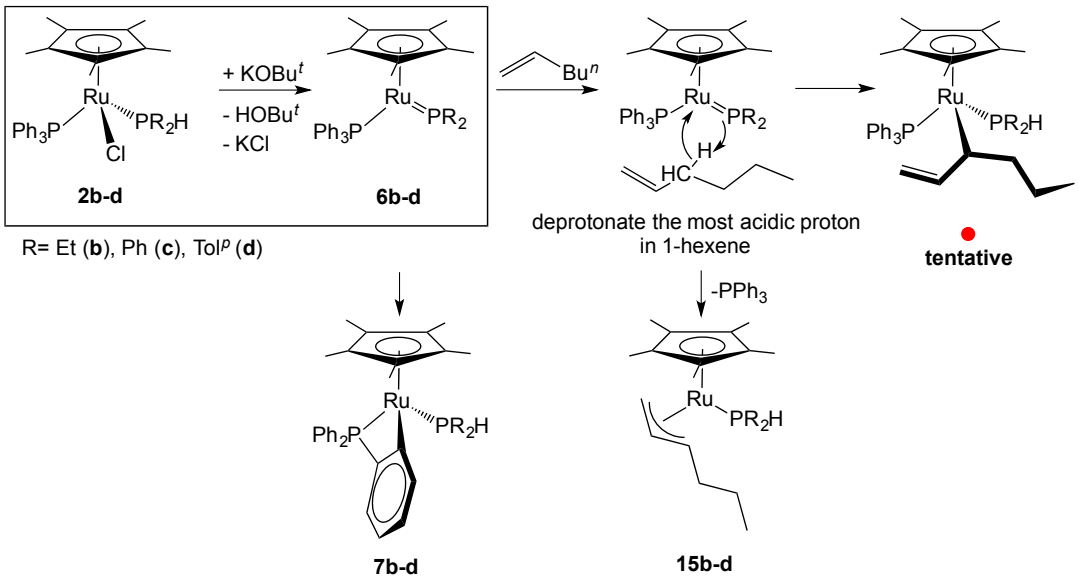

Scheme 5.7 NMR scale reactions of [**2b-d** + KOBu^t] with excess 1-hexene. The η^1-allyl complex (red dot) is observed only for R= Et (**2b**).

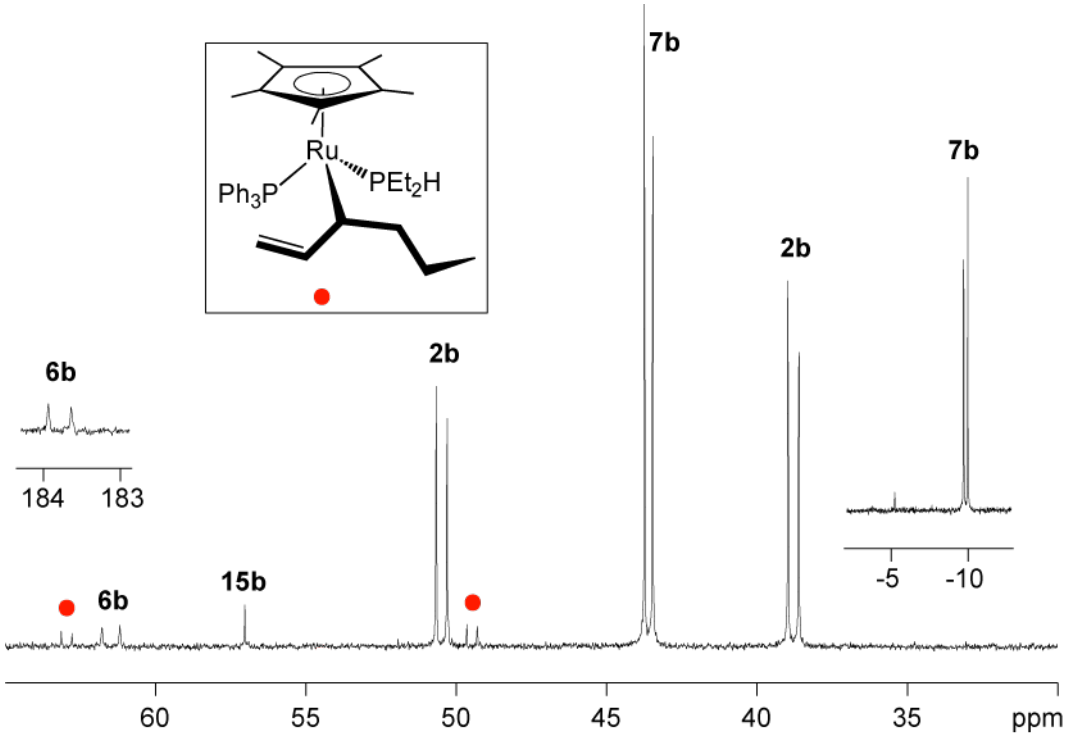

Figure 5.6 $^{31}P\{^{1}H\}$ NMR (202.51 MHz, C_6D_6) spectrum of preliminary reaction of [**2b** + KOBu^t] and excess 1-hexene after 0.5 h.

5.3.3 Detailed characterization of Ru(η^5-Cp*){η^3-$CH_2CHCH(C_3H_7)$}(PR_2H) (15c,d)

The η^3-allyl complexes **15c,d** (R = Ph, Tol^p) can be identified in the $^{31}P\{^{1}H\}$ NMR spectra by the presence of a singlet which splits into a doublet in the ^{31}P NMR spectra with a large $^{1}J_{PH}$ coupling (e.g. for **15c**: 324 Hz). These same $^{1}J_{PH}$ couplings are also observed in the ^{1}H NMR spectra. The ^{1}H NMR spectra show a diagnostic ^{1}H shift for the signal due to the central proton H_B in the allyl group (e.g. **15c** δ: 3.14-3.05 ppm, see Figure 5.7 for labeling).[18] The ^{13}C signal due to C_B (e.g. **15c** δ: 76.8 ppm) can be identified by its correlation with H_B in the $^{1}H/^{13}C\{^{1}H\}$-HSQC spectra. The ^{1}H shift for H_B is distinctly downfield from the other protons in the allyl group. C_A and C_C can be identified by their correlations with the ^{1}H signal due to H-PR_2 in the $^{1}H/^{13}C\{^{1}H\}$-HMBC spectra (Figure 5.7). H_A and H_C can be identified by their correlations with signals due to C_A and C_C in the $^{1}H/^{13}C\{^{1}H\}$-HSQC spectra. The

assignments of C_A, C_B and C_C are supported by their different coupling constants to P in the PR_2H ligands (C_A: $^2J_{PC}$ = 5 Hz; C_B: $^3J_{PC}$ = 2 Hz; C_C: $^2J_{PC}$ = 4 Hz). The rest of the protons and carbons can be identified by their correlations with signals due to these identified carbons (C_A, C_B and C_C) and protons (H_A, H_B and H_C) in the $^1H/^{13}C\{^1H\}$-HMBC spectra. The presence of orthometallated **7** and free PPh_3 make assigning signals in the aromatic range for the PR_2H ligand more complicated for both ^1H and $^{13}C\{^1H\}$ NMR spectra. The ^{13}C DEPT 135 spectra of pure orthometallated **7** (see Chapter 3, Section 3.3) and free PPh_3 can be stacked with those of mixture containing allyl complex **15** to identify the C_{ortho}, C_{para} and C_{meta} signals for the PR_2H ligand in **15**. The H_o, H_p and H_m signals can be identified by correlations with C_{ortho}, C_{para} and C_{meta} in the $^1H/^{13}C\{^1H\}$-HSQC spectra. Details of characterization are shown in Appendix E.

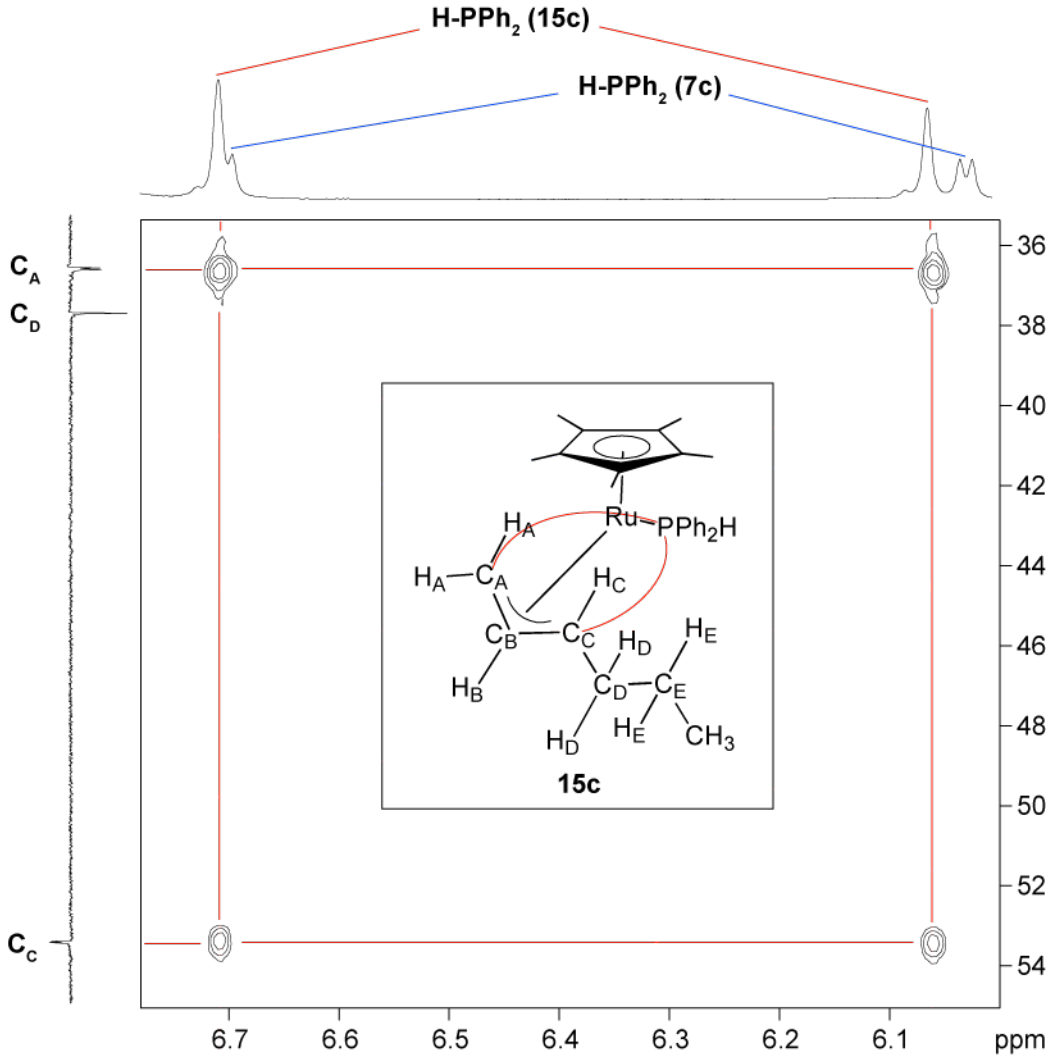

Figure 5.7 Partial $^{1}H/^{13}C\{^{1}H\}$-HMBC NMR spectrum (500.27 MHz, C_6D_6) of the reaction of [**2c** + KOBu^t] with excess 1-hexene highlighting the correlation of P-H proton signal in PPh_2H ligand with signals due to C_A and C_C in the allyl group in η^3-allyl complex **15c**.

5.3.4 Discussion of the different reactivities of Cp* phosphido 6a-d and indenyl analogues in the reactions with alkenes

As described in Section 5.1.1, indenyl phosphido **6**^{i} can undergo [2+2] cycloaddition with alkenes (acrylonitrile, styrene and 1-hexene) to give metallacyclic complexes as the major product. However, analogous metallacycles were not observed for the reactions with Cp* phosphido **6a-d** with these alkenes. The Cp* phosphido **6a-d** deprotonate the most acidic proton in these alkenes (styrene and 1-hexene) instead of attacking the unsaturated bond to form the metallacycle. In

addition, this deprotonation of alkenes (e.g., 1-hexene and styrene) was not observed for indenyl analogoues, which suggests higher basicity of the Cp* phosphido **6** relative to the indenyl phosphido **6**^{i}.

This difference may be more to do with the higher steric congestion in the Cp* system relative to indenyl analogues again. For Cp* phosphido **6a-d**, the formation of metallacycle is observed in the reaction with phenylactylene (see Secition 5.2.1). Alkynes tend to be better π-donors and therefore tend to bind more tightly to a transition metal center than do alkenes.[19] Based on this difference between phenylacetylene (alkyne) and styrene (alkene), it suggests that nucleophilic attack of the terminal phosphido ligand needs coordination of the alkene/alkyne to the Ru metal. In the Cp* system, alkenes seem to have difficulty binding to Ru metal because of its higher steric congestion compared to the indenyl system.

5.4 Reactions of benzonitrile (PhCN) with Cp* phosphido complexes 6c,b

Since diarylphosphido **6c,d** are more stable than dialkylphosphido **6a,d** (see Chapter 3, Section 3.2.3), diarylphosphido **6c,d** were generated *in situ* and reacted with five equivalent of PhCN. For the reaction of **6d**, the $^{31}P\{^{1}H\}$ NMR spectrum (Figure 5.8) shows two broad singlets (**16d** δ: 51.7 ppm, $\omega_{1/2}$ = 30 Hz and -6.0 ppm, $\omega_{1/2}$ = 58 Hz) after 3h.

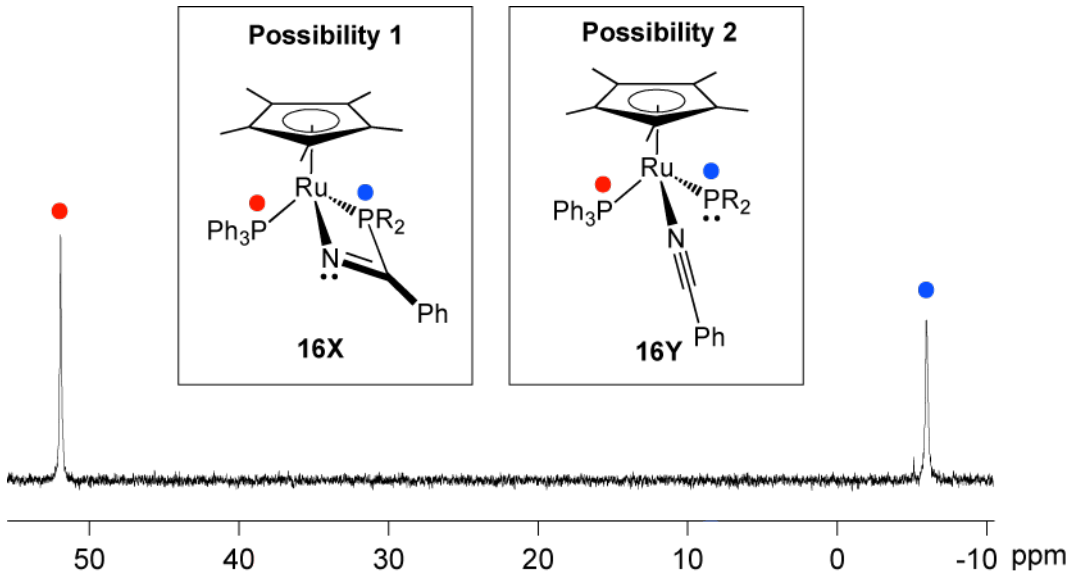

Figure 5.8 $^{31}P\{^{1}H\}$ NMR (202.51 MHz, C_6D_6) spectrum of the reaction of [**2d** + KOBu^t] with excess PhCN after 3h.

One possible structure for this type of PhCN adduct **16** is metallacycle Ru(η^5-Cp*)(κ^2-N=C(Ph)PR$_2$)(PPh$_3$) (**16X**). This tentative assignment of a metallacyclic structure is based on the diagnostic upfield ^{31}P shifts (e.g. **16d** δ: -6.0 ppm) for the 4-membered metallacycle.[2] The other possible structure is a terminal phosphido complex Ru(η^5-Cp*)(NCPh)(PR$_2$)(PPh$_3$) (**16Y**). The tentative assignment for this terminal phosphido structure is based on the $^{13}C\{^{1}H\}$ NMR spectra of these reactions, since none of quaternary carbons in coordinated PhCN are observed as a doublet (due to $^{1}J_{PC}$ coupling). The mechanisms for formation of these two possible structures are shown in Scheme 5.8. Coordinated PhCN is confirmed by its more upfield ^{1}H and ^{13}C shift relative to free PhCN. These broad ^{31}P signals suggest the existence of an equilibrium (see Scheme 5.8) between PhCN adduct **16** and planar phosphido **6**. This PhCN adduct is unstable, it will dissociate the PhCN ligand and regenerate planar phosphido **6**, then eventually form orthometallated **7d**, even in the presence of a large excess of PhCN. Adding excess of PhCN can slow down the orthometallation allowing the NMR characterizations of these PhCN adducts.

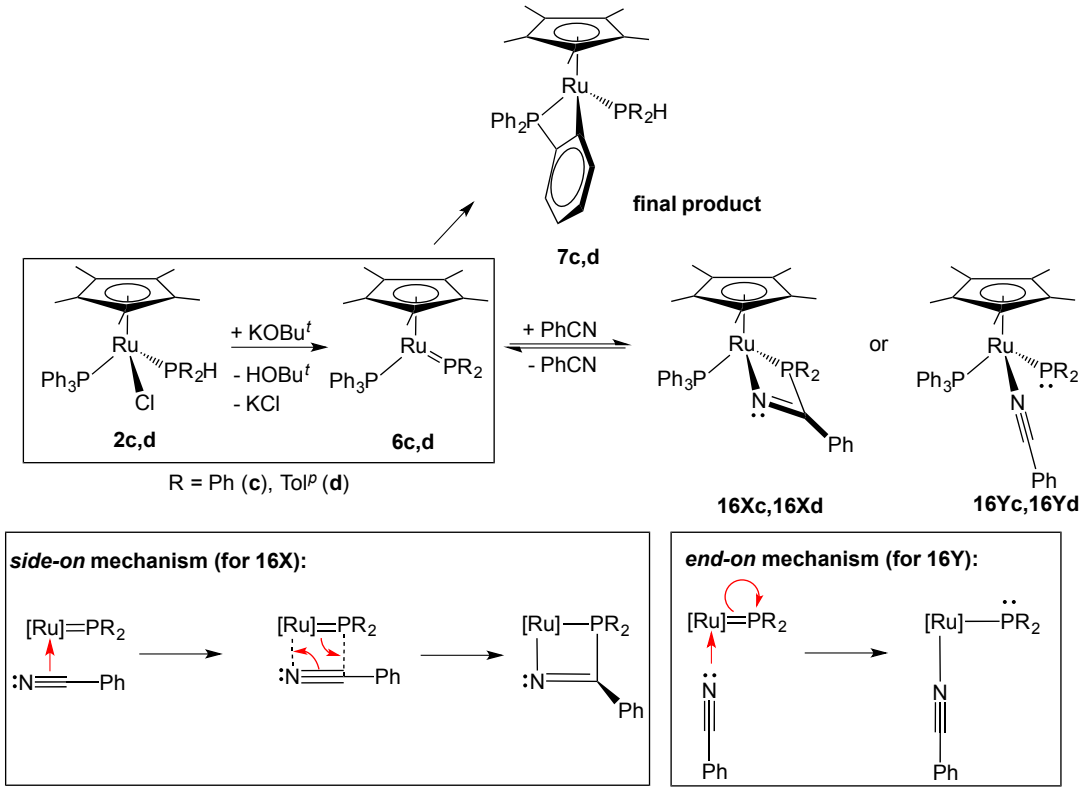

Scheme 5.8 Possible products and mechanisms for the NMR scale reaction of [**2c,d** + $KOBu^t$] with PhCN.

For the PR_2 fragment (R = Ph (**c**), Tol^p (**d**)) and PPh_3 ligand, their H_o signals can be identified by their correlations with the corresponding ^{31}P signal in $^1H/^{31}P\{^1H\}$-HMBC spectrum. The rest of the protons and carbons can be assigned using the usual 2D NMR experiments. For PhCN, there is no direct evidence to confirm the coordination mode of PhCN (**16X** or 1**6Y**). The ^1H and $^{13}C\{^1H\}$ NMR spectrum of free PhCN, compared to those of resulting PhCN adducts, shows that the PhCN adducts (Figure 5.9b and c) have more downfield ^1H shifts and more upfield $^{13}C\{^1H\}$ shifts relative to free PhCN (Figure 5.9a).

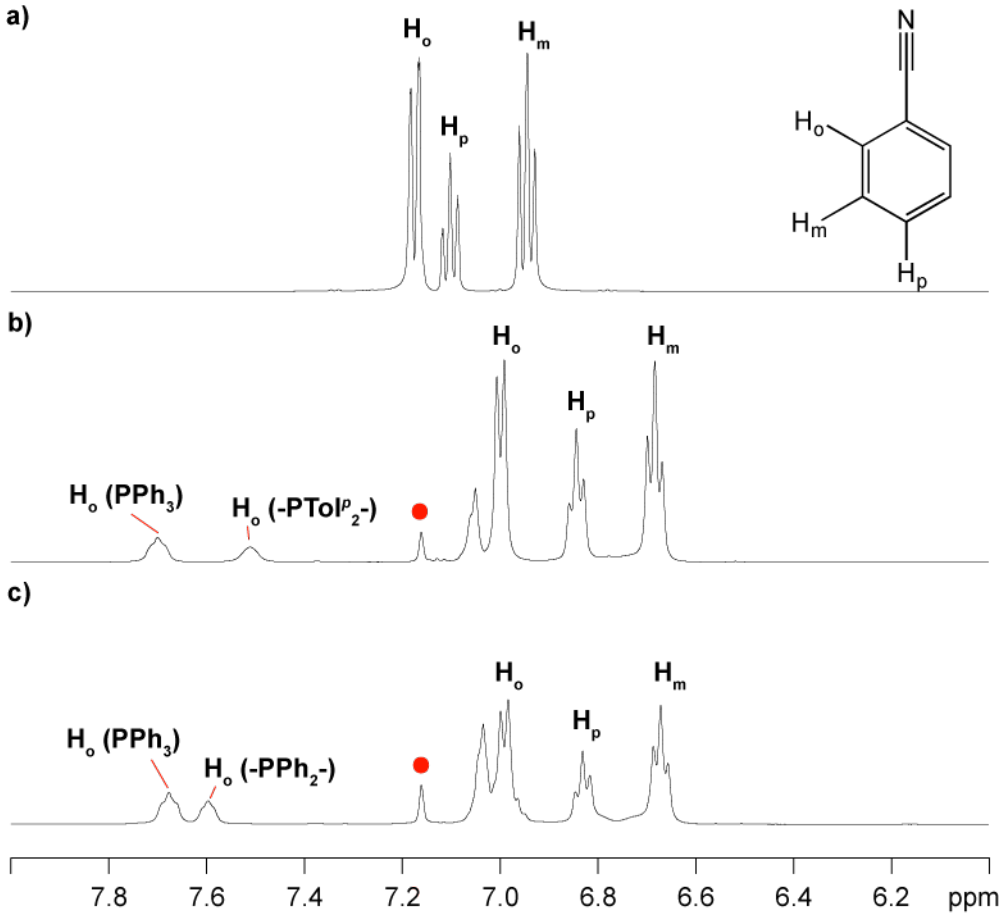

Figure 5.9 Partial ^{1}H NMR spectra (500.27 MHz, C_6D_6) of (**a**) PhCN, (**b**) the reaction of [**2d** + KOBu^t] with excess PhCN, and (**c**) the reaction of [**2c** + KOBu^t] with excess PhCN. The signals due to C_6D_5H are labeled as red dots.

5.5 Conclusion

In this chapter, the complexes **6a-d** were generated *in situ* and their reactivity was explored in a series of NMR-scale reactions with alkyne (phenylacetylene), alkene (acrylonitrile, styrene and 1-hexene) and PhCN. The products of these reactions are mostly identified and characterized by NMR. Different from indenyl analogues **6**^{i}, the Cp* phosphido **6** prefer to deprotonate the most acidic proton in these trapping reagents (phenylacetylene, styrene and 1-hexene) rather than form the metallacycles. This difference suggests the nucleophilic processes of the phosphido group are shut down by steric hindrance in the Cp* system. Since this deprotonation

of alkenes (styrene and 1-hexene) was not observed for indenyl analogues, it may suggest higher basicity of the Cp* phosphido **6** relative to the indenyl phosphido **6*i***.

PhCN can bond to Cp* diarylphosphido **6c,d**, but the resulting PhCN adducts **16** are unstable and will dissociate the PhCN ligand and regenerate planar phosphido **6c,d.**

5.6 Experimental

See Chapter 2, Section 2.6.1 for general experimental details. Complexes Ru(η^5-Cp*)Cl(PR_2H)(PPh_3) (**2a-d**) were prepared as described in Chapter 2 (Section 2.6.3). Complexes Ru(η^5-Cp*)(PR_2)(PPh_3) (**6a-d**) were generated *in situ* for reactivity studies as described in Chapter 3 (Method 1). Potassium *tert*-butoxide ($KOBu^t$) and phenylacetylene were purchased from Aldrich Chemical Co. and used as received. Styrene and 1-hexene were purchased from Aldrich Chemical Co. and dried over sodium prior to distillation under nitrogen. Benzonitrile (PhCN) and acrylonitrile were pre-dried with K_2CO_3, then fractionally distilled from P_2O_5 under dynamic vacuum. Spectroscopic data is available for most major species identified in the NMR tube reactions performed in this chapter. The ^{31}P, ^{1}H and ^{13}C NMR data can be found in Tables 5.1-5.9.

5.6.1 General method for NMR scale reactions with liquid trapping reagents

1 mL of C_6D_6 was added to the mixture of solid base $KOBu^t$ (2 mg, 0.018 mmol) and metal complex **2a-d** (**2a**: 12 mg, 0.016 mmol; **2b**: 10 mg, 0.016 mmol; **2c**: 12 mg, 0.017 mmol; **2d**: 12 mg, 0.016 mmol) in a small vial. The initially orange solutions turned dark red (for **2a,b**)/dark blue (for **2c,d**) quickly. Liquid trapping reagent was added to this mixture by microsyringe. The sample was swirled for 30s before being transferred to an NMR tube, and were then analyzed by NMR spectroscopy.

5.6.2 Reactions of [complex 2a-d + KOBu^t] with phenylacetylene

These solutions turned to yellow/orange immediately after adding phenylacetylene (3 µl, 0.028 mmol). The relative amounts of **13** and **14** observed after 3 h reaction are reported in Table 5.1. The other product is orthometallated **7**.

5.6.3 Reactions of [complex 2a-d + KOBu^t] with acrylonitrile

These solutions immediately turned to yellow/orange after adding acrylonitrile (2 µl, 0.030 mmol) and yellow solid formed. $^{31}P\{^1H\}$ NMR spectra show orthometallated **7** as final product.

5.6.4 Reactions of [complex 2a-d + KOBu^t] with 1-hexene.

These solutions slowly turned to yellow/orange after adding 1-hexene (10 µl, 0.08 mmol). The relative amounts of **15** observed after 3 h reaction are reported in Table 5.1. The other products are orthometallated **7** and branched η^1-alkyl complex Ru(η^5-Cp*)(CH(CH=CH$_2$)C$_3$H$_7$)(PEt$_2$H)(PPh$_3$) (only for R = Et (**b**))

5.6.5 Reactions of [complex 2c,d + KOBu^t] with PhCN.

These solutions immediately turned to dark red after adding PhCN (10 mg, 0.10 mmol). The relative amounts of **16** or **17** observed after 3h reaction are reported in Table 5.1.

5.6.7 Attempted isolation of Ru(η^5-Cp*){η^3-CH$_2$CHCH(C$_3$H$_7$)}(PTol$^p_2$H) (15d)

20 mL of benzene was added to a flask containing **2d** (282 mg, 0.39 mmol) and an excess of KOBu^t (23mg, 0.43 mmol), which caused the orange solution to turn deep blue. 1-hexene (200 mg, 2.38 mmol) was adding to this blue solution. The mixture was stirred for 3h at RT, and then the solution was filtered through Celite to remove solid and gelatinous byproduct KCl and HOBu^t. The benzene was removed

under vacuum. Trituration of the resulting brown oily residue with pentane (2 x 10 mL) still gave an oily residue and this residue was dissolved in pentane. The pentane was removed under vacuum. The $^{31}P\{^{1}H\}$ NMR spectrum of this resulting residue shows ~50% allyl **15d** and byproduct ~50 % PPh_3.

Table 5.1 202.51 MHz $^{31}P\{^{1}H\}$ NMR data for alkynyl complexes **13a-d**, metallacycles **14b-d**, η^3-allyl complexes **15c,d** and PhCN adducts **16**, and their relative amounts after 3h in C_6D_6 at 300 K: δ (ppm) (multiplicity, $^{2}J_{PP}$ or $\omega_{1/2}$ (Hz)).

Complex		PR_2H/-PR_2-	PPh_3	%Conversion
Ru(η^5-Cp*)(C≡CPh)(PCy_2H)(PPh_3)	**13a**	53.3 (d, 34)	59.3 (d)	20
Ru(η^5-Cp*)(C≡CPh)(PEt_2H)(PPh_3)	**13b**	41.5 (d, 38)	60.1 (d)	20
Ru(η^5-Cp*)(C≡CPh)(PPh_2H)(PPh_3)	**13c**	41.5 (d, 37)	55.8 (d)	85
Ru(η^5-Cp*)(C≡CPh)($PTol^p{}_2H$)(PPh_3)	**13d**	39.6 (d, 37)	56.2 (d)	82
Ru(η^5-Cp*)(κ^2-PhC=CHPEt$_2$)(PPh_3)	**14b**	-41.9 (d, 39)	61.9 (d)	80
Ru(η^5-Cp*)(κ^2-PhC=CHPPh$_2$)(PPh_3)	**14c**	-39.3 (d, 35)	63.1 (d)	15
Ru(η^5-Cp*)(κ^2-PhC=CHP$Tol^p{}_2$)(PPh_3)	**14d**	-40.7 (d, 35)	63.2 (d)	18
Ru(η^5-Cp*)(η^3-$CH_2CHCHC_3H_7$)(PPh_2H)	**15c**	57.2 (s)	N/A	56
Ru(η^5-Cp*)(η^3-$CH_2CHCHC_3H_7$)($PTol^p{}_2H$)	**15d**	55.4 (s)	N/A	52
Ru(η^5-Cp*)(κ^2-N=C(Ph)PPh$_2$)(PPh_3)/ Ru(η^5-Cp*)(NCPh)(PPh_2)(PPh_3)	**16Xc/ Yc**	-3.8 (s, 41)	51.6 (s, 29)	100
Ru(η^5-Cp*)(κ^2-N=C(Ph)P$Tol^p{}_2$)(PPh_3)/	**16Xd/ Yd**	-6.0 (s, 58)	51.7 (s, 30)	100

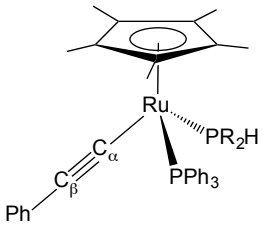

13

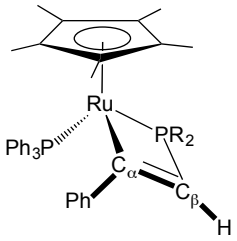

14

Figure 5.10 Structure of complex **13** and **14** showing locations of carbons on Cα≡CβPh and κ^2-PhCα=CβH fragments.

Table 5.2 500.27 MHz ^{1}H NMR data for Ru(η^5-Cp*)(C≡CPh)(PR$_2$H)(PPh$_3$) **13a-d** and Ru(η^5-Cp*)(κ^2-PhC=CHPR$_2$)(PPh$_3$) **14b-d** in C_6D_6 at 300 K: δ in ppm (multiplicity, RI, J_{avg} or $\omega_{1/2}$ in Hz, assignment).[a]

	η^5-Cp*	**PPh$_3$**	**Other**
13a	1.94 (s, 15H)	Not observed	Not observed
13b	1.62 (s, 15H)	Not observed	**H-PEt$_2$** 3.84 (d, 1H, $^1J_{PH}$ 343.4) Other signals not observed
13c	1.53 (s, 15H)	**H$_o$** 7.83-7.45 (m, overlaps H$_o$ in -C≡CPh, 6H) **H$_{m,p}$** 7.09- 6.93 [m, H$_m$ and H$_p$ overlapping, 9H (*also overlaps H$_{m,p}$ in PPh$_2$H)]	**Cα≡CβPh:** **H$_o$** 7.64-7.58 (m, overlaps H$_o$ in PPh$_3$, 2H) **H$_m$** 7.28-7.20 (m, 2H) **H$_p$** 7.05-7.03 (m, overlaps H$_{m,p}$ in PPh$_2$H and -C≡CPh, 1H) **PPh$_2$H:** **H-PPh$_2$** 6.45 (d, 1H, $^1J_{PH}$ 379.8) **H$_o$** 7.92-7.83 (m, 2H), 7.15-7.10 (m, overlaps H$_m$ in PPh$_2$H, 2H) **H$_m$** 7.15-7.10 (m, overlaps H$_o$ in PPh$_2$H, 2H) **H$_{m,p}$** 7.09- 6.93 [m, H$_m$ and H$_p$ overlapping, 4H (*also overlaps H$_{m,p}$ in PPh$_3$)]
13d	1.58 (s, 15H)	**H$_o$** 7.91-7.47 (br s, overlaps H$_o$ in PTol$^p_2$H and C≡CPh,	**Cα≡CβPh:** **H$_o$** 7.64 (d, 2H, $^3J_{HH}$ 7.5)

		6H, $\omega_{1/2}$ 145.8) **H$_p$** 7.43- 7.37 (m, 3H) **H$_m$** 7.03-6.99 (m, 6H)	**H$_m$** 7.26 (t, 2H, $^3J_{HH}$ 7.4) **H$_p$** 7.05-7.03 (m, 1H) **PTol$^p_2$H:** **H-PTol$^p_2$** 6.45 (d, 1H, $^1J_{PH}$ 377.0) **H$_o$** 7.83 (dd, 2H, $^3J_{PH}$ 11.5, $^3J_{HH}$ 7.4), 7.11 (dd, 2H, $^3J_{PH}$ 11.5, $^3J_{HH}$ 7.4) **H$_m$** 6.99-6.95 (m, overlaps H$_m$ in PPh$_3$, 2H), 6.93-6.88 (m, 2H) **CH$_3$** 2.16 (s, 3H), 1.99 (s, 3H)
14b	1.47 (s, 15H)	**H$_o$** 8.05 (br s, 2H, $\omega_{1/2}$ 58.1), 7.76 (br s, 2H, $\omega_{1/2}$ 57.2), 3rd one not observed **H$_{m,p}$** 7.07-6.98 (m, H$_m$ and H$_p$ overlapping, 9H)	**κ^2-PhCα=Cβ H:** **H$_o$** 7.60 (dd, 2H, $^3J_{HH}$ 7.7, $^4J_{PH}$ 1.5) **CH** 7.46 (dd, 1H, $^2J_{PH}$ 9.4, $^4J_{PH}$ 4.0) **H$_m$** 7.29 (t, 2H, $^3J_{HH}$ 7.6) **H$_p$** 7.19-7.17 (m, overlaps residual solvent signal, 1H) **PEt$_2$:** **CH$_2$ (A)** 1.91-1.78 (m, 2H) **CH$_2$ (B)** 1.19-1.10 (m, 1H), 0.75-0.66 (m, 1H) **CH$_3$ (A)** 1.09-1.01 (m, 3H) **CH$_3$ (B)** 0.61-0.52 (m, 3H)
14c	1.37 (s, 15H)	**H$_o$** (br s, 2H, $\omega_{1/2}$ 36.9) Other signals not observed	Not observed
14d	1.41 (s, 15H)	**H$_o$** (br s, 2H, $\omega_{1/2}$ 29.2) Other signals not observed	Not observed

[a] Structure illustrating structure of **13** and **14** [R= Cy(**a**), Et (**b**), Ph (**c**), Tol^p (**d**)] in Figure 5.10

Table 5.3 125.79 MHz $^{13}C\{^1H\}$ NMR data for Ru(η^5-Cp*)(C≡CPh)(PR$_2$H)(PPh$_3$) **13b-d** and Ru(η^5-Cp*)(κ^2-PhC=CHPR$_2$)(PPh$_3$) **14b-d** in C_6D_6 at 300 K: δ in ppm (multiplicity, RI, J_{avg} or $\omega_{1/2}$ in Hz, assignment).[a]

	η^5-Cp*	**PPh$_3$**	**Other**
13b	C$_{ring}$ 89.8 (s) C$_{methyl}$ 10.5 (s)	Not observed	Not observed
13c	C$_{ring}$ 93.1 (s) C$_{methyl}$ 10.4 (s)	C$_{ipso}$ not observed C$_{ortho}$ 134.3 (d, $^2J_{PC}$ 10), 132.2 (d, $^2J_{PC}$ 11), 128.5 (d, $^2J_{PC}$ 9) C$_{para}$ 128.4 (s)	**Cα≡Cβ Ph:** C$_{ipso}$ 132.1 (s), C$_{ortho}$ 131.1 (s) C$_{meta}$ 128.3 (s), C$_{para}$ 123.6 (s) Cβ 112.3 (s), Cα not observed **PPh$_2$H:**

		C_{meta} 127.4 (d, $^4J_{PC}$ 9)	C_{ipso} 135.0 (d, $^1J_{PC}$ 37), the other C_{ipso} not observed C_{ortho} 134.7 (d, $^2J_{PC}$ 11), 132.9 (d, $^2J_{PC}$ 9) C_{para} 129.5 (s), 128.8 (s) C_{meta} 128.1 (d, $^3J_{PC}$ 8), 127.7 (d, $^3J_{PC}$ 9)
13d	C_{ring} 93.0 (s) C_{methyl} 10.4 (s)	C_{ipso}, C_{ortho} not observed C_{para} 128.4 (s) C_{meta} 127.4 (d, $^3J_{PC}$ 9)	**Cα≡Cβ Ph:** C_{ipso} 132.1 (s), C_{ortho} 131.1 (s) C_{meta} 128.3 (s), C_{para} 123.5 (s) C_b 112.3 (s), C_a not observed **PTol$^p_2$H:** C_{para} 139.4 (s), 138.5 (s) C_{ortho} 134.8 (d, $^2J_{PC}$ 10), 133.0 (d, $^2J_{PC}$ 9) C_{ipso} 133.4 (d, $^1J_{PC}$ 41), 131.9 (d, $^1J_{PC}$ 41) C_{meta} 128.8 (d, $^3J_{PC}$ 8), 128.5 (d, $^3J_{PC}$ 9) CH_3 21.4 (s), 21.1 (s)
14b	C_{ring} 90.1 (s) C_{methyl} 11.0 (s)	C_{ipso}, C_{ortho} not observed C_{para} 128.9 (s) C_{meta} 128.7 (d, $^3J_{PC}$ 8)	**κ^2-PhCα=Cβ H:** Cα 193.4[b], C_{ipso} 149.3[c], C_{ortho} 128.2 (s), C_{meta} 127.4 (s), C_{para} 126.3 (s), Cβ 125.0 (dd, $^1J_{PC}$ 43, $^3J_{PC}$ 2) **PEt$_2$:** CH_2 (A) 19.8 (d, $^2J_{PC}$ 21) CH_2 (B) 16.1 (d, $^2J_{PC}$ 9) CH_3 (A) 9.4 (d, $^3J_{PC}$ 6) CH_3 (B) 8.6 (d, $^3J_{PC}$ 5)
14c	C_{ring} 90.5 (s) C_{methyl} 10.7 (s)	Not observed	Not observed
14d	C_{ring} 90.4 (s) C_{methyl} 10.7 (s)	Not observed	Not observed

[a] Structure illustrating labeling for Cα≡Cβ Ph and κ^2-PhCα=Cβ H carbons [R= Cy(**a**), Et (**b**), Ph (**c**), Tol^p (**d**)] in Figure 5.10.
[b] Not directly observed but tracked by the correlation in ^{1}H/^{13}C{^{1}H}-HMBC spectrum [Cα <=> H_o (in κ^2-PhCα=Cβ H); Cα <=> H on Cβ].
[c] Not directly observed but tracked by the correlation in ^{1}H/^{13}C{^{1}H}-HMBC spectrum [C_{ipso} <=> H_m (in κ^2-PhCα=Cβ H); C_{ipso} <=> H on Cβ].

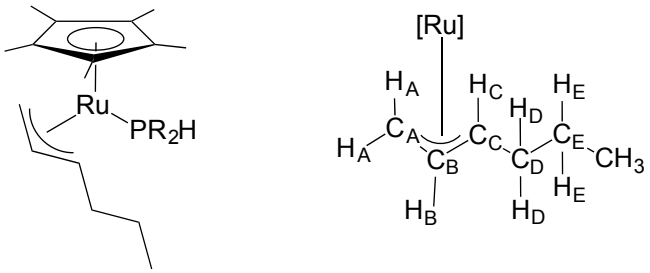

Figure 5.11 Structure of Ru(η^5-Cp*){η^3-$CH_2CHCH(C_3H_7)$}(PR_2H) **15** showing η^3-$CH_2CHCH(C_3H_7)$ allyl protons $H_{A\text{-}E}$ and carbons $C_{A\text{-}E}$.

Table 5.4 500.27 MHz ^{1}H NMR data for Ru(η^5-Cp*){(η^3-$CH_2CHCH(C_3H_7)$}(PR_2H) 15c,d in C_6D_6 at 300 K: δ in ppm (multiplicity, RI, J_{avg} or $\omega_{1/2}$ in Hz, assignment).[a]

	η^5-Cp*	**PR_2H**	**η^3-$CH_2CHCHC_3H_7$**
15c	1.62 (s, 15H)	**H-PPh$_2$** 6.39 (d, 1H, $^1J_{PH}$ 324.8) **Ph:** **H$_o$** 7.53 (dd, 2H, $^3J_{PH}$ 10.0, $^3J_{HH}$ 8.0), 7.44 (dd, 2H, $^3J_{PH}$ 10.0, $^3J_{HH}$ 8.0) **H$_m$** 7.12-7.08 (m, 4H) **H$_p$** 7.06-7.03 (m, overlaps free **PPh$_3$**, 2H)[b]	**H$_B$** 3.14-3.05 (m, 1H) **H$_A$** 2.10-2.06 (m, 1H, *cis* to **H$_B$**), 0.74 (dd, 1H, $^3J_{HH}$ 18.3, $^3J_{PH}$ 9.1, *trans* to **H$_B$**) **H$_D$** 1.97-1.90 (m, 1H), 1.62-1.55 (m, overlaps Cp* signal, 1H) **H$_E$** 1.55-1.52 (m, 2H) **H$_C$** 1.02-0.96 (m, overlaps **CH$_3$** in allyl group, 1H) **CH$_3$** 0.99 (t, 3H, $^3J_{HH}$ 7.1)
15d	1.66 (d, 15H, $^4J_{PH}$ 1.3)	**H-PTol$^p_2$** 6.43 (d, 1H, $^1J_{PH}$ 323.5) **Tol^p:** **H$_o$** 7.47 (dd, 2H, $^3J_{PH}$ 10.4, $^3J_{HH}$ 8.7), 7.43 (dd, 2H, $^3J_{PH}$ 10.3, $^3J_{HH}$ 8.4) **H$_m$** 6.98-6.93 (m, 4H) **CH$_3$** 2.07 (s, 3H), 2.05 (s, 3H)	**H$_B$** 3.15-3.06 (m, 1H) **H$_A$** 2.10-2.08 (m, 1H, *cis* to **H$_B$**), 0.74 (dd, 1H, $^3J_{HH}$ 18.5, $^3J_{PH}$ 9.1, *trans* to **H$_B$**) **H$_D$** 2.00-1.96 (m, 1H)[c], 1.61-1.58 (m, overlaps Cp* signal, 1H) **H$_E$** 1.58-1.52 (m, 2H) **H$_C$** 1.12-1.05 (m, 1H) **CH$_3$** 1.02 (t, 3H, $^3J_{HH}$ 7.2)

[a] Structure illustrating labeling for η^3-$CH_2CHCHC_3H_7$ protons $H_{A\text{-}E}$ [R= Ph (**c**), Tol^p (**d**)] in Figure 5.11.
[b] Not directly observed but tracked by the correlation in $^1H/^{13}C\{^1H\}$-HSQC spectrum (C_{para} <=> H_p).
[c] Not directly observed but tracked by the correlation in $^1H/^{13}C\{^1H\}$-HSQC spectrum (C_D <=> H_D).

Table 5.5 125.79 MHz $^{13}C\{^1H\}$ NMR data for Ru(η^5-Cp*)(η^3-$CH_2CHCHC_3H_7$)(PR_2H) **15c,d** in C_6D_6 at 300 K: δ in ppm (multiplicity, RI, J_{avg} or $\omega_{1/2}$ in Hz, assignment).[a]

	η^5-Cp*	PR_2H	η^3-$CH_2CHCHC_3H_7$
15c	C_{ring} 88.6 (d, $^2J_{PC}$ 2) C_{methyl} 10.7 (s)	**Ph:** C_{ipso} not observed C_{ortho} 134.7 (d, $^2J_{PC}$ 10), 133.6 (d, $^2J_{PC}$ 10) C_{para} 129.1 (s), 128.7 (s) C_{meta} 128.0 (d, $^3J_{PC}$ 9), the other not observed	C_B 76.8 (d, $^3J_{PC}$ 2) C_C 53.5 (d, $^2J_{PC}$ 4) C_D 37.8 (s) C_A 36.7 (d, $^2J_{PC}$ 5) C_E 27.0 (s) CH_3 14.3 (s)
15d	C_{ring} 88.4 (d, $^2J_{PC}$ 2) C_{methyl} 10.3 (s)	**Tol^p:** C_{para} 138.8 (s), 138.5 (d, $^4J_{PC}$ 2) C_{ortho} 134.7 (d, $^2J_{PC}$ 10), 133.8 (d, $^2J_{PC}$ 10) C_{meta} 128.9 (d, overlaps free **PPh_3**, $^3J_{PC}$ 9), 128.8 (d, overlaps free **PPh_3**, $^3J_{PC}$ 9)[b] C_{ipso} 133.1 (d, $^1J_{PC}$ 38), 131.2 (d, $^1J_{PC}$ 39) CH_3 21.2 (s)	C_B 76.7 (d, $^3J_{PC}$ 2) C_C 53.1 (d, $^2J_{PC}$ 4) C_D 38.0 (s) C_A 36.9 (d, $^2J_{PC}$ 5) C_E 27.1 (s) CH_3 14.3 (s)

[a] Structure illustrating Structure illustrating locations of η^3-$CH_2CHCHC_3H_7$ carbons $C_{A\text{-}E}$ [R= Ph (**c**), Tol^p (**d**)] in Figure 5.11.
[b] Not directly observed and tracked by the correlation in $^1H/^{13}C\{^1H\}$-HMBC spectrum [C_{meta} <=> CH_3 (in *p*-Tol)].

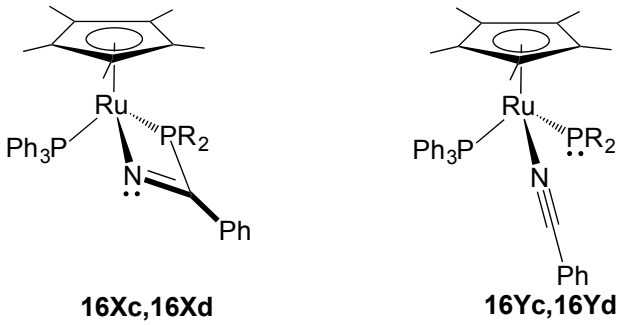

16Xc,16Xd **16Yc,16Yd**

Figure 5.12 Structure of PhCN adduct **16** showing two possible structures Ru(η^5-Cp*)(κ^2-N=C(Ph)PR$_2$)(PPh_3) (**X**) and Ru(η^5-Cp*)(NCPh)(PR_2)(PPh_3) (**Y**).

Table 5.6 500.27 MHz ^1H NMR data for PhCN adducts **16X/16Y** in C_6D_6 at 300 K: δ in ppm (multiplicity, RI, J_{avg} or $\omega_{1/2}$ in Hz, assignment).[a]

Compound	η^5-Cp*	PhCN	PR_2	PPh_3
16Xc/16Yc	1.48 (s,	**H_o** 6.99 (d, 2H, $^3J_{HH}$ 7.7)	**Ph:** **H_o** 7.60 (br s, 4H, $\omega_{1/2}$	**H_o** 7.68 (br s, 6H, $\omega_{1/2}$ 23.0)

	15H)	**H_p** 6.83 (t, 1H, $^3J_{HH}$ 7.3) **H_m** 6.67 (t, 2H, $^3J_{HH}$ 7.7)	19.1) **H_m** 7.05-7.02 (m, overlaps **$H_{m,p}$** in PPh_3, 2H), 7.00-6.97 (m, overlaps with signal of PhCN, 2H) **H_p** 6.97-6.94 (m, overlaps with signal of PhCN, 2H)	**$H_{m,p}$** 7.05-7.02 (m, overlaps with **H_m** in PPh_2, 9H)
16Xd/ 16Yd	1.50 (s, 15H)	**H_o** 7.00 (d, 2H, $^3J_{HH}$ 7.7) **H_p** 6.84 (t, 1H, $^3J_{HH}$ 7.3) **H_m** 6.68 (t, 2H, $^3J_{HH}$ 7.7)	**Tol^p:** **H_o** 7.51 (br s, 4H, $\omega_{1/2}$ 20.0) **H_m** 6.87-6.81(m, overlaps **H_p** in PhCN, 4H) **CH_3** 2.12 (s, 6H)	**H_o** 7.70 (br s, 6H, $\omega_{1/2}$ 22.4) **$H_{m,p}$** 7.08-7.03 (m, 9H)

[a] Structure illustrating PR_2 [R= Ph (**c**), Tol^p (**d**)] in Figure 5.12.

Table 5.7 125.79 MHz $^{13}C\{^1H\}$ NMR data for PhCN adducts **16X/16Y** in C_6D_6 at 300 K: δ in ppm (multiplicity, RI, J_{avg} or $\omega_{1/2}$ in Hz, assignment).[a]

Compound	η^5-Cp*	PhCN	PR_2	PPh_3
16Xc/16Yc	C_{ring} 90.3 (s) C_{methyl} 9.9 (s)	C_{para} 132.1 (s) C_{ortho} 132.0 (s) C_{meta} 128.9 (s) C_{CN} 118.8 (s) C_{ipso} 113.0 (s)	**Ph:** C_{ipso} 151.1 (d, $^1J_{PC}$ 40) C_{ortho} 135.3 (d, $^2J_{PC}$ 19) C_{meta} 127.1 (s), 127.0 (s) C_{para} 124.0 (s)	C_{ipso} 137.5 (d, $^1J_{PC}$ 37) C_{ortho} 135.1 (d, $^2J_{PC}$ 10), 135.0 (d, $^2J_{PC}$ 10) C_{para} 128.9 (d, $^4J_{PC}$ 2) C_{meta} 127.6 (d, $^3J_{PC}$ 9)
16Xd/16Yd	C_{ring} 90.2 (s) C_{methyl} 9.9 (s)	C_{para} 132.1 (s) C_{ortho} 132.0 (s) C_{meta} 128.9 (s) C_{CN} 118.8 (s) C_{ipso} 113.0 (s)	**Tol^p:** C_{ipso} 147.2 (d, $^1J_{PC}$ 44) C_{ortho} 135.4 (d, $^2J_{PC}$ 17) C_{para} 132.8 (s)[b] C_{meta} 128.0 (s), 127.9 (s)	C_{ipso} 137.8 (d, $^1J_{PC}$ 40) C_{ortho} 135.1 (d, $^2J_{PC}$ 10), 135.0 (d, $^2J_{PC}$ 10) C_{para} 128.8 (s) C_{meta} 127.6 (d, $^3J_{PC}$ 9)

[a] Structure illustrating PR_2 [R= Ph (**c**), Tol^p (**d**)] in Figure 5.12.

[b] Not directly observed but tracked by the correlation in $^1H/^{13}C\{^1H\}$-HMBC spectrum [C_{para} <=> H_o (in *p*-Tol)].

5.7 References

[1] Derrah, E. *Probing the Reactivity of Ruthenium Indenyl Complexes in P-C Bond Forming Reactions.* Ph.D thesis, University of Victoria, **2009**.

[2] Derrah, E. J.; Pantazis, D. A.; McDonald, R.; Rosenberg, L. *Angew. Chem. Int. Ed.* **2010**, *49*, 3367.

[3] Hoyle, M. M.; Pantazis, D. A.; Burton, H. M.; McDonald, R.; Rosenberg, L. *Organometallics* **2011**, *30*, 6458.

[4] Fryzuk, M. D.; Joshi, K. *Organometallics* **1989**, *8*, 722.

[5] Belli, R. G.; Burton, K. M. E.; Rufh, S. A.; McDonald, R.; Rosenberg, L. *Organometallics* **2015**, *34*, 5637.

[6] Milner, L. M.; Hall, L. M.; Pridmore, N. E.; Skeats, M. K.; Whitwood, A. C.; Lynam, J. M.; Slattery J. M. *Dalton Trans.* **2016**, *45*, 1717.

[7] Derrah, E. J.; Pantazis, D. A.; McDonald, R.; Rosenberg, L. *Angew. Chem. Int. Ed.* **2010**, *49*, 3367.

[8] Derrah, E. J.; McDonald, R.; Rosenberg, L. *Chem. Commun.* **2010**, *46*, 4592.

[9] $^{13}C\{^{1}H\}$ NMR data for phenylacetylene see: Aitken, R.A.; Atherton, J. I. *J. Chem. Soc. Perkin Transactions 1* **1994**, 1281.

[10] Dimerization of HC≡CR (R = Ph, $SiMe_3$, Bu^n and Bu^t) catalyzed by Ru(η^5-Tp)Cl(PPh_3)$_2$ and Ru(η^5-Tp)Cl(PPh_3)(py) see: Slugovc, C.; Mereiter, K.; Zobetz, E.; Schmid, R.; Kirchner, K. *Organometallics* **1996**, *15*, 5275.

[11] Dimerization of phenylacetylene catalyzed by Ru(η^5-C_8H_9)Cl(PPh_3)$_2$ and Ru(η^5-Cp)Cl(PPh_3)$_2$ see: Kirss, R. U.; Ernst, R. D.; Arif, A. M. *J. Organomet. Chem.* **2004**, *689*, 419.

[12] Dimerization of HC≡CR (R = Ph, Bu^t, $SiMe_3$, CH_2Ph, C_4H_9) catalyzed by Ru(η^5-Cp*)H_3(PR_3) (R= Ph, Cy, Me) see: Yi, C. S.; Liu, N. *Organometallics* **1996**, *15* (19), 3968.

[13] Dimerization of phenylacetylene catalyzed by Ru(η^5-indenyl)H(PPh_3)$_2$ and Ru(η^5-indenyl)(C≡CPh)(PPh_3)$_2$ see: Bassetti, M.; Marini, S.; Tortorella, F.; Cadierno, V.; Diez, J.; Gamasa, M. P.; Gimeno, J. *J. Organomet. Chem.* **2000**, *593–594*, 292.

[14] Dimerization of phenylacetylene catalyzed by Ru(η^5-C_5H_7)Cl(PPh_3)$_2$, Ru(η^5-C_5H_7)Cl($PMePh_2$)(PPh_3) and [Ru(η^5-C_5H_7)($NCCH_3$)(PPh_3)$_2$]PF_6 see: Daniels, M.; Kirss, R. U. *J. Organomet. Chem.* **2007**, *692*, 1716.

[15] Lin, A. C.; Chiang, Y.; Dahlberg, D. B.; Kresge, A. J. *J. Am. Chem. Soc.* **1983**, *105*, 5380.

[16] Zilkha, A. *J. Appl. Polym. Sci.* **1961**, *5*, 251.

[17] Yamamoto, Y.; Ogata, K.; Kuge, K.; Tatsumi K. *Inorganic Chemistry Communications* **2002**, *5*, 862.

[18] Albers, M.; Liles, D. C.; Robinson, D. J.; Shaver, A.; Singleton E. *Organometallics* **1987**, *6*, 2347.

[19] Hartwig, J. *Organotransition Metal Chemistry;* University Science Books: Sausalito, Calif., **2010**.

Chapter 6 Future work

6.1 Introduction

The work described in this thesis has provided some information on reactivity of Cp* phosphido complexes Ru(η^5-Cp*)(PR_2)(PPh_3) (**6a-b**) toward some reagents. Throughout the whole thesis, these results are discussed in the context of comparison with prior results obtained for the indenyl analogues Ru(η^5-indenyl)(PR_2)(PPh_3) (**6^i**). This project has showed the higher steric congestion and increase in basicity of the Cp* phosphido **6** relative to indenyl analogues **6^i**. This chapter describes some suggestions of how catalytic reactions could be achieved with our Cp* complexes and discuss what half-sandwich Ru complex could be a better analogue to compare with our previous indenyl complexes.

6.2 Reactions catalyzed by Cp* complexes

6.2.1 Potential hydrophosphination catalyzed by Cp* complex

As described in Chapter 2, [Ru(η^5-Cp*)(NCPh)($PTol^p{}_2H$)(PPh_3)][$B(C_6F_5)_4$] (**5d**) has been synthesized. The cationic analogues **5** with other PR_2H ligand can be synthesized by the same strategy (Scheme 6.1). The P-H bond in these cationic complexes is more acidic than that of their neutral chloride analogues Ru(η^5-Cp*)Cl(PR_2H)(PPh_3) (**2**), which might allow deprotonation by a weaker base (e.g. DBU) than $KOBu^t$ (Scheme 6.1).[1,2] The resulting phosphido complex Ru(η^5-Cp*)(NCPh)(PR_2)(PPh_3) might be useful for metal-catalyzed hydrophosphination. The proposed mechanism is shown in Scheme 6.2.

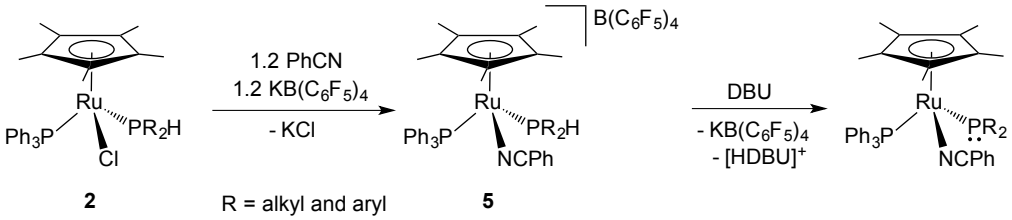

Scheme 6.1 Proposed synthesis of $[Ru(\eta^5\text{-}Cp^*)(NCPh)(PR_2H)(PPh_3)][B(C_6F_5)_4]$ (**5**) used as a precursor to generate phosphido $Ru(\eta^5\text{-}Cp^*)(NCPh)(PR_2)(PPh_3)$.

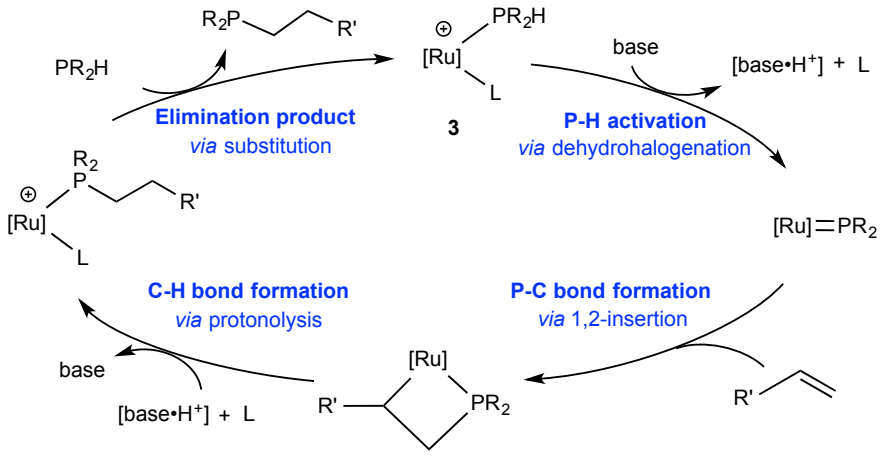

Scheme 6.2 Proposed catalytic cycle for the hydrophosphination of alkene mediated by complex **5** ([Ru] = $Ru(\eta^5\text{-}Cp^*)PR_2H$; L = PhCN).

In addition, disubstituted secondary phosphine complexes $Ru(\eta^5\text{-}Cp^*)Cl(PR_2H)_2$ (**3**) might be isolated and used as a precursor to form phosphido $Ru(\eta^5\text{-}Cp^*)(PR_2)(PR_2H)$ (Scheme 6.3). These phosphido complexes might be more stable than analogues with PPh_3 ligand $Ru(\eta^5\text{-}Cp^*)(PR_2)(PPh_3)$ (**6**), since the orthometallation could be inhibited by releasing the steric congestion at Ru (phosphine size: $PR_2H > PPh_3$) and the absence of the close C-H bond proton which can be deprotonated by phosphido (PR_2^-) ligand. Some $^{31}P\{^1H\}$ NMR spectra show the secondary phosphine phosphido $Ru(\eta^5\text{-}Cp^*)(PPh_2)(PPh_2H)$ is more stable than its analogues $Ru(\eta^5\text{-}Cp^*)(PPh_2)(PPh_3)$ (**6c**). The decreased steric crowding at Ru should allow incoming species (e.g. alkene) to approach the Ru center to form a metallacycle.

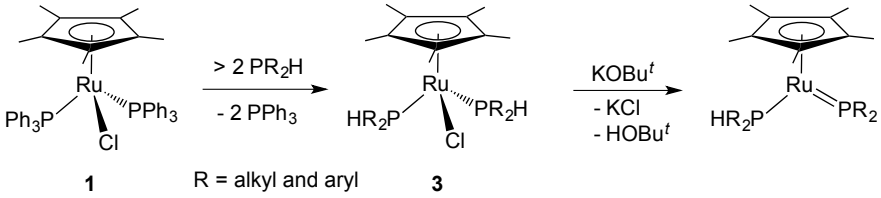

Scheme 6.3 Proposed synthesis of Ru(η^5-Cp*)Cl(PR_2H)$_2$ (**3**) used as a precursor to generate phosphido Ru(η^5-Cp*)(PR_2)(PR_2H).

6.2.2 Other reactions catalyzed by Cp* complex

Sawamoto and coworkers reported the living radical polymerization catalyzed by systematic complexes Ru(η^5-Cp*)Cl(PR_3)$_2$. [3] The Ru-catalyzed living radical polymerization proceed *via* reversible activation of a carbon-halogen bond by a Ru(II) complex (Scheme 6.4).[4] Firstly, Ru(II) attacks the halogen of an organic halide (R-X) *via* an one-electron transfer (step A) and Ru(II) is oxidized to Ru(III) followed by coordination of halide ligand at Ru center. Through this step, an initiating radical compound (R•) is formed and reacts with the monomers to keep generating an new radical specie (step B). In the end, this radical species will abstract the halogen atom from Ru(III), while simultaneously, Ru(III) is reduced to Ru(II), which is capable of terminating the polymerization and regenerating the Ru catalyst (step C). Ando et al. reported that the activity of the complexes for this living radical polymerization can be affected by the redox potential of these complexes and the redox potential found by cyclic voltammetry (CV) increased in the order Ru(η^5-Cp*)Cl(PPh_3)$_2$ (**1**) < Ru(η^5-indenyl)Cl(PPh_3)$_2$ (**1^i**) < Ru(η^5-Cp)Cl(PPh_3)$_2$.[5] The CV of Cp* complex **1** and Ru(η^5-Cp*)Cl(PCy_2H)(PPh_3) (**2a**) were studied by our group (Figure 6.1). This CV data shows unsymmetrical secondary phosphine complex **2a** has a lower redox potential relative to **1**, which suggests **2a** may be active catalyst for living radical polymerization.

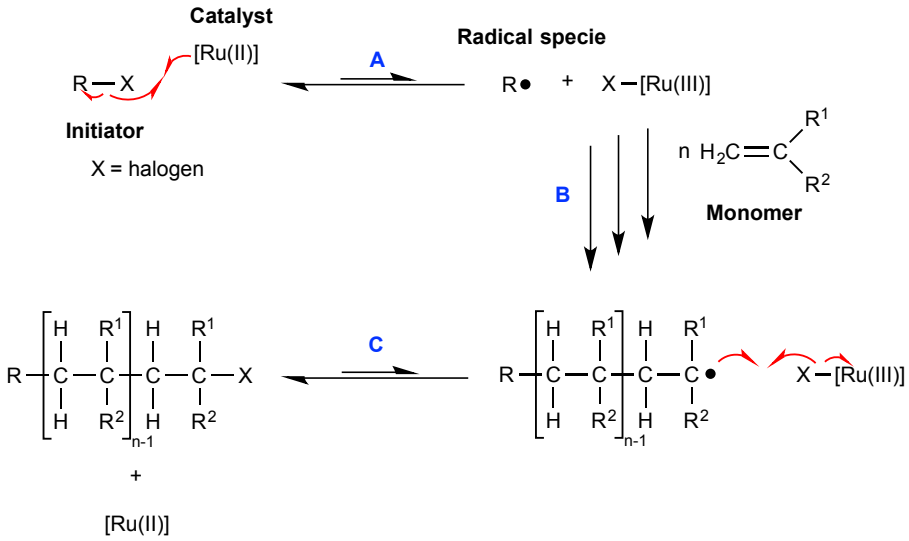

Scheme 6.4 Ru(II)-catalyzed living radical polymerization of alkene.

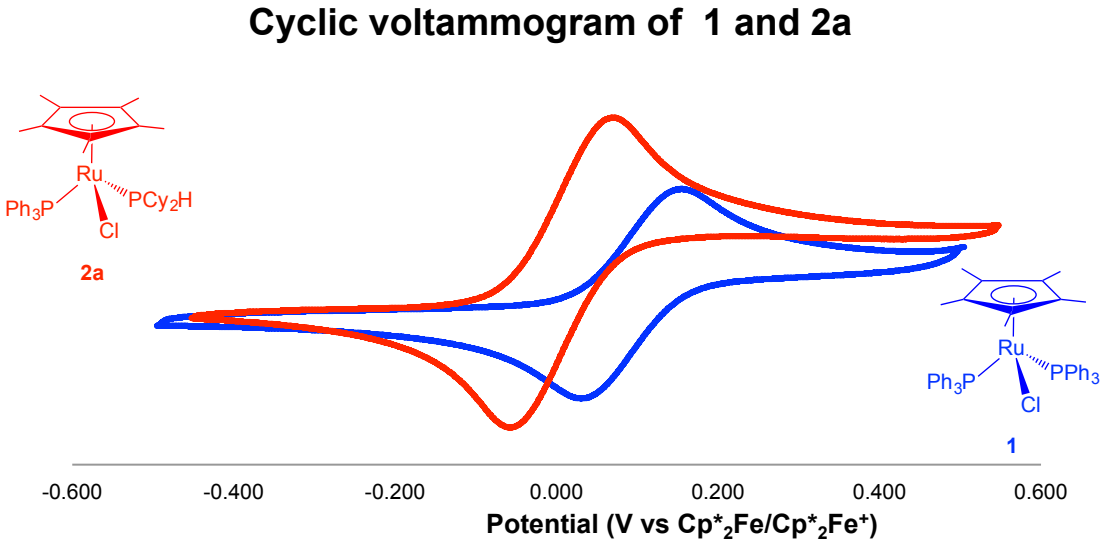

Figure 6.1 Cyclic voltammograms (CH_2Cl_2, 20 °C) of Ru(η^5-Cp*)Cl(PPh_3)$_2$ (**1**) and Ru(η^5-Cp*)Cl(PCy_2H)(PPh_3) (**2a**).

In addition, as mentioned in Chapter 5 (Section 5.2.4), Ru(η^5-Cp*)(PEt_2H)(PPh_3) (**6b**) generated in situ reacts with phenylacetylene to give alkynyl complex Ru(η^5-Cp*)(C≡CPh)(PR_2H)(PPh_3) (**13b**) which is proposed to catalyze the dimerization of phenylacetylene. It is interesting to see whether it can catalyze the dimerization of simple alkyne (e.g. 1-hexyne). This dimerization reaction of phenylacetylene has not occurred for complexes **6c,d** with larger phosphine ligands, such as PPh_2H, suggesting smaller phosphine ligands are needed to release the steric crowding at Ru

and allow phenylacetylene to approach. A new complex Ru(η^5-Cp*){P(Me)(Ph)H}(PPh_3) containing an unsymmetrically-substituted PR_2H can be synthesized to try the dimerization of phenylacetylene (Scheme 6.5). The size of P(Me)(Ph)H (commercially available) is between PEt_2H and PPh_2H and it can help better understand the effect of phosphine size on the Ru-catalyzed dimerization.

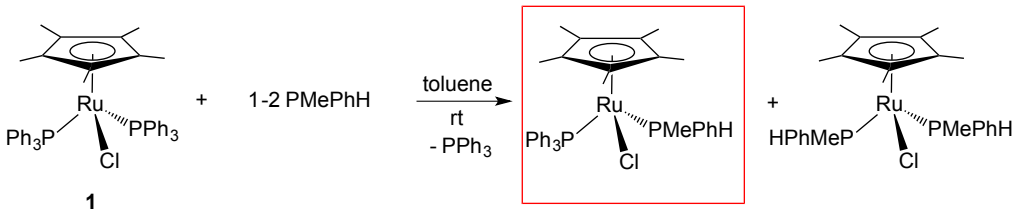

Scheme 6.5 Proposed synthesis of Ru(η^5-Cp*)Cl{P(Et)(Ph)H}(PPh_3) possibly containing disubstituted Ru(η^5-Cp*)Cl{P(Et)(Ph)H}$_2$.

6.3 Alternative lignads: Cp derivatives

From this project, the difference between Cp* and indenyl complex suggests that the Cp* ligand is not an exact analogue of the indenyl ligand because of its different electronic and steric properties. Some other ligands, which have similar structures and electron density to the indenyl ligand, could be investigated instead of the Cp* ligand. To investigate whether the indenyl effect exists in our catalytic mechanism, an indenyl analogue with a saturated 6-membered ring on the side of Cp ring might be a better choice than Cp* (see Scheme 6.6). This ligand is also commercially available. When this ligand coordinates to Ru, it has similar structure to indenyl analogue (Scheme 6.6).

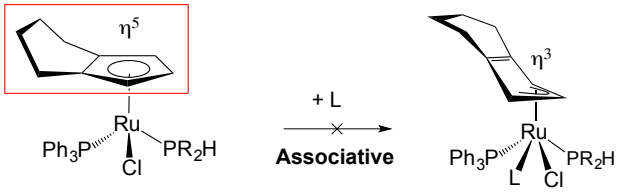

Scheme 6.6 Indenyl analogues with saturated 6-memberd ring inhibit hapticity change.

On the other hand, to optimize our half-sandwich Ru complex for hydrophosphination, the ideal auxiliary ligand should have higher electron density (more electron-rich Ru) relative to the indenyl ligand and be less bulky compared to the Cp* ligand. Hence, monosubstituted trimethylsilyl ($SiMe_3$) Cp ligand could be a good ligand to investigate. The advantage of using one $SiMe_3$ group as an alternative substituent instead of five methyl groups is that its resulting $C_5H_4(SiMe_3)$ anion is a stronger σ-donor in comparison of the indenyl group[6] and it also slightly increases the steric bulk relative to indenyl ligand. The synthesis of this ligand is not difficult; Baumgartner and coworkers reported the preparation of a series of titanium (Ti) half-sandwich complexes $Ti\{\eta^5\text{-}C_5H_{5-x}(SiMe_3)_x\}R_3$ (x = 1-3, R = Cl, Me).[7] The $C_5H_5(SiMe_3)$ can be prepared in a one-pot synthesis (Scheme 6.7). A new Ru complex based on this ligand can be used to try catalytic hydrophosphination.

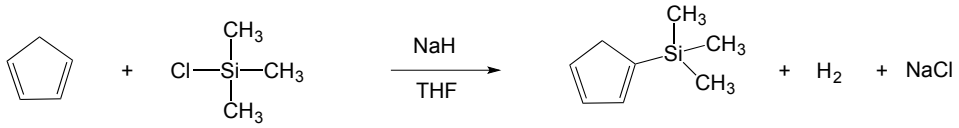

Scheme 6.7 One-pot synthesis of $C_5H_5(SiMe_3)$.

6.5 References

[1] Belli, R. G.; Burton, K. M. E.; Rufh, S. A.; McDonald, R.; Rosenberg, L. *Organometallics* **2015**, *34*, 5637.

[2] Sues, P. E.; Lough, A. J.; Morris, R. H. *J. Am. Chem. Soc.* **2014**, *136*, 4746.

[3] Ouchi, M.; Ito, M.; Kamemoto, S.; Sawamoto, M. *Chem. Asian J.* **2008**, *3*, 1358.

[4] Kamigaito, M. Ando, T. Sawamoto, M. *Chem. Rev.* **2001**, *101*, 3689.

[5] Ando, T.; Kamigaito, M.; Sawamoto, M. *Macromolecules* **2000**, *33*, 5825.

[6] Okuda, J. *Top. Curr. Chem.* **1991**, *160*, 97.

[7] Saßmannshausen, J.; Baumgartner, J. *Kinetics and Catalysis* **2009**, *50(5)*, 676.

Appendix A X-ray Crystallographic structure report for Ru(η^5-Cp*)Cl(PCy$_2$H)(PPh$_3$) (2a)

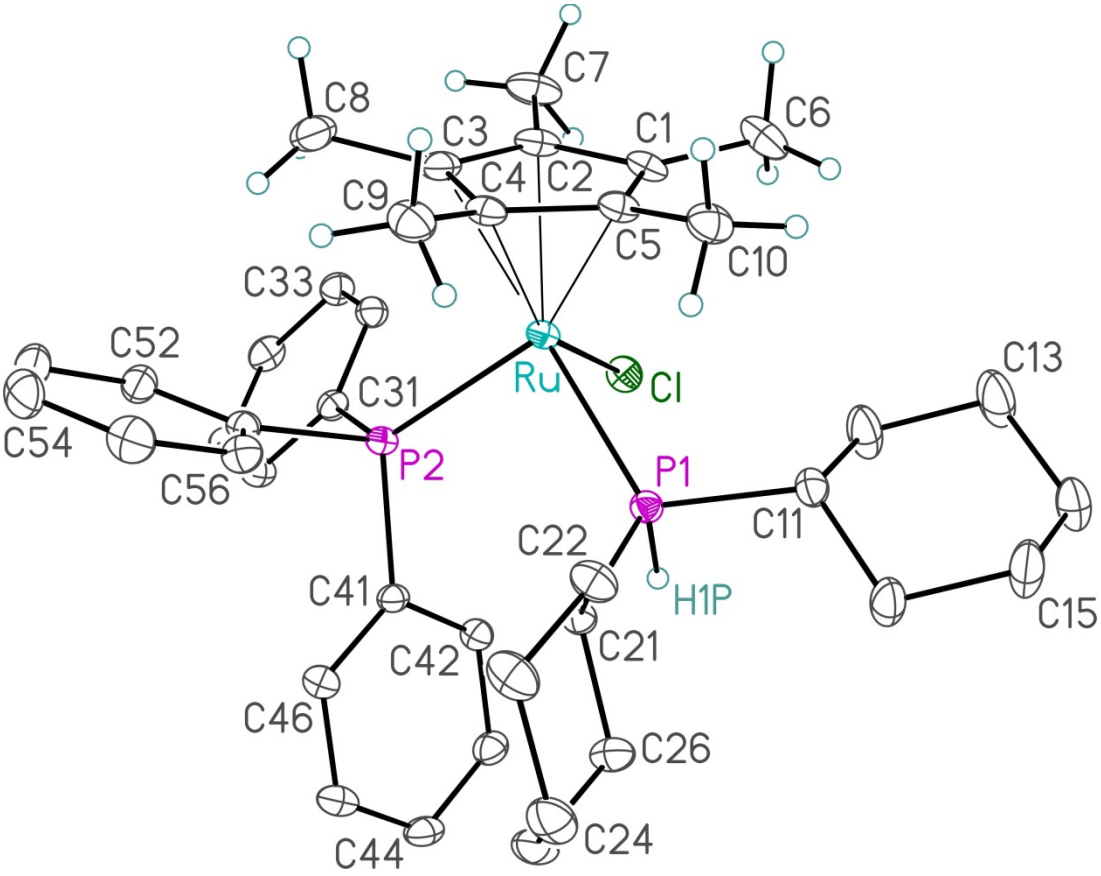

Figure A.1 Perspective view of the Ru(η^5-Cp*)Cl(PCy$_2$H)(PPh$_3$) (**2a**) molecule showing the atom labeling scheme. Non-hydrogen atoms are represented by Gaussian ellipsoids at the 30% probability level. The hydrogen atom attached to P1 and those of the pentamethylcyclopentadienyl group are shown with arbitrarily small thermal parameters; cyclohexyl- and phenyl-group hydrogens are not shown.

This structure determination, as well as that of complex 2b in Appendix B, was carried out by Dr. Robert McDonald at the X-ray Crystallography Laboratory, Department of Chemistry, University of Alberta, Edmonton, Alberta, Canada T6G 2G2. E-mail: Bob.McDonald@ualberta.ca. Phone: 1-(780)-492-2485.

Appendix A X-ray Crystallographic structure report for Ru(η^5-Cp)Cl(PCy_2H)(PPh_3) (**2a**)*

Table A.1 Crystallographic Experimental Details

A. Crystal Data	
formula	$C_{40}H_{53}ClP_2Ru$
formula weight	732.28
crystal dimensions (mm)	0.29 × 0.25 × 0.17
crystal system	monoclinic
space group	$P2_1/n$ (an alternate setting of $P2_1/c$ [No. 14])
unit cell parameters[a]	
a (Å)	13.4737 (16)
b (Å)	17.576 (2)
c (Å)	15.2841 (18)
β (deg)	99.1542 (14)
V (Å^3)	3573.4 (7)
Z	4
ρ_{calcd} (g cm^{-3})	1.361
μ (mm^{-1})	0.630
B. Data Collection and Refinement Conditions	
diffractometer	Bruker PLATFORM/APEX II CCD[b]
radiation (λ [Å]) (0.71073)	graphite-monochromated Mo Kα
temperature (°C)	–100
scan type	ω scans (0.3°) (15 s exposures)
data collection 2θ limit (deg)	56.43
total data collected	33369 (-17 ≤ h ≤ 17, -23 ≤ k ≤ 23, -20 ≤ l ≤ 20)
independent reflections	8740 (R_{int} = 0.0263)
number of observed reflections (*NO*)	7996 [$F_o^2 \geq 2\sigma(F_o^2)$]
structure solution method	Patterson/structure expansion (*DIRDIF–2008*[c])
refinement method (*SHELXL–2014*[d])	full-matrix least-squares on F^2
absorption correction method	Gaussian integration (face-indexed)
range of transmission factors	0.9665–0.8292
data/restraints/parameters	8740 / 0 / 406
goodness-of-fit (*S*)[e] [all data]	1.070
final R indices[f]	
R_1 [$F_o^2 \geq 2\sigma(F_o^2)$]	0.0286
wR_2 [all data]	0.0727
largest difference peak and hole	0.647 and –0.536 e Å^{-3}

[a]Obtained from least-squares refinement of 9987 reflections with 4.40° < 2θ < 52.78°.

[b]Programs for diffractometer operation, data collection, data reduction and absorption correction were those supplied by Bruker.

[c]Beurskens, P. T.; Beurskens, G.; de Gelder, R.; Smits, J. M. M.; Garcia-Granda, S.; Gould, R. O. (2008). The *DIRDIF-2008* program system. Crystallography Laboratory, Radboud University Nijmegen, The Netherlands.

[d]Sheldrick, G. M. *Acta Crystallogr.* **2015**, *C71*, 3–8.

[e]$S = [\Sigma w(F_o^2 - F_c^2)^2/(n - p)]^{1/2}$ (n = number of data; p = number of parameters varied; $w = [\sigma^2(F_o^2) + (0.0320P)^2 + 2.1357P]^{-1}$ where $P = [\mathrm{Max}(F_o^2, 0) + 2F_c^2]/3$).

[f]$R_1 = \Sigma||F_o| - |F_c||/\Sigma|F_o|$; $wR_2 = [\Sigma w(F_o^2 - F_c^2)^2/\Sigma w(F_o^4)]^{1/2}$.

Table A.2 Atomic Coordinates and Equivalent Isotropic Displacement Parameters

Atom	*x*	*y*	*z*	U_{eq}, Å^2
Ru	-0.07053(2)	0.29152(2)	0.24353(2)	0.02086(5)*
Cl	-0.15217(3)	0.30609(2)	0.08977(3)	0.02935(9)*
P1	0.06133(3)	0.35923(2)	0.19821(3)	0.02267(9)*
P2	-0.00778(3)	0.17600(2)	0.20435(3)	0.02058(8)*
C1	-0.18196(13)	0.36523(10)	0.29680(12)	0.0290(4)*
C2	-0.21818(14)	0.28822(11)	0.29233(13)	0.0319(4)*
C3	-0.14953(14)	0.24271(11)	0.34961(12)	0.0311(4)*
C4	-0.06756(13)	0.29048(10)	0.38887(11)	0.0272(3)*
C5	-0.09012(13)	0.36649(10)	0.35759(11)	0.0273(3)*
C6	-0.24090(17)	0.43095(13)	0.25347(14)	0.0445(5)*
C7	-0.31955(15)	0.26561(15)	0.24340(15)	0.0459(5)*
C8	-0.16622(18)	0.16261(12)	0.37689(15)	0.0441(5)*
C9	0.00839(16)	0.27085(13)	0.46878(12)	0.0389(4)*
C10	-0.03398(15)	0.43534(11)	0.39713(13)	0.0359(4)*
C11	0.04707(13)	0.46469(9)	0.19422(12)	0.0284(3)*
C12	-0.04937(16)	0.48416(12)	0.1323(2)	0.0517(6)*
C13	-0.07378(18)	0.56906(13)	0.1338(2)	0.0664(8)*
C14	0.01088(17)	0.61712(11)	0.11120(16)	0.0445(5)*
C15	0.10811(17)	0.59684(12)	0.16774(19)	0.0517(6)*
C16	0.13229(15)	0.51136(11)	0.16642(18)	0.0460(5)*
C21	0.19299(12)	0.33547(10)	0.24628(11)	0.0247(3)*
C22	0.22708(14)	0.36853(11)	0.33863(12)	0.0332(4)*
C23	0.33044(15)	0.33734(13)	0.37914(13)	0.0401(5)*
C24	0.40742(15)	0.35165(13)	0.31822(15)	0.0412(5)*
C25	0.37387(14)	0.31694(12)	0.22756(14)	0.0372(4)*
C26	0.27154(13)	0.34816(12)	0.18505(12)	0.0330(4)*
C31	-0.09822(12)	0.11250(9)	0.13750(10)	0.0232(3)*

Appendix A X-ray Crystallographic structure report for Ru(η^5-Cp)Cl(PCy_2H)(PPh_3) (**2a**)*

C32	-0.20044(13)	0.12815(10)	0.12774(11)	0.0260(3)*
C33	-0.26991(13)	0.08061(10)	0.07797(12)	0.0302(4)*
C34	-0.23789(14)	0.01698(10)	0.03753(12)	0.0324(4)*
C35	-0.13615(14)	0.00046(10)	0.04672(12)	0.0324(4)*
C36	-0.06669(13)	0.04795(10)	0.09615(11)	0.0284(3)*
C41	0.09145(12)	0.17381(9)	0.13420(10)	0.0223(3)*
C42	0.07077(13)	0.20859(9)	0.05069(11)	0.0263(3)*
C43	0.14345(15)	0.21060(10)	-0.00405(12)	0.0301(4)*
C44	0.23692(14)	0.17834(10)	0.02253(12)	0.0311(4)*
C45	0.25772(13)	0.14301(11)	0.10419(12)	0.0308(4)*
C46	0.18501(13)	0.14040(10)	0.15965(11)	0.0275(3)*
C51	0.04420(12)	0.11348(9)	0.29716(10)	0.0237(3)*
C52	0.00814(14)	0.04045(10)	0.30876(12)	0.0315(4)*
C53	0.04633(17)	-0.00228(12)	0.38295(14)	0.0413(5)*
C54	0.12223(18)	0.02622(13)	0.44534(13)	0.0431(5)*
C55	0.15954(16)	0.09805(13)	0.43462(13)	0.0400(4)*
C56	0.12032(14)	0.14165(11)	0.36149(12)	0.0305(4)*
H1P	0.0681(14)	0.3493(11)	0.1156(12)	0.022(5)

Anisotropically-refined atoms are marked with an asterisk (*). The form of the anisotropic displacement parameter is: $\exp[-2\pi^2(h^2a^{*2}U_{11} + k^2b^{*2}U_{22} + l^2c^{*2}U_{33} + 2klb^*c^*U_{23} + 2hla^*c^*U_{13} + 2hka^*b^*U_{12})]$.

Appendix A X-ray Crystallographic structure report for Ru(η^5-Cp)Cl(PCy_2H)(PPh_3) (**2a**)*

Table A.3 Selected Interatomic Distances (Å)

Atom1	Atom2	Distance	Atom1	Atom2	Distance
Ru	Cl	2.4445(5)	C13	C14	1.503(3)
Ru	P1	2.3334(5)	C14	C15	1.493(3)
Ru	P2	2.3146(5)	C15	C16	1.538(3)
Ru	C1	2.2325(16)	C21	C22	1.528(2)
Ru	C2	2.2337(17)	C21	C26	1.537(2)
Ru	C3	2.2464(17)	C22	C23	1.533(3)
Ru	C4	2.2155(17)	C23	C24	1.521(3)
Ru	C5	2.2342(16)	C24	C25	1.516(3)
P1	C11	1.8635(17)	C25	C26	1.529(3)
P1	C21	1.8565(17)	C31	C32	1.389(2)
P1	H1P	1.292(18)	C31	C36	1.397(2)
P2	C31	1.8379(16)	C32	C33	1.388(2)
P2	C41	1.8424(16)	C33	C34	1.380(3)
P2	C51	1.8423(17)	C34	C35	1.386(3)
C1	C2	1.437(3)	C35	C36	1.385(2)
C1	C5	1.424(2)	C41	C42	1.403(2)
C1	C6	1.496(3)	C41	C46	1.389(2)
C2	C3	1.416(3)	C42	C43	1.386(2)
C2	C7	1.503(3)	C43	C44	1.382(3)
C3	C4	1.440(3)	C44	C45	1.382(3)
C3	C8	1.495(3)	C45	C46	1.394(2)
C4	C5	1.435(2)	C51	C52	1.394(2)
C4	C9	1.503(3)	C51	C56	1.394(2)
C5	C10	1.502(2)	C52	C53	1.389(3)
C11	C12	1.520(3)	C53	C54	1.377(3)
C11	C16	1.525(3)	C54	C55	1.378(3)
C12	C13	1.529(3)	C55	C56	1.388(3)

Appendix A X-ray Crystallographic structure report for Ru(η^5-Cp)Cl(PCy_2H)(PPh_3) (**2a**)*

Table A.4 Selected Interatomic Angles (deg)

Atom1	Atom2	Atom3	Angle	Atom1	Atom2	Atom3	Angle
Cl	Ru	P1	84.752(16)	Ru	C1	C2	71.28(9)
Cl	Ru	P2	88.292(15)	Ru	C1	C5	71.47(9)
Cl	Ru	C1	93.67(5)	Ru	C1	C6	128.85(13)
Cl	Ru	C2	92.02(5)	C2	C1	C5	107.39(16)
Cl	Ru	C3	122.78(5)	C2	C1	C6	123.65(18)
Cl	Ru	C4	153.95(5)	C5	C1	C6	128.46(18)
Cl	Ru	C5	126.68(5)	Ru	C2	C1	71.19(10)
P1	Ru	P2	92.510(16)	Ru	C2	C3	72.07(10)
P1	Ru	C1	113.60(5)	Ru	C2	C7	128.90(13)
P1	Ru	C2	150.81(5)	C1	C2	C3	108.62(16)
P1	Ru	C3	151.60(5)	C1	C2	C7	123.22(19)
P1	Ru	C4	114.12(5)	C3	C2	C7	127.67(19)
P1	Ru	C5	96.94(5)	Ru	C3	C2	71.09(10)
P2	Ru	C1	153.89(5)	Ru	C3	C4	70.01(9)
P2	Ru	C2	116.43(5)	Ru	C3	C8	132.08(13)
P2	Ru	C3	94.95(5)	C2	C3	C4	108.10(16)
P2	Ru	C4	107.65(5)	C2	C3	C8	126.29(18)
P2	Ru	C5	144.35(5)	C4	C3	C8	124.89(18)
C1	Ru	C2	37.53(7)	Ru	C4	C3	72.34(10)
C1	Ru	C3	62.29(7)	Ru	C4	C5	71.89(9)
C1	Ru	C4	62.94(6)	Ru	C4	C9	135.88(12)
C1	Ru	C5	37.19(6)	C3	C4	C5	107.22(16)
C2	Ru	C3	36.84(7)	C3	C4	C9	125.62(17)
C2	Ru	C4	62.61(7)	C5	C4	C9	124.41(17)
C2	Ru	C5	62.14(6)	Ru	C5	C1	71.34(9)
C3	Ru	C4	37.65(7)	Ru	C5	C4	70.48(9)
C3	Ru	C5	62.21(7)	Ru	C5	C10	132.42(12)
C4	Ru	C5	37.63(6)	C1	C5	C4	108.59(16)
Ru	P1	C11	115.95(6)	C1	C5	C10	127.19(17)
Ru	P1	C21	119.51(6)	C4	C5	C10	123.33(16)
Ru	P1	H1P	113.4(8)	P1	C11	C12	108.54(13)
C11	P1	C21	108.89(8)	P1	C11	C16	117.76(13)
C11	P1	H1P	97.2(8)	C12	C11	C16	108.20(17)
C21	P1	H1P	98.3(8)	C11	C12	C13	112.03(19)
Ru	P2	C31	116.06(6)	C12	C13	C14	111.8(2)
Ru	P2	C41	119.84(5)	C13	C14	C15	111.14(19)
Ru	P2	C51	115.70(5)	C14	C15	C16	113.18(19)
C31	P2	C41	98.18(7)	C11	C16	C15	110.57(18)
C31	P2	C51	101.72(7)	P1	C21	C22	114.08(12)
C41	P2	C51	102.33(7)	P1	C21	C26	115.70(12)
C22	C21	C26	111.87(15)	C22	C23	C24	110.97(17)
C21	C22	C23	110.94(15)	C23	C24	C25	111.09(17)

Appendix A X-ray Crystallographic structure report for Ru(η^5-Cp)Cl(PCy_2H)(PPh_3) (**2a**)*

C24	C25	C26	111.19(16)	C41	C42	C43	120.23(16)
C21	C26	C25	110.54(15)	C42	C43	C44	120.69(17)
P2	C31	C32	119.86(12)	C43	C44	C45	119.62(16)
P2	C31	C36	121.47(13)	C44	C45	C46	120.16(17)
C32	C31	C36	118.67(15)	C41	C46	C45	120.66(16)
C31	C32	C33	120.69(16)	P2	C51	C52	123.35(13)
C32	C33	C34	120.12(17)	P2	C51	C56	118.57(13)
C33	C34	C35	119.93(16)	C52	C51	C56	118.01(16)
C34	C35	C36	120.03(17)	C51	C52	C53	120.69(18)
C31	C36	C35	120.56(17)	C52	C53	C54	120.44(19)
P2	C41	C42	117.58(12)	C53	C54	C55	119.72(18)
P2	C41	C46	123.79(13)	C54	C55	C56	120.13(19)
C42	C41	C46	118.63(15)	C51	C56	C55	120.99(18)

Appendix A X-ray Crystallographic structure report for Ru(η^5-Cp)Cl(PCy_2H)(PPh_3) (**2a**)*

Table A.5 Torsional Angles (deg)

Atom1	Atom2	Atom3	Atom4	Angle	Atom1	Atom2	Atom3	Atom4	Angle
Cl	Ru	P1	C11	82.04(7)	P2	Ru	C1	C5	111.46(12)
Cl	Ru	P1	C21	-144.39(6)	P2	Ru	C1	C6	-123.64(17)
P2	Ru	P1	C11	170.09(6)	C2	Ru	C1	C5	116.52(16)
P2	Ru	P1	C21	-56.34(6)	C2	Ru	C1	C6	-118.6(2)
C1	Ru	P1	C11	-9.68(8)	C3	Ru	C1	C2	-36.84(11)
C1	Ru	P1	C21	123.89(8)	C3	Ru	C1	C5	79.67(12)
C2	Ru	P1	C11	-2.70(13)	C3	Ru	C1	C6	-155.4(2)
C2	Ru	P1	C21	130.87(12)	C4	Ru	C1	C2	-79.46(12)
C3	Ru	P1	C11	-84.67(12)	C4	Ru	C1	C5	37.06(10)
C3	Ru	P1	C21	48.89(12)	C4	Ru	C1	C6	162.0(2)
C4	Ru	P1	C11	-79.29(8)	C5	Ru	C1	C2	-116.52(16)
C4	Ru	P1	C21	54.27(8)	C5	Ru	C1	C6	124.9(2)
C5	Ru	P1	C11	-44.34(8)	Cl	Ru	C2	C1	-93.39(10)
C5	Ru	P1	C21	89.22(8)	Cl	Ru	C2	C3	148.92(10)
Cl	Ru	P2	C31	-46.79(6)	Cl	Ru	C2	C7	24.6(2)
Cl	Ru	P2	C41	70.79(6)	P1	Ru	C2	C1	-10.53(18)
Cl	Ru	P2	C51	-165.89(6)	P1	Ru	C2	C3	-128.23(11)
P1	Ru	P2	C31	-131.46(6)	P1	Ru	C2	C7	107.43(19)
P1	Ru	P2	C41	-13.88(6)	P2	Ru	C2	C1	177.52(9)
P1	Ru	P2	C51	109.44(6)	P2	Ru	C2	C3	59.82(11)
C1	Ru	P2	C31	48.06(12)	P2	Ru	C2	C7	-64.5(2)
C1	Ru	P2	C41	165.64(12)	C1	Ru	C2	C3	-117.69(15)
C1	Ru	P2	C51	-71.04(12)	C1	Ru	C2	C7	118.0(2)
C2	Ru	P2	C31	44.62(8)	C3	Ru	C2	C1	117.69(15)
C2	Ru	P2	C41	162.21(8)	C3	Ru	C2	C7	-124.3(2)
C2	Ru	P2	C51	-74.48(8)	C4	Ru	C2	C1	80.41(11)
C3	Ru	P2	C31	75.97(8)	C4	Ru	C2	C3	-37.29(10)
C3	Ru	P2	C41	-166.44(8)	C4	Ru	C2	C7	-161.6(2)
C3	Ru	P2	C51	-43.13(8)	C5	Ru	C2	C1	37.72(10)
C4	Ru	P2	C31	112.23(8)	C5	Ru	C2	C3	-79.97(11)
C4	Ru	P2	C41	-130.19(8)	C5	Ru	C2	C7	155.7(2)
C4	Ru	P2	C51	-6.87(8)	Cl	Ru	C3	C2	-37.85(12)
C5	Ru	P2	C31	122.95(10)	Cl	Ru	C3	C4	-156.15(8)
C5	Ru	P2	C41	-119.47(10)	Cl	Ru	C3	C8	84.4(2)
C5	Ru	P2	C51	3.85(10)	P1	Ru	C3	C2	126.36(11)
Cl	Ru	C1	C2	88.55(10)	P1	Ru	C3	C4	8.06(17)
Cl	Ru	C1	C5	-154.93(10)	P1	Ru	C3	C8	-111.39(19)
Cl	Ru	C1	C6	-30.03(18)	P2	Ru	C3	C2	-129.01(10)
P1	Ru	C1	C2	174.42(9)	P2	Ru	C3	C4	112.69(10)
P1	Ru	C1	C5	-69.06(11)	P2	Ru	C3	C8	-6.8(2)
P1	Ru	C1	C6	55.84(19)	C1	Ru	C3	C2	37.54(10)
P2	Ru	C1	C2	-5.06(18)	C1	Ru	C3	C4	-80.76(11)

Appendix A X-ray Crystallographic structure report for Ru(η^5-Cp)Cl(PCy_2H)(PPh_3) (**2a**)*

C1	Ru	C3	C8	159.8(2)	C3	Ru	C5	C10	156.3(2)
C2	Ru	C3	C4	-118.30(15)	C4	Ru	C5	C1	-118.48(15)
C2	Ru	C3	C8	122.3(2)	C4	Ru	C5	C10	117.8(2)
C4	Ru	C3	C2	118.30(15)	Ru	P1	C11	C12	-57.71(16)
C4	Ru	C3	C8	-119.4(2)	Ru	P1	C11	C16	179.00(14)
C5	Ru	C3	C2	79.78(11)	C21	P1	C11	C12	164.09(15)
C5	Ru	C3	C4	-38.52(10)	C21	P1	C11	C16	40.80(17)
C5	Ru	C3	C8	-158.0(2)	Ru	P1	C21	C22	-79.11(13)
Cl	Ru	C4	C3	50.73(16)	Ru	P1	C21	C26	148.99(11)
Cl	Ru	C4	C5	-64.81(15)	C11	P1	C21	C22	57.36(15)
Cl	Ru	C4	C9	174.07(14)	C11	P1	C21	C26	-74.54(14)
P1	Ru	C4	C3	-175.81(9)	Ru	P2	C31	C32	-12.24(15)
P1	Ru	C4	C5	68.66(10)	Ru	P2	C31	C36	168.13(12)
P1	Ru	C4	C9	-52.5(2)	C41	P2	C31	C32	-141.28(14)
P2	Ru	C4	C3	-74.69(10)	C41	P2	C31	C36	39.08(15)
P2	Ru	C4	C5	169.77(9)	C51	P2	C31	C32	114.24(14)
P2	Ru	C4	C9	48.7(2)	C51	P2	C31	C36	-65.40(15)
C1	Ru	C4	C3	78.90(11)	Ru	P2	C41	C42	-58.21(14)
C1	Ru	C4	C5	-36.63(10)	Ru	P2	C41	C46	121.28(13)
C1	Ru	C4	C9	-157.8(2)	C31	P2	C41	C42	68.24(14)
C2	Ru	C4	C3	36.48(10)	C31	P2	C41	C46	-112.27(15)
C2	Ru	C4	C5	-79.05(11)	C51	P2	C41	C42	172.21(13)
C2	Ru	C4	C9	159.8(2)	C51	P2	C41	C46	-8.30(16)
C3	Ru	C4	C5	-115.53(15)	Ru	P2	C51	C52	120.98(13)
C3	Ru	C4	C9	123.3(2)	Ru	P2	C51	C56	-55.92(14)
C5	Ru	C4	C3	115.53(15)	C31	P2	C51	C52	-5.73(16)
C5	Ru	C4	C9	-121.1(2)	C31	P2	C51	C56	177.37(13)
Cl	Ru	C5	C1	31.82(12)	C41	P2	C51	C52	-106.92(15)
Cl	Ru	C5	C4	150.30(8)	C41	P2	C51	C56	76.19(14)
Cl	Ru	C5	C10	-91.94(18)	Ru	C1	C2	C3	62.74(12)
P1	Ru	C5	C1	120.43(10)	Ru	C1	C2	C7	-124.75(18)
P1	Ru	C5	C4	-121.09(10)	C5	C1	C2	Ru	-62.75(11)
P1	Ru	C5	C10	-3.33(18)	C5	C1	C2	C3	-0.01(19)
P2	Ru	C5	C1	-135.35(10)	C5	C1	C2	C7	172.50(16)
P2	Ru	C5	C4	-16.87(14)	C6	C1	C2	Ru	124.76(17)
P2	Ru	C5	C10	100.89(18)	C6	C1	C2	C3	-172.50(16)
C1	Ru	C5	C4	118.48(15)	C6	C1	C2	C7	0.0(3)
C1	Ru	C5	C10	-123.8(2)	Ru	C1	C5	C4	-60.94(11)
C2	Ru	C5	C1	-38.06(11)	Ru	C1	C5	C10	129.61(18)
C2	Ru	C5	C4	80.41(11)	C2	C1	C5	Ru	62.63(11)
C2	Ru	C5	C10	-161.8(2)	C2	C1	C5	C4	1.69(18)
C3	Ru	C5	C1	-79.93(12)	C2	C1	C5	C10	-167.76(16)
C3	Ru	C5	C4	38.54(10)	C6	C1	C5	Ru	-125.36(19)

Appendix A X-ray Crystallographic structure report for Ru(η^5-Cp)Cl(PCy_2H)(PPh_3) (**2a**)*

C6	C1	C5	C4	173.70(17)	C14	C15	C16	C11	-56.2(3)
C6	C1	C5	C10	4.3(3)	P1	C21	C22	C23	171.90(14)
Ru	C2	C3	C4	60.52(11)	C26	C21	C22	C23	-54.4(2)
Ru	C2	C3	C8	-128.86(18)	P1	C21	C26	C25	-172.59(13)
C1	C2	C3	Ru	-62.18(12)	C22	C21	C26	C25	54.5(2)
C1	C2	C3	C4	-1.66(19)	C21	C22	C23	C24	55.3(2)
C1	C2	C3	C8	168.96(17)	C22	C23	C24	C25	-57.1(2)
C7	C2	C3	Ru	125.74(19)	C23	C24	C25	C26	57.5(2)
C7	C2	C3	C4	-173.75(17)	C24	C25	C26	C21	-55.8(2)
C7	C2	C3	C8	-3.1(3)	P2	C31	C32	C33	-179.61(13)
Ru	C3	C4	C5	63.89(11)	C36	C31	C32	C33	0.0(2)
Ru	C3	C4	C9	-134.32(17)	P2	C31	C36	C35	179.41(14)
C2	C3	C4	Ru	-61.21(12)	C32	C31	C36	C35	-0.2(3)
C2	C3	C4	C5	2.68(18)	C31	C32	C33	C34	0.0(3)
C2	C3	C4	C9	164.47(16)	C32	C33	C34	C35	0.1(3)
C8	C3	C4	Ru	128.01(17)	C33	C34	C35	C36	-0.3(3)
C8	C3	C4	C5	-168.10(16)	C34	C35	C36	C31	0.3(3)
C8	C3	C4	C9	-6.3(3)	P2	C41	C42	C43	178.23(13)
Ru	C4	C5	C1	61.48(11)	C46	C41	C42	C43	-1.3(2)
Ru	C4	C5	C10	-128.57(16)	P2	C41	C46	C45	-177.95(13)
C3	C4	C5	Ru	-64.18(11)	C42	C41	C46	C45	1.5(2)
C3	C4	C5	C1	-2.70(18)	C41	C42	C43	C44	0.2(3)
C3	C4	C5	C10	167.25(15)	C42	C43	C44	C45	0.7(3)
C9	C4	C5	Ru	133.75(17)	C43	C44	C45	C46	-0.4(3)
C9	C4	C5	C1	-164.77(16)	C44	C45	C46	C41	-0.7(3)
C9	C4	C5	C10	5.2(3)	P2	C51	C52	C53	-176.09(15)
P1	C11	C12	C13	173.0(2)	C56	C51	C52	C53	0.8(3)
C16	C11	C12	C13	-58.2(3)	P2	C51	C56	C55	177.51(15)
P1	C11	C16	C15	-179.47(16)	C52	C51	C56	C55	0.4(3)
C12	C11	C16	C15	57.1(2)	C51	C52	C53	C54	-1.5(3)
C11	C12	C13	C14	56.5(3)	C52	C53	C54	C55	0.9(3)
C12	C13	C14	C15	-52.3(3)	C53	C54	C55	C56	0.4(3)
C13	C14	C15	C16	52.8(3)	C54	C55	C56	C51	-1.1(3)

Appendix A X-ray Crystallographic structure report for Ru(η^5-Cp)Cl(PCy_2H)(PPh_3) (**2a**)*

Table A.6 Least-Squares Planes

Plane	Coefficients[a]				Defining Atoms with Deviations			
(Å)[b]								
1	-8.430(9)	3.211(15)	12.965(7)	6.560(4)				
					C1	-0.0051(10)	C2	-0.0049(11)
					C3	0.0128(10)	C4	-0.0158(10)
					C5	0.0130(10)		
					Ru	-1.8717(8)	C6	0.141(3)
					C7	0.143(3)	C8	0.250(3)
					C9	0.317(3)	C10	0.273(3)

Distance: $Ru–C_{cent}$ = 1.872 Å (C_{cent} = C1–C2–C3–C4–C5 centroid)

Angles: C_{cent}–Ru–Cl = 120.6º, C_{cent}–Ru–P1 = 129.8º, C_{cent}–Ru–P2 = 127.4º

[a]Coefficients are for the form $ax+by+cz = d$ where x, y and z are crystallographic coordinates.

[b]Underlined atoms were not included in the definition of the plane.

Table A.7 Anisotropic Displacement Parameters (U_{ij}, Å^2)

Atom	U_{11}	U_{22}	U_{33}	U_{23}	U_{13}	U_{12}
Ru	0.01761(7)	0.02295(7)	0.02240(7)	-0.00341(4)	0.00437(5)	0.00050(4)
Cl	0.0264(2)	0.0324(2)	0.02755(19)	0.00021(16)	-0.00072(16)	0.00164(16)
P1	0.0211(2)	0.02181(19)	0.02515(19)	-0.00142(15)	0.00396(15)	-0.00026(15)
P2	0.01872(19)	0.02232(19)	0.02116(18)	-0.00201(14)	0.00463(14)	-0.00010(15)
C1	0.0242(8)	0.0347(9)	0.0294(8)	-0.0079(7)	0.0085(7)	0.0075(7)
C2	0.0218(8)	0.0432(10)	0.0329(9)	-0.0118(7)	0.0114(7)	-0.0016(7)
C3	0.0302(9)	0.0343(9)	0.0325(9)	-0.0054(7)	0.0167(7)	-0.0025(7)
C4	0.0258(8)	0.0340(9)	0.0238(8)	-0.0041(6)	0.0097(7)	0.0036(7)
C5	0.0244(8)	0.0321(9)	0.0268(8)	-0.0077(7)	0.0084(6)	0.0017(7)
C6	0.0420(11)	0.0505(12)	0.0397(10)	-0.0077(9)	0.0027(9)	0.0223(10)
C7	0.0227(9)	0.0669(15)	0.0495(12)	-0.0202(11)	0.0103(8)	-0.0032(9)
C8	0.0516(13)	0.0403(11)	0.0469(11)	-0.0029(9)	0.0278(10)	-0.0080(9)
C9	0.0416(11)	0.0491(11)	0.0267(9)	0.0001(8)	0.0071(8)	0.0106(9)
C10	0.0361(10)	0.0365(10)	0.0362(9)	-0.0124(8)	0.0094(8)	-0.0013(8)
C11	0.0320(9)	0.0224(8)	0.0308(8)	-0.0014(6)	0.0051(7)	0.0014(7)
C12	0.0292(10)	0.0278(10)	0.0927(19)	0.0034(11)	-0.0070(11)	0.0028(8)
C13	0.0347(12)	0.0328(11)	0.128(3)	0.0076(14)	0.0023(14)	0.0094(9)
C14	0.0498(13)	0.0273(9)	0.0531(12)	0.0047(9)	-0.0024(10)	0.0073(9)
C15	0.0410(12)	0.0265(10)	0.0825(17)	0.0127(10)	-0.0061(11)	-0.0037(8)
C16	0.0299(10)	0.0297(10)	0.0759(16)	0.0151(10)	0.0007(10)	0.0013(8)
C21	0.0210(8)	0.0244(8)	0.0287(8)	-0.0003(6)	0.0042(6)	0.0003(6)
C22	0.0280(9)	0.0402(10)	0.0302(9)	-0.0053(7)	0.0011(7)	0.0063(7)
C23	0.0343(10)	0.0500(12)	0.0328(9)	-0.0038(9)	-0.0039(8)	0.0118(9)
C24	0.0247(9)	0.0436(11)	0.0524(12)	-0.0038(9)	-0.0028(8)	0.0023(8)
C25	0.0245(9)	0.0449(11)	0.0437(11)	0.0013(9)	0.0097(8)	0.0039(8)
C26	0.0238(8)	0.0423(10)	0.0339(9)	0.0015(8)	0.0075(7)	-0.0011(7)
C31	0.0240(8)	0.0233(7)	0.0224(7)	-0.0005(6)	0.0041(6)	-0.0027(6)
C32	0.0250(8)	0.0258(8)	0.0277(8)	-0.0011(6)	0.0056(6)	-0.0007(6)
C33	0.0240(8)	0.0318(9)	0.0344(9)	0.0003(7)	0.0031(7)	-0.0038(7)
C34	0.0336(9)	0.0317(9)	0.0313(9)	-0.0053(7)	0.0035(7)	-0.0117(7)
C35	0.0366(10)	0.0288(9)	0.0337(9)	-0.0094(7)	0.0110(8)	-0.0051(7)
C36	0.0268(8)	0.0288(8)	0.0305(8)	-0.0046(7)	0.0077(7)	-0.0018(7)
C41	0.0226(8)	0.0214(7)	0.0246(7)	-0.0030(6)	0.0086(6)	-0.0021(6)
C42	0.0263(8)	0.0259(8)	0.0274(8)	-0.0009(6)	0.0062(7)	0.0010(6)
C43	0.0358(10)	0.0300(9)	0.0264(8)	0.0000(6)	0.0108(7)	-0.0023(7)
C44	0.0303(9)	0.0339(9)	0.0324(9)	-0.0063(7)	0.0156(7)	-0.0050(7)
C45	0.0227(8)	0.0366(9)	0.0345(9)	-0.0067(7)	0.0084(7)	0.0006(7)
C46	0.0255(8)	0.0299(8)	0.0275(8)	-0.0024(7)	0.0054(7)	0.0020(7)
C51	0.0228(8)	0.0267(8)	0.0226(7)	-0.0011(6)	0.0066(6)	0.0019(6)
C52	0.0349(9)	0.0290(9)	0.0312(9)	0.0017(7)	0.0068(7)	-0.0010(7)
C53	0.0538(13)	0.0327(10)	0.0392(10)	0.0087(8)	0.0125(9)	0.0037(9)
C54	0.0535(13)	0.0456(11)	0.0297(9)	0.0096(8)	0.0048(9)	0.0141(10)

C55	0.0381(11)	0.0522(12)	0.0274(9)	0.0000(8)	-0.0021(8)	0.0045(9)
C56	0.0290(9)	0.0348(9)	0.0276(8)	0.0000(7)	0.0041(7)	-0.0012(7)

The form of the anisotropic displacement parameter is:

$\exp[-2\pi^2(h^2a^{*2}U_{11} + k^2b^{*2}U_{22} + l^2c^{*2}U_{33} + 2klb^*c^*U_{23} + 2hla^*c^*U_{13} + 2hka^*b^*U_{12})]$

Table A.8 Derived Atomic Coordinates and Displacement Parameters for Hydrogen Atoms

Atom	*x*	*y*	*z*	U_{eq}, Å^2
H6A	-0.2615	0.4201	0.1903	0.053
H6B	-0.1991	0.4769	0.2603	0.053
H6C	-0.3007	0.4390	0.2814	0.053
H7A	-0.3721	0.2932	0.2679	0.055
H7B	-0.3291	0.2107	0.2499	0.055
H7C	-0.3236	0.2781	0.1805	0.055
H8A	-0.2077	0.1626	0.4240	0.053
H8B	-0.1013	0.1387	0.3986	0.053
H8C	-0.2006	0.1340	0.3258	0.053
H9A	0.0724	0.2958	0.4643	0.047
H9B	0.0181	0.2156	0.4717	0.047
H9C	-0.0159	0.2883	0.5225	0.047
H10A	-0.0567	0.4803	0.3616	0.043
H10B	0.0382	0.4280	0.3977	0.043
H10C	-0.0468	0.4426	0.4579	0.043
H11	0.0386	0.4819	0.2549	0.034
H12A	-0.1057	0.4548	0.1500	0.062
H12B	-0.0426	0.4690	0.0712	0.062
H13A	-0.1353	0.5795	0.0908	0.080
H13B	-0.0873	0.5831	0.1935	0.080
H14A	0.0169	0.6096	0.0481	0.053
H14B	-0.0042	0.6715	0.1199	0.053
H15A	0.1055	0.6125	0.2295	0.062
H15B	0.1631	0.6256	0.1470	0.062
H16A	0.1422	0.4963	0.1060	0.055
H16B	0.1955	0.5010	0.2074	0.055
H21	0.1925	0.2792	0.2557	0.030
H22A	0.1774	0.3555	0.3775	0.040
H22B	0.2305	0.4247	0.3347	0.040
H23A	0.3529	0.3621	0.4371	0.048
H23B	0.3252	0.2820	0.3895	0.048
H24A	0.4168	0.4071	0.3120	0.049
H24B	0.4728	0.3294	0.3448	0.049
H25A	0.3695	0.2610	0.2333	0.045
H25B	0.4243	0.3283	0.1888	0.045
H26A	0.2495	0.3223	0.1277	0.040
H26B	0.2774	0.4033	0.1734	0.040
H32	-0.2230	0.1718	0.1554	0.031
H33	-0.3396	0.0919	0.0717	0.036
H34	-0.2855	-0.0155	0.0034	0.039

H35	-0.1141	-0.0435	0.0191	0.039
H36	0.0030	0.0365	0.1020	0.034
H42	0.0067	0.2308	0.0316	0.032
H43	0.1289	0.2344	-0.0604	0.036
H44	0.2866	0.1804	-0.0151	0.037
H45	0.3217	0.1204	0.1226	0.037
H46	0.1996	0.1155	0.2154	0.033
H52	-0.0431	0.0197	0.2655	0.038
H53	0.0199	-0.0515	0.3907	0.050
H54	0.1488	-0.0035	0.4956	0.052
H55	0.2122	0.1178	0.4774	0.048
H56	0.1458	0.1914	0.3552	0.037

Appendix B X-ray Crystallographic structure report for Ru(η^5-Cp*)Cl(PEt$_2$H)(PPh$_3$) (2b)

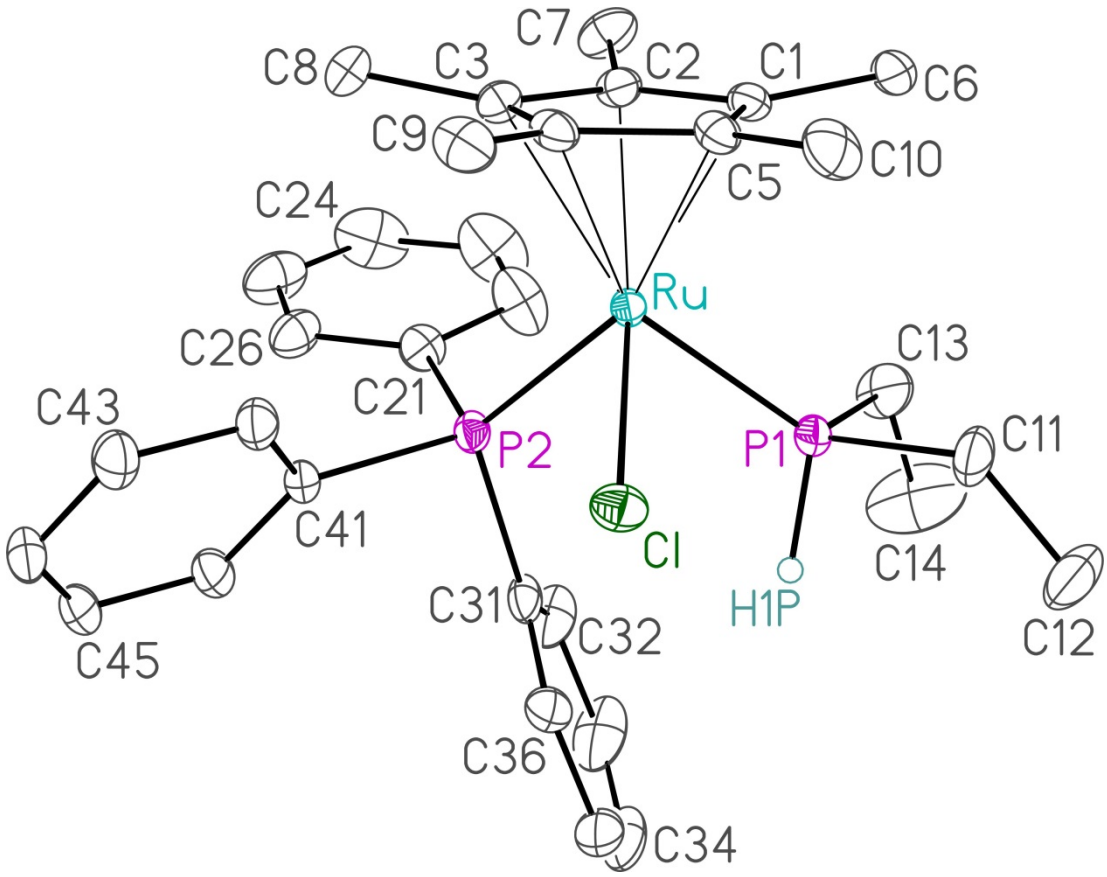

Figure B.1 Perspective view of the Ru(η^5-Cp*)Cl(PEt$_2$H)(PPh$_3$) (**2b**) molecule showing the atom labelling scheme. Non-hydrogen atoms are represented by Gaussian ellipsoids at the 30% probability level. The hydrogen atom attached to P1 is shown with an arbitrarily small thermal parameter; all other hydrogens are not shown.

This structure determination, as well as that of complex **2b** in Appendix A, was carried out by Dr. Robert McDonald at the X-ray Crystallography Laboratory, Department of Chemistry, University of Alberta, Edmonton, Alberta, Canada T6G 2G2. E-mail: Bob.McDonald@ualberta.ca. Phone: 1-(780)-492-2485.

Appendix B X-ray Crystallographic structure report for Ru(η^5-Cp)Cl(PEt_2H)(PPh_3) (**2b**)*

Table B.1 Crystallographic experimental details

A. Crystal Data

formula	$C_{32}H_{41}ClP_2Ru$
formula weight	624.11
crystal dimensions (mm)	0.36 × 0.25 × 0.24
crystal system	orthorhombic
space group	*Pbca* (No. 61)
unit cell parameters[a]	
a (Å)	17.7339 (8)
b (Å)	15.8452 (8)
c (Å)	21.8712 (10)
V (Å^3)	6145.7 (5)
Z	8
ρ_{calcd} (g cm^{-3})	1.349
μ (mm^{-1})	0.720

B. Data Collection and Refinement Conditions

diffractometer	Bruker PLATFORM/APEX II CCD[b]
radiation (λ [Å]) (0.71073)	graphite-monochromated Mo Kα
temperature (°C)	–100
scan type	ω scans (0.3°) (15 s exposures)
data collection 2θ limit (deg)	56.75
total data collected	187606 (-23 ≤ *h* ≤ 23, -21 ≤ *k* ≤ 21, -29 ≤ *l* ≤ 29)
independent reflections	12093 (R_{int} = 0.0377)
number of observed reflections (*NO*)	9868 [$F_o^2 \geq 2\sigma(F_o^2)$]
structure solution method	Patterson/structure expansion (*DIRDIF–2008*[c])
refinement method (*SHELXL–2014*[d])	full-matrix least-squares on F^2
absorption correction method	multi-scan (*TWINABS*)
range of transmission factors	0.8800–0.6316
data/restraints/parameters	12093 / 0 / 335
goodness-of-fit (*S*)[e] [all data]	1.094
final *R* indices[f]	
R_1 [$F_o^2 \geq 2\sigma(F_o^2)$]	0.0426
wR_2 [all data]	0.1326
largest difference peak and hole	1.182 and –0.432 e Å^{-3}

[a]Obtained from least-squares refinement of 9042 reflections with 4.38° < 2θ < 56.34°.

[b]Programs for diffractometer operation, data collection, data reduction and absorption correction were those supplied by Bruker. The crystal used for data collection was found to display non-merohedral twinning. Both components of the twin

were indexed with the program *CELL_NOW* (Bruker AXS Inc., Madison, WI, 2004). The second twin component can be related to the first component by a 177.3º rotation about the [0 1 0] axis in both real space and reciprocal space. Integrated intensities for the reflections from the two components were written into a *SHELXL-2014* HKLF 5 reflection file with the data integration program *SAINT* (version 8.34A), using all reflection data (exactly overlapped, partially overlapped and non-overlapped). The refined value of the twin fraction (*SHELXL-2014* BASF parameter) was 0.0723(6).

[c]Beurskens, P. T.; Beurskens, G.; de Gelder, R.; Smits, J. M. M.; Garcia-Granda, S.; Gould, R. O. (2008). The *DIRDIF-2008* program system. Crystallography Laboratory, Radboud University Nijmegen, The Netherlands.

[d]Sheldrick, G. M. *Acta Crystallogr.* **2015**, *C71*, 3–8.

[e]$S = [\Sigma w(F_o^2 - F_c^2)^2/(n - p)]^{1/2}$ (n = number of data; p = number of parameters varied; $w = [\sigma^2(F_o^2) + (0.0728P)^2 + 3.6332P]^{-1}$ where $P = [\mathrm{Max}(F_o^2, 0) + 2F_c^2]/3$).

[f]$R_1 = \Sigma||F_o| - |F_c||/\Sigma|F_o|$; $wR_2 = [\Sigma w(F_o^2 - F_c^2)^2/\Sigma w(F_o^4)]^{1/2}$.

Table B.2 Atomic coordinates and equivalent isotropic displacement parameters

Atom	*x*	*y*	*z*	U_{eq}, Å^2
Ru	0.22569(2)	0.19380(2)	0.18120(2)	0.02105(9)*
Cl	0.26329(5)	0.05050(5)	0.15333(4)	0.0364(2)*
P1	0.31331(4)	0.23175(6)	0.10927(4)	0.02939(19)*
P2	0.13141(4)	0.18634(5)	0.10872(4)	0.02553(17)*
C1	0.27205(18)	0.2776(2)	0.25236(15)	0.0289(6)*
C2	0.19366(19)	0.2951(2)	0.24556(15)	0.0295(7)*
C3	0.15292(19)	0.2197(2)	0.26320(15)	0.0305(7)*
C4	0.20591(19)	0.1569(2)	0.27894(14)	0.0296(7)*
C5	0.28080(18)	0.1920(2)	0.27167(15)	0.0287(7)*
C6	0.3339(2)	0.3422(2)	0.24787(18)	0.0395(8)*
C7	0.1593(2)	0.3809(2)	0.23778(19)	0.0459(9)*
C8	0.0692(2)	0.2169(3)	0.27128(18)	0.0419(9)*
C9	0.1912(2)	0.0709(2)	0.30450(17)	0.0415(8)*
C10	0.3525(2)	0.1469(3)	0.28856(19)	0.0454(9)*
C11	0.4099(2)	0.1971(3)	0.1280(2)	0.0528(12)*
C12	0.4644(3)	0.1896(4)	0.0771(2)	0.0662(15)*
C13	0.3253(3)	0.3412(3)	0.0838(2)	0.0560(12)*
C14	0.3395(5)	0.3545(4)	0.0191(3)	0.110(3)*
C21	0.0678(2)	0.2778(2)	0.10426(16)	0.0357(7)*
C22	0.1001(3)	0.3574(3)	0.0989(2)	0.0595(13)*
C23	0.0573(4)	0.4297(3)	0.0927(3)	0.0803(18)*
C24	-0.0205(3)	0.4233(4)	0.0932(3)	0.0775(17)*
C25	-0.0539(3)	0.3461(4)	0.0993(2)	0.0635(13)*

Appendix B X-ray Crystallographic structure report for Ru(η^5-Cp)Cl(PEt_2H)(PPh_3) (**2b**)*

C26	-0.0103(2)	0.2724(3)	0.10503(18)	0.0443(9)*
C31	0.15859(18)	0.1728(3)	0.02771(15)	0.0350(8)*
C32	0.1495(2)	0.2346(3)	-0.01642(19)	0.0538(11)*
C33	0.1782(3)	0.2224(5)	-0.0754(2)	0.0732(17)*
C34	0.2149(3)	0.1496(5)	-0.0904(2)	0.0684(17)*
C35	0.2235(2)	0.0875(4)	-0.0476(2)	0.0581(13)*
C36	0.1957(2)	0.0987(3)	0.01141(17)	0.0429(9)*
C41	0.06653(16)	0.0961(2)	0.11678(15)	0.0289(6)*
C42	0.06893(18)	0.0476(2)	0.16982(17)	0.0345(7)*
C43	0.0198(2)	-0.0204(2)	0.17780(18)	0.0409(8)*
C44	-0.0313(2)	-0.0404(3)	0.1326(2)	0.0451(9)*
C45	-0.0337(2)	0.0069(3)	0.07923(18)	0.0471(10)*
C46	0.01478(19)	0.0745(3)	0.07118(17)	0.0405(8)*
H1P	0.309(2)	0.193(2)	0.0561(19)	0.033(10)

Anisotropically-refined atoms are marked with an asterisk (*). The form of the anisotropic displacement parameter is: $\exp[-2\pi^2(h^2a^{*2}U_{11} + k^2b^{*2}U_{22} + l^2c^{*2}U_{33} + 2klb^*c^*U_{23} + 2hla^*c^*U_{13} + 2hka^*b^*U_{12})]$.

Table B.3 Selected interatomic distances (Å)

Atom1	Atom2	Distance	Atom1	Atom2	Distance
Ru	Cl	2.4437(9)	C4	C9	1.496(5)
Ru	P1	2.2915(8)	C5	C10	1.504(5)
Ru	P2	2.3071(8)	C11	C12	1.479(6)
Ru	C1	2.205(3)	C13	C14	1.452(7)
Ru	C2	2.209(3)	C21	C22	1.390(6)
Ru	C3	2.247(3)	C21	C26	1.388(5)
Ru	C4	2.244(3)	C22	C23	1.382(6)
Ru	C5	2.207(3)	C23	C24	1.385(8)
P1	C11	1.845(4)	C24	C25	1.365(8)
P1	C13	1.834(4)	C25	C26	1.406(6)
P1	H1P	1.32(4)	C31	C32	1.384(6)
P2	C21	1.840(4)	C31	C36	1.393(6)
P2	C31	1.849(4)	C32	C33	1.401(7)
P2	C41	1.843(3)	C33	C34	1.363(9)
C1	C2	1.425(5)	C34	C35	1.367(8)
C1	C5	1.429(5)	C35	C36	1.393(5)
C1	C6	1.502(4)	C41	C42	1.392(5)
C2	C3	1.448(5)	C41	C46	1.398(4)
C2	C7	1.500(5)	C42	C43	1.396(5)
C3	C4	1.411(5)	C43	C44	1.379(5)
C3	C8	1.496(5)	C44	C45	1.388(6)
C4	C5	1.448(4)	C45	C46	1.384(5)

Appendix B X-ray Crystallographic structure report for Ru(η^5-Cp)Cl(PEt_2H)(PPh_3) (**2b**)*

Table B.4 Selected interatomic angles (deg)

Atom1	Atom2	Atom3	Angle	Atom1	Atom2	Atom3	Angle
Cl	Ru	P1	83.54(3)	C2	C1	C5	108.7(3)
Cl	Ru	P2	88.78(3)	C2	C1	C6	125.0(3)
Cl	Ru	C1	129.35(9)	C5	C1	C6	125.9(3)
Cl	Ru	C2	154.70(9)	Ru	C2	C1	71.02(18)
Cl	Ru	C3	121.71(9)	Ru	C2	C3	72.48(18)
Cl	Ru	C4	92.20(9)	Ru	C2	C7	133.7(3)
Cl	Ru	C5	95.21(9)	C1	C2	C3	107.4(3)
P1	Ru	P2	91.90(3)	C1	C2	C7	125.7(3)
P1	Ru	C1	94.23(8)	C3	C2	C7	125.1(3)
P1	Ru	C2	114.92(9)	Ru	C3	C2	69.61(18)
P1	Ru	C3	152.79(9)	Ru	C3	C4	71.55(19)
P1	Ru	C4	145.94(9)	Ru	C3	C8	131.2(3)
P1	Ru	C5	108.58(9)	C2	C3	C4	108.3(3)
P2	Ru	C1	141.81(9)	C2	C3	C8	123.5(3)
P2	Ru	C2	106.78(9)	C4	C3	C8	127.7(3)
P2	Ru	C3	98.14(9)	Ru	C4	C3	71.82(18)
P2	Ru	C4	121.87(9)	Ru	C4	C5	69.64(18)
P2	Ru	C5	159.43(9)	Ru	C4	C9	128.4(2)
C1	Ru	C2	37.67(12)	C3	C4	C5	108.3(3)
C1	Ru	C3	62.66(12)	C3	C4	C9	128.1(3)
C1	Ru	C4	62.79(12)	C5	C4	C9	123.4(3)
C1	Ru	C5	37.81(12)	Ru	C5	C1	71.03(18)
C2	Ru	C3	37.91(12)	Ru	C5	C4	72.39(18)
C2	Ru	C4	62.72(12)	Ru	C5	C10	126.9(3)
C2	Ru	C5	63.38(13)	C1	C5	C4	107.3(3)
C3	Ru	C4	36.63(13)	C1	C5	C10	128.0(3)
C3	Ru	C5	62.69(12)	C4	C5	C10	124.4(3)
C4	Ru	C5	37.97(11)	P1	C11	C12	117.6(3)
Ru	P1	C11	113.53(15)	P1	C13	C14	116.9(4)
Ru	P1	C13	122.37(15)	P2	C21	C22	117.7(3)
Ru	P1	H1P	116.2(17)	P2	C21	C26	124.3(3)
C11	P1	C13	104.0(2)	C22	C21	C26	118.0(4)
C11	P1	H1P	96.3(17)	C21	C22	C23	122.3(5)
C13	P1	H1P	100.6(16)	C22	C23	C24	119.1(5)
Ru	P2	C21	116.15(12)	C23	C24	C25	119.9(5)
Ru	P2	C31	118.39(10)	C24	C25	C26	121.0(5)
Ru	P2	C41	115.24(11)	C21	C26	C25	119.7(4)
C21	P2	C31	101.58(17)	P2	C31	C32	123.7(3)
C21	P2	C41	103.47(16)	P2	C31	C36	117.8(3)
C31	P2	C41	99.46(15)	C32	C31	C36	118.2(4)
Ru	C1	C2	71.31(18)	C31	C32	C33	120.2(5)
Ru	C1	C5	71.17(18)	C32	C33	C34	120.7(5)
Ru	C1	C6	129.5(2)	C33	C34	C35	119.9(4)

Appendix B X-ray Crystallographic structure report for Ru(η^5-Cp)Cl(PEt_2H)(PPh_3) (**2b**)*

C34	C35	C36	120.3(5)	C41	C42	C43	120.8(3)
C31	C36	C35	120.7(4)	C42	C43	C44	119.9(4)
P2	C41	C42	119.3(2)	C43	C44	C45	119.9(3)
P2	C41	C46	122.1(3)	C44	C45	C46	120.4(3)
C42	C41	C46	118.6(3)	C41	C46	C45	120.5(4)

Appendix B X-ray Crystallographic structure report for Ru(η^5-Cp)Cl(PEt_2H)(PPh_3) (**2b**)*

Table B.5 Torsional angles (deg)

Atom1	Atom2	Atom3	Atom4	Angle	Atom1	Atom2	Atom3	Atom4	Angle
Cl	Ru	P1	C11	-61.86(18)	C2	Ru	P1	C11	100.1(2)
Cl	Ru	P1	C13	172.2(2)	C2	Ru	P1	C13	-25.9(2)
P2	Ru	P1	C11	-150.42(18)	C3	Ru	P1	C11	97.6(3)
P2	Ru	P1	C13	83.6(2)	C3	Ru	P1	C13	-28.4(3)
C1	Ru	P1	C11	67.3(2)	C4	Ru	P1	C11	22.5(2)
C1	Ru	P1	C13	-58.7(2)	C4	Ru	P1	C13	-103.5(3)
C2	Ru	P1	C11	100.1(2)	C5	Ru	P1	C11	31.5(2)
C2	Ru	P1	C13	-25.9(2)	C5	Ru	P1	C13	-94.5(2)
C3	Ru	P1	C11	97.6(3)	Cl	Ru	P2	C21	176.34(13)
C3	Ru	P1	C13	-28.4(3)	Cl	Ru	P2	C31	-62.36(15)
C4	Ru	P1	C11	22.5(2)	Cl	Ru	P2	C41	55.12(12)
C4	Ru	P1	C13	-103.5(3)	P1	Ru	P2	C21	-100.17(13)
C5	Ru	P1	C11	31.5(2)	P1	Ru	P2	C31	21.14(15)
C5	Ru	P1	C13	-94.5(2)	P1	Ru	P2	C41	138.61(12)
Cl	Ru	P2	C21	176.34(13)	C1	Ru	P2	C21	-0.9(2)
Cl	Ru	P2	C31	-62.36(15)	C1	Ru	P2	C31	120.4(2)
Cl	Ru	P2	C41	55.12(12)	C1	Ru	P2	C41	-122.10(18)
P1	Ru	P2	C21	-100.17(13)	C2	Ru	P2	C21	16.60(16)
P1	Ru	P2	C31	21.14(15)	C2	Ru	P2	C31	137.90(17)
P1	Ru	P2	C41	138.61(12)	C2	Ru	P2	C41	-104.62(15)
C1	Ru	P2	C21	-0.9(2)	C3	Ru	P2	C21	54.47(16)
C1	Ru	P2	C31	120.4(2)	C3	Ru	P2	C31	175.77(17)
C1	Ru	P2	C41	-122.10(18)	C3	Ru	P2	C41	-66.75(15)
C2	Ru	P2	C21	16.60(16)	C4	Ru	P2	C21	84.50(17)
C2	Ru	P2	C31	137.90(17)	C4	Ru	P2	C31	-154.19(18)
C2	Ru	P2	C41	-104.62(15)	C4	Ru	P2	C41	-36.72(16)
C3	Ru	P2	C21	54.47(16)	C5	Ru	P2	C21	74.7(3)
C3	Ru	P2	C31	175.77(17)	C5	Ru	P2	C31	-164.0(3)
C3	Ru	P2	C41	-66.75(15)	C5	Ru	P2	C41	-46.5(3)
C4	Ru	P2	C21	84.50(17)	Cl	Ru	C1	C2	-148.34(16)
C4	Ru	P2	C31	-154.19(18)	Cl	Ru	C1	C5	-30.1(2)
C4	Ru	P2	C41	-36.72(16)	Cl	Ru	C1	C6	91.3(3)
C5	Ru	P2	C21	74.7(3)	P1	Ru	C1	C2	126.55(18)
C5	Ru	P2	C31	-164.0(3)	P1	Ru	C1	C5	-115.21(18)
C5	Ru	P2	C41	-46.5(3)	Cl	Ru	P1	C11	-61.86(18)
Cl	Ru	C1	C2	-148.34(16)	Cl	Ru	P1	C13	172.2(2)
Cl	Ru	C1	C5	-30.1(2)	P2	Ru	P1	C11	-150.42(18)
Cl	Ru	C1	C6	91.3(3)	P2	Ru	P1	C13	83.6(2)
P1	Ru	C1	C2	126.55(18)	C1	Ru	P1	C11	67.3(2)
P1	Ru	C1	C5	-115.21(18)	C1	Ru	P1	C13	-58.7(2)
Cl	Ru	P1	C11	-61.86(18)	C2	Ru	P1	C11	100.1(2)
Cl	Ru	P1	C13	172.2(2)	C2	Ru	P1	C13	-25.9(2)
P2	Ru	P1	C11	-150.42(18)	C3	Ru	P1	C11	97.6(3)
P2	Ru	P1	C13	83.6(2)	C3	Ru	P1	C13	-28.4(3)
C1	Ru	P1	C11	67.3(2)	C4	Ru	P1	C11	22.5(2)
C1	Ru	P1	C13	-58.7(2)	C4	Ru	P1	C13	-103.5(3)

Appendix B X-ray Crystallographic structure report for Ru(η^5-Cp)Cl(PEt_2H)(PPh_3) (**2b**)*

C5	Ru	P1	C11	31.5(2)	Ru	P2	C31	C32	-111.1(3)
C5	Ru	P1	C13	-94.5(2)	Ru	P2	C31	C36	63.6(3)
Cl	Ru	P2	C21	176.34(13)	C21	P2	C31	C32	17.4(3)
Cl	Ru	P2	C31	-62.36(15)	C21	P2	C31	C36	-167.9(3)
Cl	Ru	P2	C41	55.12(12)	C41	P2	C31	C32	123.3(3)
P1	Ru	P2	C21	-100.17(13)	C41	P2	C31	C36	-61.9(3)
P1	Ru	P2	C31	21.14(15)	Ru	P2	C41	C42	10.9(3)
P1	Ru	P2	C41	138.61(12)	Ru	P2	C41	C46	-168.9(3)
C1	Ru	P2	C21	-0.9(2)	C21	P2	C41	C42	-116.9(3)
C1	Ru	P2	C31	120.4(2)	C21	P2	C41	C46	63.2(3)
C1	Ru	P2	C41	-122.10(18)	C31	P2	C41	C42	138.6(3)
C2	Ru	P2	C21	16.60(16)	C31	P2	C41	C46	-41.2(3)
C2	Ru	P2	C31	137.90(17)	Ru	C1	C2	C3	63.8(2)
C2	Ru	P2	C41	-104.62(15)	Ru	C1	C2	C7	-130.7(4)
C3	Ru	P2	C21	54.47(16)	C5	C1	C2	Ru	-61.7(2)
C3	Ru	P2	C31	175.77(17)	C5	C1	C2	C3	2.1(4)
C3	Ru	P2	C41	-66.75(15)	C5	C1	C2	C7	167.6(3)
C4	Ru	P2	C21	84.50(17)	C6	C1	C2	Ru	125.6(3)
C4	Ru	P2	C31	-154.19(18)	C6	C1	C2	C3	-170.6(3)
C4	Ru	P2	C41	-36.72(16)	C6	C1	C2	C7	-5.1(5)
C5	Ru	P2	C21	74.7(3)	Ru	C1	C5	C4	-63.8(2)
C5	Ru	P2	C31	-164.0(3)	Ru	C1	C5	C10	122.5(4)
C5	Ru	P2	C41	-46.5(3)	C2	C1	C5	Ru	61.8(2)
Cl	Ru	C1	C2	-148.34(16)	C2	C1	C5	C4	-2.0(4)
Cl	Ru	C1	C5	-30.1(2)	C2	C1	C5	C10	-175.7(3)
Cl	Ru	C1	C6	91.3(3)	C6	C1	C5	Ru	-125.6(3)
P1	Ru	C1	C2	126.55(18)	C6	C1	C5	C4	170.6(3)
P1	Ru	C1	C5	-115.21(18)	C6	C1	C5	C10	-3.1(6)
C1	Ru	C5	C4	116.0(3)	Ru	C2	C3	C4	61.4(2)
C1	Ru	C5	C10	-123.7(4)	Ru	C2	C3	C8	-126.6(3)
C2	Ru	C5	C1	-37.03(18)	C1	C2	C3	Ru	-62.9(2)
C2	Ru	C5	C4	79.0(2)	C1	C2	C3	C4	-1.4(4)
C2	Ru	C5	C10	-160.8(4)	C1	C2	C3	C8	170.5(3)
C3	Ru	C5	C1	-79.77(19)	C7	C2	C3	Ru	131.6(4)
C3	Ru	C5	C4	36.25(19)	C7	C2	C3	C4	-167.0(3)
C3	Ru	C5	C10	156.5(4)	C7	C2	C3	C8	4.9(6)
C4	Ru	C5	C1	-116.0(3)	Ru	C3	C4	C5	60.4(2)
C4	Ru	C5	C10	120.3(4)	Ru	C3	C4	C9	-124.9(3)
Ru	P1	C11	C12	158.1(4)	C2	C3	C4	Ru	-60.2(2)
C13	P1	C11	C12	-66.6(5)	C2	C3	C4	C5	0.2(4)
Ru	P1	C13	C14	-140.6(5)	C2	C3	C4	C9	174.9(3)
C11	P1	C13	C14	89.3(6)	C8	C3	C4	Ru	128.3(4)
Ru	P2	C21	C22	51.6(4)	C8	C3	C4	C5	-171.3(3)
Ru	P2	C21	C26	-129.3(3)	C8	C3	C4	C9	3.4(6)
C31	P2	C21	C22	-78.3(4)	Ru	C4	C5	C1	62.9(2)
C31	P2	C21	C26	100.8(3)	Ru	C4	C5	C10	-123.1(3)
C41	P2	C21	C22	178.9(3)	C3	C4	C5	Ru	-61.8(2)
C41	P2	C21	C26	-2.0(4)	C3	C4	C5	C1	1.1(4)

Appendix B X-ray Crystallographic structure report for Ru(η^5-Cp)Cl(PEt_2H)(PPh_3) (**2b**)*

C3	C4	C5	C10	175.1(3)	P2	C31	C36	C35	-174.5(3)
C9	C4	C5	Ru	123.2(3)	C32	C31	C36	C35	0.6(5)
C9	C4	C5	C1	-173.9(3)	C31	C32	C33	C34	0.6(7)
C9	C4	C5	C10	0.1(5)	C32	C33	C34	C35	0.3(7)
P2	C21	C22	C23	177.2(5)	C33	C34	C35	C36	-0.7(7)
C26	C21	C22	C23	-1.9(7)	C34	C35	C36	C31	0.3(6)
P2	C21	C26	C25	-177.9(3)	P2	C41	C42	C43	179.0(3)
C22	C21	C26	C25	1.2(6)	C46	C41	C42	C43	-1.1(5)
C21	C22	C23	C24	1.5(9)	P2	C41	C46	C45	-179.2(3)
C22	C23	C24	C25	-0.4(10)	C42	C41	C46	C45	1.0(5)
C23	C24	C25	C26	-0.3(9)	C41	C42	C43	C44	0.5(6)
C24	C25	C26	C21	-0.1(7)	C42	C43	C44	C45	0.3(6)
P2	C31	C32	C33	173.7(3)	C43	C44	C45	C46	-0.4(6)
C36	C31	C32	C33	-1.0(6)	C44	C45	C46	C41	-0.2(6)

Table B.6 Least-Squares Planes

Plane	Coefficients[a]			Defining Atoms with Deviations (Å)[b]			
1	-0.43(3)	4.89(2)	20.795(11)	6.478(7)			
				C1	0.012(2)	C2	-0.010(2)
				C3	0.005(2)	C4	0.002(2)
				C5	-0.009(2)		
				Ru	-1.8582(15)	C6	0.208(6)
				C7	0.262(6)	C8	0.195(6)
				C9	0.119(6)	C10	0.091(6)

[a]Coefficients are for the form $ax+by+cz = d$ where x, y and z are crystallographic coordinates.

[b]Underlined atoms were not included in the definition of the plane.

Table B.7 Anisotropic displacement parameters (U_{ij}, Å^2)

Atom	U_{11}	U_{22}	U_{33}	U_{23}	U_{13}	U_{12}
Ru	0.01968(12)	0.02312(14)	0.02036(14)	0.00036(8)	-0.00037(8)	-0.00225(8)
Cl	0.0430(4)	0.0285(4)	0.0378(5)	-0.0042(3)	-0.0019(3)	0.0052(3)
P1	0.0246(4)	0.0375(5)	0.0260(4)	-0.0034(3)	0.0028(3)	-0.0079(3)
P2	0.0217(3)	0.0317(4)	0.0232(4)	0.0026(3)	-0.0018(3)	-0.0036(3)
C1	0.0340(16)	0.0274(15)	0.0253(15)	-0.0055(13)	0.0027(12)	-0.0069(12)
C2	0.0345(16)	0.0276(16)	0.0264(16)	-0.0019(12)	0.0052(13)	-0.0009(13)
C3	0.0330(16)	0.0349(17)	0.0235(15)	0.0007(12)	0.0033(12)	-0.0028(13)
C4	0.0393(17)	0.0281(16)	0.0213(15)	-0.0002(12)	-0.0024(12)	-0.0066(14)
C5	0.0306(16)	0.0314(17)	0.0242(15)	-0.0016(12)	-0.0047(12)	-0.0017(13)
C6	0.0405(18)	0.0382(19)	0.0396(19)	-0.0109(16)	0.0077(15)	-0.0164(16)
C7	0.057(2)	0.0329(19)	0.048(2)	0.0026(16)	0.0165(18)	0.0105(17)
C8	0.0337(18)	0.053(2)	0.0396(19)	-0.0044(17)	0.0123(15)	-0.0054(16)
C9	0.060(2)	0.0355(19)	0.0290(18)	0.0082(14)	-0.0030(16)	-0.0101(17)
C10	0.0415(19)	0.054(2)	0.041(2)	0.0003(17)	-0.0149(17)	0.0023(18)
C11	0.0218(15)	0.093(4)	0.044(2)	-0.006(2)	0.0013(15)	-0.0031(18)
C12	0.040(2)	0.105(4)	0.053(3)	-0.001(3)	0.015(2)	0.018(2)
C13	0.069(3)	0.040(2)	0.060(3)	0.001(2)	0.024(2)	-0.019(2)
C14	0.190(8)	0.069(4)	0.072(4)	0.032(3)	0.046(5)	0.011(5)
C21	0.0338(17)	0.0397(19)	0.0336(17)	0.0037(15)	-0.0064(14)	0.0041(14)
C22	0.056(3)	0.042(2)	0.081(3)	0.013(2)	-0.028(2)	-0.001(2)
C23	0.091(4)	0.044(3)	0.106(5)	0.010(3)	-0.035(4)	0.011(3)
C24	0.087(4)	0.063(3)	0.083(4)	-0.004(3)	-0.026(3)	0.037(3)
C25	0.051(2)	0.084(4)	0.055(3)	-0.005(3)	-0.002(2)	0.030(3)
C26	0.0366(18)	0.056(2)	0.040(2)	0.0008(18)	0.0021(16)	0.0113(17)
C31	0.0233(14)	0.058(2)	0.0238(15)	0.0030(14)	-0.0042(12)	-0.0130(15)
C32	0.042(2)	0.081(3)	0.039(2)	0.020(2)	-0.0021(17)	-0.002(2)
C33	0.054(3)	0.131(5)	0.035(2)	0.036(3)	0.000(2)	-0.010(3)
C34	0.042(2)	0.135(5)	0.028(2)	-0.001(3)	0.0056(17)	-0.027(3)
C35	0.043(2)	0.094(4)	0.037(2)	-0.024(2)	0.0075(17)	-0.015(2)
C36	0.0405(18)	0.057(2)	0.0310(19)	-0.0096(16)	0.0005(15)	-0.0112(18)
C41	0.0233(13)	0.0342(17)	0.0294(15)	-0.0033(12)	0.0016(12)	-0.0073(12)
C42	0.0269(15)	0.0396(19)	0.0370(18)	0.0005(14)	-0.0008(13)	-0.0048(14)
C43	0.0378(18)	0.0366(19)	0.048(2)	0.0039(16)	0.0038(16)	-0.0072(15)
C44	0.0316(16)	0.043(2)	0.060(3)	-0.0105(18)	0.0092(17)	-0.0146(16)
C45	0.0347(17)	0.064(3)	0.043(2)	-0.0148(19)	-0.0017(16)	-0.0197(18)
C46	0.0339(17)	0.053(2)	0.0349(18)	-0.0049(16)	-0.0035(14)	-0.0119(16)

The form of the anisotropic displacement parameter is:

$\exp[-2\pi^2(h^2a^{*2}U_{11} + k^2b^{*2}U_{22} + l^2c^{*2}U_{33} + 2klb^*c^*U_{23} + 2hla^*c^*U_{13} + 2hka^*b^*U_{12})]$

Appendix B X-ray Crystallographic structure report for Ru(η^5-Cp)Cl(PEt_2H)(PPh_3) (**2b**)*

Table B.8 Derived atomic coordinates and Displacement Parameters for Hydrogen Atoms

Atom	*x*	*y*	*z*	U_{eq}, Å^2
H6A	0.3397	0.3707	0.2873	0.047
H6B	0.3210	0.3837	0.2164	0.047
H6C	0.3812	0.3141	0.2370	0.047
H7A	0.1579	0.4098	0.2774	0.055
H7B	0.1079	0.3751	0.2219	0.055
H7C	0.1897	0.4139	0.2090	0.055
H8A	0.0446	0.2395	0.2346	0.050
H8B	0.0549	0.2510	0.3069	0.050
H8C	0.0531	0.1584	0.2776	0.050
H9A	0.1368	0.0600	0.3046	0.050
H9B	0.2106	0.0679	0.3464	0.050
H9C	0.2166	0.0285	0.2792	0.050
H10A	0.3958	0.1824	0.2780	0.055
H10B	0.3555	0.0935	0.2661	0.055
H10C	0.3527	0.1356	0.3326	0.055
H11A	0.4310	0.2372	0.1582	0.063
H11B	0.4064	0.1414	0.1483	0.063
H12A	0.5132	0.1708	0.0931	0.079
H12B	0.4458	0.1485	0.0473	0.079
H12C	0.4704	0.2447	0.0572	0.079
H13A	0.2793	0.3730	0.0950	0.067
H13B	0.3677	0.3662	0.1070	0.067
H14A	0.3448	0.4150	0.0111	0.132
H14B	0.3859	0.3253	0.0073	0.132
H14C	0.2971	0.3321	-0.0047	0.132
H22	0.1535	0.3622	0.0996	0.071
H23	0.0810	0.4832	0.0882	0.096
H24	-0.0507	0.4725	0.0892	0.093
H25	-0.1073	0.3421	0.0998	0.076
H26	-0.0343	0.2191	0.1094	0.053
H32	0.1236	0.2853	-0.0067	0.065
H33	0.1721	0.2654	-0.1054	0.088
H34	0.2344	0.1421	-0.1305	0.082
H35	0.2486	0.0366	-0.0582	0.070
H36	0.2022	0.0552	0.0409	0.051
H42	0.1044	0.0609	0.2009	0.041
H43	0.0217	-0.0528	0.2143	0.049
H44	-0.0650	-0.0864	0.1380	0.054
H45	-0.0688	-0.0071	0.0480	0.056
H46	0.0129	0.1063	0.0344	0.049

Appendix C NMR spectra of isolated compounds

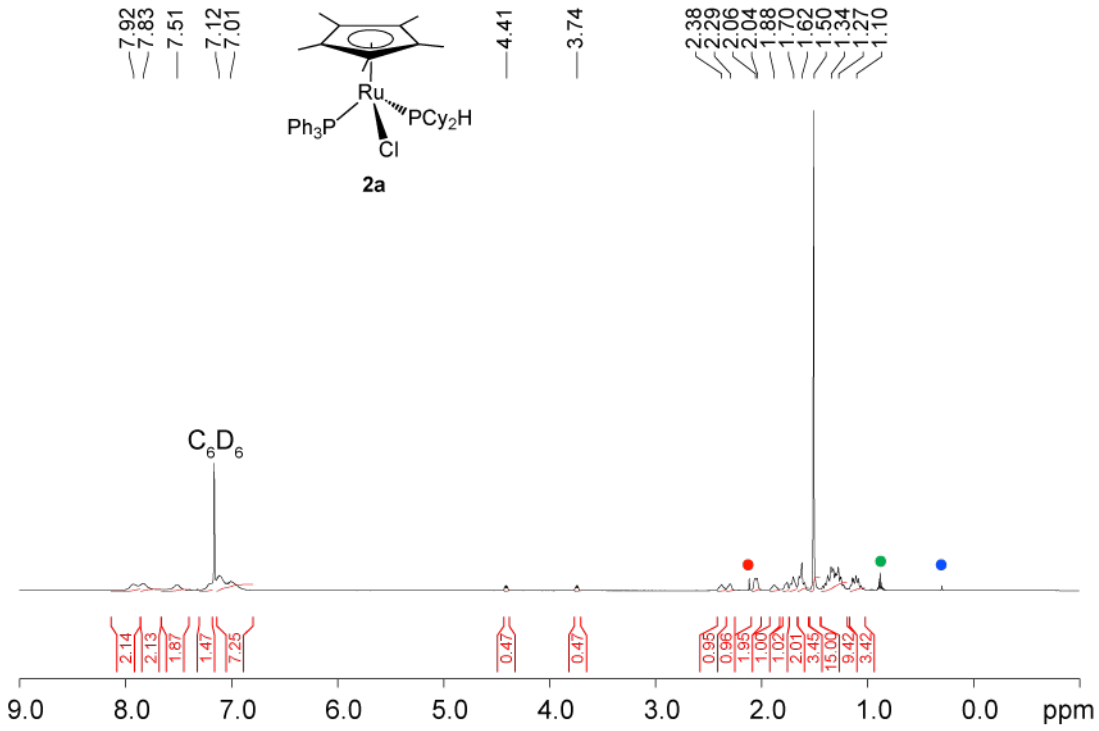

Figure C.1 ^{1}H NMR spectrum (500.27 MHz, C_6D_6) of complex **2a**. The signals due to other compounds are labeled as red dot (toluene), blue dot (grease) and green dot (pentane).

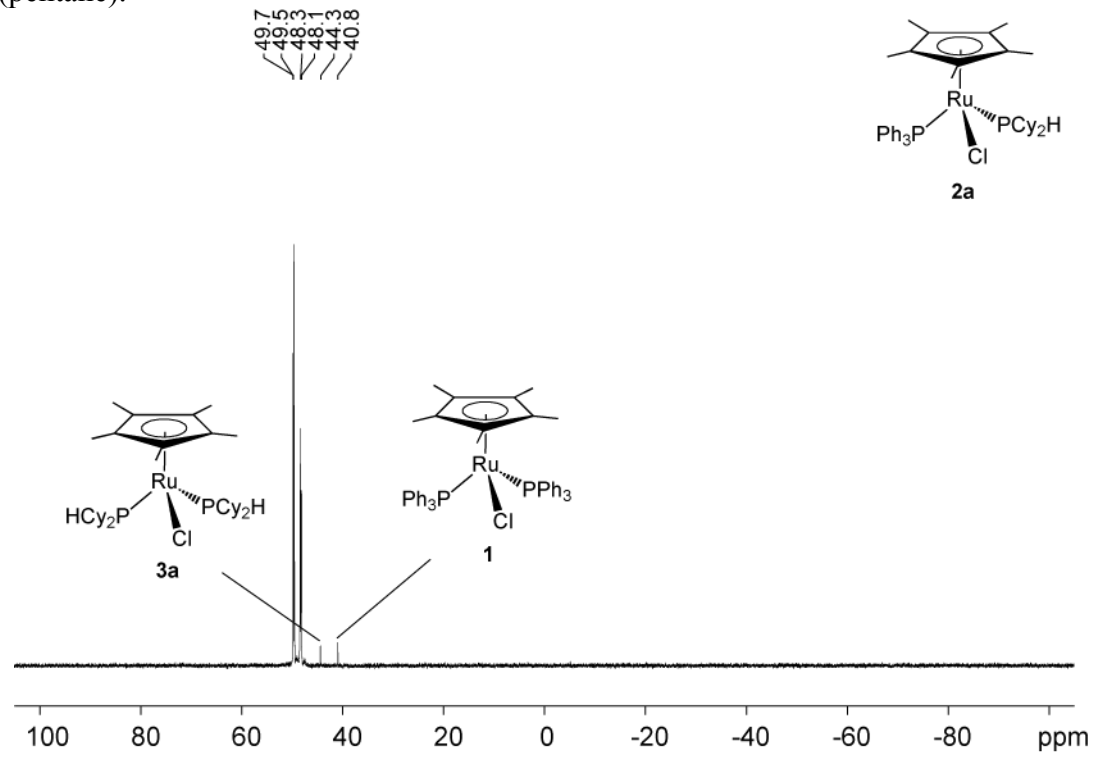

Figure C.2 ^{31}P{^{1}H} NMR spectrum (202.51 MHz, C_6D_6) of complex **2a**.

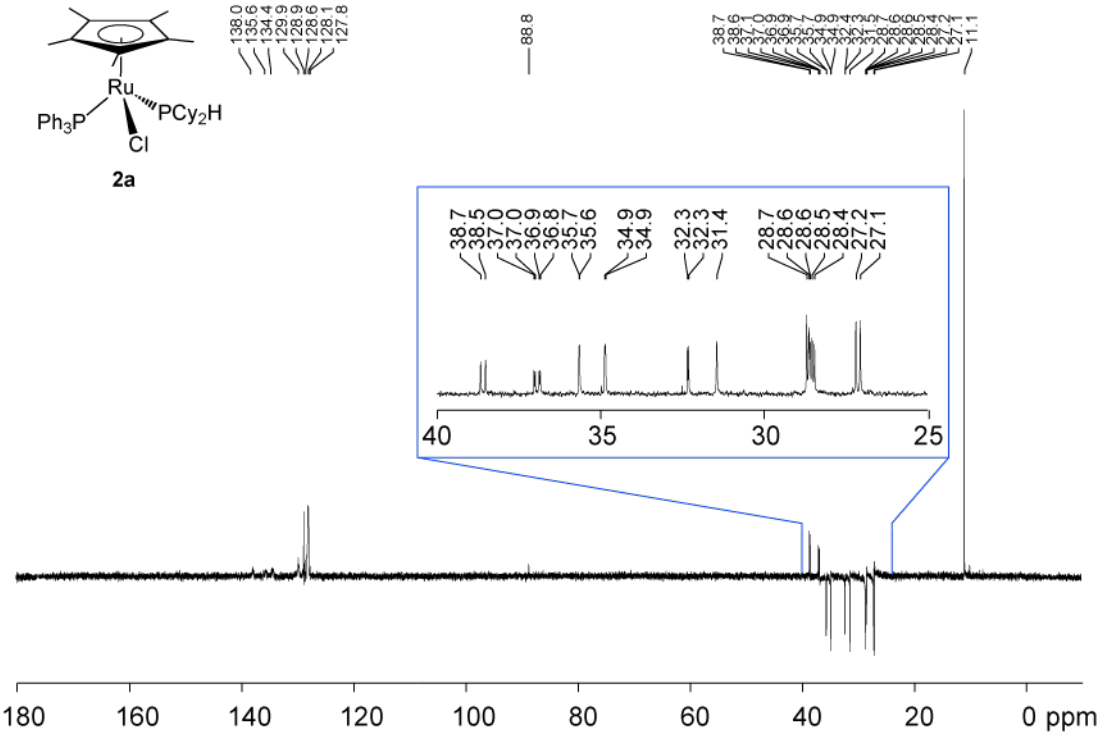

Figure C.3 ^{13}C DEPT 135 and $^{13}C\{^{1}H\}$ NMR (inset) spectrum (125.79 MHz, C_6D_6) of complex **2a**.

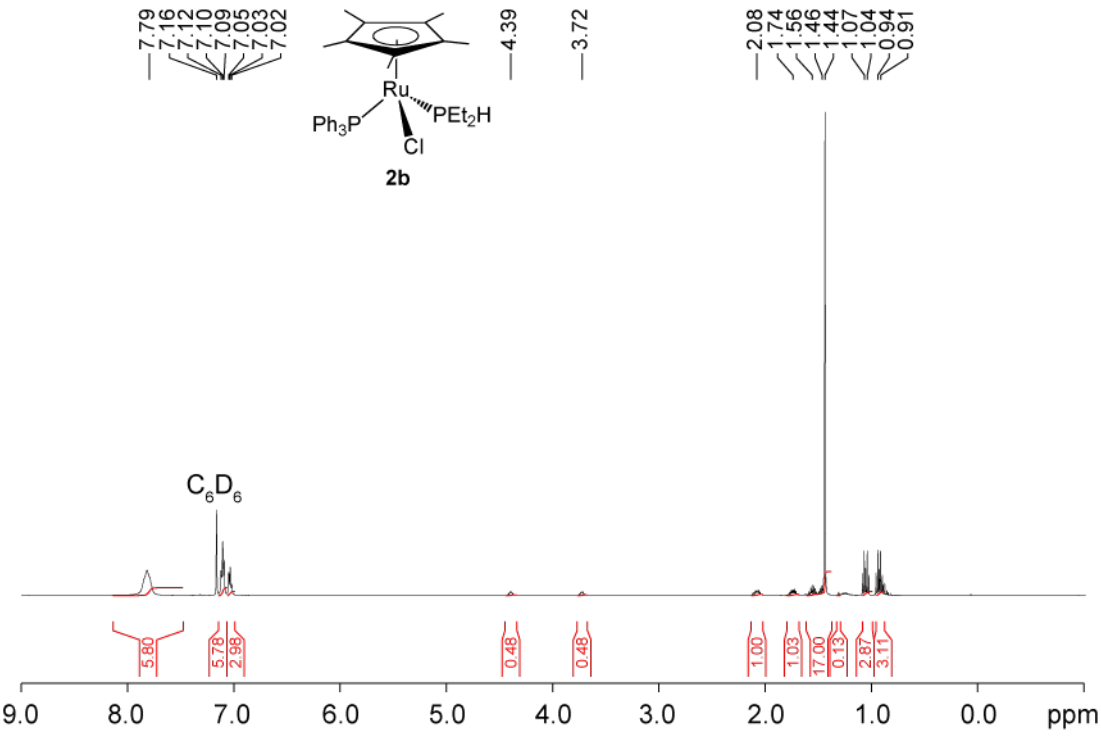

Figure C.4 ^{1}H NMR spectrum (500.27 MHz, C_6D_6) of complex **2b**.

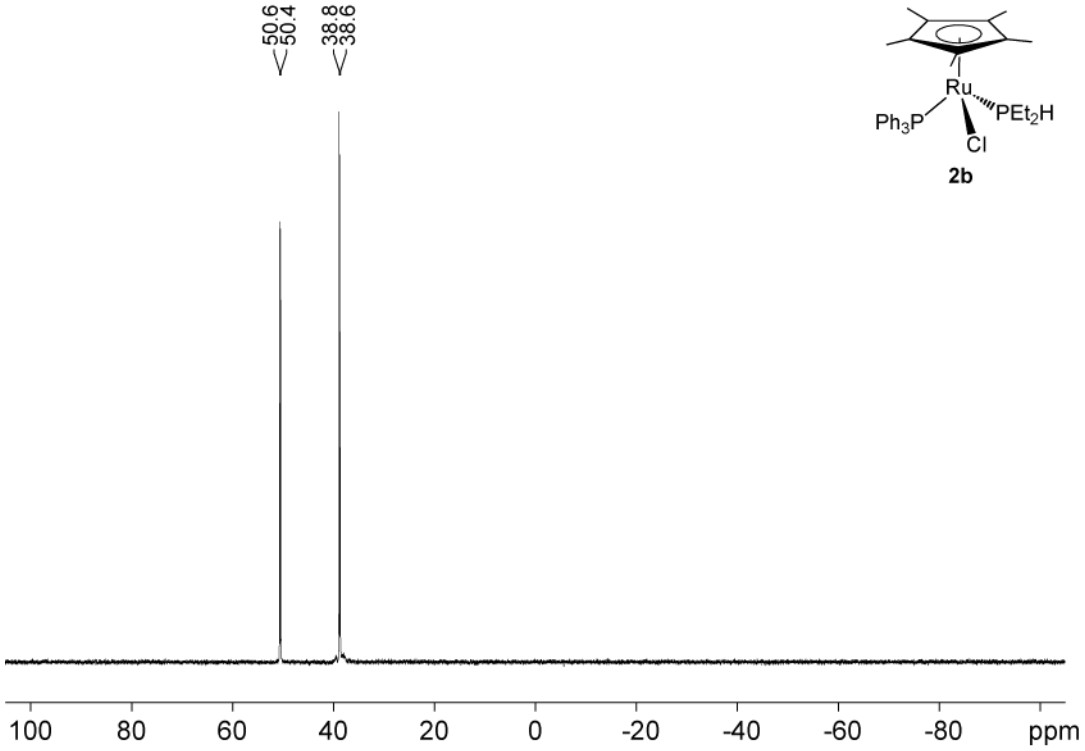

Figure C.5 $^{31}P\{^{1}H\}$ NMR spectrum (202.51 MHz, C_6D_6) of complex **2b**.

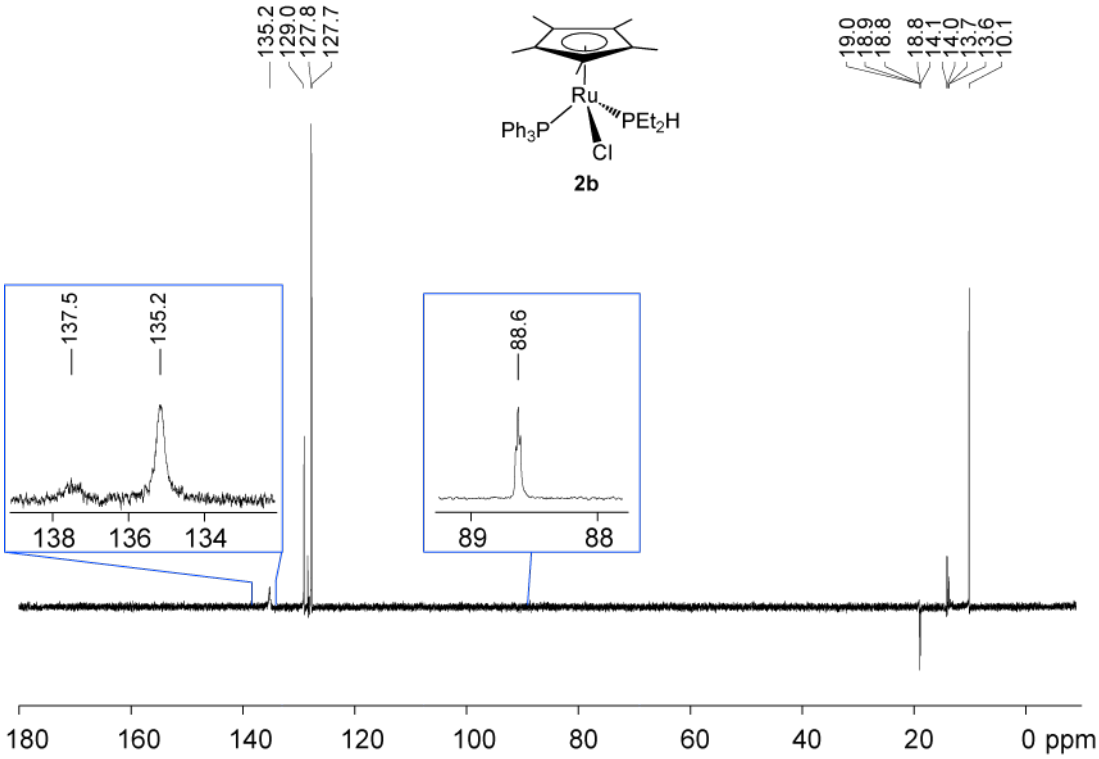

Figure C.6 ^{13}C DEPT 135 and $^{13}C\{^{1}H\}$ NMR (inset) spectrum (125.79 MHz, C_6D_6) of complex **2b**.

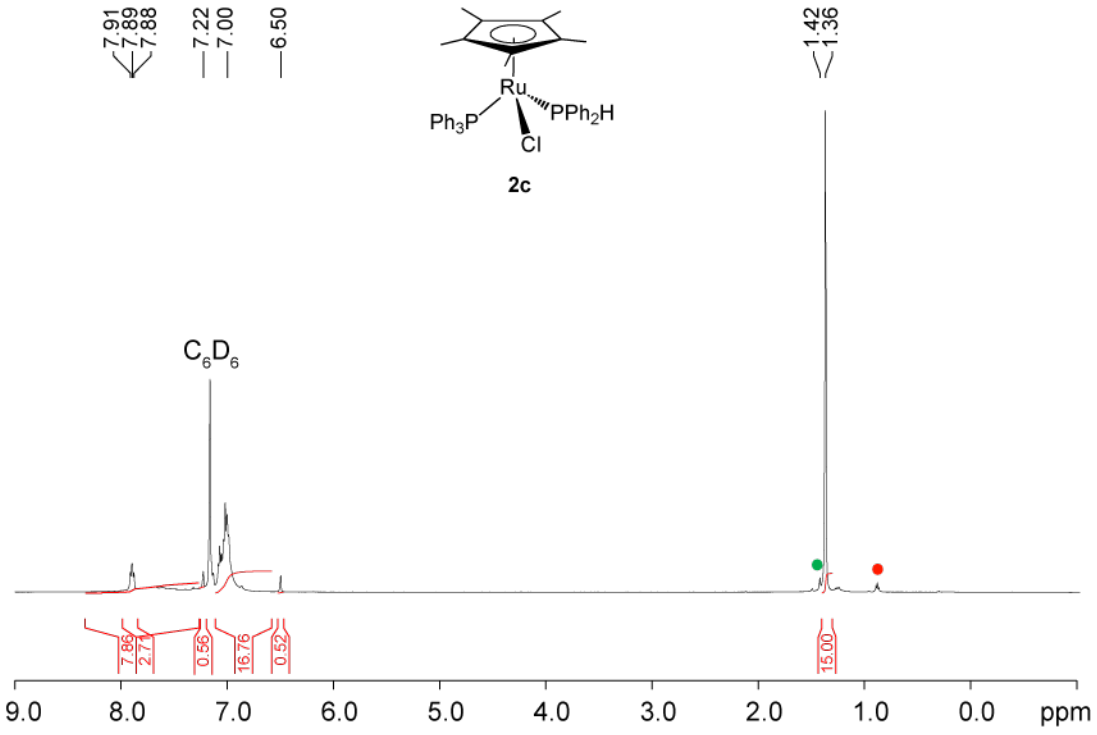

Figure C.7 ^{1}H NMR spectrum (500.27 MHz, C_6D_6) of complex **2c** containing a small amount of disubstituted **3c** (green dot). The signal due to toluene is labeled as red dot.

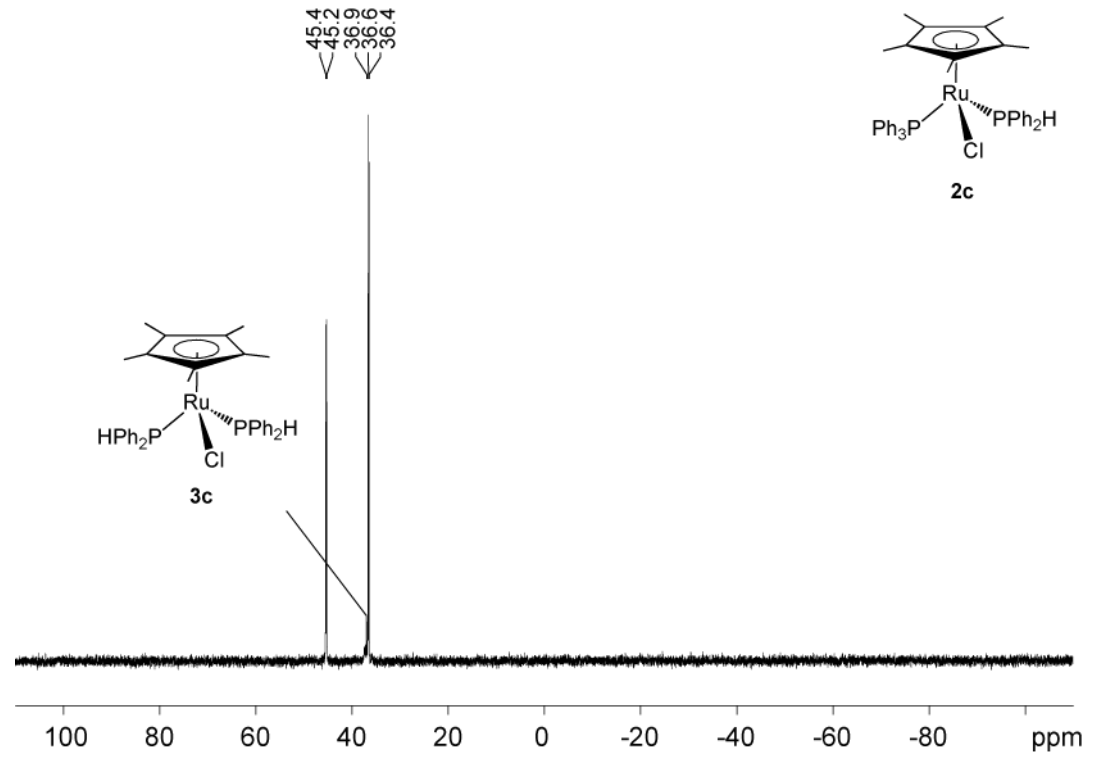

Figure C.8 ^{31}P{^{1}H} NMR spectrum (202.51 MHz, C_6D_6) of complex **2c** containing a small amount of disubstituted **3c**.

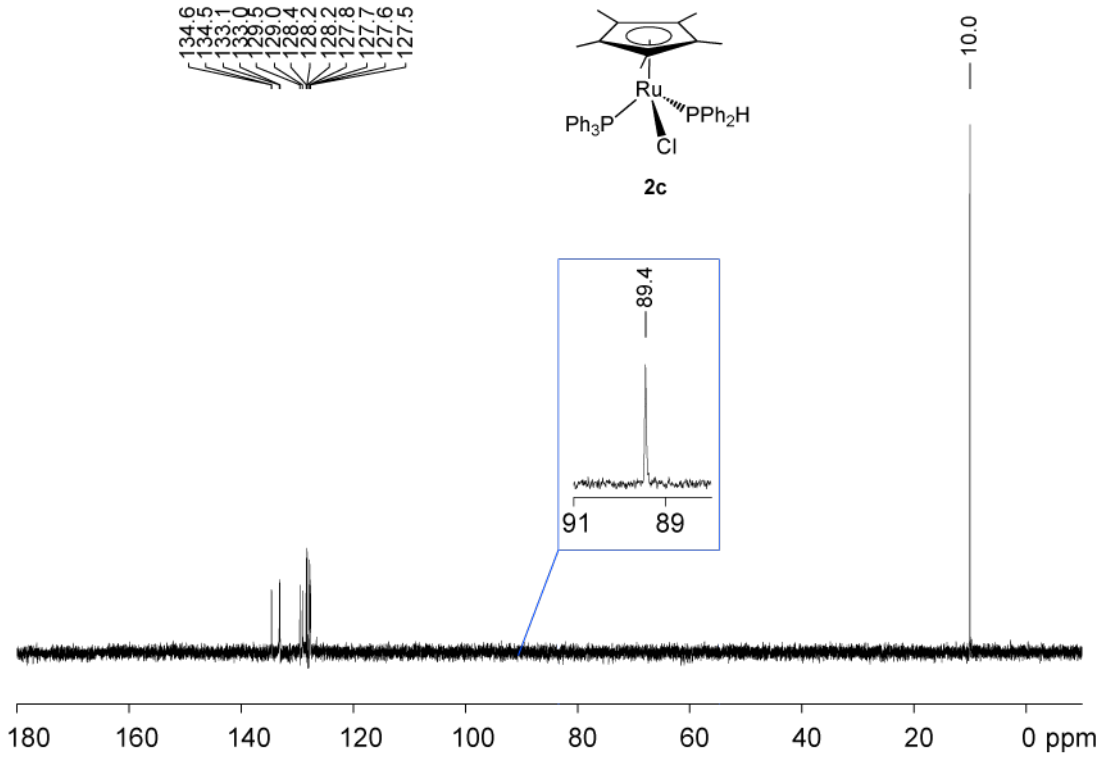

Figure C.9 ^{13}C DEPT 135 and $^{13}C\{^{1}H\}$ NMR (inset) spectrum (125.79 MHz, C_6D_6) of complex **2c**.

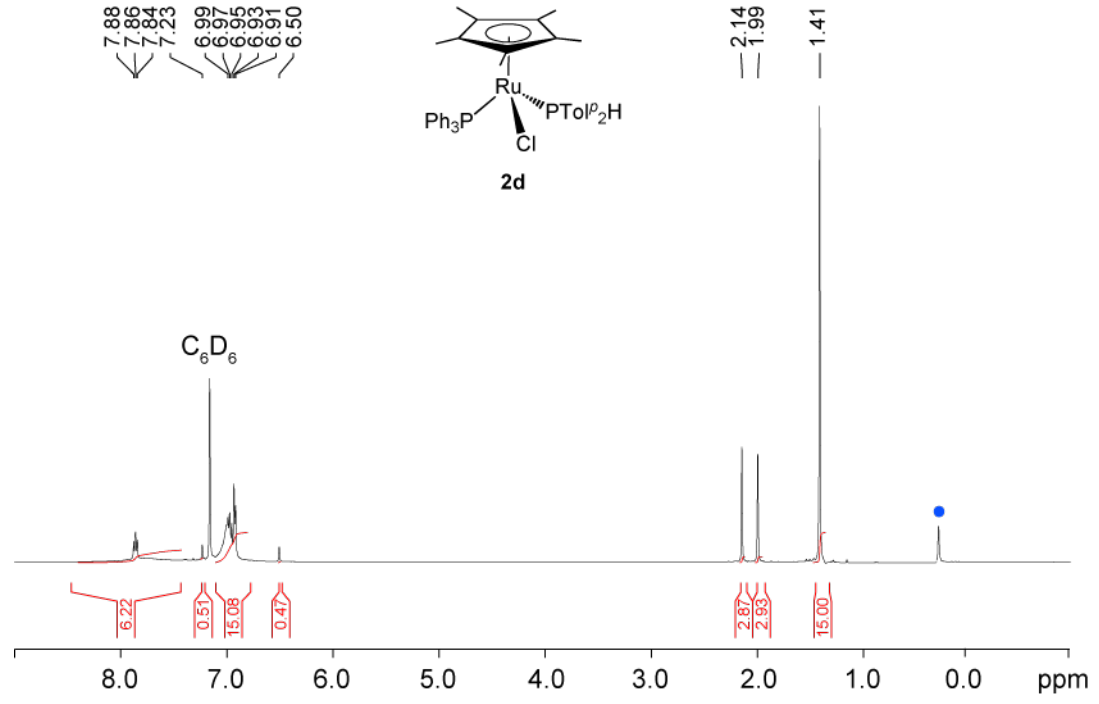

Figure C.10 ^{1}H NMR spectrum (500.27 MHz, C_6D_6) of complex **2d**. The signal due to grease is labeled as red dot.

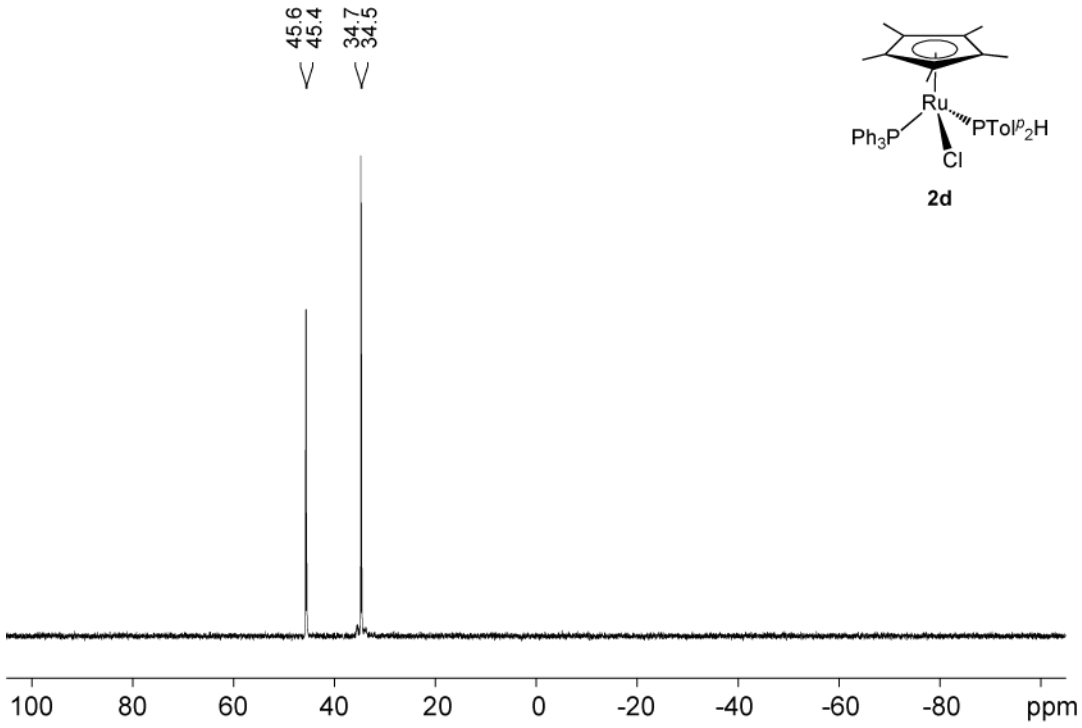

Figure C.11 $^{31}P\{^{1}H\}$ NMR spectrum (202.51 MHz, C_6D_6) of complex **2d**.

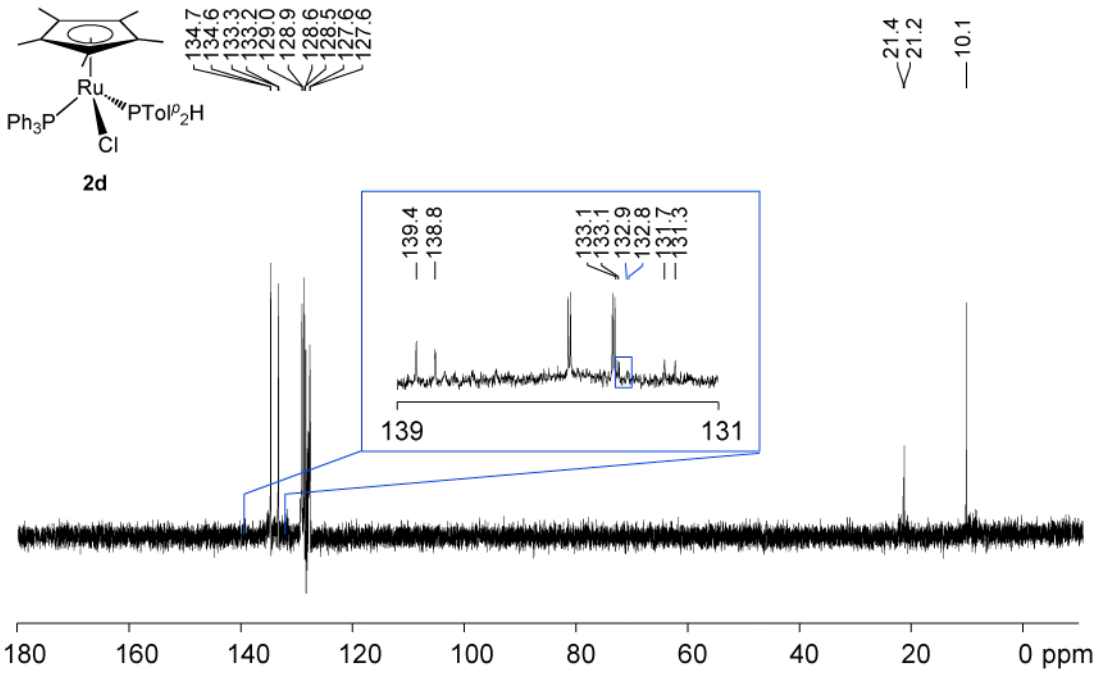

Figure C.12 ^{13}C DEPT 135 and $^{13}C\{^{1}H\}$ NMR (inset) spectrum (125.79 MHz, C_6D_6) of complex **2d**.

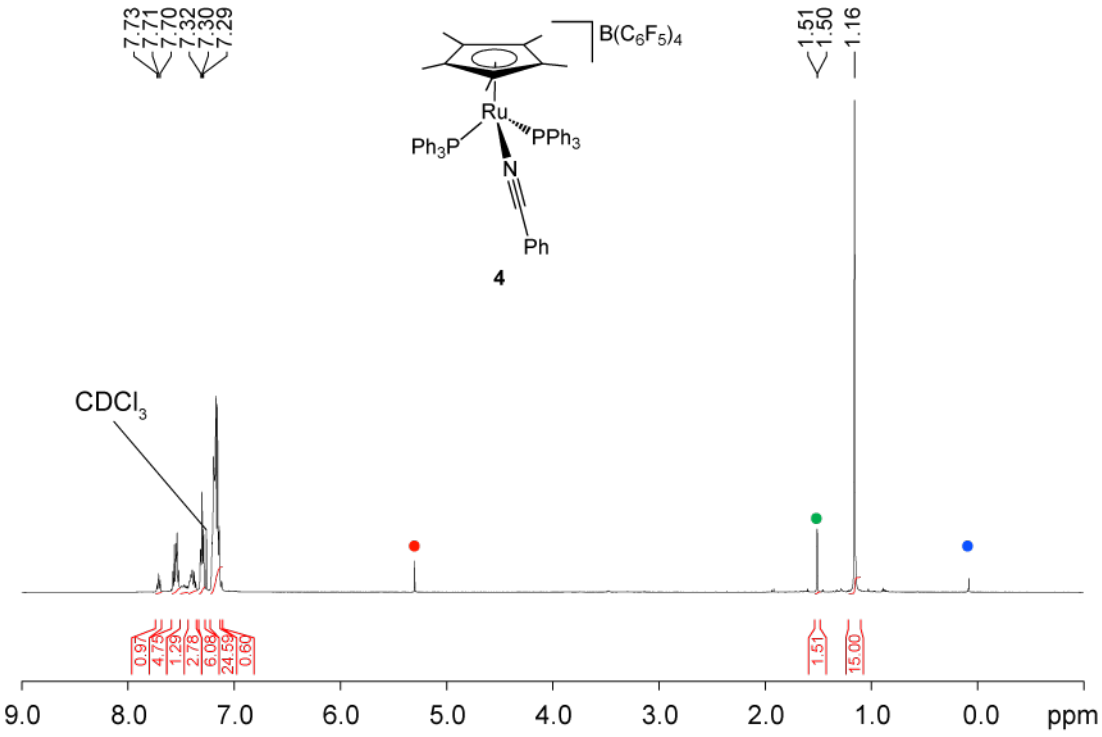

Figure C.13 ^{1}H NMR spectrum (500.27 MHz, $CDCl_3$) of complex **4** containing a small amount of [Ru(η^5-Cp*)(NCPh)$_2$(PPh$_3$)][B(C$_6$F$_5$)$_4$] (green dot). The signals due to other compounds are labeled as red dot (CH_2Cl_2) and blue dot (grease).

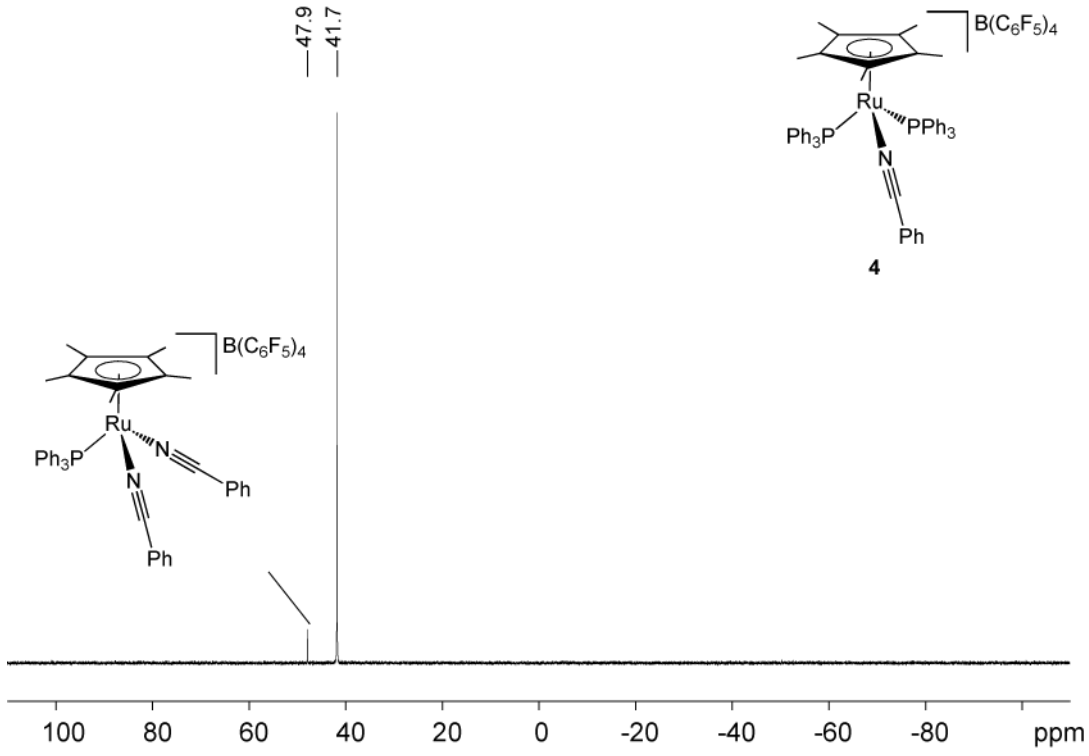

Figure C.14 ^{31}P{^{1}H} NMR spectrum (202.51 MHz, $CDCl_3$) of complex **4** containing a small amount of [Ru(η^5-Cp*)(NCPh)$_2$(PPh$_3$)][B(C$_6$F$_5$)$_4$]

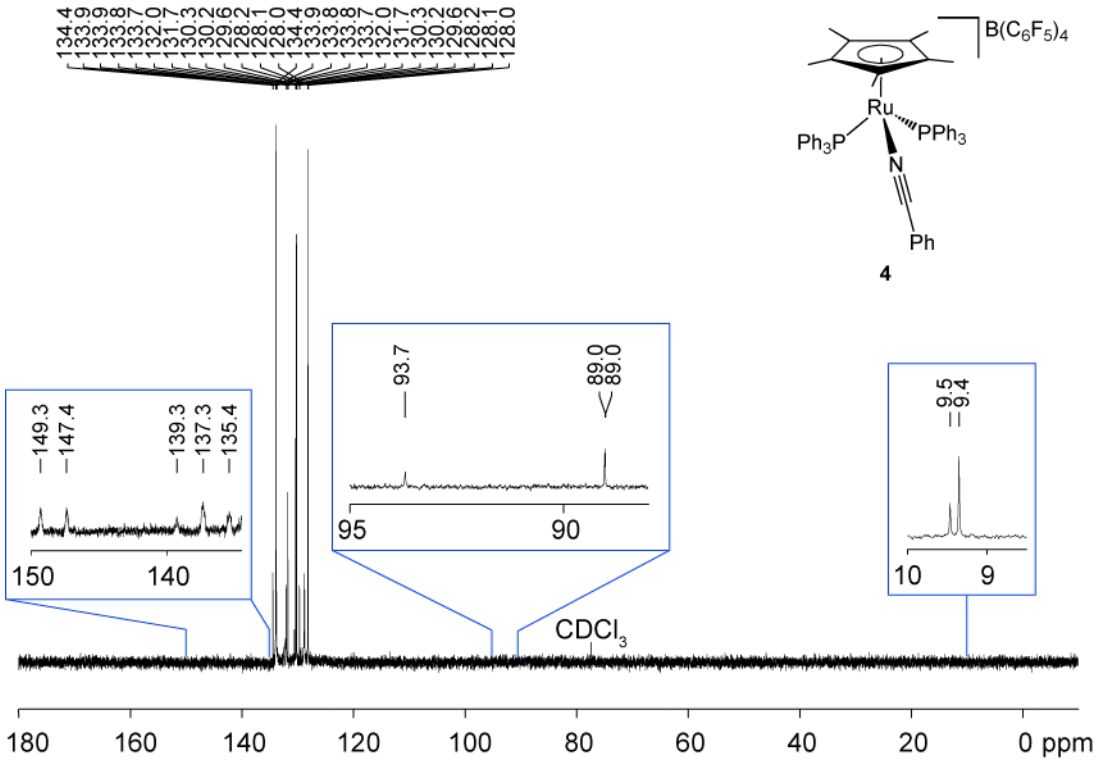

Figure C.15 ^{13}C DEPT 135 and $^{13}C\{^{1}H\}$ NMR (inset) spectrum (125.79 MHz, $CDCl_3$) of complex **4**.

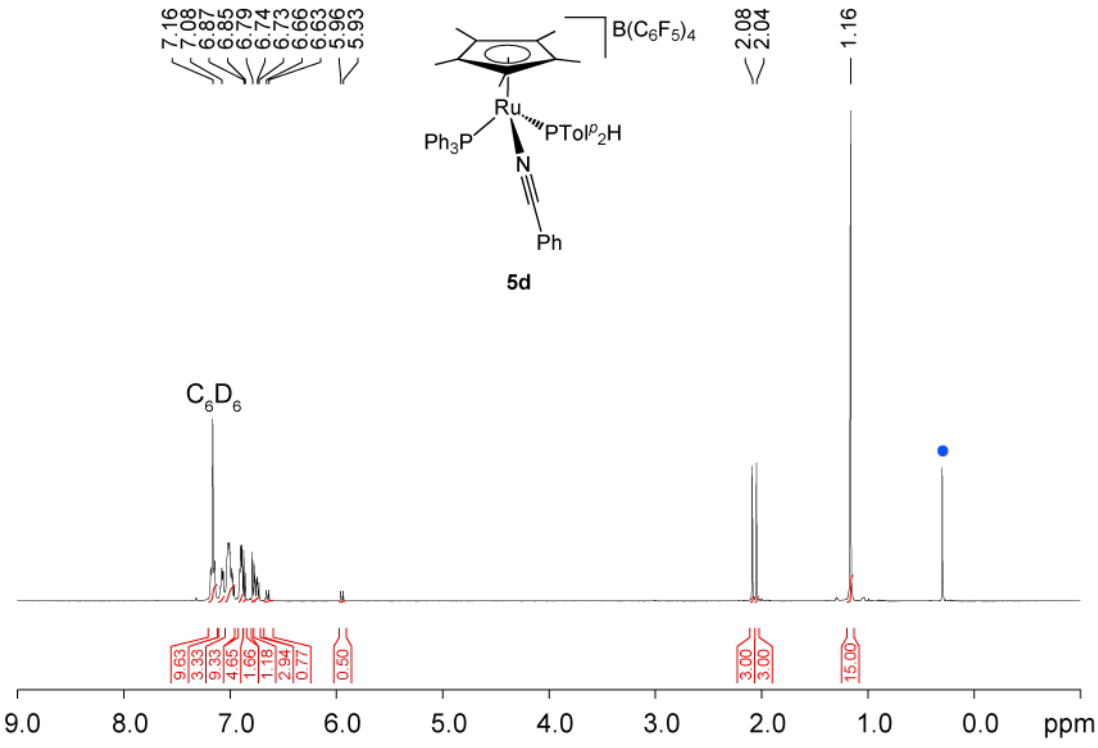

Figure C.16 ^{1}H NMR spectrum (500.27 MHz, C_6D_6) of complex **5d**. The signal due to grease is labeled as blue dot.

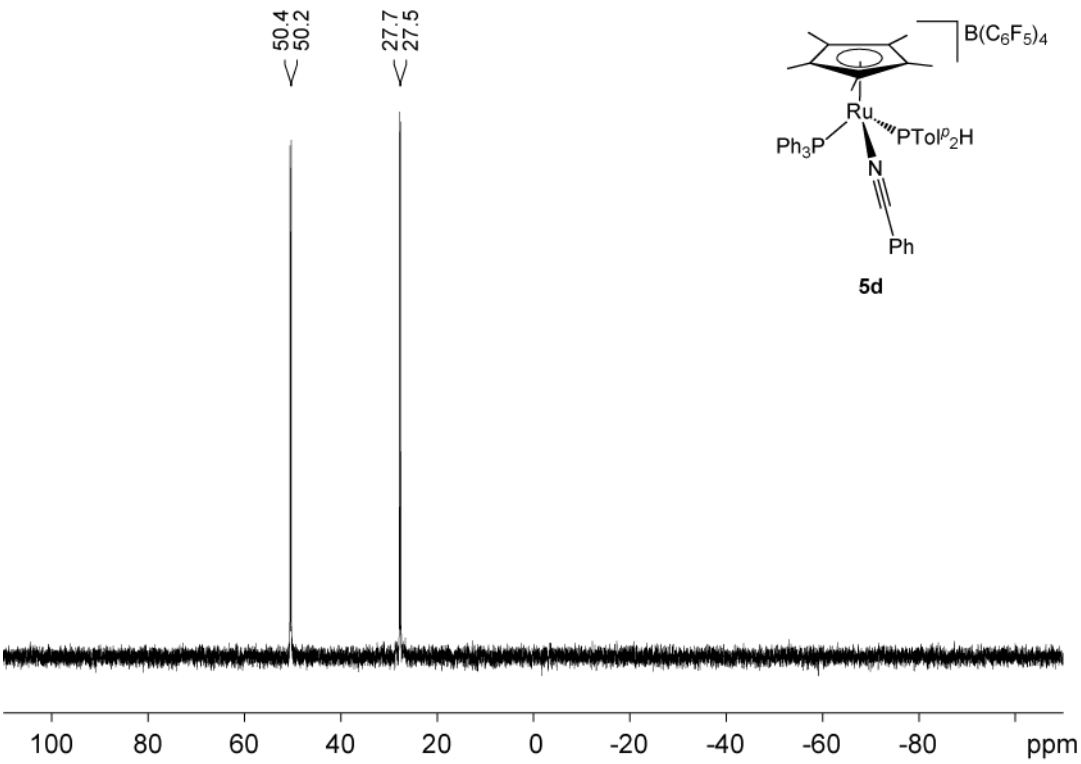

Figure C.17 $^{31}P\{^{1}H\}$ NMR spectrum (202.51 MHz, C_6D_6) of complex **5d**.

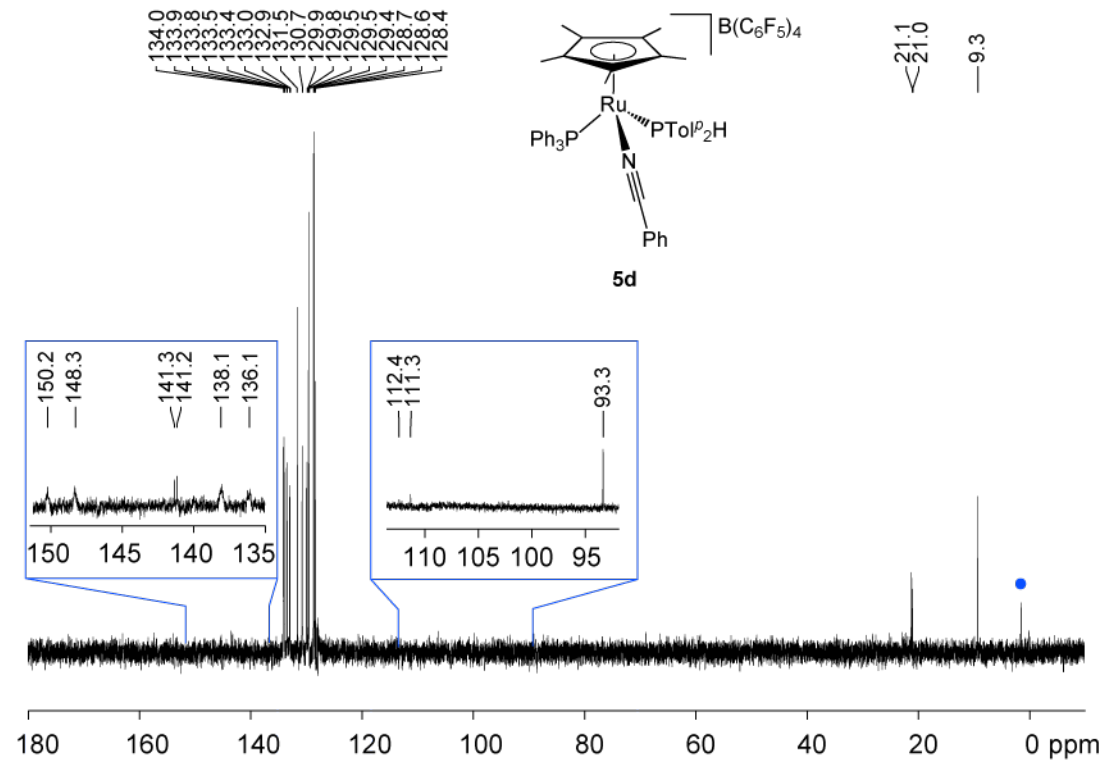

Figure C.18 ^{13}C DEPT 135 and $^{13}C\{^{1}H\}$ NMR (inset) spectrum (125.79 MHz, C_6D_6) of complex **5d**. The signal due to grease is labeled as blue dot.

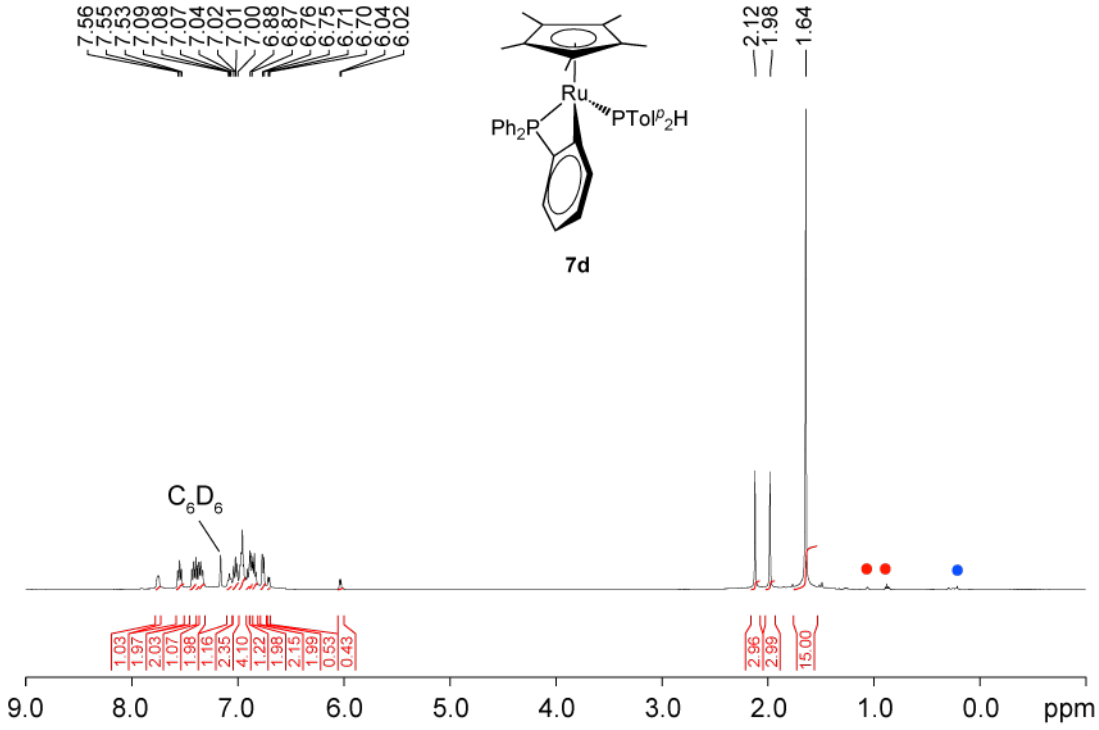

Figure C.19 ^{1}H NMR spectrum (500.27 MHz, C_6D_6) of complex **7d**. The signals due to other compounds are labeled as red dot (pentane) and blue dot (grease).

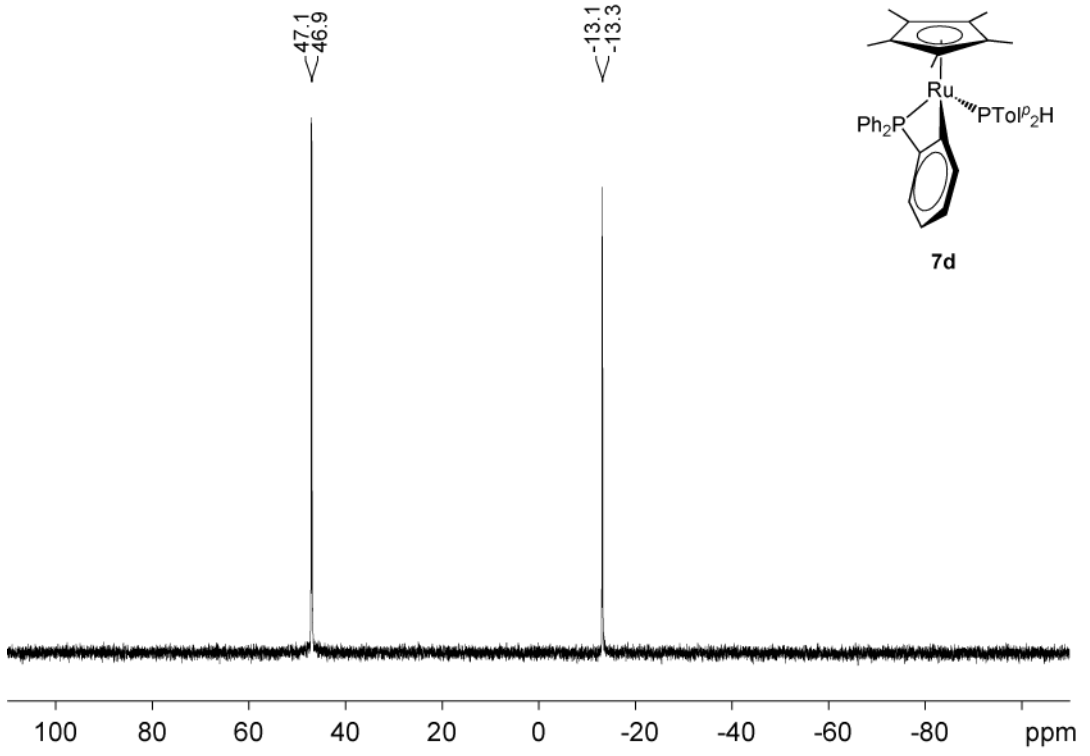

Figure C.20 ^{31}P{^{1}H} NMR spectrum (202.51 MHz, C_6D_6) of complex **7d**.

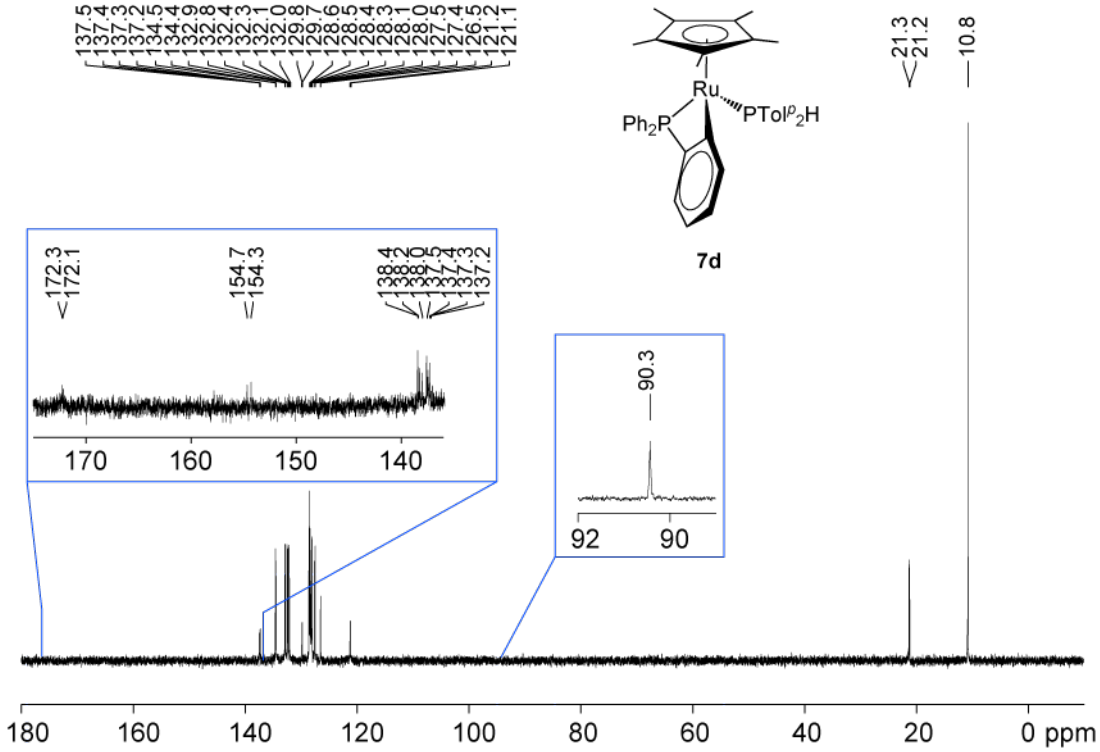

Figure C.21 ^{13}C DEPT 135 and ^{13}C{^{1}H} NMR (inset) spectrum (125.79 MHz, C_6D_6) of complex **7d**.

Appendix D Stacked $^{31}P\{^{1}H\}$ spectra for monitoring the dehydrohalogenation of 2a-d

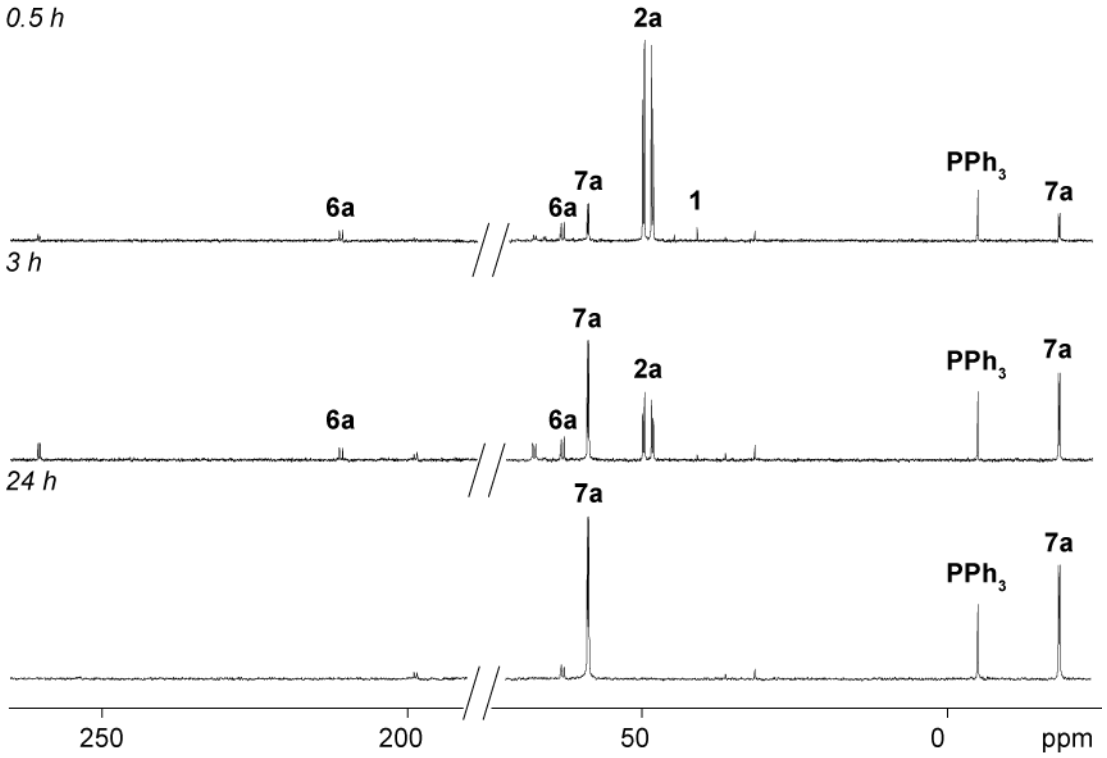

Figure D.1 $^{31}P\{^{1}H\}$NMR spectra (500.27 MHz, C_6D_6) of the dehydrohalogenation of [**2a** + KOBu^{t}] (0.5h, 3h and 24h). The other signals without label are described in Chapter 3.

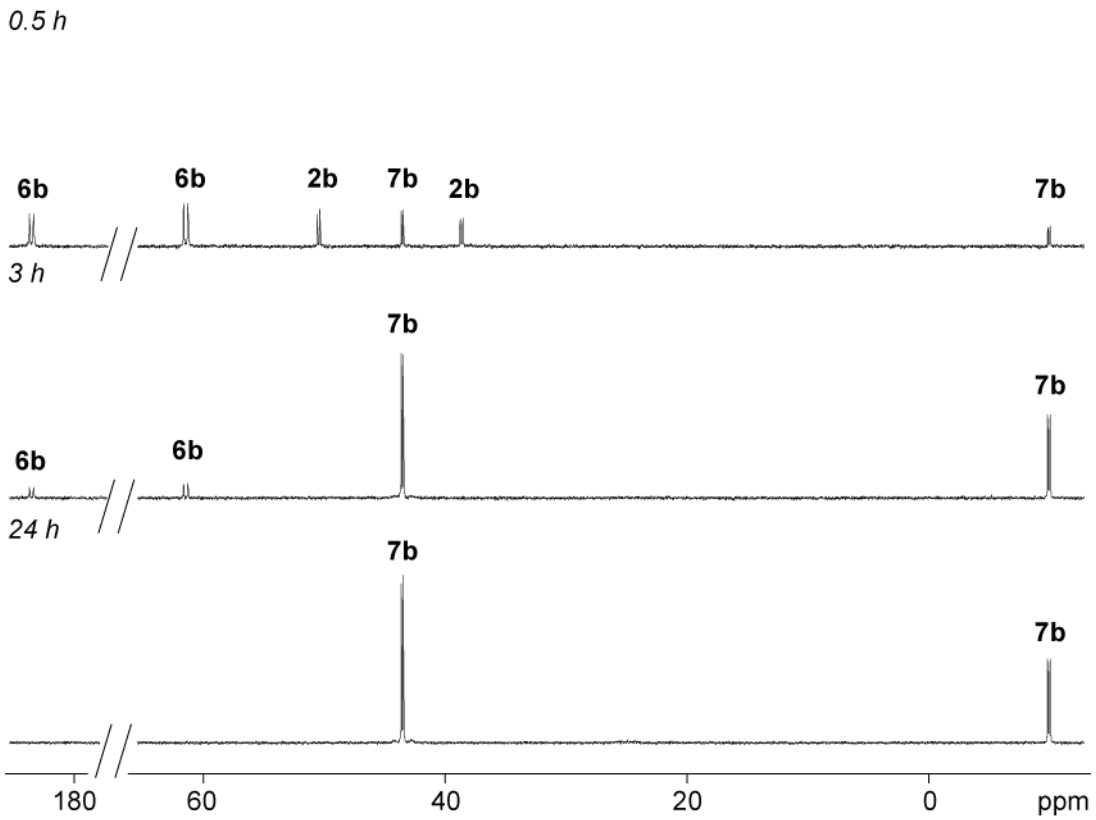

Figure D.2 $^{31}P\{^{1}H\}$NMR spectra (500.27 MHz, C_6D_6) of the dehydrohalogenation of [**2b** + KOBu^t] (0.5h, 3h and 24h).

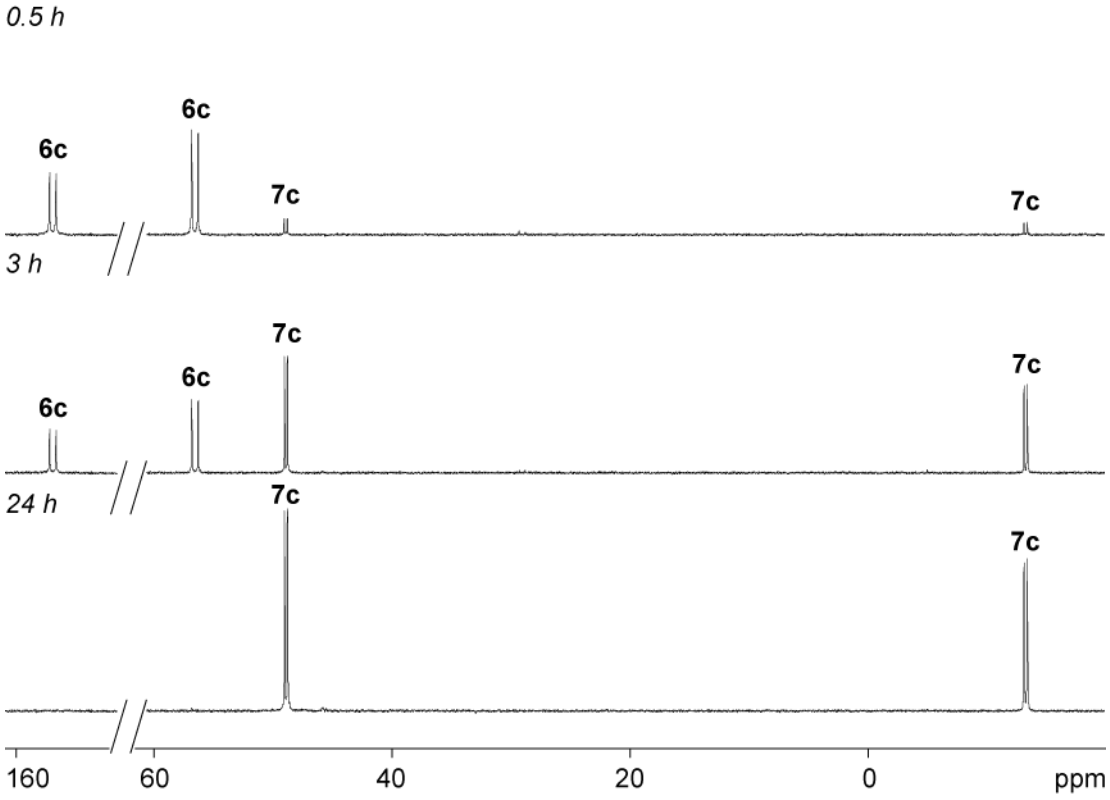

Figure D.3 $^{31}P\{^{1}H\}$NMR spectra (500.27 MHz, C_6D_6) of the dehydrohalogenation of [**2c** + KOBu^t] (0.5h, 3h and 24h).

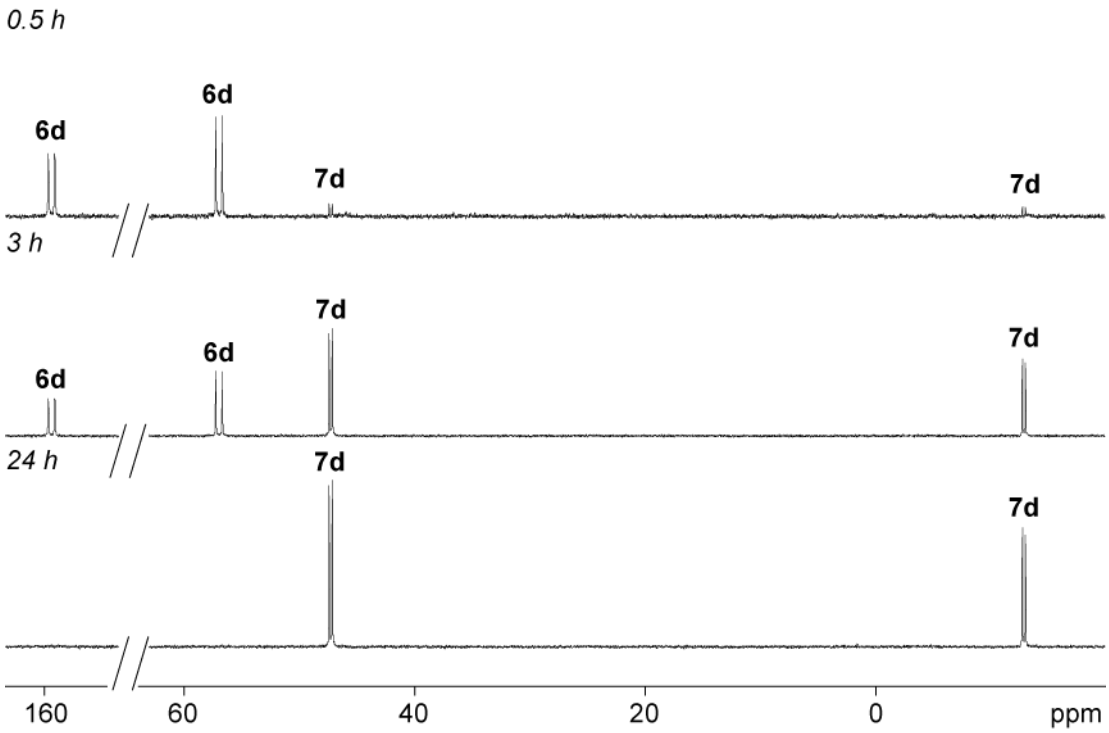

Figure D.4 $^{31}P\{^{1}H\}$NMR spectra (500.27 MHz, C_6D_6) of the dehydrohalogenation of [**2d** + KOBu^t] (0.5h, 3h and 24h).

Appendix E Sample guide to NMR assignments.

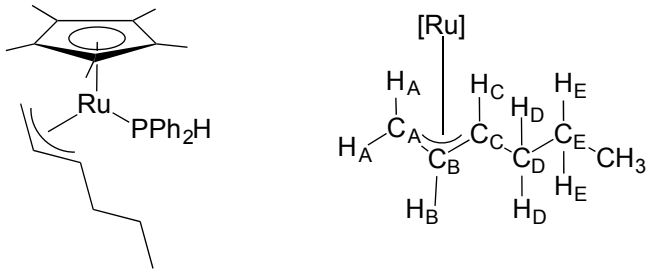

Figure E.1 Structure of Ru(η^5-Cp*){η^3-$CH_2CHCH(C_3H_7)$}(PPh_2H) (**15c)** showing η^3-$CH_2CHCH(C_3H_7)$ allyl protons $H_{A\text{-}E}$ and carbons $C_{A\text{-}E}$.

Characterization of Ru(η^5-Cp*){η^3-$CH_2CHCH(C_3H_7)$}(PPh_2H) (**15c**) (δ in ppm) shown as an example

For Cp*:

1. Distinct ^{1}H shift **CH_3 (Cp*)** δ: 1.62 (s, 15H).
2. **CH_3 (Cp*)** <=> **C_{methyl} (Cp*)** in ^{1}H/^{13}C-HSQC found ^{13}C **methyl (Cp*)** δ: 10.7 (s).
3. **CH_3 (Cp*)** <=> **C_{ring} (Cp*)** in ^{1}H/^{13}C-HMBC found ^{13}C **C_{ring}** δ: 88.6 (d, $^2J_{PC}$ 2).

For $HPPh_2$:

1. Diagnostic ^{1}H shift for **$HPPh_2$** and $^1J_{PH}$ coupling confirmed by ^{31}P NMR δ: 6.39 (d, $^1J_{PH}$ 324.8).
2. Stacked ^{1}H and ^{13}C{^{1}H} spectra of **15c**, **PPh_3** and **7c** to remove the signal due to **PPh_3** and **7c**.
3. Diagnostic ^{13}C shift for **C_{ortho}** in the Ph ring δ: 134.7 (d, $^2J_{PC}$ 10), 133.6 (d, $^2J_{PC}$ 10) (the two Ph groups are diastereotopic).
4. **C_{ortho}** <=> **H_o** in ^{1}H/^{13}C-HSQC found ^{1}H **Ho** δ: 7.53 (dd, 2H, $^3J_{PH}$ 10.0, $^3J_{HH}$ 8.0), 7.44 (dd, 2H, $^3J_{PH}$ 10.0, $^3J_{HH}$ 8.0).
5. **H_{ortho}** <=> **C_{para}** in ^{1}H/^{13}C-HMBC found ^{13}C **C_{para}** δ: 129.1 (s), 128.7 (s).
6. **C_{para}** <=> **H_p** in ^{1}H/^{13}C-HSQC found ^{1}H **H_p** δ: 7.06-7.03 (m, overlaps with signal of **PPh_3**, 2H).
7. Diagnostic ^{13}C shift for **C_{meta}** in the Ph ring δ: 128.0 (d, $^3J_{PC}$ 9).
8. **C_{meta}** <=> **H_m** in ^{1}H/^{13}C-HSQC found ^{1}H **H_m** δ: 7.12-7.08 (m, 4H).

For η^3-allyl group:

1. ^{1}H signal for **H_B ($H_{central}$)** assigned by its diagnostic shift δ: 3.14-3.05 (m, 1H).
2. **H_B** <=> **C_B** in ^{1}H/^{13}C-HSQC found ^{13}C **C_B** δ: 76.8 (d, $^3J_{PC}$ 2).
3. **H_B** <=> **C_D** in ^{1}H/^{13}C-HMBC and negative phase of signal **C_D** in ^{13}C dept 135 found ^{13}C **C_D** δ: 37.8 (s).
4. **C_D** <=> **H_D** in ^{1}H/^{13}C-HSQC found ^{1}H **H_D** δ: 1.97-1.90 (m, 1H), 1.62-1.55 (m, overlaps Cp* signal, 1H) (these protons are diastereotopic).
5. **C_D** <=> **CH_3** in ^{1}H/^{13}C-HMBC found ^{1}H **CH_3** δ: 0.99 (t, 3H, $^3J_{HH}$ 7.1).
6. **CH_3** <=> **C_{methyl}** in ^{1}H/^{13}C-HSQC found ^{13}C **C_{methyl}** δ: 14.3 (s).
7. **H-PPh_2** <=> **C_C** in ^{1}H/^{13}C-HMBC, distinct downfield ^{13}C shift and positive phase of signal **C_C** in ^{13}C DEPT 135 found ^{13}C **C_C** δ: 53.5 (d, $^2J_{PC}$ 4).
8. **H-PPh_2** <=> **C_A** in ^{1}H/^{13}C-HMBC and negative phase of signal **C_A** in ^{13}C dept 135 found ^{13}C **C_A** δ: 36.7 (d, $^2J_{PC}$ 5).

9. $\mathbf{C_C}$ <=> $\mathbf{H_C}$ in $^{1}H/^{13}C$-HSQC found ^{1}H $\mathbf{H_C}$ δ: 1.02-0.96 (m, overlaps $\mathbf{CH_3}$ in allyl group, 1H).
10. $\mathbf{C_A}$ <=> $\mathbf{H_A}$ in $^{1}H/^{13}C$-HSQC found ^{1}H $\mathbf{H_A}$ δ: 2.10-2.06 (m, 1H, *cis* to $\mathbf{H_B}$), 0.74 (dd, 1H, $^{3}J_{HH}$ 18.3, $^{3}J_{PH}$ 9.1, *trans* to $\mathbf{H_B}$).
11. $\mathbf{CH_3}$ <=> $\mathbf{C_E}$ in $^{1}H/^{13}C$-HMBC and negative phase of signal $\mathbf{C_E}$ in ^{13}C DEPT 135 found ^{13}C $\mathbf{C_E}$ δ: 27.0 (s).
12. $\mathbf{C_E}$ <=> $\mathbf{H_E}$ in $^{1}H/^{13}C$-HSQC found ^{1}H $\mathbf{H_E}$ δ: 1.55-1.52 (m, 2H).